ISSN 0973-0540

ANNALS OF THE INDIAN NATIONAL ACADEMY OF ENGINEERING

Volume : XV April 2018

INDIAN NATIONAL ACADEMY OF ENGINEERING

GOVERNING COUNCIL

Office Bearers

President	:	Dr. B.N. Suresh
Vice-Presidents	:	Dr. Indranil Manna
	:	Dr. Purnendu Ghosh
	:	Dr. Pradip
Chief Editor of Publications	:	Dr. Purnendu Ghosh
Executive Director	:	Brig RajanMinocha

The Indian National Academy of Engineering (INAE) is an autonomous institution partly supported by the Department of Science and Technology, Govt. of India and is recognized as a Scientific and Industrial Research Organization (SIRO) by the Department of Scientific and Industrial Research, Govt. of India.

Registered Office

Indian National Academy of Engineering
Unit No. 604-609, SPAZE, I Tech Park, 6th Floor, Tower A, Sector 49, Sohna Road
Gurgaon – 122 002 (India)
Phone: (91) – 0124 – 4239480
Fax: (91) – 0124 – 4239481
Email : inaehq@inae.in
Website : www.inae.in

Published by the Indian National Academy of Engineering, New Delhi
Printed at the Naman Stickers, 96 B, 4D Campus, Murlipura, Jaipur, Ph. : 0141-2742220

ISSN 0973-0540

ANNALS OF THE INDIAN NATIONAL ACADEMY OF ENGINEERING

Volume : XV April 2018

CONTENTS

PRESENTATIONS BY INAE YOUNG ENGINEER AWARDEES 2017

Annals of the Indian National Academy of Engineering
Vol. XV, April 2018

EDITORIAL

The Indian National Academy of Engineering (INAE) functions as an apex body that promotes the practice of engineering and technology in solving problems of national importance. Its activities include formulation of technology policies, promotion of quality engineering education, and encouraging R&D activities.

The Annual Convention of the INAE is an event where Fellows of the Academy assemble to welcome the newly elected Fellows and to participate in the General Body Meeting to discuss and share their ideas pertinent to the activities of the Academy, and the growth of engineering profession. In addition to this, the INAE recognises excellence and proficiency in engineering profession through its awards.

The Annual Convention of the INAE was held at TCS Chennai during December 14-17, 2017. The Proceedings of the Annual Convention contains the presentations made by the newly elected Fellows and the young engineer awardees. The INAE sincerely appreciates the efforts of the Fellows of the Academy in bringing out this volume of the Annals. INAE looks forward to receiving your valuable response.

April, 2018

Purnendu Ghosh
Chief Editor

Annals of the Indian National Academy of Engineering
Vol. XV, April 2018

Indigenous Development of Multi Gigawatt Pulsed Power Technology and Applications in BARC

Archana Sharma[1]

Abstract
In BARC, Pulsed power technology is being developed since 1970s. It has achieved many milestones in terms of pulsed power systems capacity, topologies and their utilization in various domain of investigations such as relativistic electron beam (REB), flash X-rays (FXR), high power microwaves (HPM), ultrawide band (UWB) generation and magnetic pulse welding (MPW) for dissimilar metals. These systems are being made compact and repetitive to meet the industrial requirement. All sub-systems are indigenously developed and demonstrated successfully. A few of them are transferred to industry also.

Keywords : Pulsed power technology, High power microwaves, flash x-rays, magnetic pulse welding

1 Introduction

Multi gigawatt pulsed power technology was earlier required for fusion applications and to simulate nuclear electromagnetic pulse (NEMP) simulation for R&D institutes and defense applications. Now a days, this technology is widely used to demonstrate their applications in industries for wood curing, water treatment, nano powder generation and pulse welding etc. In BARC, the research work started on pulsed power technology to be used for fusion experiments and flash x-rays generation in the beginning using **K**ilo **A**mpere **L**inear Injector series (KALI75-KALI5000) as shown in Fig.1 [1].

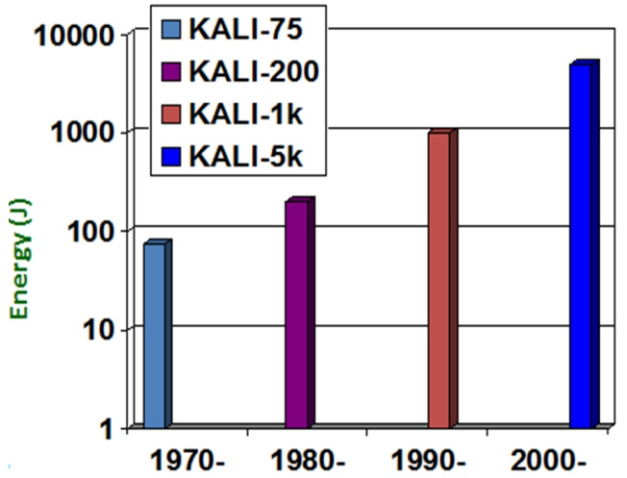

As systems capacity is increased their utilization was also expanded to high power microwave generation and electromagnetic forming/welding. The essence of pulsed power technology is to charge slowly and discharge fast. Each and every sub-systems is developed with the conscious decision of reducing inductance and field enhancement at desired place only. Various types of high voltage pulsed power systems have been developed based on tesla transformer, Marx generator, coaxial pulse forming lines (PFL), Blumlein and relativistic electron beam (REB) diodes.

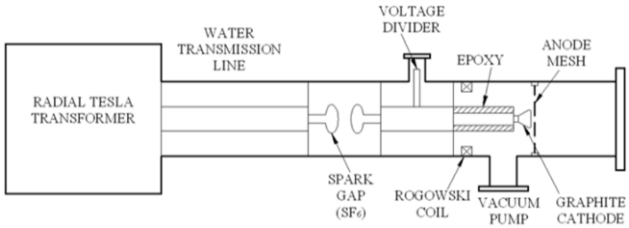

Fig.2 Schematic of Pulsed Power System

[1]Accelerator and Pulse Power Division, Bhabha Atomic Research Centre, Mumbai-400085

In order to transfer high voltage (>100kV) and high current (>5 kA) pulsesin sub-microseconds, sparkgap switches are widely deployed wherein by changing pressure only, operating voltage can be varied. It is a simple and robust device with a limitation on repetition rate. Intensive work has been done on switch characteristics and REB diode performance[2]. Another challenge in this technology is to measure the pulse amplitude and shape. There is no diagnosis off the shelf available to measure intense beam power, voltage and current. As a part of development Rogowski coils, sparkgaps switches, aqueous solution based load and voltage divider were in house developed. To make system repetitive, sparkgaps switches have inherent limitations of discharge/recombination process delay, therefore magnetic pulse compression (MPC) based switches were used and linear induction accelerators were developed to do technology demonstration of repetitive pulsed power system by LIA-200: 200kV,5kA,1-100Hz [3]. In this paper , system and their usage as high power microwave (HPM), flash (X-rays) and Magnetic pulse welding (MPW) will be illustrated in the following sections.

2 KALI-30GW System

This system consists of HVDC power supply, Marx generator coupled with transformer oil based Blumlein type PFL. It is developed by all indigenous components and materials.The Marx generator is immersed in transformer oil for insulation and cooling whereas all sparkgaps were in pressurized gas medium. Charging inductor and pre-pulse switches are the vital components of this system which are generally not mentioned in the literature. Design of Blumlein is also analyze din terms of voltage distribution and electric field optimization. This system has been used to produce REB pulses and convert them to either FXR or HPM [4]. Experimental studies were done for different types of high power microwave devices based on virtual cathode oscillators, axial and co-axial type, reflex triode with graphite and velvet cathode to optimize the electron beam to HPM conversion efficiency.

Fig. 3: Photograph of KALI-30GW system(1MV,30kA,80ns)

The system is tested for 1MV,30kA,80ns output pulse with reflex triode to produce high power microwave pulses.These HPM is used to study the vulnerability threshold of various electronics devices and circuitry.

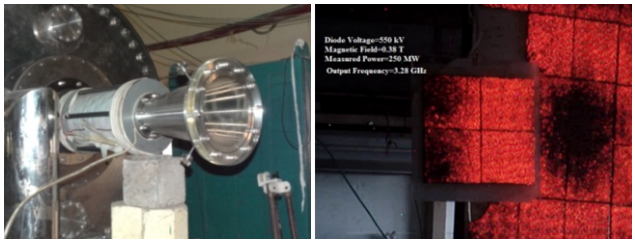

Fig. 4 Backward wave oscillator & output HPM on Neon bulb arrays in TM01 mode

Recently an indigenously designed and developed backward wave oscillator (BWO) is tested with this pulsed power system and 1GW HPM in TM_{01}[5] mode is measured successfully as shown in Fig. 3. It also enabled to develop high gain antenna and filed probe to measure the power and frequency of out put pulses.

3. Flash X-Rays generation

Any X-ray machine can penetrate through opaque object and get the imaging. the capacity of penetration depends on the density (attenuation coefficient :μ), thickness (t) of the object and voltage of the electron beam ($I= I_0 e^{-\mu t}$). The dose which is received by the detector is proportional to the product of voltage and current (dose α $IV^{2.8}$).

Distribution of dose is measured with respect to distance and angle using TLDs and OSLDs. maximum dose generated so far is 12R/pulse at window. Image plate is used for radiography and tungsten pin (anode) gets eroded after a few shots need to be replaced, which can be seen by reduced dose for same parameters.

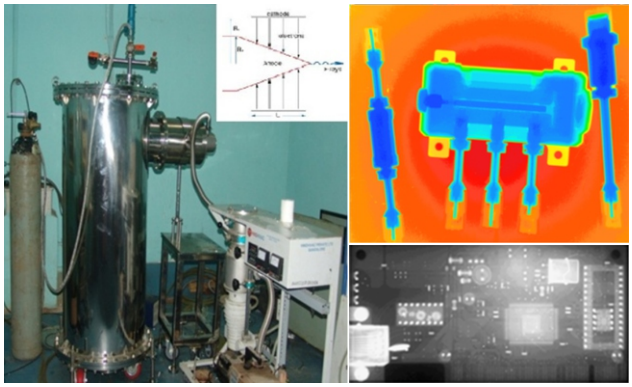

Fig.5: Marx based FXR source and Radiography

This source is based on bremstrahlung radiation and it has wide energy distribution of X-rays. It is exposed in <100ns hence fast dynamic even t can be captured without blur. Such systems are developed using FXR diode of tungsten anode and graphite cathode as shown in Fig.5, coupled with gas filled Marx generator. This technology has been developed from 200kV to 1000kV, 100ns FXR output pulse and radiography has been done [6].

4Electro-Magnetic Pulse Welding

In BARC capacitor bank technology has been developed for electromagnetic manufacturing (EMM) applications [7]. It is varied from 40-800kJ, 100kA-1000kA, 10-40kHz (short circuit Frequency). It operate in single shot mode. It can generate magnetic pressure upto 1GPa. This magnetic pressure corresponds to 50T pulsed magnetic field in pulsed.

Fig.6Indigenous Electro-Magnetic welding Setup

It is being used for dissimilar metal welding in lap joint for sheet to sheet and tube to tube or rod. This technique is similar to explosive welding wherein weld interface will have a wavy nature as shown inFig. 7.

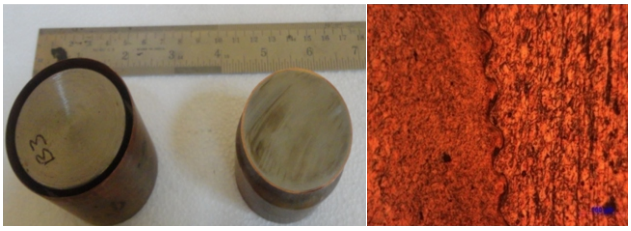

Fig.7 Magnetic pulse welding and interface metallograph

This is a clean and green process without any need of pre-post weld treatment on the job. It does not require any filler materials, gas emission etc. It can be automated for higher throughput. It has been demonstrated for Al/Al, Cu/soft iron, Al/copper, steel/Al and steel Cu etc. leak tightness of the order of 10^-9mbarl/s has been achieved. This technology is available with ECIL, Hyderabad and M/S Artech Welder, Pune.

This system can also be used for electro pulsing to alter the material properties as per need. It has the advantage of getting the materials hardening without losing ductility unlike thermal hardening process.The high pulse magnetic field has distinct area of choice for many physicist to develop probes for various parameters in materials study.

5 Pulse Neutron Generation

Pulsed current discharge from a capacitor bank to a plasma focus device is used and in a D-D environment with an optimiseddeuterium gas pressure and current pulse [8], it gives burst of pulsed neutron/ It can be used for prompt gamma neutron activation analysis (PGNAA).

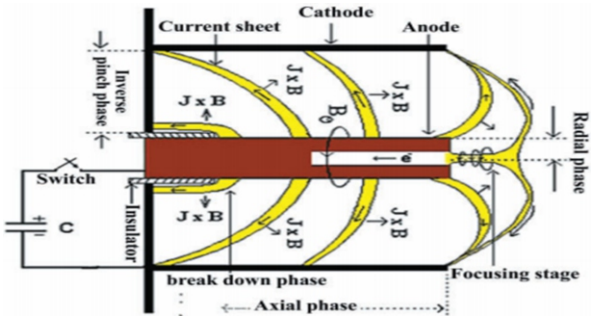

Fig.8: Principle of Plasma focus for operation

It can be used for neutron based studies in universities to measure, shield and detect and deploy for trace analysis of different kind of materials purity. This is an D-D reaction as given below:

$$D + D \rightarrow {}^{3}He + n\ (2.45MeV)$$

To use these neutron it can be suitable thermalised using high density polyethylene sheets. Various detectors (NaI, silver activation based and He-3/BF3 gas filled detectors are available for experiments. This source can also be used to calibrate the detectors without radioactive source (Pu/Be). Efforts are being made to do neutron radiography using these systems in the lab.

Table-1 Pulsed Neutron Source Parameters

System type	: Transportable	Portable
DD neutron yield per pulse	: 4×10^{9} n/p (average)	10^{5} – 10^{6} n/p (average)
Neutron energy (DD)	: ~2.45 MeV (typical)	~2.45 MeV (typical)
Pulse duration (FWHM)	: ~50 ns (typical)	~25 ns (typical)
Plasma focus head	: Replenishable & Demountable type	Replenishable & Demountable type
Total energy stored	: 10 kJ (maximum)	340 Joules (maximum)
Total capacitance	: 50 µF (12.5 µF × 4 Nos.)	22.5 µF (1.9 µF × 12 Nos.)
Charging voltage	: 20 kV (maximum)	5.5 kV (maximum)
Energy transfer switch	: Pseudospark (4 Nos.)	Sparkgap (1 No.)
Peak discharge current	: 600 kA (maximum)	120 kA (maximum)
Minimum time between shots	: 180 s	200 ms
Size of plasma focus head	: 0.2 m (ϕ) × 0.3 m (h)	0.025 m (ϕ) × 0.1 m (h)
Overall weight of system	: 300 kgs (approx.)	10 kgs (approx.)

Two types of dense plasma focus based neutron source has been developed and their parameters are listed in the table above. This technology is also available for transfer if approaced to headttcd@barc.gov.in. Specialisation is achieved on the design of high tesla coil and field measurememnt upto 60T within 25µs.

6 Acknowledgement

The author is grateful to BARC for giving the opportunity towork in this exciting field of pulsed power technology. Thanks are due to Shri R.K.Rajawat, AD,BTDG and Shri D.Venkateshawarlu, RD,BARC-Vizag. Lastly sincere acknowledgement to colleagues of PPSS, APPD and PPEMD, this work could be completed with their active team efforts

7 References

1. **Rakhee Menon , Amitava Roy, SabyasachiMitra , Archana Sharma , JayantaMondal, Kailash Mittal , K V Nagesh , D P Chakravarthy , (2008),** "Generation and Dose Distribution Measurement of Flash X-ray in KALI-5000 System", *Rev. Sci. Instrum. 79, 103301*.

2. **Amitava Roy, S. Mitra, R. Menon, D. D. P. Kumar, SenthilKumar,Archana Sharma, K. C. Mittal, K.V. Nagesh, D. P. Chakravarthy, (2009),**"Prepulse Suppression on a High Power Electron Beam Accelerator using a Dielectric Cathode Holder", *IEEE Transactions on Plasma Science, Vol. 37, pp. 67-75*.

3. **Archana Sharma, A.M. Shaikh, K. Senthil, S. Mitra, R. Chandra, S. Vishnu, S. Sandeep, AmitavaRoy**,"Preliminary results of Linear Induction Accelerator LIA-200", A. Sharma, et. al., *Journal of Instrumentation, 2010 JINST 5 P05001*, [2010].

4. **Archana Sharma, A.M. Shaikh, K. Senthil, S. Mitra, R. Chandra, S. Vishnu, S. Sandeep, Amitava Roy** ,"First results of KALI-30 GW with 1 MV flash X-raysgeneration and characterization by Imaging plate", *Journal of Instrumentation, JINST 9 P07011*, [2014].

5. **Romesh C., J. Mondal, V. K. Sharma, A.S. Patel, S. K. Singh, K. Senthil, A. Roy, S. Mitra, Archana Sharma, R. K. Rajawat,** ("Relativistic Backward Wave Oscillator Operation in Low Magnetic Field Region", *National Symposium on Vacuum Technology and Its Applications to Electron Beams, Nov. 2015, (IVSNS - 2015), at BARC, Mumbai.*, [2015].

6. **Rakhee K Menon, Sabyasachimitra , Ankur Patel , Raghwendra Kumar ,**

Gaurav Singh , K Senthil , Ranjeet Kumar , Tanmay S Kolge , Amitava Roy , S Acharya, Debabrata Biswas , Archana Sharma, (2017), "Development of Cable Fed Flash X-ray (FXR) System", *Review of Scientific Instruments 88, 083307.*

7. **P.C.Saroj, M.R.Kulkarni, Satendra Kumar and D.P.Chakravarthy,** (2014),"Design and Development of 40 kJ, 20 kV EMM system,"Internal report BARC, Mumbai

8. *R Verma*, *R Shukla*, **E Mishra, P Dhang, P Dey,Archana Sharma,** (2017),"*Indigenous Development of Pulsed Neutron Generators for Analytical Applications*," *BARC News letter, March-April, 2017, pp.22-26.*

Annals of the Indian National Academy of Engineering
Vol. XV, April 2018

Indigenous Capacity Building for High Temperature Materials for Space

S. C. Sharma[1]

As space based services reach door-step of the common man and become an integral part his daily life, 'low cost access to space' becomes watchword for material scientists. Towards this, development of reusable launch vehicles (RLVs) is absolutely imperative mainly due to the fact that they can bring down the launch cost by an order of magnitude as compared to that of expendable vehicles. Additionally, RLVs are important as they (i) improve mission success probability, (ii) enable in-orbit servicing of space systems, retrieval of payloads for refurbishment and reuse, and re-fuelling of satellites, (iii) facilitate setting up of manufacturing bases for advanced materials and medicines in micro-gravity environment, and (iv) reduce launch preparation time. Design and realization of a RLV are governed largely by operational limits of available high temperature materials.

Material sensitive architecture of RLVs poses formidable challenges with respect to high temperature materials as they are expected to fulfill a combination of conflicting requirements to meet severe environmental conditions and mission demands. Concentrated efforts are made to indigenously develop these high temperature materials and Thermal Protection Systems (TPSs), their processing technologies and productionize them on industrial level for operational phase of RLVs.

Thermal Protection Systems (TPSs)

Thermal protection of the reusablelaunch vehicle (RLV) during its atmospheric reentry is the most critical phase of the whole mission. Thermal Protection System (TPS) occupies about-fifth of the total weight of a reentry type of space vehicle. Various external contours of an RLV experience different levels of heat flux during atmospheric reentry. Design of TPS is evolved considering mainly severity of the heat flux to which various parts of a RLV are exposed.

TPS for medium heat-flux conditions

Silica Tiles are used to thermally protect those regions of a Reusable Launch Vehicle (RLV) which experience medium heat-flux conditions (temperatures around 1400 ^{0}C) during atmospheric reentry phase. They should be of light weight, able to withstand maximum acoustic loads of 145 dB, aerodynamic pressures upto 140 Pa and have a life span of minimum 100 flights. A Silica based thermally insulating system with oxide structure and low coefficient of thermal expansion (CTE) has excellent thermal shock and oxidation resistance.

Process technology evolved and established for Silica Tiles was based on Silica sol-gel approach. Vacuum moulded Silica performs were impregnated with Silica sol-gel. Subsequent to hydrolysis, they were sintered to yield the silica billets with the density of only 0.30 g/cc. They contained fibrespredominated by the matrix phase. Sintering parameters were optimized to obtain amorphous structure with very low CTE. The upper surfaces of the tiles were coated with special high emissivity coatings which ensured the re-radiation of majority of the thermal loads falling on the RLV during highly hostile atmospheric reentry conditions.

[1]Propellants, Polymers, Chemicals & Materials Entity Vikram Sarabhai Space Centre, Trivandrum 695022

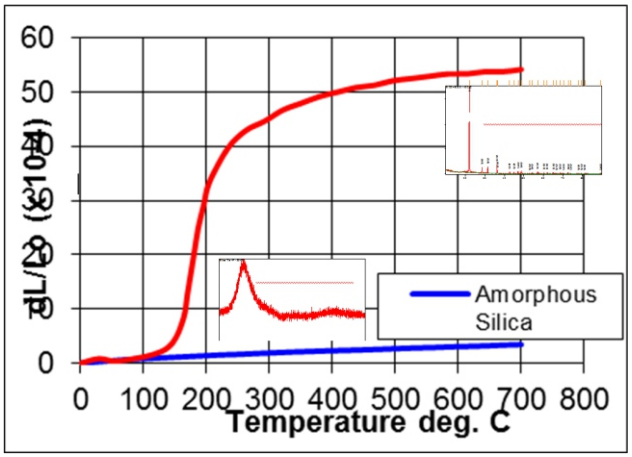

Thermal expansion characteristics of amorphous and crystalline Silica structures

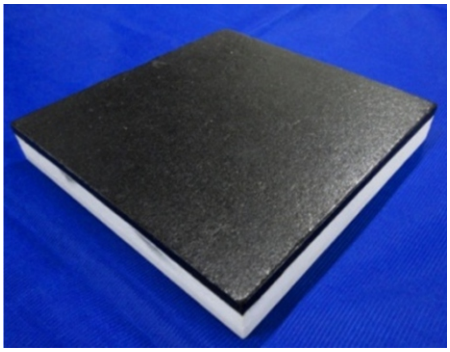

Silica tile with high emissivity coating

The Silica Tiles were successfully tested for their thermal response under Kinetic Heat Flux conditions and thermal shock resistance under an atmosphere wherein oxy-hydrogen gas mix was used to get the required temperatures. Temperature and acoustic emission data in real time were acquired. Samples were stable upto 1400^{0}C. They were also subjected to plasma wind tunnel test at CIRA, Italy and acoustic test at an internal facility in ISRO.

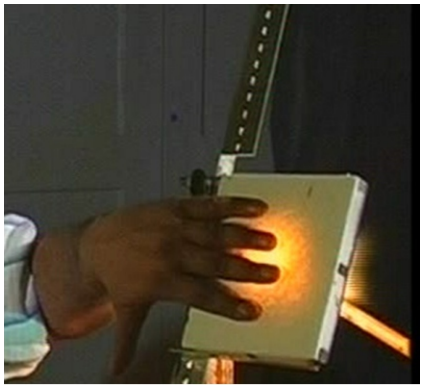

Thermal Shock Test on Silica Tile

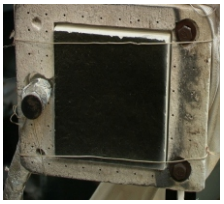

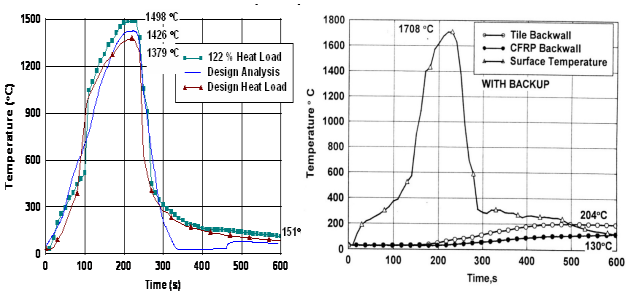

Thermal response of Silica tile showing temperature at various depth of the tile

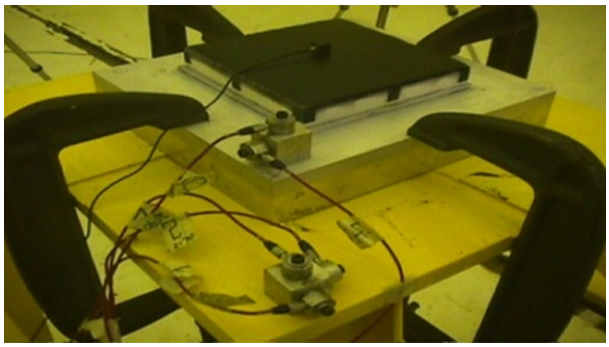

Silica tile under Acoustic test

Having validated the Silica Tile process technology for Space Capsule Recovery Experiment (SRE) which incorporated around 250 of these tiles, the process innovation for the tile was further evolved for RLV-TD. The next generation of Silica tiles has superior mechanical properties and better machinability characteristics. These characteristics were called for to meet the performance-critical requirement of complex geometrical contours of RLV-TD. More than 450 tiles have been integrated with windward surfaces of the RLV-TD.

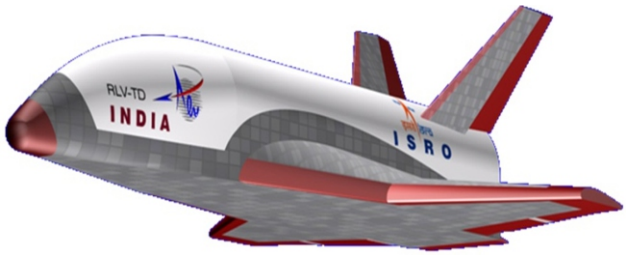

Silica tiles of different contours for Windward Regions of RLV-TD

The Silica tiles signify the "LAB to LUANCH" success highlighting upgradation of a LAB scale process technology to the LUANCH pad and ultimately accomplishing their to and fro journey through the realms of infinite space.

TPS for high heat-flux conditions

Owing to its excellent thermal shock resistance, a carbon based structure remains the first choice for the high heat-flux regions namely nose-cone and other leading edges of the RLV. However, currently used reinforced carbon composite (RCC), has two areas which call for further improvement : (i) its density of about 2.0 g/cc imposes penalty for space application, and (ii) its good thermal conductivity makes it a poor heat insulator material for TPS application.

A foamed carbon addresses to both these issues. It is a porous structure with very low levels of density. Porosity, while imparts excellent thermal insulation characteristics, struts or ligaments of the foam, by virtue of being made of carbon, impart very good thermal shock resistance to the foams.

Process route successfully established for synthesizing carbon foams is based on the use of a sacrificial substrate or thermo-degradable polymeric scaffolding which is impregnated by polymeric resin.For synthesizing C-foams of varying morphological features and density, sacrificial substrate of different pore-sizes and resin of various concentrations were employed. Minimum density of 0.041 g/cc and maximum density of 0.210 g/cc are achieved with the following two combinations of resin-concentration and cell-size: 10%-30PPI and 90%-80PPI respectively.

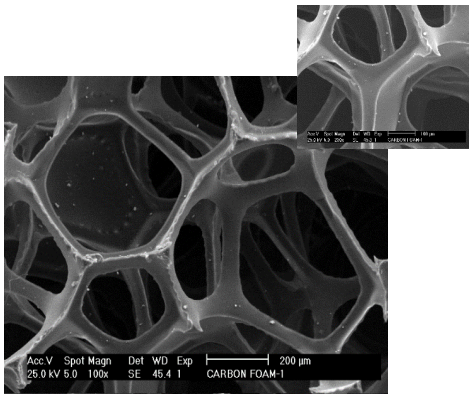

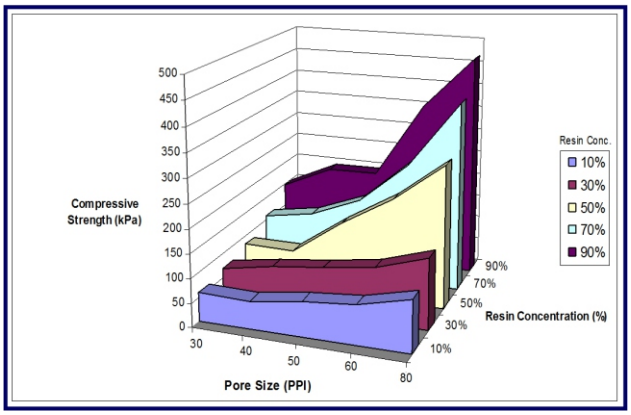

Cell morphology of the reticulated foam structure made of a 3-D network of struts and variation in the foam density with cell-size of substrate foam and concentration of the resin

Foams were subjected to high temperatures to realize graphitic structure and High Resolution Transmission Electron Microscopy (HRTEM) was conducted mainly to study the effect of thermal treatments on the crystallinity in carbon structure. Fourier Transform Infrared (FTIR) spectroscopy was performed to evaluate the effectiveness of various processing operations in realizing a carbon based foam-structure. Effectiveness of the process used to synthesize the carbon foam was validated by TGA results which showed carbon yield of more than 95% after graphitization treatment. These results of carbon yield as were further corroborated by the Fourier Transform Infrared (FTIR) spectroscopy.

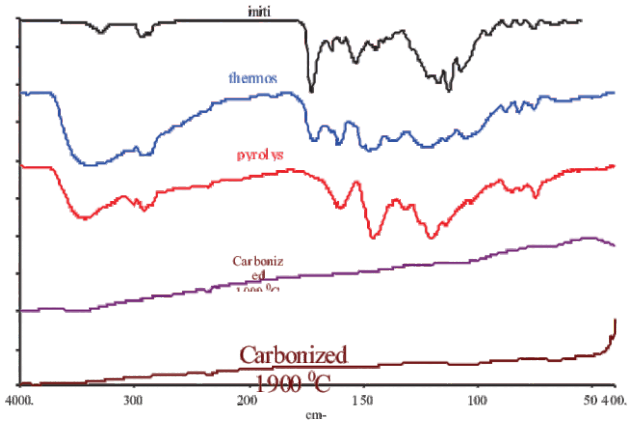

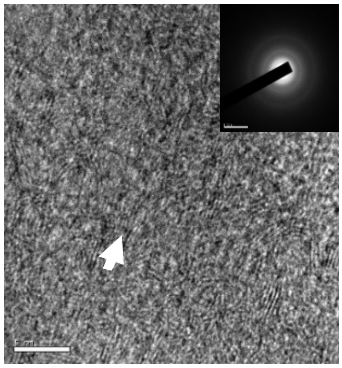

IR spectrum for carbon foam samples under various stages of processing and HRTEM - LF Image alongwith microdiffraction pattern of graphitized foam sample

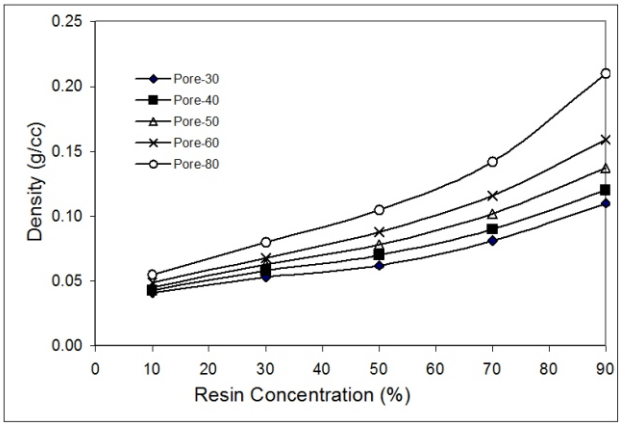

Variation in compressive strength of C foam with pore size and resin concentration

200x200x20 mm C foam of 30 PPI

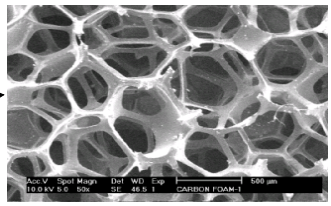

Cell morphology of the reticulated foam structure

Computational thermal response of carbon foams under the stipulated heat flux conditions was estimated using Fourier Heat Conduction expression. To validate the above computational thermal response analysis of carbon foams, Kinetic Heating Simulation (KHS) test was conducted on foam TPS panels.During KHS test, 17.5 mm thick carbon foam TPS panel records maximum back-wall temperatures as 226.7, 258.5 and 251.1 ^{0}C at three locations which are in close proximity with the predicted temperature and meet the TPS requirement for RLV.

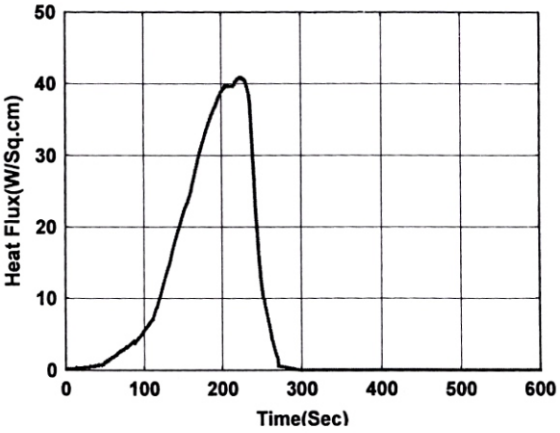

Computational thermal response of carbon foam

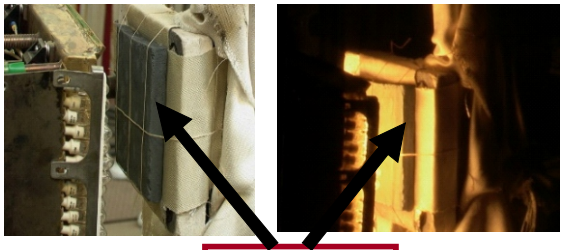

Validation of C foam tile under Kinetic Heat Flux Test

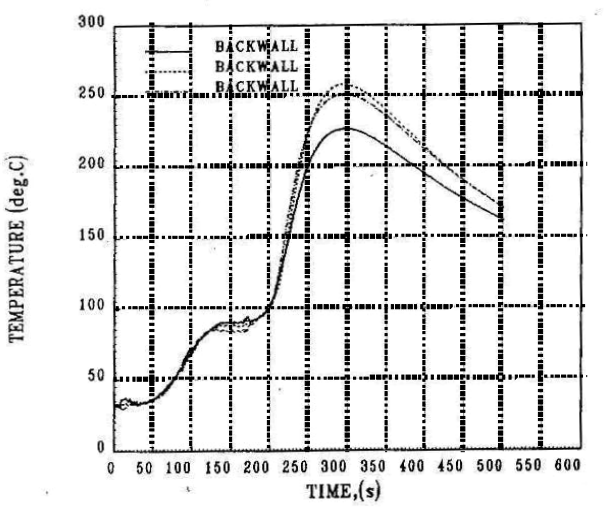

Back-wall temperatures on three locations of C foam tile under Kinetic Heat Flux Test

Ultra High Temperature Ceramics

RLV based future concepts such as 'Two Stage To Orbit (TSTO)' and 'Single Stage TO Orbit (SSTO)' offer tremendous promise to enormously reduce the cost of space transportation. TSTO and SSTO launch vehicles will employ sharp leading edges mainly to reduce the aerodynamic drag during hypersonic atmospheric re-entry. Consequently, these edges will experience extremely high heat fluxes. Zirconium diboride based Ultra High Temperature Ceramics (UHTCs) can be used up to temperature as high as 2500°C and therefore they are potential candidate materials for TSTO and SSTO missions. Using Powder Metallurgy approach, process-parameters for ZrB_2 have been optimized and leading edge structures with the geometrical shape as Pylon were successfully tested under very high enthalpy conditions.

Development of process technology for ZrB_2 based UHTC adopted Powder Metallurgy route.$MoSi_2$ and SiC powders were incorporated in the ZrB_2matrix mainly to enhance the sinterability of the composite. Process-parameters for ZrB_2were optimized in terms of pressure-temperature-time cycle.

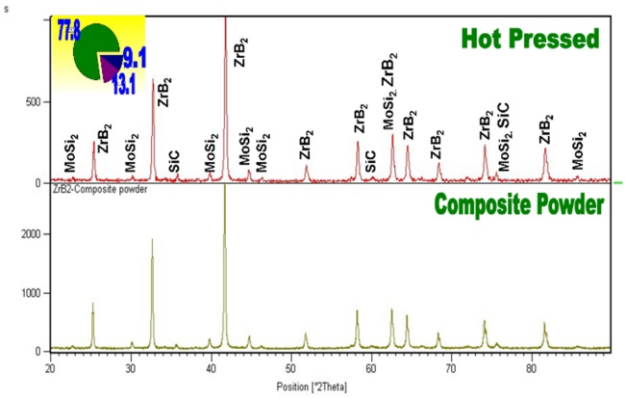

Phase analysis of ZrB_2Composite

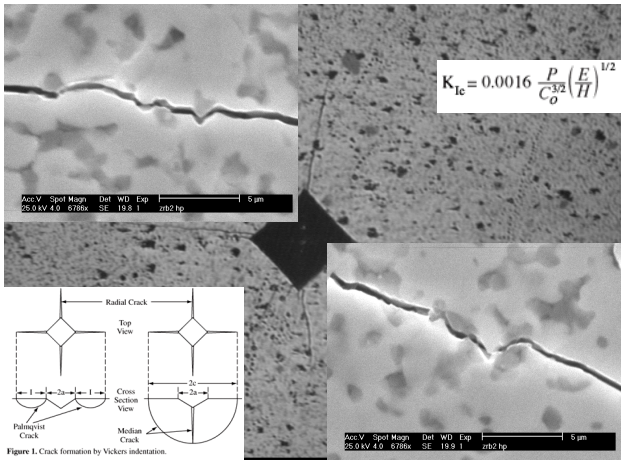

Transgrannular propogation of Crack in ZrB_2 Composite

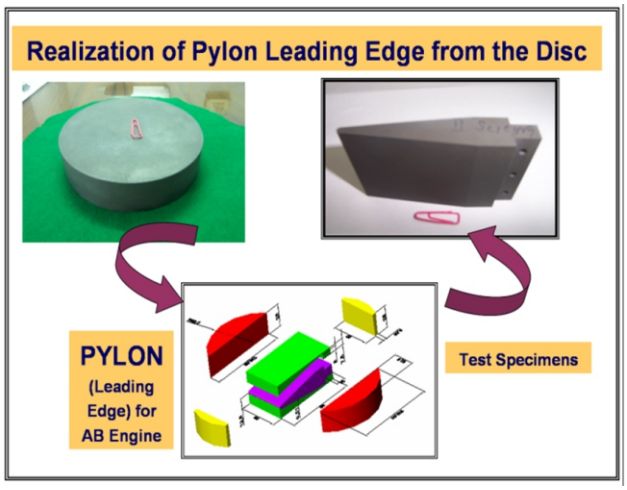

Hot pressed block of ZrB_2 Compositeandplan for realization of components and test-specimens from the block

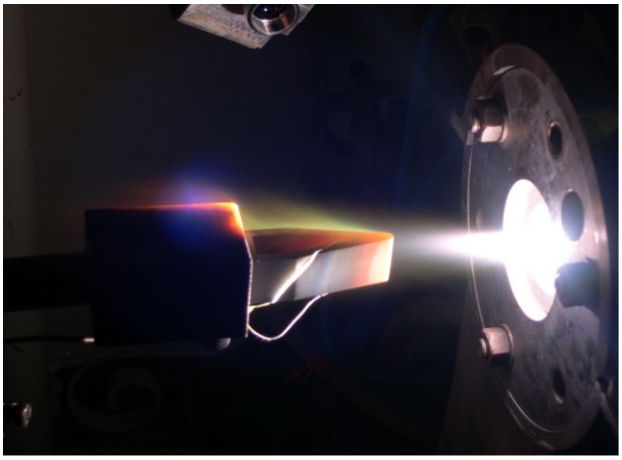

High Enthalpy test on ZrB_2 base composite

Randomly Oriented C/C Composite and C/SiC Composite

Carbon/carbon (C/C) composites are known for their fascinating high temperature properties (e.g., high thermal-shock resistance, low density, high thermal conductivity, etc.) Process technology was evolved for a 'randomly oriented, hybrid carbon-fiber-reinforced, mesophase-pitch-derived, carbon-matrix C/C' composite. Process variables and parameters were mainly focused at tailoring the hot-pressedproperties of the composite using various combinations of short carbon fibers, partial hot-pressing-assisted carbonization under low heat, and complete carbonization under higher heat.Process yielded good enhancement in density and mechanical properties of the compacted and densified samples.

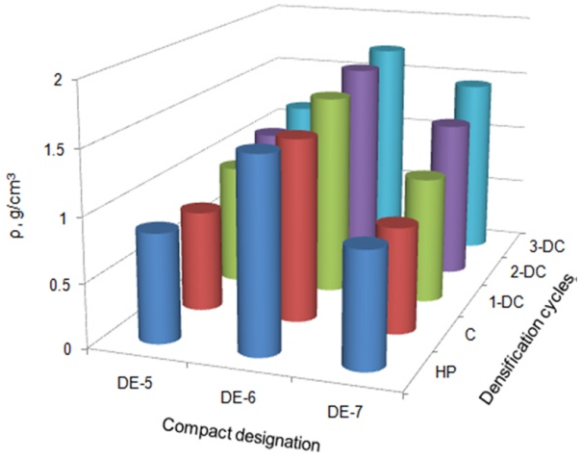

Density of compacts hot-pressed at various reinforcement wt% and SEM images of compacts after hot pressing and carbonization

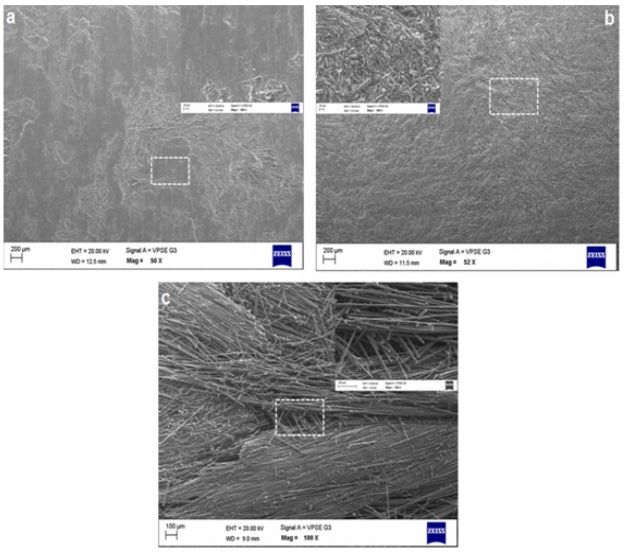

Scanning electron micrographs showing morphology of the orientation of fibres

Carbon/silicon carbide (C/SiC) composites have evoked considerable interest for applications in a wide temperature range due to their excellent properties at elevated temperature such as strength, stiffness, oxidation resistance, lowdensity, creep resistance, chemical stability, and low wear.For the effective processing of the C/SiC composites, the agglomeration-free distribution of Carbon Fibres (CFs) in the SiC matrix plays a key role in interphase bonding, crack propagation, mode of failure, etc. A methodology involving the exfoliation of CFs and their dispersion in SiC powder matrix without any dispersing agent was established and demonstrated successfully. The probable mechanism behind the rapid and effective dispersion of CFs, resulting from the inclusion of an exfoliation step in the method was also explained.

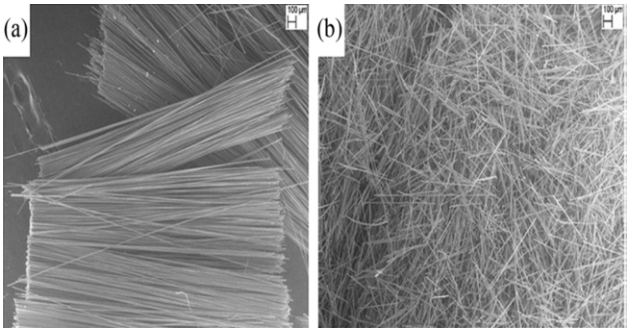

Scanning electron microscope micrographs of, (a) un-exfoliated carbon fiber tows (b) exfoliated carbon fibers

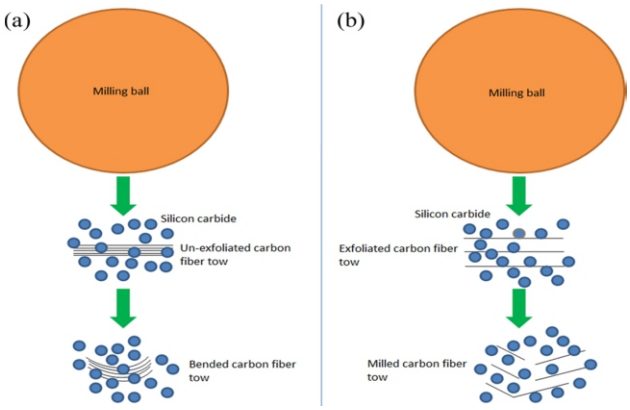

Conceptual models of interaction of milling ball with carbon fibers and silicon carbide powder for, (a) un-exfoliated carbon fiber tow, (b) exfoliated carbon fiber tow.

Silica Aerogel

With extremely low density and low thermal conductivity, silica aerogels find a range of important applications in space programmes. They have already been used for thermal insulation in interplanetary spacecrafts and comet dust collector.

Processing technology for silica aerogel was developed using two-step sol-gel synthesis. After preparation of the Sol and gelation on the bath, chemically modified Gel was super critically dried under optimum conditions of pressure and temperature. Achieved tap density of the Aerogel is in the range of 0.07-0.1 g/cm^3. BET specific surface area is 570 m^2/g obtained by N_2-sorption technique. Porosity of 96% is achieved for a mean tap density of 0.1 g/cm^3. Pore volume & pore size were calculated to be 6 cm^3/g and 30-50 nm respectively. This establishes the material as 'mesoporous'. Refractive index was calculated and found to be 1.0152 which is close to that of air. The contact angle measurement of a water droplet on the aerogel surface revealed itshydrophobicity (contact angle of 145°).

Granular Silica aerogels

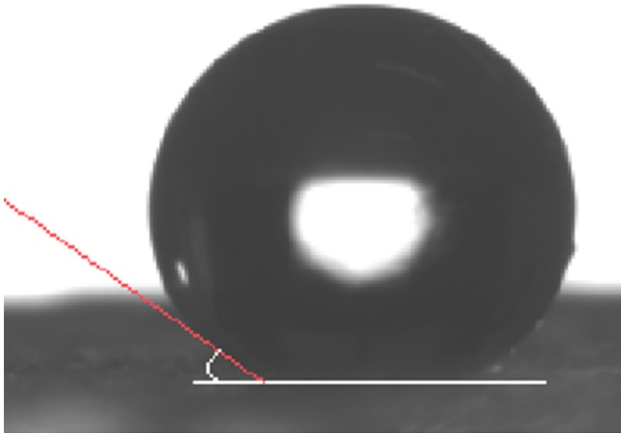

Aerogel showing a contact angel of 145^0

SiC Coating

Process technology for SiC coating was developed mainly to provide high temperature oxidation protection to carbon/carbon (C/C) based structures for high heat flux regions of RLV. Preceramic precursor route was evolved for the coating process. Various parameters for slurry preparation, application method, curing and sintering temperature and duration etc. were optimized at lab-scale first. After a series of qualification tests, the coating technology was applied to actual flight hardware which also underwent various tests by simulating the structural and high temperature conditions.

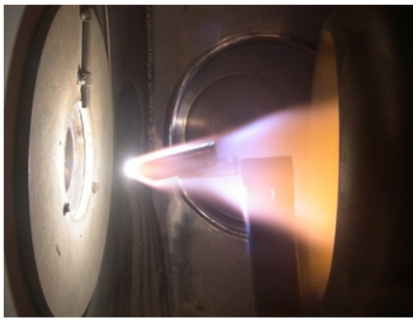

During the test

After the test

SiC coated C/C sample undergoing Arc Jet test

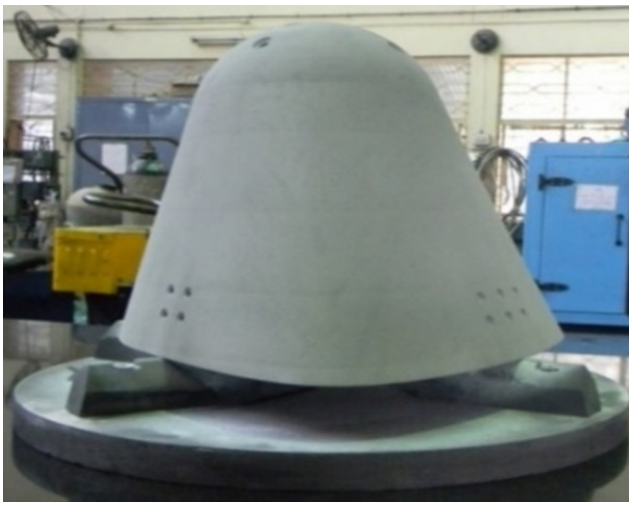

SiC Coated C/C Nose Cap

Conclusions

- Reusable launch vehicle (RLV) technology is essentially required for bringing cost effectiveness in space based services for the common man. High temperature materials play a very important role in RLV technology.

- For ISRO's RLV programme, a variety of high temperature materials have been developed and successfully inducted into the programme.

- For medium heat flux regions of RLV, Thermal Protection System (TPS) based on silica tiles was developed. These tiles were first successfully flight-proven through Space capsule Recovery Experiment (SRE) and subsequently they demonstrated their capability during flight of RLV-Technology Demonstrator (RLV-TD).

- To meet the requirement of large number of silica tiles, process-technology for tiles was scaled-up through industry.

- Special coating technologies were also developed for these high temperature applications. They include high emissivity coatings, high temperature oxidation resistance coatings etc.

- Ultra-light carbon-foam based TPS is developed for the high heat flux regions of RLV. The foam TPS has successfully undergone various high temperature tests.

- Technology development programme is in progress for Zirconium Diboride (ZrB_2) based composites for hypersonic RLVs such as Two-stage-to-orbit (TSTO) and Single-stage-to-orbit (SSTO) missions.

- Process-technology is also developed for the carbon/silicon carbide (C/SiC) composite and silica aerogel for high temperature application in Indian space programme.

Acknowledgement

The author wishesto acknowledge the untiring efforts of his colleagues in Materials and Mechanical Entity and Propellants, Polymers, Chemicals and Materials Entity ofVikram Sarabhai Space Centre, who, as a team, made the development programme for high temperature materials a success.

Annals of the Indian National Academy of Engineering
Vol. XV, April 2018

Designing Robust Software : From Theory to Practice

Sriram K. Rajamani[1]

Abstract Designing robust software is a difficult endeavor. Unlike other engineering endeavors such as designing bridges, buildings or motors, we understand less about what it takes to design software in a reliable and robust manner. In this paper, we give a perspective on this topic, influenced by what we have learned over the years working on this topic.

Keywords: software quality, static analysis, runtime analysis, software design

1. Malleability and Quality

Unlike bridges or buildings, software is malleable. Software is easy to change, and hence it is tempting to start with a rough design, and evolve it iteratively as requirements evolve. To ensure robustness, experience has shown the need to complement such iterative design with validation efforts to ensure that quality metrics are met. Quality metrics range from robustness, security, and acceptable performance. Several methods such as testing, static analysis, runtime instrumentation, runtime monitoring, and code generation can be used to ensure high quality. Practitioners in the industry use pragmatic techniques such as testing, whereas academics investigate static analysis based on formal methods (such as formal verification), which promise more robustness, but are hard to apply to real-world software. In this article, we describe our efforts in bridging the gap between theory and practice, and point to directions for future work.

2. Static Analysis and Testing

When we test a program, we observe its behavior on some executions to increase our confidence in its quality. While testing can prove presence of defects, it cannot prove their absence [1]. Static analysis refers to a class of techniques which analyze a program during compilation, without running the program. Such analyses tend to analyze all behaviors of a program and hence have the potential to establish absence of certain kinds of defects. However, sophisticated static analysis techniques, such as formal verification, are costly in terms of time and effort. In our experience, validation techniques to ensure high software quality involve three aspects: (1) automation, (2) scale and (3) depth of the property being validated. All approaches we know of, fare well in one or two of these three aspects, and not all three. For example, type systems enjoy automation and scale, but check only weak properties of the software such as type and memory safety. Deductive verification with preconditions and postconditions can verify deep properties, but at the expense of either scale or automation. To perform deductive verification of large programs, manual annotations in terms of invariants are needed. In our work, we have made several attempts to explore these tradeoffs. We designed the SLAM software model checker [2] which demonstrated that automated verification of interface properties was possible on low-level software. Static Driver Verifier, which is a product built with the SLAM engine (and now uses more advanced verification engines) has been evolving and shipping with every release of Windows for more than a decade now. We have also explored combining testing and verification using the Yogi analysis engine [3].

Runtime instrumentation is another way to combine static and static and dynamic analysis. In

[1]Managing Director, Microsoft Research Bangalore

this approach, the compiler generates runtime checks to ensure that specific properties (such as memory safety) are satisfied. Then, static analysis is used to eliminate as many of these checks as possible (by constructing proofs that such tests will never fail). In addition, we can also show that in the presence of these runtime checks (by assuming that these runtime checks pass), higher level properties, such as protocol adherence, can be formally verified [4].
More generally, combination of techniques such as testing, formal methods, type systems, static analysis, model checking are needed to ensure software quality [9].

3. Modeling and Code Generation
Static and dynamic analysis are best used for existing code written in existing programming languages. When there is opportunity to work with early stages of a software project, there is more scope to work in design-level tools to reason about the software at a higher level of abstraction. Often, design-level representations (also called "models") are easier to analyze since they are less detailed than code. Such opportunities can be exploited when possible.

For new code, we can attempt writing models of the code at higher levels of abstraction, perform analysis at the level of models to ensure robustness and quality, and then use compilers to generate code. We have successfully demonstrated this approach for writing asynchronous code using the P language [5]. In general, coming up with domain specific languages and compilers to guarantee specific class of properties of programs is a promising and pragmatic approach to improve software quality, though the approach has limitations in terms of generality.

4. Security and Privacy
In the age of the internet and cloud, security and privacy have become important aspects of software quality assurance. Since data is increasingly becoming the fuel of the internet economy, it is important to be able to state policies about use of data, and quality tools to enforce conformance of the policies at the implementation level. Formal approaches to state and check such data use policies are fundamental to protecting data privacy [6]. Also, as we put customer data in the cloud, there is a great need to provide customers of cloud computing complete control over their data: no one should be able to access the data without the customer's permission. Even if there are malicious employees in the cloud service provider, or hackers break into the data center, they still should not be able to get access to customer data. A robust solution to cloud security requires re-thinking the software stack, ranging from new kinds of hardware (such as Intel SGX), and new kinds of software architectures, and new kinds of validation tools [7].

5. Artificial Intelligence and Machine Learning
Modern software is undergoing dramatic changes because of improvements in artificial intelligence and machine learning. Tools and techniques for software quality need to be dramatically changed to account for pervasive use of machine learning. Unlike manually written software, where a programmer writes code, machine learning enables machines to learn models based on scenarios (usually provided as a list if input-output examples) and use these models to perform predictions. Quality of software which uses such learned models is a difficult problem, specifically if we want to provide guarantees about the software's behavior. In most cases, the behavior of learned models to new (our unseen, so far) inputs is hard to predict. Also, understanding the software development life cycle for machine learning is still in its infancy. When a machine learned model produces incorrect results, errors can be in the training data, model parameters or in the training algorithm itself. We have made some initial attempts in designing debugging tools for machine learning [8], but the area is relatively new, and has a lot of room for future work.

6. Summary
In summary, software quality continues to be a practical problem and intellectual challenge which requires continued research. In addition to quality requirements on functionality, new

requirements such as security and privacy are placing more demands on quality assurance. Contemporary trends such as machine learning require radically new tools to support the entire software development life cycle. Hence, software quality will continue to be an active and productive research area in the years to come.

7. Acknowledgment

We thank our collaborators, for contributions to our joint work, and for being sources of inspiration and learning over the years.

8. References

1. Edsger W. Dijkstra: The Humble Programmer, ACM Turing Lecture, 1972 (also available as EWD340)

2. Thomas Ball, Vladimir Levin, Sriram K. Rajamani: A decade of software model checking with SLAM, Commun. ACM 54(7): 68-76 (2011)

3. Nels E. Beckman, Aditya V. Nori, Sriram K. Rajamani, Robert J. Simmons, SaiDeep Tetali, Aditya V. Thakur: Proofs from Tests. IEEE Trans. Software Eng. 36(4): 495-508 (2010)

4. Madhu Gopinathan, Sriram K. Rajamani: Enforcing object protocols by combining static and runtime analysis. OOPSLA 2008: 245-260

5. Ankush Desai, Vivek Gupta, Ethan K. Jackson, Shaz Qadeer, Sriram K. Rajamani, Damien Zufferey: P: safe asynchronous event-driven programming. PLDI 2013: 321-332

6. Shayak Sen, Saikat Guha, Anupam Datta, Sriram K. Rajamani, Janice Y. Tsai, Jeannette M. Wing: Bootstrapping Privacy Compliance in Big Data Systems. IEEE Symposium on Security and Privacy 2014: 327-342

7. Rohit Sinha, Manuel Costa, Akash Lal, Nuno P. Lopes, Sriram K. Rajamani, Sanjit A. Seshia, Kapil Vaswani: A design and verification methodology for secure isolated regions. PLDI 2016: 665-681

8. Aleksandar Chakarov, Aditya V. Nori, Sriram K. Rajamani, Shayak Sen, Deepak Vijaykeerthy : Debugging Machine Learning Tasks. CoRR abs/1603.07292 (2016)

9. James R. Larus, Thomas Ball, Manuvir Das, Robert DeLine, Manuel Fähndrich, Jonathan D. Pincus, Sriram K. Rajamani, Ramanathan Venkatapathy, Righting Software. IEEE Software 21(3): 92-100 (2004)

Annals of the Indian National Academy of Engineering
Vol. XV, April 2018

Growth of Indigenous Defence industrial Base Through Multi-disciplinary Technology Development & Policy Enablers

Jayant Damodar Patil[1]

Abstract This paper brings out the changing contours of Defence Industry in India and highlights the efforts put in by the author in shaping the policy landscape for the Defence & Aerospace sector with an intent to encourage indigenization. The paper also chronicles the unique achievements in development of a basket of multi-disciplinary products and technologies leading to the realization of over a hundred systems in three decades for the author's organization.

Keywords: Defence Policy, Indigenization, Multi-Disciplinary Technology Development, Stabilization, Under-water Platform, Launcher, RF

1 Background

Historically, Defence Procurement in India has primarily stayed either with the Government owned sector or through direct imports through the Government-to-Government (G-G)/ Foreign Military Sales(FMS) route.

Over decades, post-Independence, India's Defence needs banked on Manufacturing ToT and saw growing import content in our National security preparedness due to failure of not being able to stay in tune with advancement of technology. Technologies in Defence sector being strategic in nature, are associated with control and denial regimes in respect of flow of defence technologies from one country to another.

As a recommendation of the post Kargil review committee, Defence manufacturing was opened up for participation by the Indian Private Industry in May 2001. On the Policy front, Government permitted unrestricted entry of Private Sector (including FDI) subject to licensing. The intent towards encouraging indigenization has been addressed through the Defence Procurement Procedures released over the years from 2005 onwards.

As the economy has moved towards a more liberalized form over the years,the author's Company, L&T,undertook a journey of building critical weapons & sensor systems in a period spanning about three decades, and realized over hundred indigenous defence equipment and systems both through in-house R&D efforts and in partnership with DRDO.

The road to inter-disciplinary system development, required industry to master elemental technologies such as DC servo-drives, servo-hydraulics, RF and Digital Signal Processing, under-water platform hull manufacturing, structural optimizations, and controls. The basket of technologies and new products thus developed have built an enviable track record in Defence Systems for L&T.

2 Policy Changes

The Indian government having recognized the importance of Manufacturing sector in boosting GDP growth, is pushing hard through its Make in India campaign to promote indigenous production and place the country on the world map as a leading manufacturing destination. This initiative has the potential to realize India's ambitious plans to grow manufacturing sector from the current 17% of GDP to 25% over the next decade by harnessing mainly the energies of the country's youth. However, no

[1]Sr. Vice President & head, Defence & Aeraspace Business and Member of the Board L&T Heavy Engineering and L&T SHip Building, Larsen & Turbo Ltd., Mumbai

country can aspire to achieve regional supremacy by remaining dependent for majority of its defence & security needs. Thus a concurrent push to 'Design in India' and 'Digital India'needs to be at the core of our policy making and implementation of “Make in India”. Theseare critical policy initiatives to enable indigenous design, engineering, development and manufacture of one's own defence requirements.

With planned Defence Capital Acquisitions to the tune of INR 14-16 lakh crore over the next decade and a vision to enhance defence indigenization from current levels of 35-40% to 70-75%, this sector alone can contribute an additional ~40 Lakh Cr or 1.7-1.8% to India's GDP over the next ten years with economy growing at 8-10% YoY (considering the multiplier effect across tierised value chain that one expects from defence manufacturing).

India's Defence Sector is a monopsony. The Country's defence procurement historically depended primarily on G-to-G relationships and consequently theMinistry of Defence (MoD) chose to create and trust only Government owned companies as production agencies. The ownership syndrome in MoD also maneuvered production of indigenously developed defence products (by DRDO and industry partners) to DPSUs and other government owned entities with mixed success. In case of complex systems the DPSUs remained as prime contractors, supported by Private players as development partners to DRDO. This model with implicit handling and margin at the hands of prime contractors yielded poor financial efficacy. Post opening up of the sector in 2001, the private sector majors and development partners to DRDO evolved into system integrators and competitively positioned themselves to design, develop and manufacture complex platforms like Submarines, Warships, Radars, Artillery Guns, Armoured Systems, etc.

Globally, governments control export of defence technologies, being strategic by nature, and hold the Intellectual Property (IP) rights as well (through Govt. funding); and companies are not at liberty to part with them, at will. Having made large investments over several decades, sovereign nations do not share critical technologies, without commensurate benefits and controls having geo-political implications leading to control / denial regimes. G-G relationships, thus play a decisive role in making available requisite level of technology, mandate IP control framework and demand appropriate FDI limits.

Multiple expert committees like Kelkar committee, Ramarao Committee, Sisodia (IDSA) committee, Naresh Chandra Committee, Ravinder Gupta committee, articulated structural changes in MoD / MoD Wings / DRDO, Creation of Cadre for Acquisition, Indigenization, Recognition of Centers of Excellence and need for long term investments towards creating Indigenous Product Capability. The author has represented his Company, led Industry forums and been invited on Government Panels to steer and define these Policy initiatives.

Concurrent policy innovations include ease of licensing, increasing license tenure, Export Guidelines and On Line Approval processes, new offset guidelines, new “Make” procedure, and addressing level playing field for all players. A new category, IDDM has been introduced for Indigenously Designed Developed and Manufactured Products with highest priority in the Procurement categorization hierarchy.

It was with this backdrop, that the Dhirendra Singh Committee recommended a Strategic Partnership model for MoD and Private sector as an imperative to cut imports, implement Make-in-India and create system integrators in addition to already established DPSUs. This would transform India's defence production from hitherto being 'import dependent' to it being a 'foreign-exchange neutral' one, create jobs, build competition and help stretch the budgets to acquire higher capabilities through force multipliers. The recommendations of the

Expert committee were accepted by the MoD and Hon Raksha Mantri entrusted the responsibility to formulate a rational, fair, scientific and transparent process for selection of Strategic Partners, including criteria for prequalification and then final qualification, to a task force under the chairmanship of Dr V K Aatre, ex Secretary R&D and Head of DRDO. This composite committee comprised best minds in the Industry across sectors including Defence (Services and Acquisition), R&D, Finance and Law.The task force submitted its report in April '16 and proposed a comprehensive three-step process.

The MoD leadership then decided to consult the industry in an open forum. Thus, five sub-groups were constituted by MoD with clear terms of reference, and chaired by representatives of Apex Industry Chambers, with representatives from MoD, select members of earlier Expert committees, Service HQs, DRDO, and Industry for focussed discussions to harness the "practitioners" views on the selection process, measurement criteria and covenants, in the context of specific segments and suggest required changes. The author was Chairman of the sub-group on Submarines. The five sub-groups hailed the idea of SP and the objective to select the best, technically competent, financially capable, and reliable long term strategic partner. The innovation of "Identifying & supporting Strategic Partners for complex system integration platform programs" marks a new beginning towards recognizing the capabilities and strengths of Private Sector, and their inclusive participation in Defence sector.

Aided by these policy reforms, the Indian Defence Industry is maturing by the day. Under the new policy regime, we see programs being categorized under 'Buy Indian' signaling that we are no longer fully dependent on any external agency for the core of our products. There are also increasing number of programs under 'Buy & Make (Indian)' category, indicating preference to trust Indian companies over Foreign OEMs, with a mandate of >50% indigenous content. Also visible are the increasing number of local industry players competing for Buy Global contracts putting them shoulder to shoulder with international players. Although this has to scale up in a big way, Industry confidence would be further buoyed through active support of MoD by conclusion of development contracts under the "Make" Programs and initiating acquisition under the Indigenously Designed, Developed and Manufactured (IDDM) category.

Towards efforts in Policy Reform, the author has attained the distinction of being an Industry Veteran and Expert and was included in the core group of FICCI Defence Division for advise on the various positions taken by FICCI wrt MoD besides being an invitee to numerous Think Tanks and special interactive sessions at IDSA, Vivekananda Foundation (VIF), Centre for Joint Warfare Studies (CENJOWS), Observer Research Foundation (ORF), Pahle India etc.

The author was specially invited to join the Prof Rama Rao Committee for restructuring of DRDO 2007-08 and was a Member of the DATE / NRI (Decision Aid for Technology Evaluation / National Resource Index) committee for Structural Engineering leading to TRL classification.

The author has also been Member of Numerous Review committees for range of DRDO projects across Weapon Systems and Engineering Systems Programs including PRC's, ATPs, FRRs, LAB, PFR.

In the Aerospace sector, the author was a Member of 12th Plan Review Committees for MoD & Dept. of Space and a Member, CIT, PSLV Privatization, ISRO. The author's Company has been involved in the Aerospace Sector as ISRO's manufacturing partner industry for serial production of solid rocket motors besides a host of other hardware such as payload heat shields, solar array deployment devices, tankages and in the productionisation of the PSLV hardware since the mid 80's.On account of his specialization in Industrial R&D, the author has represented ISRO in a Failure Analysis Committee for Launch Pad 1 wheels and a Committee headed by Prof Rama

Rao for feasibility of realisation of Solid rocket motors by Flow Forming.

Besides these, the author has been Member of National Defence Executive Committees of FICCI, CII and ASSOCHAM, Chairman of FICCI Defence R&D Committee and Chairman of CII Defence Shipbuilding & Marine Committee.

2.1 Incentive model for Higher Indigenization in Defence

Today, none of the Indian Defence companies feature in the Top 2500 Global List of R&D spenders. The private sector accounts for roughly 35% of India's total R&D spending. In order to ensure Defence indigenization, every Indian company needs to be encouraged to innovate and keep pace with technology. The author has led the development of a strong industrial R&D Center in his Company with focus on many elemental technologies to facilitate the path for new product development backed by investments in Manufacturing Technologies driving 'Make in India' and boosting Defence Manufacturing.

Having brought about a slew of important policy reforms in the last three years, the Govt. has sown the seeds for a strong defence economy to concurrently facilitate enhanced participation of the Private Sector as well as nurture and support the Government owned entities. All it needs to do is take a few more bold steps, speed up decision making, delayer approval stages, and eliminate repetitive process steps to unleash and actively promote indigenization. It is an imperative that the Make-in-India for defence is a journey that, with time, will evolve into Make-forIndia, and later lead to Made-in-India.

Increasing indigenization in Defence Manufacturing has always been an important mandate of the Defence Procurement Procedure (DPP). This assumes even bigger significance under 'Make in India' where the focus needs to be on doing the critical value add in India and not just delivering from within the country. While DPP 2016 has addressed this partially by increasing the floor level for Indigenous content from 30% to 40%, it is important to incentivize the Industry for achieving indigenous content substantially higher than the specified minimum in the form of price preference and purchase preference. This incentive will drive the industries to compete in achieving higher and higher indigenization. While Purchase preference is to promote higher indigenous content and job creation in India, the price preference is for promoting higher Tax revenue collection through tierised value chains on increased quantum of indigenous content and the multiplier effect thereof, besides higher GDP creation. One of the ways of achieving this is to provide an incentive of upto a maximum of 10% be paid to the Industry for achieving substantially higher indigenous content over the minimum specified for the procurement category.

For e.g. in case of Buy (Indian) where the minimum stipulated Indigenous content is 40%, achieving higher indigenous content may be incentivized through accelerated benefit in slabs of 20%, as below:

48 to 56% - 1%
56 to 64% - 2.5%
64 to 72% - 5%
72 to 80% - 8%
Above 80% - 10%

It is noteworthy that the purchase preference has been institutionalized by Department of Defence Production in select acquisition cases involving DPSUs. This is provided for higher indigenous content beyond 20% as long as the L2 with higher indigenous content matches the L1 price. The urgent need is for institutionalizing the same in the MoD acquisition process and provide graded price preference to enhanced indigenization and promote Make-in-India.

3 Multi-Disciplinary Technology Development

The Defence sector epitomizes capability building that is driven by technology to gain

asymmetric advantage through capability investments in the form of force multipliers. Technology leadership, self-reliance (in-house development) in technologies and investments in building tech-savvy human resources greatly mitigates project technical risks. This also enables us address obsolescence risks, build sustenance and insulate us from the vagaries of monopolistic pricing by external technology providers and help build competitiveness and gain operational efficiency. Strong foundation of our Defence sector was built on in-house technology development as a differentiator and risk mitigator. L&T has built a bouquet of home-grown technologies which have enabled us to successfully build products and solutions with innovation to maneuver the technology risks inherent across our business portfolio. Also these technologies have been leveraged and deployed across projects and user domains to reduce our exposure to foreign technology collaborators as well as enabled us to seek any required technology support at our terms in niche domains thus leveraging evolving policy that is getting Indian Industry centric. Some of the key technology elements across disciplines developed by the L&T under the guidance of the author are described below.

3.1 Stabilization Technology

Experience with the development of DRDO launch equipment gave the confidence to undertake independent development of Naval Weapon Systems. A key technology element in Naval Weapon Systems and Sensors is stabilization technology which was developed and mastered and deployed across a range of ship based systems.

3.1.1 Dhanush – Stabilized Vertical Launch System

The weapon system is a state-of-the-art electro-hydraulically stabilized vertical launch system (SVLS) for the vertical launch of a missile. This complex and innovative system, without any parallel in the world, has been indigenously developed from concept to realization through exemplary collaborative development between Program AD (DRDO) and L&T, with valuable suggestions and input from the Indian Navy. State-of-the-art concurrent engineering techniques such as 3-D solid modeling, finite element analysis methods, and advanced control simulation techniques were employed for the development to ensure successful realization of the system without hard prototype route.

The challenge for such a launch stabilization system is to stabilize a high inertia, large mass imbalance (inverted pendulum) on a hydraulically driven platform having low stiffness and damping. The system configuration involved a 2-axis gimbal and a set of three high-pressure servo hydraulic actuators to provide correcting (balancing) moments.Flow to the three hydraulic actuators was controlled by servo valves, which were, in turn, controlled by an embedded controller. The launch platform was free to rotate about roll and pitch axes constrained by end limits.

The missile was clamped onto the platform using an innovative clamping device at the base. A backup support system was provided in the form of a pair of grabs pivoted on the stabilized launch basket and reaching above the missile center of gravity. Just prior to lift-off, the grabs were opened hydraulically. The launch stabilization control system has to maintain the platform position horizontal within specified accuracy and roll-pitch rates. Additionally, the system was to compensate for the disturbances such as wind force, etc.

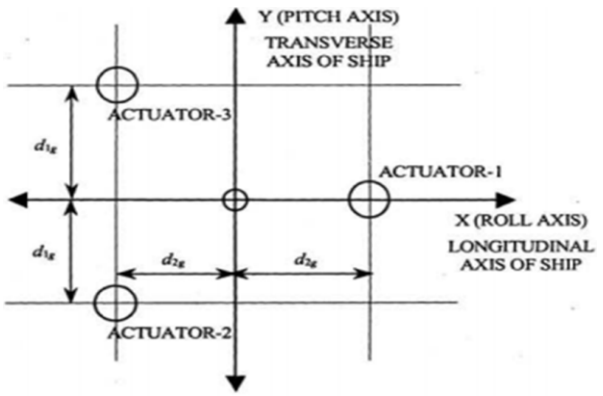

Figure above gives the orientation of the piston actuators. The actuators were oriented in such a way that two of these (2nd and 3rd) compensated for pure roll motion and all the three together compensated for pitch motion.

3.1.2 FourAxis Stabilized RF tracking Platform

Another application of stabilization technology is a ship borne high precision RF tracking system (4 Axis). This system has been developed for tracking aerial targets with maximum dynamics of 30°/s velocity and 30°/s2 acceleration, while maintaining a tracking accuracy of ±0.1°.Major challengeswere in the design of the high stiffness structures, low backlash drive trains and development of optimized control loops to achieve desired response & accuracy, keeping stability margins within the limits.

The configuration involved elevation over azimuth over a roll- pitch gimbal. This architecture has been conceptualized to overcome very high azimuth acceleration requirements due to roll and pitch and to take care ofthe stringent tracking accuracy requirement.

High Torque BLDC Direct drive motors were used for tracking pedestal (Azimuth and Elevation axis) in order to meet the bandwidth and accuracy requirements and to avoid the backlash. BLDC motor with reduction gear is used for stabilization platform (Roll and Pitch axis) where the requirements are considerably less compared to the tracking pedestal requirements. Several analyses and optimization techniques have been evolved during simulation phase.

The system has been successfully tested in DRDO premises with aerial targets.

3.2 Under-water Platform Technology

3.2.1 Hull Manufacturing Technology

A noteworthy contribution of the author has been in the development of indigenous technologies for submarines. These include hull manufacturing technologies and various equipment and weapon technologies.

Figure above shows 4 Axis RF Tracking System

The underwater platform consists of two hulls i.e.the light outer hull and the inner pressure hull. The light hull is the outer non-watertight hull which provides a hydro-dynamically efficient shape. The pressure hull is the inner hull that bears the enormous external pressure of the ocean at any depth and maintains the structural integrity and thus provides the ultimate safety to the crew and the equipment on board.

Being a military platform the challenge lies for the designer in striking the fine balance between the scantlings used for structural members and limiting the structural weight of the platform for a given displacement (weight of the submarine). Needless to say while higher scantlings would provide the much needed structural integrity they would also increase the steel weight thereby bringing down the payload carrying capacity of the platform.

While the design of light hull provides the hydrodynamic shape to the platform it also needs to bear the slamming loads, on surface, and the docking loads. Thin plates with dense stiffening are used to form the panels of the light hull. Containing the distortion due to welding of dense stiffening on a thin plate to maintain the form and profile presents an uphill task to the production engineer. Add to this the continual reduction in plate thickness of these panels along the circumference of the hull as one moves from bottom to top poses a nearly insurmountable challenge for integration of these panels to form a nearly perfect circular shape. Exact quantification

of the heat input due to welding and its consequences on the overall shape of the panel is the basis for determining the pre-camber, developing the right sequence and the process of welding.

The pressure hull on the other hand is an elastic design and is made of relatively (compared to light hull) higher thickness while based on the theory of thin shells (r/t~120). The leeway i.e. the tolerances on the circular shape of the hull (out of circularity is 0.002r, r-radius of shell) that the designer permits has a direct bearing on the factor of safety. To limit the structural weight the factor of safety is relatively very low compared to commercial pressure vessels and thereby once again poses a challenge to the fabricator.

In addition to devising the jigs and fixtures and welding processes, exacting measurement and quality plans ensure adherence of the fabricated structure to stringent tolerances defined by the designer. The complexity of forming (limiting the thinning of the shell) the dish ends of the pressure vessels is unparalleled for external pressure vessels.

The manufacturing technology perfected by L&T for underwater hull fabrication over a period of years is recognized world over and has enabled India to join a band of select nations who build submarines.

3.3Fire Control Systems Technology

Success and effectiveness of any weapon systems depends on how accurately it can deliver the munitions at the target end. Traditionally this accuracy of firing is more a function of firing tables and the gunner expertise apart from a host of external factors like the target behavior, environmental conditions, ammunition, etc. With the advent of new technologies, it is possible to minimize the human intervention and at the same time make the system itself more intelligent to improve system accuracy through high end computation of the ballistics and firing tables.

L&T embarked on this journey of self-reliance in this crucial technology of Fire Control Systems in the late 1980s, with the implementation of Fire Control Systems for Artillery Rockets and Missile Launchers.

At the beginning of this century, L&T started developing the ballistics and fire control systems for upgrades for in-service Air Defence Guns like the Zu-23 and L70 Guns. Being legacy systems in service, with no design data available, L&T had to start from the first principle of Internal Ballistics with accurate prediction of the muzzle velocity and CFD modeling of various shells. The algorithm developed accounts for various environmental factors like the air temperature, density, earth's rotation, gravity, etc. In addition to these factors various launcher related parameter are modeled in the overall ballistic module. These modules are experimentally verified in test conditions and further fine-tuned prior to field validation. Various steps involved in this exercise are illustrated in the following figure :

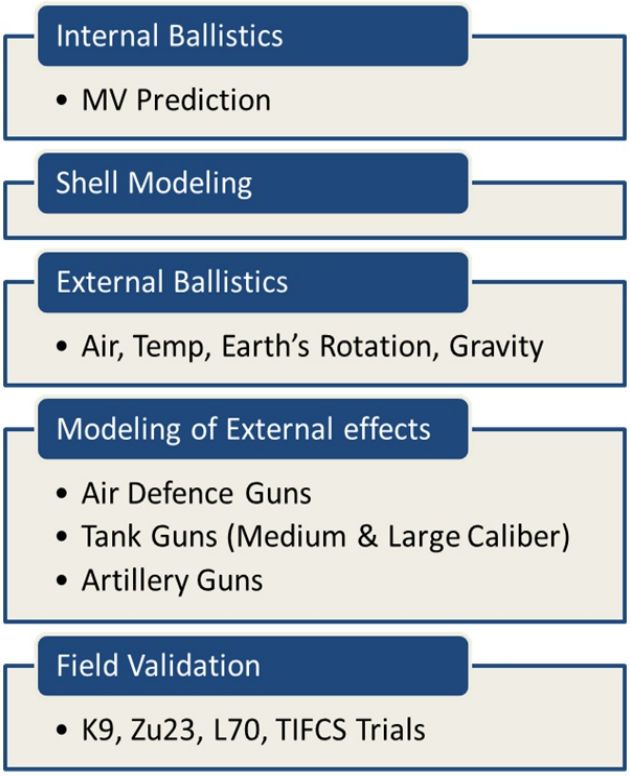

A detailed ballistic algorithm is developed in-house that takes into account not only various ammunition related parameters but also the target parameters like the target maneuver and generates the trajectory and estimates the hit probability.

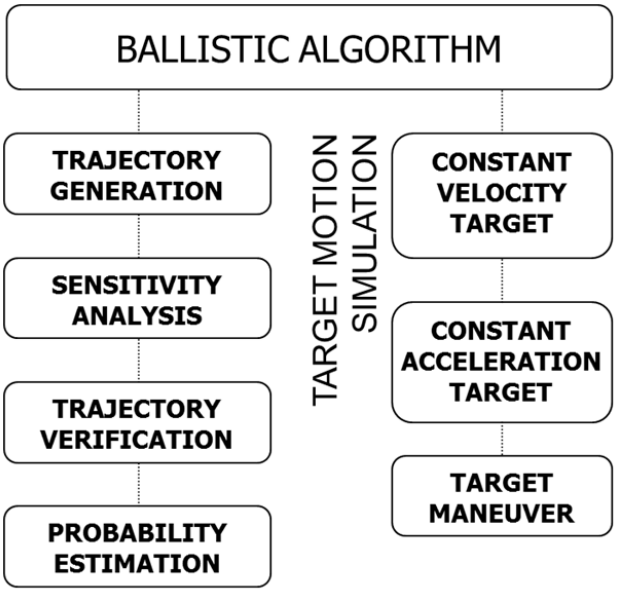

For generating the trajectory, the algorithm requires inputs in terms of target range. This range is achieved with the help of the Laser Range Finders. Based on multiple inputs of ranges, the target velocity vector is calculated by the algorithm, which also serves as an input to the tracking system. The ballistic module, in addition to the LRF inputs, gets inputs from visual sensors like the Thermal Imager. The thermal imager is mounted on a stabilized pedestal, which is used to acquire the target initially by the gunner. Once the target is acquired and 'Locked' by the gunner, the tracking algorithm takes over and predicts the future position of the target. The sighting system keeps the target in range by continuously updating its position to this future position, while the gun is slaved to the sight.

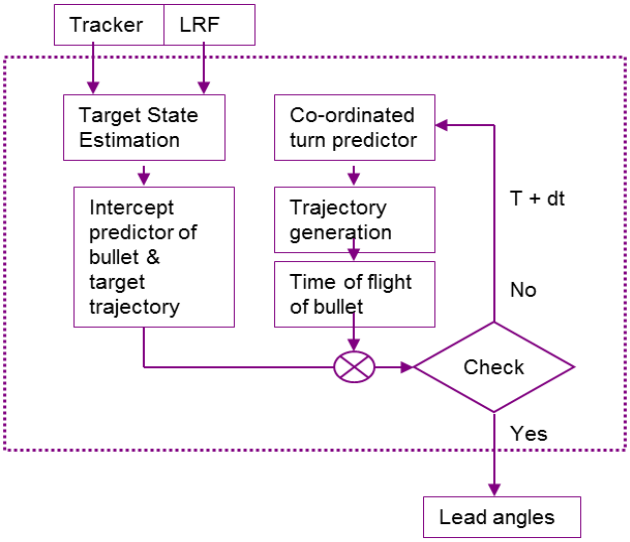

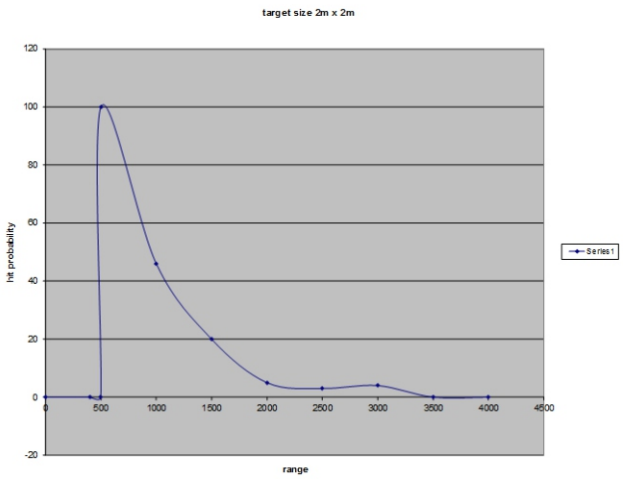

Figure 1 : Typical Hit Probability Simulation

Criticality of such system is processing inputs from multiple sensors like the LRF, sighting system, position sensors as well as ammunition data simultaneously in real-time, calculate and converge on the ballistic solution and issue the commands to the weapon system for positioning as well as firing within a very small window of time. State of the art hardware with open architecture has been designed in-house for this purpose, while the algorithms have been converted into efficient codes which can provide solutions in real time.

Following pictures illustrate the actual solutions implemented on the Zu-23 and L-70 Gun Upgrades.

Figure 3 : Target Hit This FCS development is highly modular and has been implemented in various formats like the 23mm and 40mm Air Defence Role, to 125mm MBT firing to 155mm Artillery guns, increasing the hit probability of basic weapon.

Figure 3 : Target Hit

3.4 Launcher Technology

Over the years, L&T has worked on variety of Launchers for different applications, from ATGMs to SAMs to Surface to Surface Missiles, Artillery Rockets to Air Defence Guns to Artillery Guns. The variety of ammunition ranges from a medium caliber air defence shot to a highly intelligent guided missiles. Each of the weapon system has unique requirements in terms of Launcher Technologies. For example an Artillery System requires a very robust and accurate positioning system, while a Surface to Air Missile

or Air Defence Gun requires a quick reaction system with very high tracking accuracy. On the other hand, the strategic missiles require a simpler vertical launch systems. The same weapon, if required to be launched while on move, like from the ship or a battle tank, requires stabilized launcher system in addition to the other features.

In 2001, DRDO embarked on an ambitious journey of developing an interceptor missile, L&T was the chosen partner for the ground systems including the Launcher System. L&T designed a unique Universal Launcher for this requirement.

Universal Launcher is a high mobility, multi-role, state-of-the-art weapon system for launching this AD Missile, the endo-atmospheric interceptor in providing TBM defence capability to India. The Launcher was designed for a guided, under slung missile configuration, which was attempted for the first time. It features a unique design catering tothree different modes, i.e. Position, Tracking and Vertical modes of firing for flexibility of mission. The Modular design adopted, has built in expandability in the system for adapting the article configuration with the launcher. The entire system is fully“Networked” and built for total all-electric operation including auto leveling using low voltage DC servo technology for its obvious advantages of battery backed operation with dual redundant power supply system.

Few of the salient features of this system are:

1. Silent mode of operation with all electric operation.

2. Auto leveling of launcher on electro mechanical Outriggers.
3. 360^0 azimuth movement for effective endless tracking.
4. Ball screw linear actuator driven by electric motors for high rigidity - high accuracy elevation drive.
5. All electric DC Low Voltage system for enhanced crew safety.

Thus this unique technology demonstrator launcher is an amalgamation of most of the latest technologies in the launcher domain.

3.4.1Under-water launchers & Simulators

L&T has created a unique facility at its Talegaon Plant, where land based firing of Torpedoes and Tube Launched Missiles (TLMs) can be carried out. The facility consists of a pressurized vessel which is filled with water, to simulate launch conditions at various depths of the sea. The Torpedo Tube is integrated with the vessel and full scale firing can be performed.

A unique, in-house designed arrestor system has been installed in the vessel, which brings the article to a safe stop. This facility can be used to fine tune the performance of the system before installation on board, as well as for crew training.The arrestor system has been proven in push-out launches of up to 35 m/s exit velocity for a 1.6 ton article and can be used for articles up to 2.4 tons weight. The entire preparatory and launch activities of the facility are controlled through a remotely located operating system.

All critical parameters of launch are recorded using a data-acquisition system that provides real-time data related to article acceleration and velocity as it exits

The torpedo tube itself is a unique design which caters to both push-out and swim-out modes of operation. Air push-out mode is achieved using high pressure compressed air stored in an air bottle mounted on the torpedo tube and flow is controlled using a highly customized in-house developed firing valve capable of pumping in extremely high flow rate of air. A higher diameter of the muzzle section allows swim-out launches to be performed from the same tube, thus giving it a universal underwater launcher characteristic.

The Torpedo Tube has already been proven in swim-out launch for two torpedoes of Western Origin. Push out launches have been successfully demonstrated on dummy torpedoes simulating dimensional and mass characteristics of these articles. The Torpedo Tubes developed by L&T can be adapted for launching all types of torpedoes and tube launched missiles presently available in the international market. Any adaptations or modifications required in the tube to make it compatible with a particular article can be easily undertaken. L&T has also developed a novel Elastomeric Ejection System for Bubble Less Push-Out Ejection of TLMs from Underwater Platforms.

3.5 RF Technology

A multi-pronged approach was used for developing expertise in this technology segment.

- Working closely with ISRO for the Development & Supply of two precision instrument grade tracking Radars, one in C-band & the other in S-band. Both these Radars have played a key role in tracking the missions ISRO from SHAR, Sriharikota. C- Band radar has a range of 4300 km in Transponder mode and a resolution of one meter with an absolute accuracy of 4 m.
- Concurrently working with DRDO & BEL in the development and production of Rohini and Revathi Radar platforms and other subsystems. Further, we developed Antenna systems for LRDE Radar programs (Arudhra and Ashwini) and Medium Power Radar (MPR) of ELTA.
- Collaboration with Indian and foreign technology partners for building this capability within the country.

The 4-axes stabilized gimbaled telemetry platform described earlier comprises of S & Ka band tracking system for monitoring re-entry objects. This is a "first of its kind" system and the main challenge here was the development of a dual band Antenna and feed system. In addition to the dual RF tracking system, it was also equipped with long range Electro-optic system capable of tracking an incoming object.

For an MoD trial evaluation L&T realized an Air Defence Fire Control Radar with in-house developed capability as a replacement of the aging Flycatcher Radars of the Indian Army. This system consists of surveillance Radar, Tracking Radar, Electro-optical system and fire control computer for control of two Anti-Aircraft L70 guns.

Another important MoD program undertaken was 3D-ASR for Indian Navy. An essential operational requirement of a Naval Ship is detection and classification of air targets at long ranges. A complete picture of the air space around the ship is needed in order to have effective Fleet Air Defence. Such crucial capability can be effectively provided by a Three Dimensional Long range Surveillance Radar. A 3D radar system simultaneously conducts three dimensional search of the air space and sea surface area around the ship. It automatically detects targets in the air and surface and creates tracks which could be sent to the radar console or the Combat Management System (CMS).

4 Conclusion

This paper brings out the evolution of the Indian Defence Industry and the establishment of a Defence Industrial Base in the country through the lifespan of the author's career as a technologist and technocrat. During this period large Industrial R&D's in the Private Sector have developed capabilities in system engineering and realization of Platforms & System of Systems. Through a process of multi-disciplinary digital simulations and computer aided engineering, experimentation, prototyping and enhancement of previously developed technologies a range of over hundred indigenous products have been developed and deployed in this period. This has given a great boost to indigenization and self-reliance for Indian Defence, which coupled with many enabling Policy Initiatives has paved the path for realization of Indigenously Designed Developed and Manufactured WeaponPlatforms and Systems.

Annals of the Indian National Academy of Engineering
Vol. XV, April 2018

Indigenous design and development of State of the art industrial Hypersonic Wind Tunnel & Shock Tunnel

S. Pandian[1], B. Murugan[2] and K. Srinivasan[3]

Abstract:
Aerodynamic and Aerothermal characterization of aerospace vehicles in hypersonic Mach no. regime is very much vital for successful reentry and interplanetary missions. Similarly hypersonic becomes very important in design and development of supersonic combustion ramjets (SCRAMJET). In order to meet the above testing requirements of present and future missions of ISRO, two industrial facilities, viz., 1m Hypersonic Wind Tunnel and 1m Shock Tunnel have been indigenously designed, developed and established at Vikram Sarabhai Space Centre, Thiruvananthapuram. Towards this the technologies under embargo were developed through ISRO, Indian Industries and Academic Institutions collaboration. The simulation capabilities and the salient features of these facilities are brought out in this paper.

1.0 Introduction

Aerospace vehicles encounter severe aerothermal environment during reentry phase / interplanetary missions due to hypervelocity conditions. The salient flow characteristics of hypersonic Mach number are formation of thicker boundary layers, entropy layers, thin shock layer, shock layer-boundary layer interactions, high temperature effects such as dissociation and ionization of air due to high kinetic energy, etc. (fig. 1). The effect of the flow features on the aerospace vehicles need to be clearly understood for vehicle performance evaluation, optimal design of control system and thermal protection system.

Simulation of these flow conditions in wind tunnel and measurement of aerodynamic forces and moments, pressures, heat transfer rates on a scaled model provide vital inputs for the proper aerothermaldesign of the aerospace vehicle to withstand the severe operating environment. The most important simulation parameters are Reynolds number and Mach number for force and pressure measurements whereas simulation of velocity and enthalpy are essential for heat transfer measurements. Hypersonic Wind Tunnel is used for force and pressure measurements and Shock Tunnel is used for heat transfer measurements

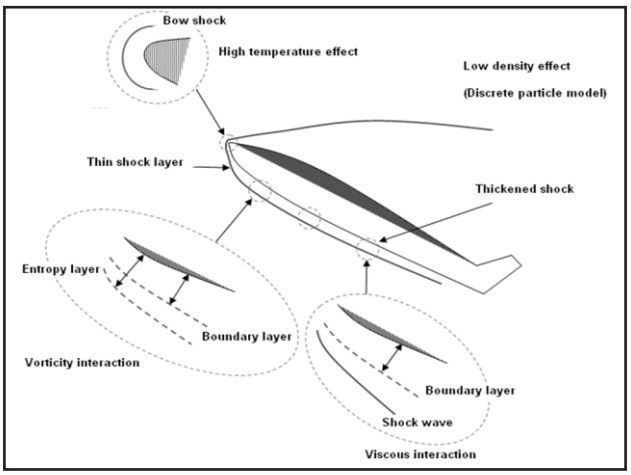

Fig. 1 Hypersonic flow characteristics

In order to meet the hypersonic aerothermal simulations required for present and future missions of ISRO, two facilities viz., 1m Hypersonic Wind Tunnel and 1m Shock Tunnel have been indigenously designed, developed and established at Vikram Sarabhai Space Centre (VSSC) in association with leading Indian industries.

2.0 Facilities Overview :

The schematic of Hypersonic Wind Tunnel (HWT) is shown as fig. 2 and schematic of Shock Tunnel (ST) is shown as fig. 3.

[1] Director, ISRO Propulsion Complex, Mahendragiri
[2]Head, Hypersonic Wind Tunnel Division, VSSC, Trivandrum
[3] Head, Wind Tunnel Data Division, VSSC, Trivandrum

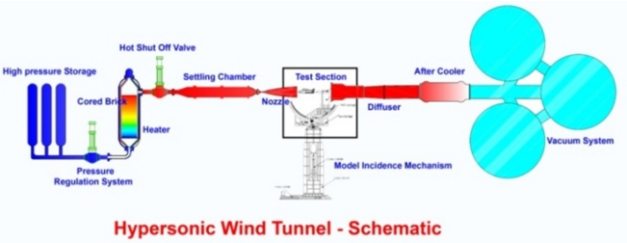

Fig. 2 - Schematic of HWT

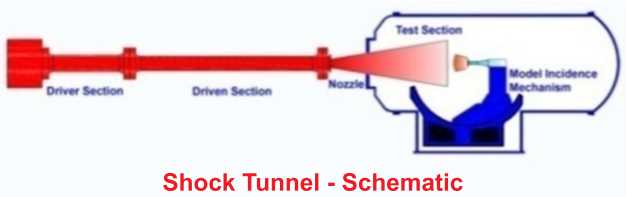

Fig. 3 - Schematic of ST

The overall specifications of HWT is given in table 1 and overall specifications of ST is given in table 2.

Table 1 - Specifications of HWT

Type	Enclosed free jet
Size	1 m (nozzle exit dia.)
Mach no.	6, 8, 10 & 12
Reynolds no.	80 million per m (max.)
Operating pressure	100 bar (max.)
Operating temperature	1550 K (max.)
Run time	20-40 sec.
Angle of attack	-10° to 50° (pitch) ±10° (yaw)
Applications	Force measurements, Steady & unsteady pressure measurements, IR thermography

Table 2 - Specifications of ST

Size	1 m (nozzle exit dia.)
Velocity	5 km/s
Enthalpy	12.5 MJ/kg
Mach no.	6, 8, 10 & 12
Angle of attack	-10° to 50°
Run time	1-6 ms
Applications	Heat transfer rate measurements, Supersonic combustion experiments.

These facilities are established as state of art facilities and first of its kind in the country in terms of size and simulation capabilities. With the establishment of these facilities, India joined the elite club of nations such as USA, Russia, Japan & France having large scale facilities for hypersonic flow field simulation.

3.0Design& development challenges:

The operating conditions of these facilities are dictated by the simulation requirements of Reynolds number and Mach number in the case of HWT, and velocity and enthalpy in the case of High Pressure System (HPS) with a storage pressure of 300 bar & 132 m^3; Vacuum System (VAS) with Horton spheres of volume 6600 m^3 evacuating to a vacuum level of 10^{-2} mbar; Heater System with alumina cored brick bed as heat storage medium, LPG storage system with 100 tonnes capacity and LPG burner to heat the alumina cored brick bed; Model incidence mechanism with four degrees of freedom and accurate servo control closed feedback system; PLC based operation & control system with 300 channels instrumentation, 700 mm diameter Schlieren Optical System for flow visualization etc., were required to meet the simulation requirements of Hypersonic Wind Tunnel. Because of the high pressure-high temperature operating conditions and massiveness of the systems, aerothermal& mechanical design of these sub-systems posed a real challenge.

The realization of the above facilities paved the way for the indigenous development of technologies, facing technology denial, such as cored bricks, hot shut off valve and massive 15-5 PH forgings. Besides, the development of above facilities posed many challenging aero and aero thermal problems, intricate engineering, high precision machining, massive fabrication, stringent quality procedures and above all extra safety measures due to usage of high pressure air, Liquid Petroleum Gas (LPG), hydrogen, oxygen and ignition system.

4.0 Technology developments:

I. Heater System :

Heater system is used to preheat the test medium (air) to the required temperature in order to avoid liquefaction when it expands through the nozzle. The temperature requirement increases with Mach number. Alumina pebbles / alumina cored bricks stacked inside the heater vessels are used as heat storage medium. Since alumina pebbles generate dust during tunnel blowdown, usage of alumina pebbles in the heaters of hypersonic wind tunnels is not a preferred option. Also, for alumina pebbles the operational temperature is limited by the high temperature creep, which occurs due to the high stress at the point of contact of pebbles. Therefore, it was decided to use alumina cored bricks as heat storage medium in the heaters of 1 m Hypersonic Wind Tunnel., But this technology could not be imported due to embargo. Hence, it was decided to indigenously develop & manufacture alumina cored bricks.

A. Cored bricks:

These alumina cored bricks have to withstand the high temperature and frequent thermal cyclic loads due to heating and blowdown operations of the tunnel.

Development of cored brick is interdisciplinary in nature involving thermal, material and mechanical fields.

The desirable properties of the brick include ability to withstand high thermal shock, high temperatures and resistance to thermal stresses, good abrasion resistance and resistance to crack propagation. Alumina was chosen as the material for brick due to its high melting point.

During the development process of cored bricks,lot of parameters was varied. The major parameters varied were alumina percentage in composition, particle size, proportion of temporary and permanent binders, loads applied on the bricks during pressing and sintering duration.

In the developmental process, the thermal, mechanical and material properties were evaluated

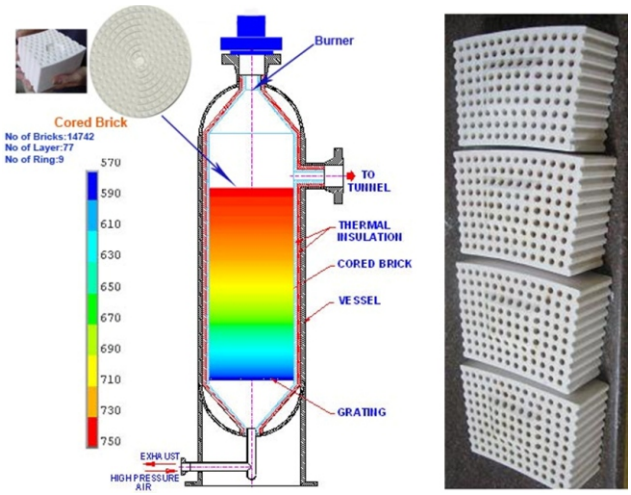

Fig. 4 - Heater schematic & cored bricks

through coupon level tests. The properties were evaluated through tests at various laboratories available at VSSC, M/s. SEPR and CGCRI, Kolkata to obtain chemical composition; physical properties such as density, apparent porosity; thermal properties such as thermal conductivity, specific heat, coefficient of thermal expansion, refractoriness under load, thermal cyclic tests; mechanical properties such as cold crushing strength, abradability index as per relevant standards& dust characterization tests (a special facility was rigged up for these tests). The above testing requirements / procedures were finalised after carrying out necessary thermal analysis. During the development process, 400 samples are subjected to 11 different types of tests for characterization and qualification of cored bricks.

As part of qualification and acceptance tests, ultrasonic inspection is carried out on all the sintered bricks for qualifying them, in addition to the sample level tests for evaluation of standard properties. Dimensional and visual inspections are also carried out on all bricks. Finally, the bricks are assembled up to every 1.5 m height and alignment of holes is checked. Bricks are trimmed to get better alignment.

B. Hot Shut-off Valves:

Hot Shut off Valves (HSV) are the most critical valve components in the hypersonic wind tunnel, operating at high pressures and temperatures as

high as 1550K. The HSV-4, positioned downstream of Heater II, will isolate high pressure high temperature air on upstream side from vacuum on downstream side. On initiation of blowdown, during initial opening the valve is choked and hence the valve gate experiences extremely high heat flux i.e. 200 times higher than that experienced by Apollo re-entry module. In fully open condition, the valve downstream seat experiences high heat flux for the blowdown duration of 40s. This valve is also an import substitute as it could not be imported due to embargo.

The valve gate experiences extreme heat flux during initial opening due to choking. Detailed thermal analysis shows that even for a short duration, high temperature super-alloys also cannot withstand the thermal loads. In order to alleviate the problems during initial opening, multiple strategies are implemented for valve operation. First, the actuation of the valve has to be fast during initial opening, hence reducing the choking duration. Secondly, based on flow field analysis and transient shock movement after initial opening, a constrictor plate is positioned at downstream location to facilitate reduction of choking period.

For fully open condition, detailed design and analysis shows temperature beyond material limits and resulting stresses much higher than strength of material. The downstream seat faces hot flow impingement, making it the most critical component in the valve. A variety of flow path modifications are attempted for studying the effect on heat flux.

Gaseous film cooling with cold air is introduced through an annular gap near the downstream seat inside the existing valve to alleviate high heat flux and related problems on downstream seat. The levels of film cooling need to be optimal i.e. lesser would lead to thermal/structural problems, and excessively high would defeat the purpose of heating the air. Film cooling is optimized by varying film cooling mass flow and annular gap using CFD/FE analyses for different Mach number conditions. The effectiveness of gaseous film cooling in valve type geometry is validated in a sub-scale experimental set-up. In order to minimize realization delays and cost escalation, an ingenious configuration is arrived which required no modification on the basic valve. All new elements are add-ons to the original valve with ease of assembly. Film cooling circuit elements are sized appropriately in order to deliver a pre-defined cold air mass flow.

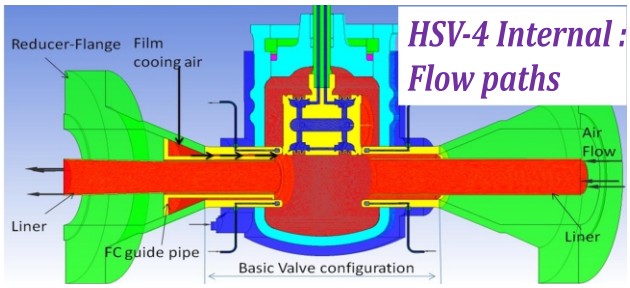

Fig. 5 - Hot Shut Off Valve -4

The implementation of film cooling inside a gate valve makes it a unique indigenous product suitable for high temperature/high pressure applications. An elegant way to configure new add-on elements around an existing valve led to a modular product.

Pressure testing and functional testing were carried out to qualify the valve for operating conditions. Low pressure pneumatic leak tests, high pressure hydro leak tests, shell hydro test and actuator function test were completed at factory. The functional test required a novel testing scheme and set-up in order to simulate the operating conditions of high pressure and high temperature. The functional qualification test was successfully carried out at 400 deg C temperature and 120 bar pressure with Nitrogen gas medium.

5.0 Model Incidence Mechanism:

Model incidence mechanisms with model injection capability are used in hypersonic wind tunnels to alleviate the tunnel starting / stopping loads. The complexity of the system increases with increase in number of degrees of freedom. A model incidence mechanism with four degrees of freedom (axes) has been designed & realized for HWT. The system has the capability to inject the model into the flow within 0.5 seconds after the flow is established. The test model can be maneuvered during the test, in the angle of attack

range of -10 to +50 in the pitch plane and ±10 in the yaw plane. The system has the provision to move 1000 mm (off-line movement) along the flow direction to accommodate longer models.

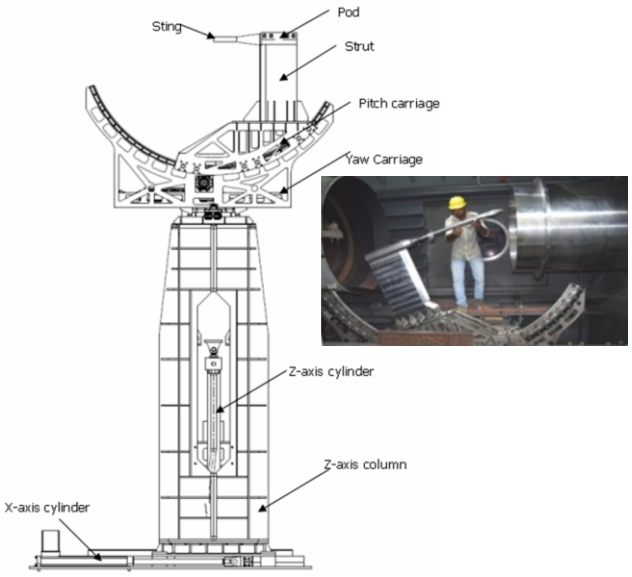

Fig. 6 - Schematic & photograph of Model Incidence Mechanism

The schematic diagram of the system is shown in fig. 61. All the four axes are operated by linear hydraulic actuators. The complete system is located on the X-axis platform. The horizontal X-axis movement is effected by a pair of hydraulic actuators in an open loop and after the desired location is reached, the platform is clamped by a spring mechanism. The pitch & yaw axes are mounted on a saddle. This saddle is moved vertically by a hydraulic actuator between two columns with linear guide ways to achieve the Z-axis movement. This movement is controlled by a servo valve with an optical encoder to provide the position feedback for the control system. The pitch axis motion is achieved by moving a carriage over a circular rail with circular guide ways. The carriage is moved by a hydraulic linear actuator with a rack mounted on it, which drives a pinion. The yaw axis movement is achieved by moving a hydraulic linear actuator mounted with a rack which drives a bull gear to achieve the angular movement. Both the axes are operated by a servo valve with position feedback from optical encoder.

In the case of Z-axis (injection axis), the maximum velocity to be attained is 4 m/s with an acceleration of 40 m/s^2 and the injection mass is more than 3 tonnes. This requirement demands a minimum hydraulic system pressure of 240 bar and flow rate of 3000 lpm, but the quantity of hydraulic fluid required is 30 litres for one cycle. Since, no online pumping system can meet this demand of 240 bar with a flow rate of 3000 lpm, it was decided to design the hydraulic power pack with a set of accumulators with nitrogen back-up bottles to store the energy and operate the system in blow down mode. A hydraulic power pack is designed with 11 accumulators to store the energy by adopting standard design procedures. These accumulators are charged with hydraulic fluid to the required pressure by a hydraulic pump with a flow rate of 50 lpm.

Servo valves, of reputed make, which can handle a maximum flow rate of 5000 lpm is selected for Z-axis movement, servo valve with a flow rate of 150 lpm is selected for pitch axis & valve with a flow rate of 20 lpm is selected for yaw axis. The servo valves are positioned close to the actuators in order to have fast response.

The hydraulic actuators are designed with a minimum factor of safety of 3 even under buckling.

The structural design philosophy is not only to keep the stresses on the components within the specified limits and also to keep the deflections very minimum. Therefore, design is not only strength based but also stiffness based. This is done to minimize the difference between the measured angle of attack and the true angle of attack. A detailed finite element analysis was carried out by generating a model including all the structural elements, guide ways, LM rails, hydraulic actuators, oil stiffness, etc., of the model incidence mechanism. The analysis was carried out for the loads corresponding to the maximum dynamic pressure operating conditions for both winged body (max. normal force & pitching moment) and blunt body (max. axial force) configurations.

This system has been realized, tested, integrated & commissioned and being used during the tunnel testing to precisely inject and maneuver the model

in pitch & yaw planes with respect to the flow axis.

6.0 Nozzles :

Hypersonic Wind Tunnel facility is designed to operate at Mach number 6, 8 10 & 12. Nozzle contours are designed using Method of Characteristics and the contour is corrected accounting the boundary layer displacement thickness. The design is carried out to achieve a minimum core diameter of 500 mm & flow inclination < 0.2 and accordingly, the exit diameter of Mach 6 & 8 nozzles were fixed as 1000 mm and for Mach 10 & 12 nozzles as 1180 mm. The contour is designed for a nominal operating pressure of 30 bar and the corresponding temperature to avoid liquefaction of air.

Subsequently, detailed mechanical design and thermo-structural analysis are carried out to ensure the structural integrity of the nozzles and adequate factor of safety (as per ASME code) for the operating conditions. The nozzle is split into 8 segments considering the manufacturing / machining feasibility. Since the heat transfer rates are very high at the throat region, suitable materials are chosen to withstand the operating temperature & pressure. The material of construction of the nozzle segments are given in table 7.3. The throat segment of Mach 6 nozzle is un cooled and water-cooled for other nozzles. All the divergent sections and subsonic sections are designed with a wall thickness of 20 mm considering design, manufacturing & handling aspects. Throat section of Mach 6 nozzle is designed with a wall thickness of 10 mm (for effective heat transfer) and throat sections of other nozzles have a wall thickness of 6 mm for effective cooling.

Subsonic sections, throat section (Mach 6 nozzle only) and divergent-1 sections are machined from integral forgings (including flanges) of 15-5 PH stainless steel. Manufacturing of large size 15-5 PH forgings is one of the technologies developed for manufacturing of nozzle segments of Hypersonic Wind Tunnel and shock tubes of Shock Tunnel. Throat sections of Mach 8, 10 & 12 nozzles are machined from solid rods of copper-beryllium alloy. This material is chosen to derive the benefit of copper for good thermal conductivity and beryllium for mechanical strength. Divergent sections- 2 to 6 are fabricated by rolling and welding of stainless steel plates. These welds are qualified using dye-penetrant test and radiography test (100%).

Both internal and external profiles of the nozzle segments are machined using CNC vertical lathes. The design co-ordinates of the nozzle segments at 1 mm interval are used as machining program in CNC machines. A tolerance (radial) of 20 m was specified for throat segment, 50 m for divergent-1 segment and 60 m for subsonic & divergent segments 2 to 6 for the internal profile. Surface finish of 0.8 to 1.6 μm is specified for the internal surfaces of the nozzle segments. CNC machine with high precision capability and CMM machine with very good accuracy were required. Special fixtures & radial clamps for holding the job in the machine, dampened boring bar of L/D >10, special carbide tool inserts for machining the Cu-Be alloy were all required to precisely machine the throat within the specified profile accuracy & surface finish.

After completion of machining, the internal profile along four generators (90 apart) and other dimensions of the segments are inspected in CMM machine (contour measuring machine). The initial setting, referencing & inspection procedures were evolved for profile inspection in CMM machine.

The entire nozzle assembly was assembled within a concentricity of 1 mm and integrated with the tunnel axis within 1 mm linear accuracy and 0.1 angular accuracy.

Fig. 7 - Photograph of nozzles

7.0 Vacuum System:

The various tunnel operating conditions of the Hypersonic Wind Tunnel requires, 10^{-2} mbar for Vacuum System (VAS). The vacuum system consists of two chains of vacuum pumping system with a capacity of 1,20,000 m^3/hr. Each pumping chain consists of 4 no. of mechanical booster pump & 3 no. of rotary piston pumps.

Two chains are separately connected to vacuum spheres. There are 3 Nos. of Horton spheres. Each Horton sphere has diameter of 16 m and volume of 2200m^3, made of SA516 Grade 70 carbon steel of 24 mm thick designed as per ASME Sec. VIIIDiv 2. Weight of the vessels is 580 ton. The 3 vacuum vessels are interconnected and total volume of the 3 spheres is 6600 m^3.Each sphere consists of 60 petals, 1 top cap and 1 bottom cap. The petals were formed at factory. Subsequently, a mock up assembly was made at factory and dimensions were checked. The entire fabrication of the spheres was carried out in-situ. All the weld joints (approx. 4 km) were qualified by radiography. Subsequently, the vessels were pressure tested & helium leak tested for vacuum operation qualification. The inside surfaces of the vacuum spheres were painted with special primer coating.

Fig. 8 - Vacuum spheres

8.0 LPG storage system:

Hypersonic Wind Tunnel system is equipped with storage heater which uses hydro carbon fuel (LPG) for heating the bed of storage heater. For this purpose, LPG is stored in the two tanks. The storage tanks are buried under the sand. This type of storage facility is called mounded storage. The mounded storage reduces the probability of external flame impingement on the vessels. Thus the vessels are protected from BLEVE (Boiling Liquid Expanding Vapor Explosion). The mounded storage is installed and commissioned as per Oil Industry and Safety Directorate (OISD 150) guidelines.

The LPG storage system is located 45 m away from the nearest building. A pump and a compressor are provided to unload the LPG from LPG tanker. Liquid LPG is taken from storage tank to vapourizer where heat is added and LPG is converted into gaseous form. Gaseous LPG is injected into the heater at a controlled pressure and flow rate for combustion. The distances between various systems are maintained as per OISD. Distances among LPG storage tanks, pump & compressor and Vapourizer are 15 m.

There are 4 retainer walls around the mound. The height of the retainer walls are 1.2 m on one side and 4.5 m on the other side. The height of the retainer walls on other two sides varies from 1.2 m to 4.5 m. Each LPG storage vessel is placed on 2 concrete pedestals. Inside the mound (and around the LPG vessels), sand was rammed with water. The compactness of the sand was to be maintained above 90%. The compactness was tested at every 0.6 m level (with 4 samples). It was found to be 98%. Over the sand, UPVC sheet, MS net, PCC and Paver blocks were laid.

The following safety features are implemented in LPG storage system: (i) Cathodic Protection System to prevent corrosion & longevity of storage tanks life (ii) Fire Fighting Water Sprinkler System to douse accidental fire during operation & loading of LPG into the storage tanks (iii) Leak & fire detection system, etc.

Fig. 9 - LPG storage system

9.0 Instrumentation & Control :

State of the art technology is used for data acquisition and control of the 1m Hypersonic Wind Tunnel. PLC based control system is working on Dual redundant Hot Standby concept. Control system monitors more than 100 input parameters and controlling more than 60 events. Considering the safety of operation triple mode redundancy is implemented in critical valve operations. Critical parameters are under continuous surveillance and in case of abnormal behaviour system sends abort command to shut down the process.

National Instruments make PXI based Real time Data Acquisition system is configured as distributed data acquisition stations. More than 150 analog channel data is acquired in 7 stations. All stations are configured in prime/redundant mode. Data is stored separately from prime and redundant channels. Model related pressure measurement is carried out using ESPs and force measurements are done using 6 component strain gauge balances. System has the capability to acquire data from 4 ESPs and from 5 balances at a time. All the DAQ stations are connected to control room through network. During the wind tunnel test data is coming to control room at lower rate for online data display purposes and after the test whole data is transferred to SCADA system automatically.

More than 20 types of sensors are used in the entire wind tunnel complex to measure different parameters. Vacuum gauges ranges from 0.1 mbar to 1000 mbar are used for vacuum measurements. GP 50 pressure sensors are used for pressure measurement ranging from 0.5 bar to 350 bar. These sensors are with built-in amplifiers to give either 0 - 5 V or 4 - 20 mA output. Specially made B-type and K-type thermo wells are used for temperature measurements.

10. HWT test results :

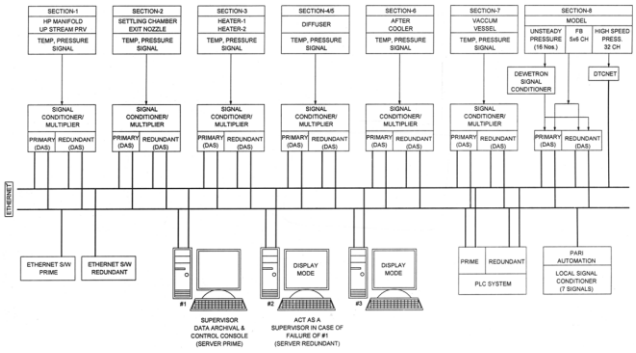

Fig. 10 - Schematic of DAQ & Control System

After successful completion of realization & integration of the facility, nozzle calibration & force measurements on standard AGARD-HB2 model were carried out and compared with other tunnel results. Subsequently, the tunnel has been used for generating data for RLV-TD, Supersonic Combustion Ramjet flight experiment, GSLV TPS Qualification, GSLV MK-III force measurements, etc.

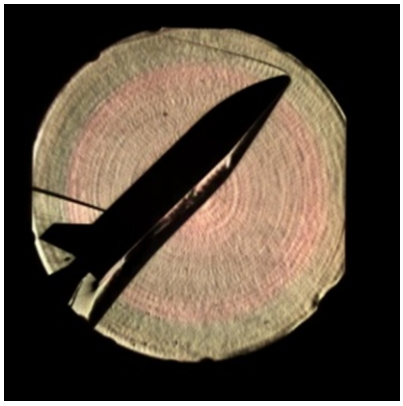

Fig. 11 - RLV-TD schlieren

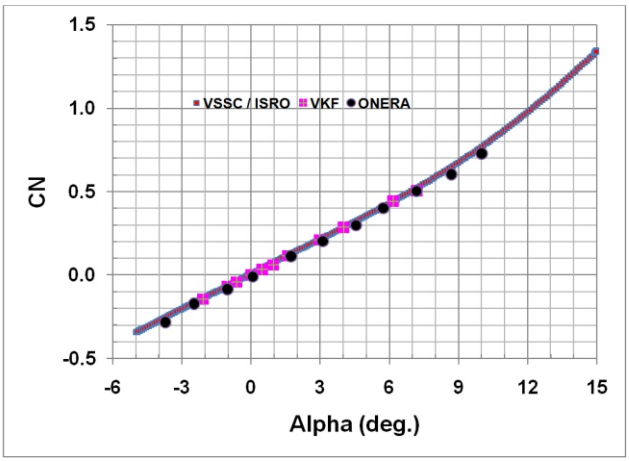

Fig. 12 - AGARD HB2 data

11.0 Shock Tunnel :

A. Large 15-5 PH forgings :

The shock tubes of the shock tunnel are designed to produce a total enthalpy of 25 MJ/kg (in Free Piston Shock Tunnel (FPST) mode) which requires 1000 bar stagnation pressure and 10,000 K stagnation temperature. The run time in a shock tunnel is 1-6 ms.The design is driven not only by the pressure but also by the fatigue. Each run in shock tunnel produces, 20 stress reversals which call for a material with high fatigue strength. Considering these requirements, a material of high yield strength ~ 1000 MPa with endurance limit of Precipitation hardened 15-5 PH steel meets many of these demands and apart from possessing high strength, it is non-corrosive, easily machinable and is supported by ASME section VIII Div 3 which is the design code. Because of these obvious advantages, 15-5 PH material is chosen as the material of construction of shock tunnel.

At the time of development, 15-5 PH forgings are manufactured up to a diameter of 150mm. However, in the present case, the diameter of the flange is 650mm and hence this poses many challenges in realization in terms of (i) Capacity limitation in ingot melting, (ii) Forging of Massive section of 345mm and 715mm with a length of 4100mm within narrow forging temperature schedule (iii) Realization of the forging to meet stringent UT quality level and Mechanical Properties, (iv) Establishment of suitable Heat treatment condition for trepanning and further downstream machining operations.

Various parameters like ageing temperature, heating rates, heating time, double ageing, Resolution annealing, etc., are varied and after many successfully coupon levels trials, forgings process is finalized.

B. Machining of 15-5 PH forgings :

The 15-5 PH forgings are massive in size and the process demands a honing internal surface finish. In order to achieve the bore a special trepanning tool was made and a material with ID of 100mm was initially trepanned. Further, the ID was increased in steps to closer shock tube ID of 180mm. Finally honing operation was carried out to achieve the required internal surface finish.

Fig. 13 - 15-5 PH forging & machined tube C. Combustion driver

In order to achieve higher shock speeds in the shock tube, the speed of sound of the driver has to be increased. One way of increasing the speed of sound is by heating a lighter gas (He) with H_2–O_2 combustion. The combustion driver also has the advantage of increasing the test time by suitably tailoring the tunnel at various enthalpies by varying a4. Hence, a combustion driven shock tunnel was developed at VSSC. One of the challeneges in combustion driver is to ensure smooth, detonation free combustion for all mixtures. Towards development of a combustion driver, a pilot combustion driver was designed and developed at VSSC .In this driver, various parametres like number & spacing of spark plugs, mixing time loading sequence, etc., were studied and based on the experimental results a combustion driver with spark plugs in two helical fashion was arrived and the spacing of the spark

plug was 0.12D. A typical pressure trace in combustion driver showing a maximum post combustion pressure of 350 bar and run time achieved for various enthalpies is shown in fig. 14.

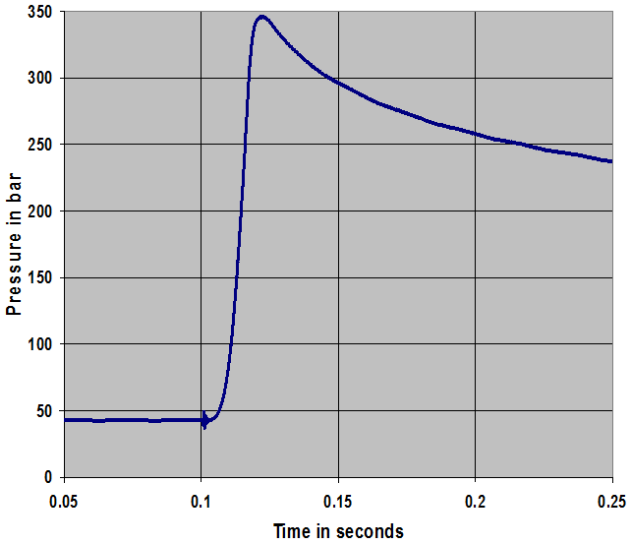

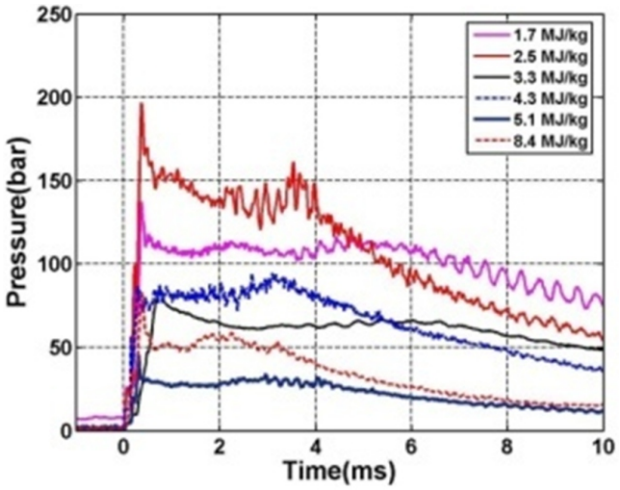

Fig. 14 - Post combustion pressure

D. Instrumentation :

As the shock tunnel has ms runtime, high speed data acquisition system is necessary. Shock tunnel data acquisition system consists of NI based cards for acquiring and storing the pressure and temperature signals. The control system of shock tunnel is based on PLC .Total 93 channels are used for control. Current system has a capability to acquire 77 channels for monitoring overall performance of tunnel. Out of 77 channels 16 channels are used for calculating different parameters (Mach number, shock speed, P2, P4, P5 etc) related to shock tunnel. 32 numbers of channels are dedicated to model related parameters. The complete chain diagram of model related acquisition is given in Error! Reference source not found.. The electrical signal generated by the transducer must be optimized for the input range of the ADC card (PXI 6133). Hence, signal conditioning is carried out to amplify low level signals and filter the high frequency noise, for more accurate measurements, Dewetron preamplifier is used which has a capability for providing excitation to sensors and at the same time can provide maximum gain of 10000 at wideband frequency.

It also isolates the transducer signal from the computer for safety purpose. An analog second order low pass Butterworth filter (10 or 30 kHz) is set in the Dewetron to remove unwanted high frequency noise. After signal conditioning, signal is transferred to PXI 6133 card which digitizes the data. This card has a sampling rate is 3 MHz sampling per Channel with 14 bit ADC resolution and has a FS range of 5V.

E. Results:

Shock tunnel was successfully used for demonstrating supersonic combustion of H2

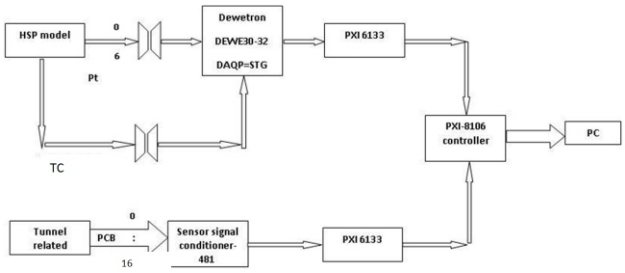

Fig. 15 - Data acquisition configuration

fuelled scramjet. In the tests, gH2 was injected and air at 2200K at 190 bar in the settling chamber is expanded to Mach 6.7 flow and supersonic combustion was demonstrated.

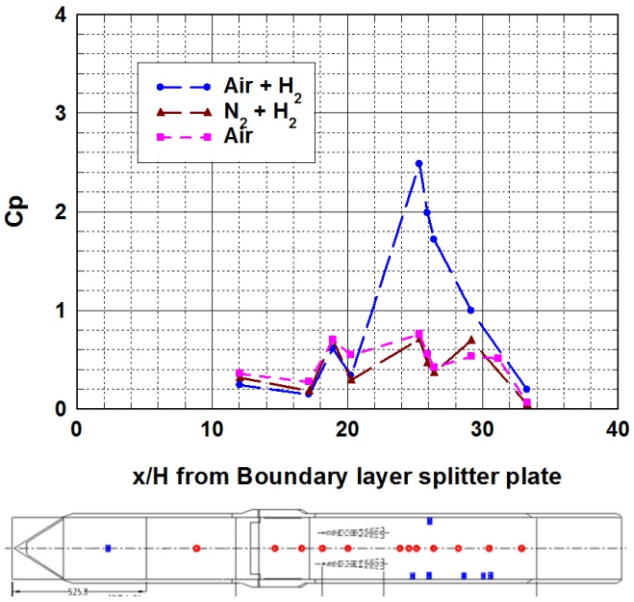

Fig. 16 - Supersonic combustion test results

Conclusions :

Two state of the art world class facilities have been indigenously developed & established at VSSC to generate design data for present and future missions of ISRO in hypersonic Mach no. regime. New technologies such as alumina cored bricks, hot shut-off valves, large size 15-5 PH forgings with integral flanges have been developed indigenously. These facilities have been Made in India with the support of Indian Industries.

Acknowledgements :

Authors wish to express their gratitude to Shri. A.S. Kiran Kumar, Chairman, ISRO and Dr. K. Sivan, Director, VSSC for their continuous support & guidance in realizing these facilities. The contributions of HWTP team including Shri. D.S. Antuvan, Former PD, Shri. S. Subash, Shri. Amitava Mandal, Shri. AnkurNagpal, Shri. Varghese Jacob & others are greatly acknowledged.

Annals of the Indian National Academy of Engineering
Vol. XV, April 2018

Transformation of Engineering Education in India

Anil D. Sahasrabudhe[1]

Abstract : The number of engineering colleges in India have increased manifold since independence more so in the last one and a half decades. This has certainly helped in improving the Gross Enrolment Ratio (GER) from mere 0.7% at the time of independence to 24.5% in 2017. Thus mission of the government for increasing access and equity has been achieved to a great extent. However, the quality is much to be desired. It is in this context that the experience of the author in engineering education from Indian Institute of Science, Bangalore, NERIST in remote north east in Arunachal Pradesh, then in IIT Guwahati and College of Engineering Pune has been made use of effectively after assuming the mantle as Chairman of AICTE, a regulatory body for technical education in India. Several reforms such as regular revision of curricula, mandatory accreditation, mandatory industry internship, innovation and entrepreneurship cells, startup policy, smart India hackathon developing an indigenous MOOCs portal SWAYAM have been introduced to transform the face of engineering education in India.

Keywords : Engineering, Education, GER, Accreditation, Industry Interaction

1 Engineering Education in India

Engineering education in India dates back to starting of 4 engineering institutes in Roorkee: Thomason college (1847); Pune: Poona College (1854); Shibpur, Kolkata: Bengal Engineering College (1856); and Guindy, Chennai: College of Engineering Guindy (1794, 1858). Most of these institutes provided skill education in civil engineering in their formative years, and subsequently started formal degree education in civil engineering, mechanical engineering and electrical engineering followed by other engineering disciplines. Institutes such as Universities of Bombay, Calcutta and Madras (1857), University of Allahabad (1887), Indian Institute of Science Bangalore (1909), Banaras Hindu University (1916), Aligarh Muslim University (1875, 1920), Punjab University (1882, 1947) were all started providing general, science and engineering education till independence. There were hardly 25 engineering institutes with less than 2500 intake at the time of independence. IITs at Kharagpur, Bombay, Kanpur, Madras and Delhi (1951, 1958, 1959, 1959, 1961) were started post-independence. Regional engineering colleges (now called National Institutes of Technologies) were also started post independence. Today there are as many as 3285 colleges affiliated to about 101 universities with a whopping intake capacity of 15.53 lakhs. There are as many as 23 specialized affiliating technical universities in different states of India. The growth of number of institutes during the last decade is shown in Table 1.

Table 1. Growth of technical institutions in India

Growth of Technical Institutions in the Country (UNDER GRADUATE)

YEAR/PROGRAM	ENGG	PHARMACY	ARCH	HMCT
2007-08	1668	854	82	73
2008-09	2388	985	82	81
2009-10	2972	1029	82	81
2010-11	3222	1041	84	83
2011-12	3286	1053	84	83
2012-13	3369	1036	100	80
2013-14	3384	1029	105	81
2014-15	3391	1025	114	77
2015-16	3387	1033	117	77
2016-17	3285	1034	114	74

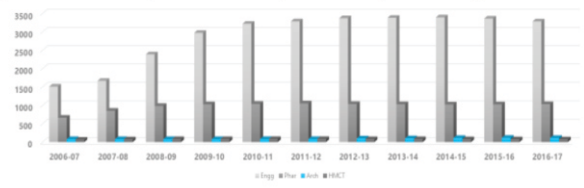

[1] Chairman, All India Council for Technical Education, New Delhi

Table 2 shows the growth in number of seats available in engineering and technical disciplines.

Table 2. Growth in intake capacity in technical education in India

Growth of INTAKE in Technical Institutions in the Country (UNDER GRADUATE)

YEAR/PROGRAM	ENGG	PHARMACY	ARCHIT	HMCT
2006-07	659717	76030	5085	5840
2007-08	701214	77582	5189	5959
2008-09	753910	78763	5268	6050
2009-10	1093380	80370	5375	6174
2010-11	1219347	81594	5457	6268
2011-12	1379149	83259	5568	6395
2012-13	1538767	83519	7325	6160
2013-14	1620958	85474	8144	6520
2014-15	1700655	89119	9834	6340
2015-16	1673186	89813	10311	6328
2016-17	1553711	84787	9161	6028

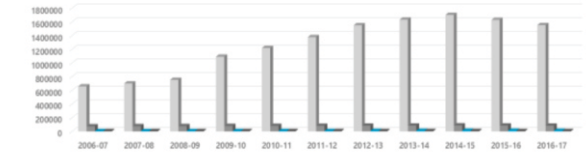

Unfortunately, in recent times more than 50% of the seats remain vacant creating a challenge for economic viability and quality of technical education being imparted. The employability of engineering graduates ranges from 25% to 40 % according to reports from several industry bodies such as CII, NASSCOM, FICCI and ASSOCHAM and surveys by agencies such as Aspiring Minds, EY, World bank etc. There has been a trend of closing of the institutes or disciplines reducing the number of available seats by the managements of these institutes with the principle of survival of the fittest. There has also been closing of colleges or reducing the number of seats by the regulator AICTE as disciplinary action for not maintaining the norms and standards announced by AICTE. Thus supply and demand gap is gradually decreasing. The MHRD had appointed a committee chaired by Mr. Kaw, former Secretary of Education for reviewing the technical education scenario in India and suggest reforms in statutory regulatory body of AICTE. The committee has submitted its report in 2015. Major recommendations of the committee are given below.

1. AICTE to be a constitutional autonomous apex authority
2. To concentrate on mentoring and development
3. To focus attention on research and innovation
4. Rating to be the fulcrum of regulation
5. To improve the sub-standard institutions
6. Provision for internship
7. Robust accreditation
8. National testing service
9. Permanent staff
10. Charting the territories
11. Distance and life-long education
12. Vocational education
13. Quantum jump in allocation of funds
14. India to be a technical education superpower

Taking a cue from the report and to address the challenge of employability and vacant seats, a number of reforms have been introduced for transforming the scenario and bringing in quality in technical education.

2 Educational Experience

2.1 Indian Institute of Science, Bangalore (IISc)

The first experience in higher education and research was from Indian Institute of Science Bangalore during Masters in Mechanical Engineering (1980-1982) and PhD in Mechanical Engineering (1984-1989) in the area of acoustics of mufflers.

The major work involved aeroacoustic evaluation of perforated muffler components (1), application of finite element method to study acoustics of mufflers, matrix condensation and transfer matrix techniques in the 3-D analysis of expansion chamber mufflers (2), design of expansion chamber mufflers incorporating 3-D effects (3), and analysis of inertance due to higher order mode effects in sudden area discontinuities (4). This research helped in understanding 3-D effects on acoustics of mufflers paving the way for better design of mufflers at all frequencies.

Figure. 1. Main building of Indian Institute of Science

The course work done during this period, literature survey, effective use of library resources, and computational facilities methodology of research created lasting impression through regular interactions with supervisor Professors M. L. Munjal and S. Anantharamu.

2.2 North Eastern Regional Institute of Science and Technology, Itanagar

The experience in setting up an institute of science and technology in the remotest part of north eastern India in Arunachal Pradesh (1987-1995) was both a challenge and an opportunity. The institute was started in the year 1986 with a totally different model of higher education with a modular pattern. This was the first of its kind experiment in India.

Figure. 2. NERIST in its formative years (1987)

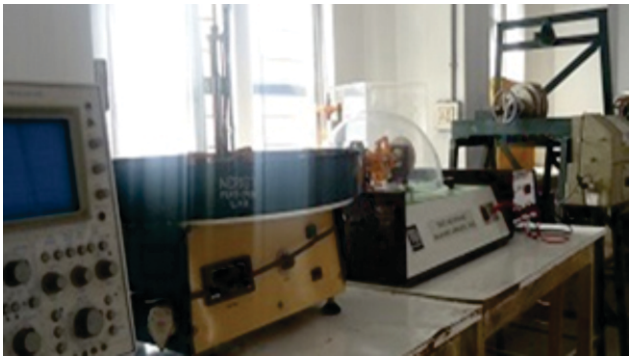

Figure. 3. Dynamics laboratory of NERIST

The entry of students was after class X into a two-year certificate module which catered to basic science education as well as one of the trades such as construction technology, carpentry, welding, I.C. engine technician, electronics technician, TV repair technician, electrician, horticulture etc. useful for employment. There was provision to move out after this two year vocational education or to continue further into a two year Diploma module in formal engineering disciplines like civil engineering, mechanical engineering, electrical engineering, electronics engineering, computer engineering, forestry etc. There was provision for lateral entry into Diploma module for students who had done ITI or class XII Science with different bridge courses depending on type of background of students. There was a provision for exiting with a Diploma or continuing further into a 2-year Degree module in engineering in respective fields. There was a provision for lateral entry of students even at this stage for externally obtained 10+3 Diploma holders or BSc degree holders with different bridge courses for each of these category of students. Thus it was an unique experiment in engineering education creating practical hands on engineers Today, NERIST has several alumni from first generation education and have taken important positions in Government and private sector industries. The institute is now a Deemed university and also offers MTech, MSc and PhD programmes in science and technology. This model of NERIST was then replicated in Sant Longowal Institute of Engineering and Technology, Central Institute of Technology, Kokrajhar and Ghani Khan Choudhury Institute of Engineering and Technology, Malda.

The National Skill Qualification Framework (NSQF) which is being implemented today by National Skill Development Authority (NSDA) and National Skill Development Council (NSDC) through All India Council for Technical Education, (AICTE), University Grants Commission (UGC) and Ministry of Skill Development and Entrepreneurship is a classic variant of the scheme being run in NERIST and three other similar institutes for over 25 years,

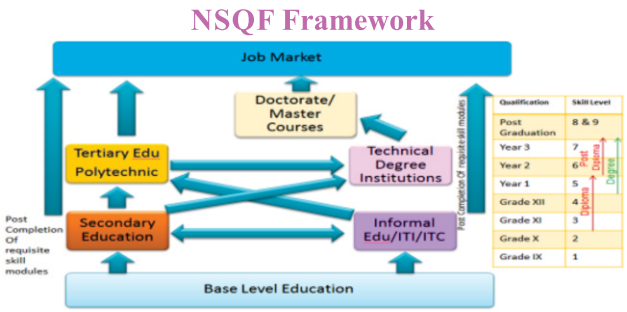

Figure. 4. National Skill Qualification Framework

2.3 Indian Institute of Technology Guwahati (IITG)

The sixth IIT was to come up in the state of Assam in Guwahati as per Assam Accord. Unlike all earlier IITs which were set up with the support of different countries, this was an indigenous IIT being set up after a gap of 4 decades. The challenges were not only in terms of building infrastructure in the low water logging area but also in terms of attracting and retaining faculty. The rich experience in starting this new IIT starting from an Institution of Engineers building, and faculty housing scattered all over the city of Guwahati to moving into a temporary transit accommodation on the campus, followed by state of the art buildings was exhilarating. The academic administrative systems, curricula were all developed by the team IIT with the 4 decades of rich experience of all other IITs. Today, IIT Guwahati is not only one of the most beautiful campuses in India, but ranked amongst the top 50 new institutes of the world. During the formative years, setting up of teaching laboratories and then research laboratories, building the IIT work culture, managing placement of students with hardly any local industry support, organizing conferences and seminars and working shoulder to shoulder with all sister IITs was indeed an enriching experience.

Figure. 5. Administrative building, central library and auditorium of IIT Guwahati

Figure 6. Picturesque guest house of IIT Guwahati

The research and development carried out during this period from 1995 to 2006 includes prediction of surface roughness and dimensional deviation by measuring cutting forces and vibrations in turning process (5) and vibration analysis and optimal control of rotating pre-twisted thin-walled beams using MFC actuators and sensors (6), development of a mobile road maintenance system for Border Road Organization (7) and setting up of a technical back up unit of Khadi and

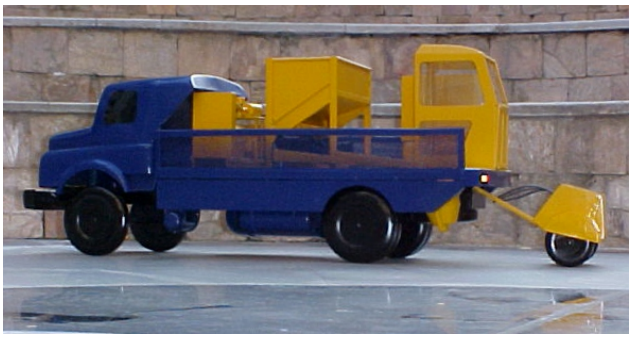

Figure. 7. Mobile Road Maintenance System

Village Industries Commission (KVIC) for developing innovative solutions to help develop rural technologies in improving quality and productivity (8) among many other projects.

Development of a new design for biogas plant accounting for the cold climate of the region, different type of bamboo and cane products for school, home and hospital furniture, new design of loin loom for weaving for reducing drudgery and improve productivity are some of the projects initiated under KVIC project. These projects have

resulted in utilizing local resources for increasing employability of local artisans.

Figure. 8. Prototype of loin loom

2.4 College of Engineering, Pune (COEP)

Once a great institute, Poona college of engineering (1854) which boasts of alumni like Bharatratna Sir M. Visvesvaraya (1881-1884), Professor Thomas Kailath (1953-1956), Dr. C. K. N. Patel (1954-1957) and Dr. Vijay Kelkar (1960-1963) had been academically sliding from eighties and was in a very bad shape by 2001. The state Government gave full autonomy to the college thanks to a report submitted by a committee headed by Dr. F. C. Kohli (2004). Dr. Kohli has been the chairman of Board of Governors since then and has been a driving force behind autonomy of the college. The author got an opportunity to turn around the college (2006-2015) and bring it in the reckoning amongst top 15 colleges in India.

Figure. 9. Main building of College of Engineering

Some of the initiatives undertaken include faculty and student empowerment. The faculty were given first hand experience of IIT by sending faculty for a full semester to IIT Bombay and make them attend PG classes, take tests, assignments and examinations along with regular students and challenging them to secure a minimum of 8 grade points on a scale of 10. Faculty were motivated to observe other processes such as academic system, laboratory equipment, library system including research activities etc. Similarly, to give the students a taste of IIT education, an exclusive 2 Mbps connectivity was established between IIT Bombay and COEP, multiple video conferencing equipment were placed in IIT Bombay and COEP and live lectures of best IIT Faculty were made available. This was done in 2007 when the term MOOCS and on line education did not exist. It was indeed a futuristic and visionary step.

For empowering students, as many as 32 student clubs were established for giving them an opportunity to give a taste of overall development of self and society. The 24X7 access to computer centre, internet, laboratories and workshop was provided to students. The net result was teams from COEP won several national level competitions like BAJA (all terrain four wheeler vehicle design, fabrication and running a race competition), ROBOCON, music, drama, street play competitions, Microsoft innovation challenge awards amongst others. Student satellite team comprising of UG students designed and fabricated a pico satellite SWAYAM with an innovative idea of passive stabilization of satellite and the same was launched by ISRO. This brought in a vibrant academic ambiance in the entire institute.

Figure. 10. All terrain four-wheel vehicle designed and fabricated by students for BAJA (1st place)

Students created three Guinness book of world records; 292 students skipping on a single rope 14 times (2006), longest painting (598 meters) on a theme big bang to modern times (2008), 3248 students solving Rubik cube within half an hour (2012). Such events and many other co-curricular activities have created a vibrant academic ambiance on the campus reaching for excellence in every domain.

Figure. 11. World record of longest painting

Figure. 12. Students solving Rubik cube

Figure. 13. COEP's Bhau Institute of Innovation, Entrepreneurship and Leadership

The research contribution during this period (2006-2015) include visco-elastic stress strain model of solid rocket propellants (9), application of wavelet transforms for diagnosis of rolling element bearings (10), experimental analysis of damping performance of visco-elastic material using constrained layer damping treatment (11) among other works.

3 All India Council for Technical Education (AICTE)

The AICTE established by an Act of Parliament in 1987 which regulates technical education in India gave an immense opportunity to the author in the capacity as chairman for transforming engineering education in India.

The number of technical institutes and number of seats in technical education had increased several fold since independence especially in the decades starting from 1990s to 2015. The access and equity was achieved but quality was much to be desired. As a result, about 45-50% seats are remaining vacant since 2010, employability of graduates in question from 2006 and only about 25-30% students getting placement through placement offices of colleges raising an alarm to check the menace of unemployability.

Meanwhile, MHRD had set up a committee with Mr. M. K. Kaw as chairman of an AICTE review committee which submitted its report in 2015. Major concerns raised included funding, outcomes, rating of institutions, innovation and research in institutes, accreditation and lack of autonomy to colleges.

Several measures have been undertaken in the last two and half years to improve the quality of technical education.

There were many quality improvement schemes like pursuing PhD by faculty members under QIP in IITs, Research Promotion Scheme, Modernisation and Removal of Obsolescence, Faculty development programme started by AICTE over the years, which were dormant due to lack of funding and effective monitoring. These were resurrected by innovative way of using interest earned from corpus for starting the schemes and then getting central government funding in due course. INAE-Distinguished Visiting Fellow, INAE-Travel Grant Scheme for young researchers, INAE- Teachers Research Fellowship Scheme are some of the schemes which were streamlined and have begun execution. AICTE has also engaged with IITs and ISTE to offer faculty development programmes of one week to two week duration. Many faculty, students and institutes have started taking advantage of these schemes. AICTE has been continuing to provide Post Graduate Scholarships to about 40000 students pursuing Masters programme in engineering, architecture and pharmacy.

Other scholarship schemes for women, persons with differential abilities (PwD), SC/ST students, Prime Minister's Special Scholarship Scheme for students from J and K are some other schemes operated by AICTE.

Most significant new schemes include Train the Teacher Scheme for attracting talented students to teaching profession, Adjunct Faculty Scheme for attracting persons from industry to teaching, Unnat Bharat Abhiyan for adopting villages by colleges, reaching out to them and using technology interventions for improving the quality of life and Margdarshan (Mentoring scheme) for mentoring sub-standard colleges by well performing colleges thereby improving the overall quality of technical education.

Two new interventions include organsing a Smart India Hackathon for technical students. 598 problem statements from 29 Government departments and ministries were offered as challenge to the students and invited their ideas for solving them in the very first edition of hackathon. More than 40000 students applied in teams of 6 with at least one female member in every team; we shortlisted 1250 teams and conducted 36 hour long non-stop hackathon on April 1 and 2 in 26 centres all over India. Prime Minister came live at 11 pm to motivate and inspire the students. Out of all the prize winning solutions, 52 of these solutions have been taken forward to create robust solutions for implementation by the concerned department/ministry. This has energized the entire technical education system and many state level and local college level hackathons have started off. The confidence level amongst students has increased manifold. In the current year the hackathon is going to be much bigger with more government departments and many state governments coming forward. It is expected to have participation of more than a lakh students. Hardware hackathon to create products is also going to be organized this year.

Second initiative is that of creating a student start up policy. The policy was launched by the then honorable President of India Shri Pranab Mukherjee on Nov 16, 2016 from the Rashtrapati Bhavan during visitors conference. An implementation committee has been set up so that through a hub and spoke model, AICTE is reaching out to 1000 colleges who are encouraged to not only have entrepreneurship related courses as part of the curriculum, but also start incubators and create 10 startups a year. This is likely to have immense effect on not only employability but in creating jobs from the campuses.

AICTE was also given a mandate to develop an indigenous MOOCs platform “SWAYAM” which was carried out successfully by AICTE with the support from MHRD. Today there are as many as 750+ courses in different disciplines on this platform. As many as 6,00,000+ students have registered on the portal. As many as 150+ nations have shown keen interest and are watching our progress. Students from 64 nations have registered for these courses. This is likely to become the largest MOOCs platform providing education at any time any where for anyone.

Figure. 14. Smart India Hackathon

AICTE has instituted three important national awards this year apart from industry institute interaction awards being awarded in association with CII. These are Chhatra Vishwakarma Awards for innovative projects, Clean and Green campus awards, and Best student startup awards. This has created both competition and collaboration between different colleges.

AICTE has also undertaken several key measures to improve quality of technical education.

1. Regular revision of curriculum : AICTE has advised colleges to conduct revision of curriculum annually. To support the colleges and universities, AICTE has developed curricula in all major disciplines of engineering both at UG and PG level and offered these as model curricula for colleges to adopt/adapt, tweak if necessary and offer latest state of the art courses. A number of senior Professors from IITs and industry persons helped AICTE in this exercise.
2. Teacher induction module: AICTE has developed three two months each modules in pedagogy and a fresh teacher has to undergo this 6 month programme to become eligible for teaching. Those in service will have to complete this programme in the next 2-3 years as per their convenience.
3. Student induction programme: For the first time, a three week student induction programme has been devised for freshmen. This programme is envisaged to break the ice and create level playing field for all students irrespective of background from where they come, sensitize students to the healthy habits, society, nation, and nature.
4. Model question papers : AICTE is devising a new way of assessing students as per outcomes desired by the institute and the programme. The testing is based on Bloom's taxonomy.
5. Mandatory internship: All students have to undergo at least 4-6 weeks internships, three times during their engineering programme so that students understand nuances of industry and become employable and industrious.
6. Industry Interaction Cell: Each institute has to have an Industry interaction cell nt just for placements, but for curriculum development, co-teaching, support for live industry projects.
7. Innovation Cell: Every institute is encouraged to start an innovation cell thereby students get access to all laboratory and workshop facilities 24X7, creating a congenial and creative academic ambiance leading to better research and outcomes.
8. Entrepreneurship or incubator cell: Every institute is advised to start entrepreneurship cell and offer entrepreneurship courses for students to become job creators.

AICTE has also emphasized on using institutional facilities to run skill development programmes for school drop outs during evenings and make use of facilities effectively.

Last but not the least, AICTE has started an exercise to create a perspective plan for the nation whereby we just do not start colleges in any area, but in only those areas where new technologies are likely to come up and hence jobs are going to be crated, thus well planned manpower useful to society is created

4 Conclusions : These are challenging times. Nation is changing. Technical education plays an important role in the economy of a nation. Being a regulator and facilitator, AICTE has started off a large number of initiatives, the positive outcome of which has started becoming visible. There is a lot of concerted effort required to achieve the desired goal of making India's technical education system which is already the largest in the world into the best in the world.

5. References :

1. **Munjal, M. L; Rao, K. N; Sahasrabudhe, A. D.** (1987) Aeroacoustic Analysis of Perforated Element Mufflers, *Journal of Sound and Vibration,* Vol.114, No. 2, pp 173-188.

2. **Kulkarni, P. G; Sahasrabudhe, A. D;** (2013) Application of Wavelet Transform for Fault Diagnosis of Rolling Element Bearings, *International Journal of Scientific and Technological Research*, Vol. 2. No. 4, pp 138-148

3. **Hujare, P. P; Sahasrabudhe, A. D;** (2014) Experimental investigation of damping performance of visco-elastic material using constrained layer damping treatment, *Procedia Materials Science*, Vol. 5, pp 726-733

4. **Sahasrabudhe, A. D; Ramu, S. A; Munjal, M. L.** (1991) Matrix Condensation and Transfer Matrix Techniques in the 3-D Analysis of Expansion Chamber Mufflers, *Journal of Sound and Vibration,* Vol.147, No. 3, pp 371-392.

5. **Sahasrabudhe, A. D; Munjal, M. L; Ramu, S. A.** (1992) Design of Expansion Chamber Mufflers Incorporating 3-D Effects, *Noise Control Engineering Journal*, Vol. 38, No.1, pp 27-38.

6. **Sahasrabudhe, A. D; Munjal, M. L; Ramu, S. A.**(1995) Analysis of Inertance due to Higher Order Mode Effects in Sudden Area Discontinuities, *Journal of Sound and Vibration,* Vol.185, No. 3, pp 515-529.

7. **Sahasrabudhe, A. D; Risbood, K. A; Dixit, U. S.** (2003) Prediction of Surface Roughness and Dimensional Deviation by Measuring Cutting Forces and Vibrations in Turning Process, *Journal of Materials Processing Technology,* Vol.132, No. 1-3, pp 203-214.

8. **Vadiraja, D. N; Sahasrabudhe, A. D.** (2009) Vibration Analysis and Optimal Control of Rotating Pre-twisted Thin-walled Beams using MFC Actuators and Sensors, *Thin Walled Structures,* Vol. 47, No. 5, pp 555-567.

9. **Ramachandran, K; Sahasrabudhe, A. D; Nadkarni, S; Dixit, U.S; Kalaga, R.** (2002), Development of Mobile Road Maintenance System, *Border Roads Organization.*

10. **Sahasrabudhe, A. D and others** (2003) Setting up of Technical Backup Unit at IIT Guwahati for R and D Interface with Khadi and Village Industries Sector.

11. **Shekhar, H; Sahasrabudhe, A. D;** (2010) Maxwell Fluid Model for Generation of Stress-Strain Curves of Visco-Elastic Solid Rocket Propellants, *Propellants, Explosives, Pyrotechnics*, Vol. 35 No. 4, pp 321-325

Annals of the Indian National Academy of Engineering
Vol. XV, April 2018

Acoustical Materials For Noise Control

A. R. Mohanty[1]

Abstract : Some of the major achievements of the research group of the author in noise control are presented here. This paper begins with a brief about sound pressure levels and introduces the concepts of path noise control. The three basic properties of acoustical material are discussed along with a brief on the measurements of the same. A recent development in the use of natural materials for noise control and a case study of noise control in a domestic dryer using natural material is discussed. This is followed by the use of micro-perforated panel for improvement of sound absorption at low frequencies. The use of sonic crystals for noise control is also discussed.

Keywords : Sound absorption, jute, noise reduction, micro perforation, sonic crystals.

1 Introduction

Worldwide there is an increasing demand for quieter products and environment, due to global competiveness amongst manufactures, adherence to regulations and customer awareness. Manufacturers are developing products apart from being efficient, which have a long life cycle, low carbon foot print and also better in its sound quality. The sound quality is the study between the actual measured sound parameters through a set of pre-defined metrics to the actual human perception. Sound Pressure Level measured in the decibel scale, weighted by the A weighting at different octave bands measured in dBA scale is accepted through the industry as an accepted parameter to quantify the noise of a product. Of course, it has to be measured in a free-field environment typically at a distance of 1 m from the product. A free-field environment is chosen so that reflections from the boundaries do not affect the measured SPL values. Though a better rating of the product noise evaluation is its sound power level (SWL) also represented in the decibel scale.

Sound, which a human being hears by its ears is actually a manifestation of the air molecule vibrations incident on the eardrum. A small fluctuating sound pressure level of 1 Pa RMS is large enough to produce a SPL of 94 dB at our eardrum. God has created our eardrum to be a very sensitive equipment having a high dynamic range and a non-linear frequency response. Actually the A-weighting function takes care of this non-linear response of the human ear. There are limits of sound pressure level to which a human being can be subjected for a particular duration.

In India, for a 8 hour period the human being must not be subjected to more than 90 dB. For an equivalent of exposure if the level is increased by 6 dB, the duration should be reduced to 4 hours and so on.

A human being thus exposed to a high level of SPL at 150 dB to even few seconds is note permissible, and would create a permanent hearing damage. The threshold of pain of a human being is to a level of around 150-160 dB. On the other hand of the hearing scale, the faintest sound a human being can hear is given as 0 dB, which corresponds to a sound pressure of 20×10^{-6} Pa.

Noise, which we hear from machineries is due to the vibro-acoustics transfer of mechanical energy from the machine either through the medium of solid, liquid and gas or a combination of the media, finally onto the vibrations of our eardrum.

[1]Department of Mechanical Engineering, IIT Kharagpur, Kharagpur 721302

Abstract : Some of the major achievements of the research group of the author in noise control are presented here. This paper begins with a brief about sound pressure levels and introduces the concepts of path noise control. The three basic properties of acoustical material are discussed along with a brief on the measurements of the same. A recent development in the use of natural materials for noise control and a case study of noise control in a domestic dryer using natural material is discussed. This is followed by the use of micro-perforated panel for improvement of sound absorption at low frequencies. The use of sonic crystals for noise control is also discussed.

Keywords : Sound absorption, jute, noise reduction, micro perforation, sonic crystals.

1 Introduction

Worldwide there is an increasing demand for quieter products and environment, due to global competiveness amongst manufactures, adherence to regulations and customer awareness. Manufacturers are developing products apart from being efficient, which have a long life cycle, low carbon foot print and also better in its sound quality. The sound quality is the study between the actual measured sound parameters through a set of pre-defined metrics to the actual human perception. Sound Pressure Level measured in the decibel scale, weighted by the A weighting at different octave bands measured in dBA scale is accepted through the industry as an accepted parameter to quantify the noise of a product. Of course, it has to be measured in a free-field environment typically at a distance of 1 m from the product. A free-field environment is chosen so that reflections from the boundaries do not affect the measured SPL values. Though a better rating of the product noise evaluation is its sound power level (SWL) also represented in the decibel scale.

Sound, which a human being hears by its ears is actually a manifestation of the air molecule vibrations incident on the eardrum. A small fluctuating sound pressure level of 1 Pa RMS is large enough to produce a SPL of 94 dB at our eardrum. God has created our eardrum to be a very sensitive equipment having a high dynamic range and a non-linear frequency response. Actually the A-weighting function takes care of this non-linear response of the human ear. There are limits of sound pressure level to which a human being can be subjected for a particular duration.

In India, for a 8 hour period the human being must not be subjected to more than 90 dB. For an equivalent of exposure if the level is increased by 6 dB, the duration should be reduced to 4 hours and so on.

A human being thus exposed to a high level of SPL at 150 dB to even few seconds is note permissible, and would create a permanent hearing damage. The threshold of pain of a human being is to a level of around 150-160 dB. On the other hand of the hearing scale, the faintest sound a human being can hear is given as 0 dB, which corresponds to a sound pressure of 20×10^{-6} Pa.

Noise, which we hear from machineries is due to the vibro-acoustics transfer of mechanical energy from the machine either through the medium of solid, liquid and gas or a combination of the media, finally onto the vibrations of our eardrum.

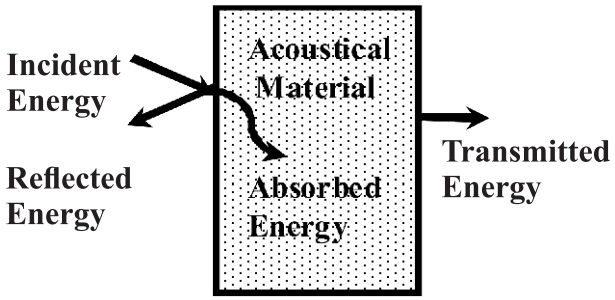

Figure 1: Phenomenon of sound interaction with an acoustical material.

2.1 Measurement of sound absorption coefficient

The sound absorption coefficient of materials can be estimated by measuring the surface impedance of the material. The standing wave tube was initially used to measure such impedances, however it is time taking since the measurements have to be done for one frequency at a time. However in 1977, Seybert and Ross in their path breaking paper reported a new technique of measuring the surface impedance of a material

using a two microphones in a plane wave tube with a random excitation [Seybert and Ross (1977)]. Based on this paper the ASTM E-1050 standard for the same was developed. The author as a graduate student was involved in the round robin test of materials developed for sound absorption using such a plane wave tube. Commercial systems have since been made available in the market. The author has developed the ACUPRO system for determination of sound absorbing materials [Mohanty, Seybert and Strong (1991)]. Since then the author has developed such systems and commercially sold to many organizations in India through IIT Kharagpur. A view of the impedance tube used for measuring sound absorbing properties of materials developed by the author at IIT Kharagpur is shown in Fig. 2.

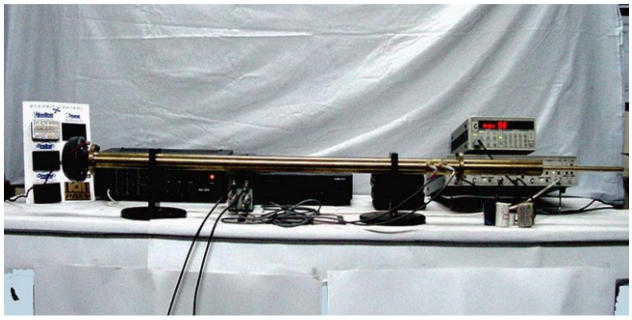

Figure 2 : Impedance tube developed at IIT Kharagpur

There are other methods also available for measurement of sound absorption co-efficient for random incident waves. However for the sake of comparison of sound absorbing materials, NRC value of the material suffices.

3 Sound Barrier Materials

Sound barriers are materials which block sound, thus have a high transmission loss. These materials are heavy. The transmission loss is a function of frequency of the incident sound wave and the density of the material. With every doubling of the frequency the transmission loss of a material increases by 6 dB. And also with every doubling the thickness of material the transmission loss also increases by 6 dB. There is a frequency at which there is a significant dip in the transmission loss of the material, this frequency is known as the coincident frequency. While selecting materials for noise attenuation the allowable range of noise reduction must be less than the coincident frequency, which depends on the material elasticity and thickness. Few examples of sound barrier materials used for noise control are heavy thick sheet metal, loaded elastomer or bitumen sheets and concrete.

3.1 Measurement of sound transmission loss

From an extension of the two microphone, random excitation theory developed by Seybert and Ross in 1977, Song and Bolton have developed a four microphone method in a plane wave impedance tube to find the sound transmission loss of the material as well as other sound propagation properties of the material like its characteristic complex acoustic impedance ; complex speed of sound in the material and its complex density [Song and Bolton, (2000)]. An ASTM and ISO standard now exist for measuring the transmission loss in an impedance tube and also of large panels using the sound intensity method by measuring using a reverberant room and an anechoic chamber.

At the laboratory level the author has developed a test setup to find out the transmission loss of small samples [Fatima and Mohanty (2011)]. The sound transmission loss is also represented with a single number given as a STC (Sound Transmission Class) Rating.

4 Damping Materials

From the theory of vibrations it is known that the vibration response at a system's response can be brought down by increasing the damping. Usually damping patches are put on areas having high displacements at resonance. These areas are the anti-node points for the particular mode of vibration [Mohanty and Fatima (2013)].

4.1 Measurement of damping factor of materials

The damping factor in materials can be found by the traditional log-decrement method. For determining damping factor at a particular mode of vibration the half-power bandwidth method

can be used. Many commercial analyzers are available based on the Oberst-Beam Method and ASTM standards also exist for such measurements. The commercially available dynamic mechanical analysers (DMA) can be used for such measurements and they can also be used to find out damping factors in materials at different temperatures.

5 Natural Materials

With growing concerns towards the environment, designers are looking forward to the use of environmental friendly materials for product development. Though the aim is not to replace completely the metals or synthetic materials by these environment friendly materials. For the former have high strength and long life. However in few applications the use of composites made up of a combination of natural fiber based materials and a binder have many advantages. Like they are environmental friendly, less weight, economical and in few places are also available abundantly in nature. Natural based fiber materials like flax, ramie, hemp, banana fiber, coir, jute, cotton can be used to produce biocomposites which have many industrial applications. These biocomposites are being used to manufacture machinery enclosures, furniture, highway crash barriers, geo-textiles, as reinforcement in concrete, apparels, bags, yarns, carpets and building materials. However, they have a strong potential to be used for noise control applications as well [Mohanty and Fatima(2013); Fatima and Mohanty (2012)].

Biocomposites made of natural materials are an excellent replacement for the above materials since they are abundantly available in nature and are economic to process. In order to use biocomposites for noise control their two important acoustical properties need to be known, normal specific sound absorption coefficient and the sound transmission loss. Another important property of the material which is used to control the vibration of the structure generating noise is its damping factor. There exist standards by which all the above properties can be measured in the laboratory.

Natural fibers have recently been utilized for making composite materials and they offer several advantages over synthetic materials. While these natural fibers can be extracted from many sources such as sisal, jute, coir, flax, hemp, pineapple and banana; jute has been promoted as the most readily available, environment friendly, abundant, economic and bio-renewable source. It is specifically cultivated in large quantities in the eastern part of India and in Bangladesh. It is a lignin-cellulose fiber which is composed primarily of the plant materials; cellulose (major component of plant fiber) and lignin (major components wood fiber). It falls into one of the bast fiber category (fiber collected from bast or skin of the plant) along with kenaf, industrial hemp, flax (linen), ramie and so forth.

Jute is used in various forms for noise control applications. The raw jute fiber after cleaning are used to produce jute yarn by a spinning process. The jute yarn is then weaved to make jute textile or cloth. Stacks of jute yarn laid in a random or a definite sequence are pressed under temperature to produce jute felt. The jute felt/fiber in turn can be chemically treated with a bonding agent usually natural rubber latex as a resin and pressed under certain temperature to form jute based biocomposite panels. In few instances the raw fibers after appropriate processing can be chopped and used as fills in noise control blankets and pads. In jute mills where jute based textiles are manufactured, during the trimming operations of these textiles many waste trims are produced. These trims can be used as acoustical fills as well, for noise control.

5.1 Acoustical Properties of Jute Materials

The properties of sound absorbing coefficient and transmission loss is measured as per the existing test standards. However there has been a empirical model developed by Delany and Bazley, which has been used to estimate the sound absorbing properties of jute materials by using its flow resistivity which is relatively simple to measure in comparison to the acoustical impedance tube [Delany and Bazley (1970); Fatima and Mohanty (2016)].

For the sake of completeness the empirical equation of Delany and Bazley used in the present study to predict the characteristic impedance, Z_c and complex wave number, k' of the natural fibrous material is given in Eqs. (1) and (2), respectively.

$$Z_c = \rho c\left[1+0.586\left(\frac{f}{\sigma}\right)^{-0.75} - j0.768\left(\frac{f}{\sigma}\right)^{-0.73}\right] \quad (1)$$

$$k' = \frac{\omega}{c}\left[1+0.0857\left(\frac{f}{\sigma}\right)^{-0.70} - j0.1749\left(\frac{f}{\sigma}\right)^{-0.59}\right] \quad (2)$$

where ρ is the density of the ambient air, c is the speed of sound in ambient air, σ is the flow resistivity and f is the frequency. All the quantities given in Eqs. (1) and (2) are in SI units. The above equations are used for fibrous materials which satisfy the relationship $0.01 < \frac{f}{\sigma} < 1.00$

For a bulk sound absorbing material of thickness d, the surface impedance of the material is given as per Eq. 3

$$Z_{in} = -jZ_c \cot(k'd) \quad (3)$$

Then, from the relationships given in Eqn. (4) between the complex reflection co-efficient, R and the surface impedance of the material, the normal specific sound absorption co-efficient, α can be calculated using Eqn. (5).

$$Z_{in} = \rho c\frac{1+R}{1-R} \quad (4)$$

$$\alpha = 1-|R|^2 \quad (5)$$

In a recent work the coefficients in Eqn. (1) and (2) have been updated for jute material by the Particle Swarm Optimization technique [Bansod and Mohanty (2017)]. The expressions thus developed can be used for estimating the impedance of the boundary where these materials are used as sound absorbers. A similar numerical work, has been done by the author at the beginning of his academic career where the measured acoustical impedance of a headliner material was used to reduce the noise of a truck cabin [Mohanty, St. Pierre, Narayanasami (2000)].

5.2 Manufacturing of jute composites

The natural rubber based jute composites are prepared as per the following procedure. Jute felt of 400 gsm(gram per square meter) specimens are dried in an oven for 1hour to remove the water content in the specimen. The jute felt are treated with 1% NaOH (alkali) solution for 1 hour. This alkali treatment is used to remove the impurities in the specimens. These alkali treated jute felts are again washed by water till they become alkali free. The washed jute felts are dried in an oven at 80^0C for an hour. The dried felt is then dipped in 1% (by volume) natural rubber solution for 1 hour. Excess rubber latex is drained off and the rubber treated jute felts are dried in a dry room for 1 hour. Jute based natural rubber latex composite is prepared by compressing ten pieces of natural rubber treated jute felts in a hydraulic press at 140^0C with a load of 8 tonne for 15 minutes. Similarly 2.5% natural rubber, 5% natural rubber and 10% natural rubber jute composites are prepared keeping all other parameters same. In all the sample preparations, natural rubber is used as bonding agent between the interfaces of the fibers [Mohanty and Fatima (2015)]. Fig. 3 shows a view of the hydraulic press used for fabricating the jute composite panels by compression moulding.

Figure 3: A 300 Ton hydraulic with a chemically treated jute felt on the platen for compression moulding.

6 Noise control applications

Our research group at the Indian Institute of

Technology Kharagpur has used the developed jute based materials in several home appliances like refrigerators, vacuum cleaners and domestic dryer [Fatima and Mohanty (2012); Mohanty and Fatima (2010); Fatima,Mohanty, Paradhe, and Tamizharasan (2013)]. The group has also used these materials for noise control in major automotive components. Some of this work is proprietary in nature and are not disclosed in details. However for the benefit of the readers of this article a case of noise control in a domestic clothes dryer and an application in architectural acoustics is described in the following sections

6.1 Natural material for building acoustics

In a design of acoustic space in the interior of a building, the acoustic clarity of the room is characterized by its reverberation time, apart from the background noise level. The reverberation time is defined as the time taken for the noise level in the room to decrease by 60 dB. Different acoustics space like a concert hall, class room, office space, cinema hall, indoor sports gymnasium have different requirements of reverberation time. This reverberation time depends on the amount of absorption present in the room and is a function of the surface area and volume of the room, which is given by the well known Sabine's equation [Mohanty and Fatima(2016)]. We have also used jute based ceiling tiles in our laboratory for controlling the reverberation time. A view of the laboratory ceiling is shown in Fig. 4.

Figure 4: Jute based fibers used as ceiling tiles

6.2 Noise Control in a domestic clothes dryer

The physical dimensions and mass of the clothes dryer in which noise control measures were implemented are 530 mm × 600 mm × 720 mm and 26 kg respectively. Motor rating and heater rating are 300 W and 1.8 kW, respectively. The drum used inside the dryer for placing the wet clothes is epoxy coated; a maximum of 5.5 kg of wet clothes can be dried in this dryer in an operation cycle. The dryer has a safety cut-off which limits the temperature inside the drum to 105^0C. All the experimental trials were done in the clothes dryer while running empty.

For the noise source identification of the dryer a sound intensity based mapping was done using a two-microphone sound intensity probe. The measured sound intensity contours of the five surfaces of the dryer are given in Fig. 5. Overall sound power was measured in the frequency range of 31.5-8000 Hz at each of the grid points by a sound intensity probe which was held at distance of 150 mm from the dryer surface[10].

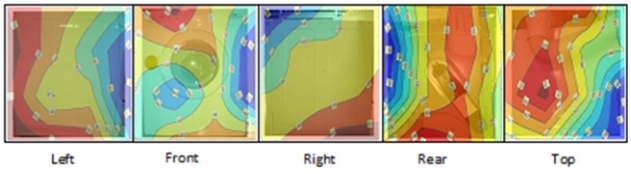

Figure 5: Sound intensity level in dBA of domestic dryer without acoustical treatment.

From Fig. 5, it is seen that the region around the motor driving the drum by a belt drive was the most dominating noise radiator, followed by the dryer exhaust at the rear top location. The overall sound intensity level at the region around the motor was 68.6 dBA and that around the dryer exhaust is 67 dBA

The application of jute based acoustical materials to the dryer was carried out for two configurations. In the first configuration, jute felt lining was applied to the rear inner wall of the outer shell of dryer as shown in Fig. 6. With such a treatment there was a marginal reduction to 68.7 dBA. In the next configuration all the inner walls were lined with 5 mm jute felt and the inner top was backed with a jute composite panel. There

was a reduction of 5.9 dB in the overall sound power level, and the overall sound power level reduced to 63.5 dBA. The octave band sound power spectra of the dryer with and without the jute material treatment is shown in Fig. 7.

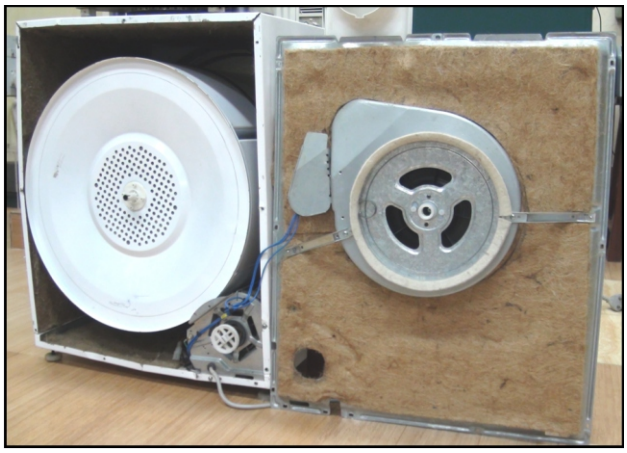

Figure 6: Inside view of the dryer shell with jute treatment.

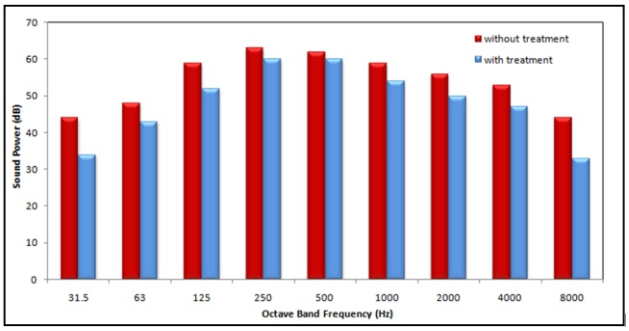

Figure 7: Octave band spectra of the radiated sound power of the dryer.

7 Emerging Areas of Research in Noise Control

Well developed mathematical models exist for the prediction of the sound absorption coefficient of porous material, based on their physical parameters like pore diameter, porosity, tortuosity, viscous and thermal characteristics length. Research is being done to develop porous materials through Even metal foams are being developed for sound absorption in harsh environment. 3D printing where these parameters can be varied to obtain the desired sound absorption. 3D printing is also being used to manufacture micro-perforated panel, where effective absorption can be obtained and low frequency absorption can be improved by maintain a cavity depth. Research into acoustical metamaterials and in particular in the human hearing frequency range the development of phonic crystals for sound attenuation. Some of the work done at IIT Kharagpur in this area is given in the following sub sections.

7.1 Microperforated panels

Micro-perforated panel (MPP) surrounded by air is modeled using the Maa's model [Maa (1987)]. The perforated holes are in the submillimetric size and considered as a parallel connection of the perforated holes. Each perforated hole can be assumed as a short tube. The common layout of MPP with the air back and rigid backing is shown in the Fig. 8.

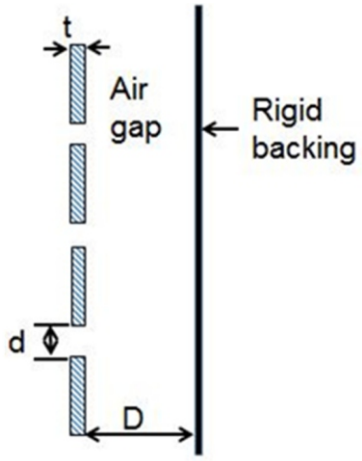

Figure 8: MPP backed by air cavity

Models exits for sound transmission through such short tubes. These models were further considered as short tube compared to the wavelength and taking into account the viscous effect inside these short tubes. The specific impedance of the short tube is calculated as the ratio of pressure difference Δp on both side of the thin plate and particle velocity $\bar{u}$ through the cross section.

$$z = \frac{\Delta p}{\bar{u}} = j\omega\rho_{air} t\left[1-\frac{2}{\sqrt{-j}\beta}\frac{J_1\left(\sqrt{-j}\beta\right)}{J_0\left(\sqrt{-j}\beta\right)}\right]^{-1} \quad (7)$$

where ω is angular frequency, ρ_{air} is mass density of air, t is the panel thickness, J_1 and J_0 are the Bessel functions of first kind and of order one and zero respectively. $\beta = d\sqrt{\omega\rho_0/4\eta}$ is the perforation

constant, where η is dynamic viscosity of air and d is the hole diameter. The perforation constant β is the ratio of radius to the thickness of viscous boundary layer inside the hole. In case of perforated panel, end correction should be applied to the real and imaginary part of the transfer impedance. The end correction for resistance term takes care of the frictional losses on the surface of the plate. The end correction for reactance term considers oscillation of the mass. This effect can be considered as effective additional tube length. The end corrections for resistance and reactance part are $0.5\sqrt{2\omega\eta\rho_0}$ and $8d/3\pi$ respectively. According to the Maa theory, the impedance of the MPP is given by Eqn. 8.

$$Z_{mpp} = r + j\omega m \tag{8}$$

$$r = \frac{32\eta t}{\sigma \rho_{air} c d^2}\left(\sqrt{1+\frac{\beta^2}{32}} + \frac{\sqrt{2}}{32}\beta\frac{d}{t}\right) \tag{9}$$

and $m\omega$ is the normalized specific acoustic reactance and given by

$$m = \frac{t}{\sigma_{MPP} c}\left(1+\frac{1}{\sqrt{9+\frac{\beta^2}{2}}}+0.85\frac{d}{t}\right) \tag{10}$$

where$t$ and d is the thickness and hole diameter of MPP respectively, η is the coefficient of viscosity and ρ_{air} is the mass density of air. Perforation ratio σ_{MPP} for MPP is defined as the ratio of perforated area to the total area of MPP.

The sound absorption mechanism of porous material and MPP is different. Porous material absorbs sound by viscous and thermal losses whereas mechanism of sound absorption of MPP is of resonant type. When MPP is backed with the porous material layer, it gives sound absorption over broader frequency range, but still it remains resonant type. Fig. 9 shows the experimental sound absorption results of the sound absorber composed of 25 mm thick jute felt layer with and without MPP. It is clear that the addition of MPP over jute felt layer significantly enhances the sound absorption over broader frequency range. Therefore, MPP helps to improve the sound absorption performance in the low to mid-frequency region. As the sound absorption performance of MPP can be tuned, it is possible to shift the sound absorption peak towards lower frequencies. Hence, MPP provides good results in low frequency sound absorption.

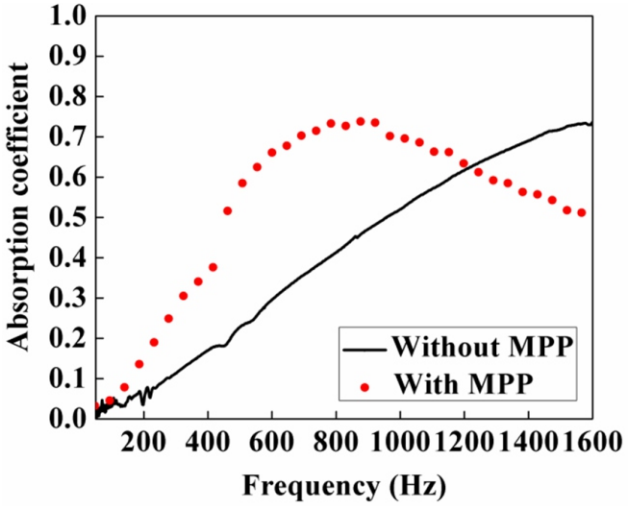

Figure 9: Measurement of normal incidence sound absorption performance of jute felt with and without MPP

7.2 Sonic crystals for noise control

Sonic crystals are noise barriers with periodic arrangement of sound scatterers arranged in different lattice configurations and embedded in a matrix or host material. The scatterers have high acoustical impedance compared to the matrix which is generally a fluid medium, e.g. air, water.The periodicity of the scatterers can be along one, two or three dimensions forming 1-D, 2-D and 3-D Sonic crystals respectively. The scatterers are responsible for multiple scattering of the reflected and incident sound waves. A numerical modelling of a scatterer was done (Panda and Mohanty, 2017)

The pressure variation across the Sonic crystal at different frequencies of 1810 Hz, 3000 Hz, 5250 Hz and 7000 Hz are shown in Fig. 10 (a), (b), (c), (d) respectively. Out of the four frequencies 1st and 3rd frequencies happen to fall inside 1st and 4th band gaps. Sound attenuation can be clearly observed at those frequencies in Fig. 9 (a) and (c)

respectively. For the other two frequencies, which lie outside the band gaps, sound wave passes through the crystals with not much attenuation.

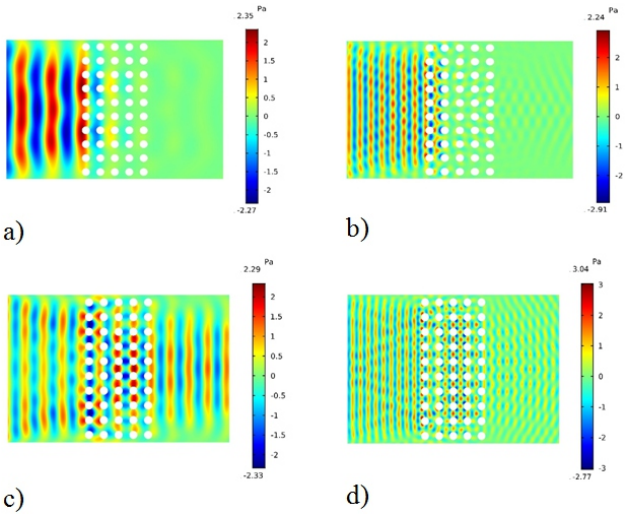

Figure. 10 : Pressure variation at different frequencies of (a) 1810 Hz (b) 3000 Hz (c) 5250 Hz (d) 7000 Hz.

8 Conclusions

Noise control many a times are an after thought after the design has been completed. The noise control specialist is thus with a dilemma whether to control the source noise or the path noise control. Designers seldom allow any design modifications at the source at a later stage, thus the noise control specialist is left with providing acoustical treatments in the path to bring about noise control. Predominantly two types of acoustical materials are preferred for noise control being either the sound absorbing material and sound barrier material. Very commercially viable natural materials are being developed for noise control as developing them either as absorbers or barriers. A recent development has been in the use of layered materials with micro-perforated facing to improve the low frequency sound absorption, which would otherwise require an increased thickness of the traditional sound absorbing materials. Research in acoustic metamaterials and sonic crystals have also demonstrated that by bringing about scattering and reflections through a geometric arrangements of rigid bodies significant sound transmission loss at selected frequencies can also be obtained. We at IIT Kharagpur are continuing our research in all the above mentioned fronts for noise control.

9 References :

1. **Bansod, P. V; Mohanty, A. R.** (2016), Inverse acoustical characterization of natural jute sound absorbing material by the particle swarm optimization method, Applied Acoustics, Vol. 112, pp. 41-52.

2. **Delany, M. E; Bazley, E.N.** (1970) Acoustical properties of fibrous absorbent materials, Applied Acoustics, Vol. 3,No. 2, pp.105-116.

3. **Fatima, S; Mohanty, A. R.** (2011) Acoustical and fire retardant properties of jute composite materials. Applied Acoustics, Vol. 72, No.2-3, pp 108-114 .

4. **Fatima, S; Mohanty, A. R.** (2012), Noise control of home appliances the green way, Noise and Vibration Worldwidepp. 26-34.

5. **Fatima, S;Mohanty, A. R; Paradhe, S; Tamizharasan, S. T.** (2013), Vibro-Acoustic Source Path Characterization of a Domestic Refrigerator, Proceedings of the 20th International Congress on Sound and Vibration Bangkok, Thailand, July 7-11.

6. **Fatima, S; Mohanty A. R.** (2015), Noise Control Using Green Materials, S&V Sound and Vibration Instrumentation Issue.

7. **Fatima, S; Mohanty, A. R.** (2016), Acoustical Characterization of Bulk Natural Fibrous Material using Flow Resistivity, Inter NOISE 2016, 21-24 August, Hamburg, Germany.

8. **Maa, D.Y.** (1987), Micro-perforated wide band absorber, Noise Control Engineering Journal Vol. 29 pp. 77-84.

9. **Mohanty, A. R; Seybert, A. F; Strong, W. F.** (1991), Acoustical Property Determination by a PersonalComputer System, Proceedings of Noise-Con 91, New York, pp. 597-602.

10. **Mohanty, A. R; St. Pierre B. D; Suruli-Narayansami, P.**(2000), Reduction of Structure-Borne Noise in a Truck Cab Interior by Numerical Techniques, Applied Acoustics, Vol. 59, No. 3, pp.1-17.

11. **Mohanty, A. R; Fatima, S.** (2010), Jute as an acoustical material for noise control of a domestic dryer, Proceedings of the 17th International Congress on Sound and Vibration, Cairo, Egypt, July 18-22.

12. **Mohanty, A. R; Fatima, S.** (2013), An Overview of Automobile Noise and Vibration Control, Noise and Vibration Worldwide, Vol 44, No. 6, pp. 10-19.

13. **Mohanty, A.R; Fatima,S.** (2014) Bio composites for Industrial Noise Control in the book Bio composites : Fundamentals to Industrial Applications, Editors V. K. Thakur and M. Kessler.2014, CRC Press (ISBN:9781771880329).

14. **Mohanty, A. R; Fatima, S.** (2016), Improvement of interior acoustics and speech quality of small office using natural material , Inter NOISE 2016, Hamburg, Germany.

15. **Panda, D; Mohanty, A. R.** (2017), Sonic crystals for highway noise reduction, Proceedings of National Symposium on Acoustics, 28th-30th October.

16. **Seybert, A. F; Ross, D. F.** (1977), Experimental determination of acoustic properties using a two microphone random-excitation technique, Journal of Acoustical Society of America Vol.61, pp.1362–1370.

17. **Song, B.H; Bolton, J.S.** (2000), A transfer-matrix approach for estimating the characteristic impedance and wavenumbers of limp and rigid porous materials, Journal of Acoustical Society of America, Vol.107, No.3, pp.1131-52.

Acknowledgements

I take this opportunity to thank my former and present research students, many of whom have helped our group, study, develop and use natural materials for noise control. I thank all my government sponsors and industrial clients who have supported me in my many projects and have joined hands with me in developing and producing quieter products. Lastly, I am immensely indebted to my PhD adviser at the University of Kentucky, USA, Prof. Andrew F. Seybert, who introduced me to the wonderful branch of engineering dealing with Acoustics and Industrial Noise Control, who has now retired from active professional life and is enjoying his life sailing and reading philosophy and biology in his pastime.

Annals of the Indian National Academy of Engineering
Vol. XV, April 2018

The importance of group delay functions in speech synthesis

Hema A Murthy[1]

Abstract : Bigdata analytics has become ubiquitous and is being exploited in every domain. The availability of large amounts of speech data and compute resources, have enabled the development of practical speech based applications. Given the Indian context, where there are about 1600 languages, with alteast 30 languages spoken by more than 1 million people building speech based systems for Indian languages is a Herculean task.

The proposed paper presents an approach where the large data requirement can be relaxed by performing appropriate signal processing that is relevant to a given domain. Initially examples from various domains like network data, and music are presented. Then a specific example from speech technology, namely speech synthesis is detailed to emphasise the need for signal processing in tandem with machine learning for speech synthesis.

The quality of vocabulary independent speech synthesis is crucially dependent upon the availability of accurate phone boundaries. The boundaries in speech are not explicitly modeled by machine learning algorithms. A group delay based segmentation algorithm is used to segment the waveform at the syllable-level. Iterative Baum-Welch reestimation procedure at the syllable-level is used to estimate phone-boundaries. This hybrid system is used to develop a speech synthesis system for Tamil where it is shown that the word error rate, and pair comparison tests improve significantly.

1 Introduction

The proliferation of small form factor smart phones has led to a significant growth in speech based applications. Siri (Apple, USA), google voice assistant (Google,USA), Cortana (Microsoft, USA), Amazon alexa (Amazon, USA) are several applications of voice based technologies. All these applications permit two-way communication in English. Although google's voice assistant provides assistance in Hindi, there are hardly any speech recognition/speech synthesis applications that are available in Indian languages. High quality speech recognition and synthesis systems require huge amounts of training data, since both systems use machine learning extensively. Collecting a large amount of data (about 1000 hours for speech recognition, and about 100 hours for speech synthesis) is a difficult task. The primary reason for the poor quality of recognition/synthesis systems built from small amount of data is that the phone-models produced with small amounts data are inaccurate. Speech synthesis suffers significantly from this issue, as the consumer of the speech output from the system is a human. The problem with machine learning algorithms for speech labeling is that the boundaries between phones is not explicitly modeled. This leads to phone boundaries that are not accurate. This issue is addressed in this paper, by using a group delay based approach to speech segmentation. The signal based properties of various sounds are exploited during the segmentation process.

The rest of the paper is organised as follows. Section 2 briefly reviews the approach used in machine learning for various domains. It concludes with a possible modification to the machine learning algorithm for faster convergence. Section 3 gives an overview of

[1]Department of Computer Science and Engineering, IIT Madras, Chennai, India

speech synthesis systems, and Section 4 discusses the issues in building speech synthesis system using low resources. Section 5 explains the theory of group delay functions especially in the context of segmentation of speech utterances. In this Section we also describe our approach to segmentation of continuous speech using group delay functions. Section 6 discusses our experiments with various Indian languages. Section 7 concludes the paper.

2 Big Data Analytics

Heavy duty computers and GPUs, and the availabilty of data owing to connectivity, have made big data analytics a reality. A number of different applications ranging from text, natural language processing, image/vision, recommenders for music, recommendation systems for shopping and music, to speech recognition and synthesis have benefited extensively. Big data analytics is primarily based on statistical learning. The primary objective of these systems is to classify/predict from the current observations using past learned information.

Current data analytics systems consist of two phases, namely, the training and testing phase. Figure 1 shows the conventional approach to machine learning system. In the context of natural signals like speech, the speech varies signficantly from session to session, and speaker to speaker. In order to capture invariant features required as in speech recognition/ synthesis, these systems require a very large amount of data. Systems like google's voice assistant use thousands of hours of data training. Further, the training process is iterative as the problem of learning is not well-posed. Thus the data is repeatedly presented to the system so that robust models are ultimately learned.

The focus of the effort in my lab is to reduce the amount of data required for training by using clever signal processing based on the domain. Figure 2 shows the modification that is made to the conventional machine learning system. The objective of our work is to use information from the domain in the form of signal processing to make the training process efficient. Appropriate signal processing that is relevant for a given domain is performed. The features extracted are used in an iterative framework. Figure 3 shows the effect of intervention using signal processing

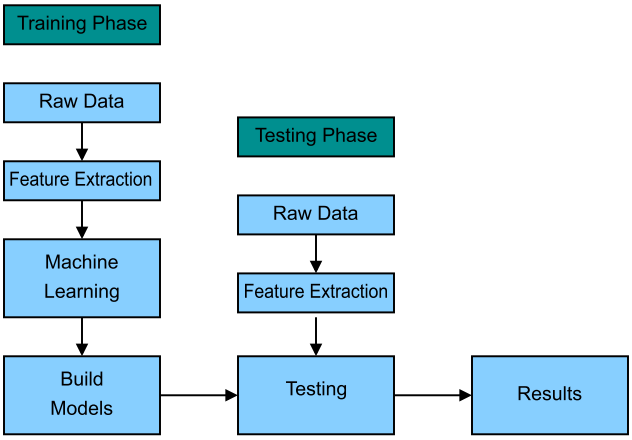

Figure 1: Overview of Steps: Machine Learning

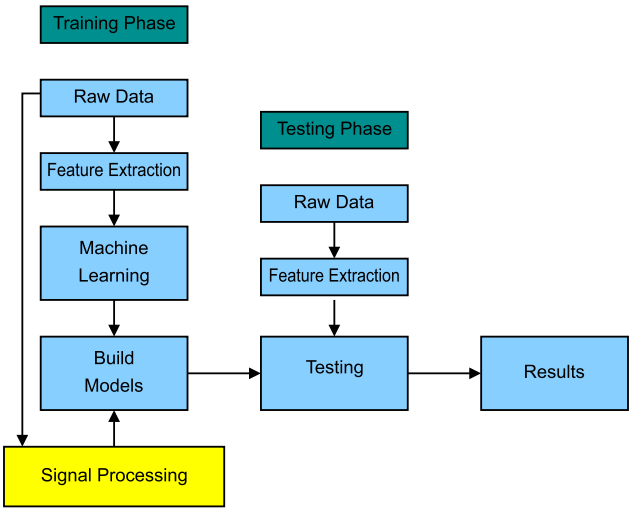

Figure 2: Overview of Steps : Event Drive Machine Learning

for detection of systematic downloading (Bhandari et al., 2014). A time series model of the data download statistics is made. The roots of the transfer function are obtained and a clustering is performed. It is observed that during normal traffic the system exhibits stable behaviour, while during a systematic download the system tends to be unstable (as indicated by red crosses in the Figure). A simple single class support vector machine (SVM) classifier is used to detect rogue downloads. Figure 4 shows another example where intervention using signal processing is used in the context of music(Sarala and Murthy,

2013). Machine learning is applied to the task of segmenting a continuous recording of a Carnatic music concert into items. In a Carnatic music concert, the number of applauses is much larger than the number of items. Signal processing and machine learning are first used to detect the location of applauses. Next each inter applause segment is identified as belonging to one of vocal, violin, composition, percussion solo (thaniavarthanam). Adjacent music segments are then merged using machine learning based melody matching.

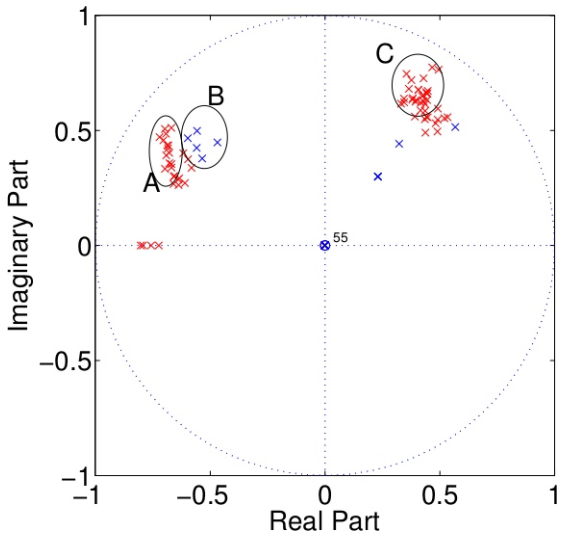

Figure 3: Signal processing and machine learning to detect systematic downloading.

The foregoing examples show the importance of signal processing in machine learning in the context of a specific task. In the following sections, we discuss in detail the use of signal processing to build practical speech synthesis systems using machine learning. Vocabulary independent speech synthesis requires accurate boundary information for building robust subword models. In particular, group delay functions are used for segmentation of speech into subword units. Machine learning models are built for the subword units.

3 Speech synthesis

Vocabulary independent speech synthesis is important for a number of applications, namely, readers for the visually challenged, readers for small form factor smart phones, and enablers for the language challenged. The objective of vocabulary independent speech synthesis systems is to produce natural sounding speech given a text as input. Two different types of text to speech synthesis systems are popular in the literature, namely, unit selection based concatenative speech synthesis systems(Black et al., 1998) and model based speech synthesis systems(Zen et al., 2009). In either system, large amount of data is collected from a native speaker from different domains. Vocabularly independence is ensured by building subword models, which generally correspond to phonemes in context 1. The waveforms and corresponding transcriptions are aligned at the phone-levels. Statistics of phones in various contexts are accumulated to learn models that are robust, and generalisable. During synthesis, a given text sentence is parsed into a sequence of subword units at the phone-level. In unit selection systems, a classification and regression tree (CART) is learned to determine the optimal sequence of waveforms that need to be concatenated to produce speech. In statistical parametric synthesis systems, a sequence of phone models are concatenated. An optimal sequence of vocal tract parameters and source parameters are generated. A vocoder converts these sequences to a waveform.

4 Issues in low resource speech synthesis

The primary issue with speech synthesis is the requirementof accurate phone boundaries, so that phone models can be built accurately. Owing to coarticulation between phones, it is difficult to obtain exact phone boundaries. As boundaries only at the level of a sentence are known, machine learning models fail to model the boundaries accurately when the amount of data available for

[1]Any language consists of about 35 consonants and 15-18 vowels.

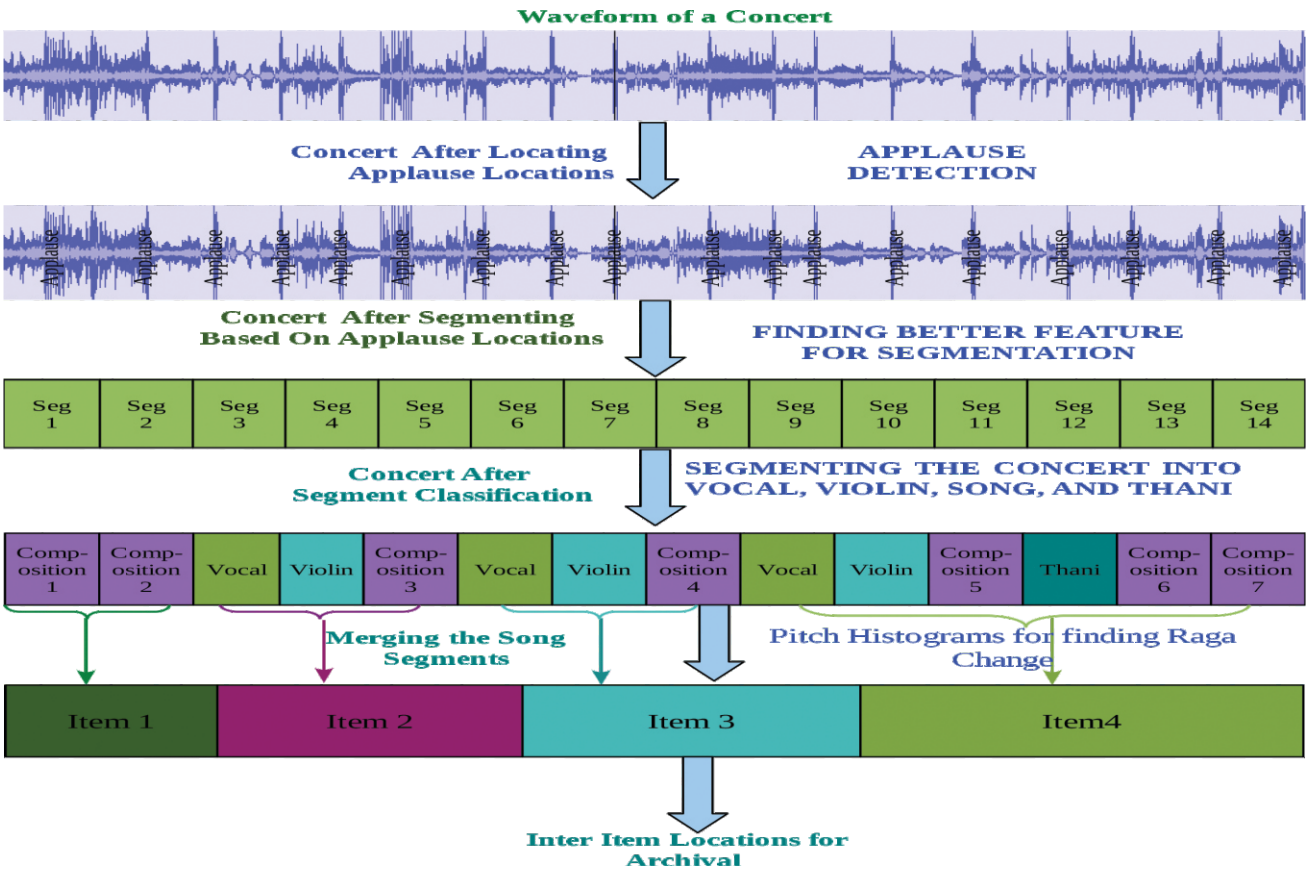

Figure 4: Applause detection and segmentation of a concert into items

training is small (see Figure 5). Observe that the waveform is made up of units that seem to have an onset, nucleus and a code (Figure 6). These units correspond to syllables which are the fundamental production units. Signal processing algorithms based on group delay processing are used to segment the waveform at the syllable level. The syllable-level waveforms are then further segmented at the phone level using machine learning. The phone-level waveforms from various contexts are then accumulated to build to robust phone models. The following Section briefly introduces group delay functions and its application to speech segmentation.

The nucleus is a sonorant, characterised by a vowel. A syllable is defined by the regular expression C*VC*, where C is consonant and V is vowel. From Figure 7, it is clear that the envelope of the short-term energy function consists of an onset, attack and decay. This characteristic is emphasised in group delay filtering as indicated in the Section 5.

5 Theory of group delay functions and its application to segmentation of speech

The time delay of the amplitude envelopes of various sinusoidal components through a device is defined as group delay. Group delay function of a discrete signal $x[n]$, $\tau_p(e^{j\omega})$ is defined as the negative derivation of Fourier transform phase and is given by(Murthy and Yegnanarayana, 2011)

$$\tau_p(e^{j\omega}) = -\frac{d\{\arg(X(e^{j\omega}))\}}{d\omega}. \quad (1)$$

ω is the angular frequency, $X(e^{j\omega})$ is the Fourier transform of the signal $x[n]$ and $\arg(X(e^{j\omega}))$is the phase function.

Taking logarithm on both sides,

$$\log X(e^{j\omega}) = \log(|X(e^{j\omega})|) + j\{\arg(X(e^{j\omega}))\} \quad (2)$$

$$\arg(X(e^{j\omega})) = Im[\log X(e^{j\omega})]. \quad (3)$$

where, Im corresponds to the imaginary part. The group delay function can be computed by (Oppenheim and Schafer, 1990; Yegnanarayana et al., 1984),

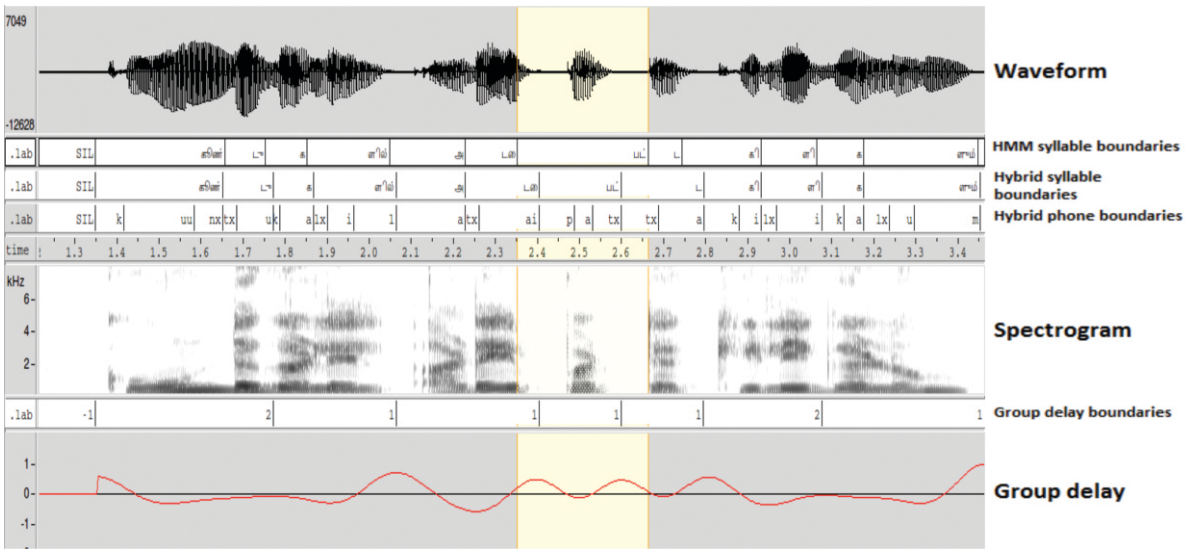

Figure 5: Example – without boundary correction

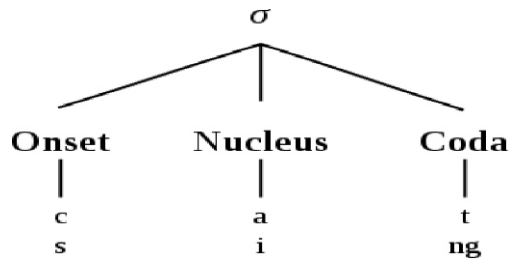

Figure 6 : Characteristics of a syllable

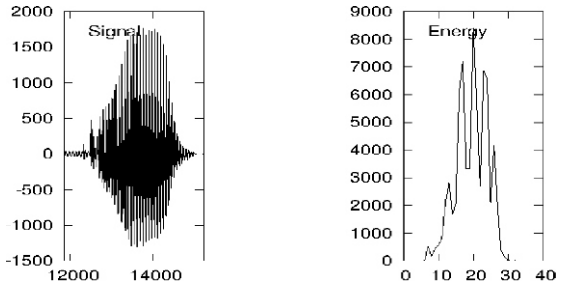

Figure 7 : The acoustic characteristics of a syllable

$$\tau(e^{j\omega}) = -Im\ \frac{d(\log(X(e^{j\omega})))}{d\omega} \qquad (4)$$

$$\tau(e^{j\omega}) = \frac{X_R(e^{j\omega})Y_R(e^{j\omega}) + Y_I(e^{j\omega})X_I(e^{j\omega})}{|X(e^{j\omega})|^2} \qquad (5)$$

where the subscripts R and I denote the real and imaginary parts, respectively. $X(e^{j\omega})$ and $Y(e^{j\omega})$ are the Fourier transforms of $x[n]$ and nx[n], respectively. Owing to the presence of $|X(e^{j\omega})|^2$ in the denominator of 5, the group delay function is only defined for minimum phase systems. Figure 8 shows a system with two poles, and the corresponding magnitude and group delay spectra. It can be shown for minimum phase systems (Sebastian et al., 2016) that the group delay function have a higher resolution compared to that of the magnitude spectrum. This is illustrated in Figure 9, where decay rate of group delay function and that of the magnitude is shown for a single pole system. From the Figure it can be seen that the group delay function decays faster than that of the magnitude spectrum.

Figure 10 gives the flow chart for group delay based syllable segmentation of speech. The short-term energy function of a speech utterance is computed. This function is a positive function. This is considered as magnitude spectrum, and symmetrised. This signal is then inverted to make the valleys peaks and viceversa. Minimum phase group delay processing via the root cepstrum shows gives the syllable boundaries.

The syllable boundaries and the text are matched first. Iterative boundary correction is performed

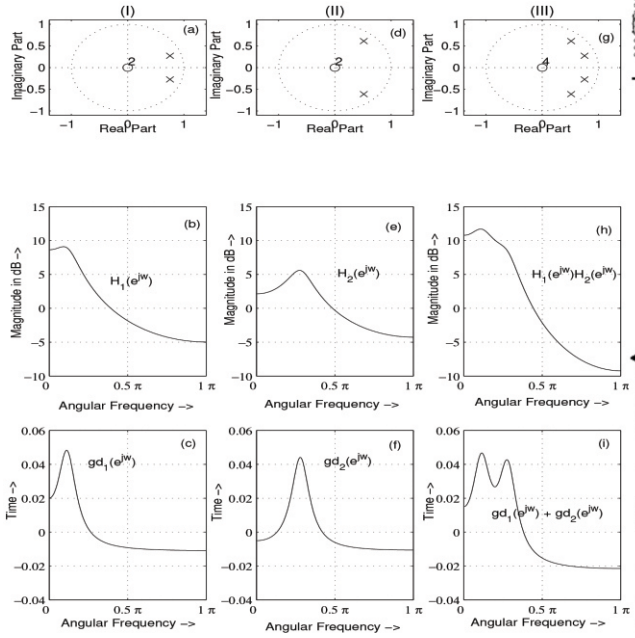

Figure 8 : Resolving power of the group delay spectrum : z-plane, magnitude spectrum and group delay spectrum I) a pole inside the unit circle at (0:8; π8), II) a pole inside the unit circle at (0:8; π4) and III) a pole at (0:8; π8) and another pole at (0:8; π4), inside the unit circle.

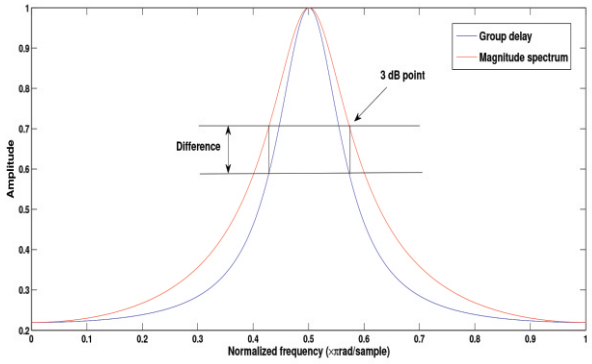

Figure 9: Comparison of group delay spectrum and magnitude spectrum for a single pole.

in the hidden Markov model-deep neural network framework (Povey et al., 2011). Segmentation at

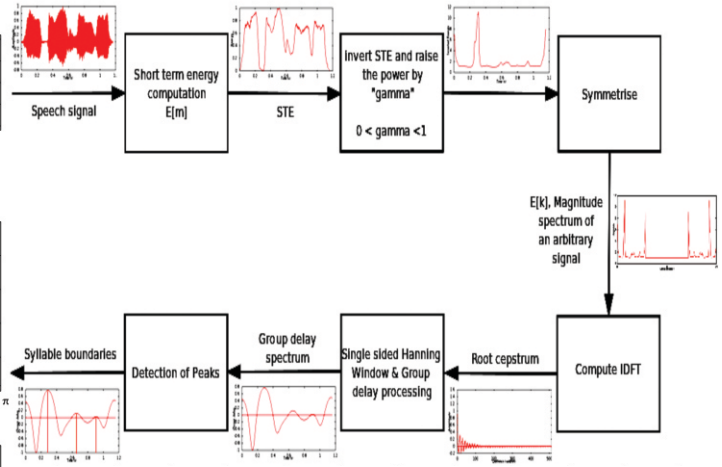

Figure 10: Steps involved in group delay segmentation algorithm for obtaining syllable boundaries

the phone level is obtained using embedded Baum-Welch reestimation at the syllable level. The phone level segments are used to build robust phone models. Using these models phone level alignments are obtained for a given utterance of speech. Figure 11 compares the segmentation at the phone level obtained using the baseline HMM segmentation and hybrid segmentation. This figures shows the corrected boundary for Figure 5.

6 Experiments

Experiments are performed using the database available at http://www.iitm.ac.in/donlab/tts/ for Tamil. The segmentation given by the hybrid method is compared with that of the conventional HMM based method. Phone-based HTS systems were built for Tamil. Subjective evaluations were performed on these TTS systems. Semantically unpredictable sentences (SUS) were synthesised, and the listeners were asked to transcribe the same. Word error rates (WER) were obtained, and it was observed that the WER for hybrid segmentation (Table 1) is lower than that of the conventional method.

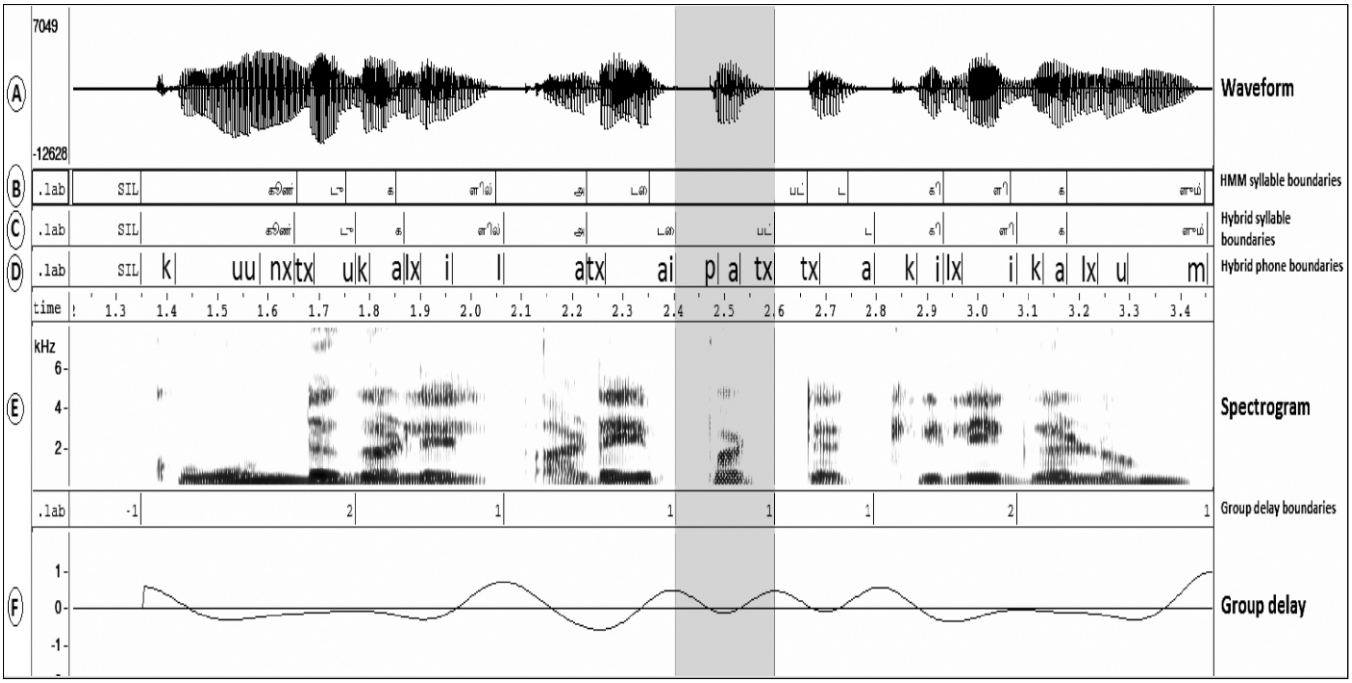

Figure 11: Comparison of baseline HMM segmentation with hybrid segmentation

Table 1 : Comparison using WER

System	WER
HTS - Phone (HMM Segmentation)	4.04%
HTS - Phone (Hybrid Segmentation)	1.01%

Pair comparison (PC) test (Salza et al., 1996) was also performed. For this comparison, the HTS system built with the hybrid segmentation method is referred to as "A" and the HTS system built with HMM based segmentation is referred to as "B". The results of PC test are shown in Table 2.

Table 2 : Pair comparison using tests

HTS - Phone		
A-B	B-A	A-B+B-A
70	15	77.5

From the Table 2, it is evident that the hybrid system is preferred. The proposed automatic hybrid segmentation algorithm, and additional new spectral cues are used in the HMM-DNN framework to build speech synthesis systems for 13 different Indian languages. Different synthesis systems are available at http://www.iitm.ac.in /donlab/tts/.

7 Conclusions

The objective of this work is show the importance of knowledge based signal processing in machine learning. The work presented in this paper shows that domain knowledge enables better convergence of machine learning algorithms for various tasks. In particular, we take the case of speech synthesis and show that use of signal processing in tandem with machine learning enables good quality TTS systems even for low resource languages.

Acknowledgements

I would like to thank Prof. B Yegnanarayana for introducing me to the world of group delay functions. I would like to thank all my current and past research scholars for helping me along the way through my journey in research, and believing in the use of "signal processing and machine learning in tandem, for building robust low resource systems."

References :

1. A. Bhandari, S. Khare, and H. A. Murthy. Systematic downloading: Analysis and detection. In 2014 8th International Conference on Signal Processing and Communication Systems (ICSPCS), pages 1–9, Dec 2014. doi: 10.1109/ICSPCS.2014.7021098.

2. A W Black, P Taylor, and R Caley. The Festival speech synthesis system. http://festvox.org/festival/, 1998.

3. Hema A Murthy and B Yegnanarayana. Group delay functions and its application to speech processing. Sadhana, 36(5):745–782, November 2011.

4. A V Oppenheim and R W Schafer. Discrete Time Signal Processing. Prentice Hall, Inc., New Jersey, 1990.

5. Daniel Povey, Arnab Ghoshal, Gilles Boulianne, Lukas Burget, Ondrej Glembek, Nagendra Goel, Mirko Hannemann, Petr Motlicek, Yanmin Qian, Petr Schwarz, Jan Silovsky, Georg Stemmer, and Karel Vesely. The kaldi speech recognition toolkit. In IEEE 2011 Workshop on Automatic Speech Recognition and Understanding. IEEE Signal Processing Society, December 2011. ISBN 978-1-4673- 0366-8. IEEE Catalog No.: CFP11SRW-USB.

6. P.L. Salza, E. Foti, L. Nebbia, and M. Oreglia. MOS and pair comparison combined methods for quality evaluation of text to speech systems. Acta Acustica, 82:650–656, 1996.

7. Padi Sarala and Hema A. Murthy. Inter and intra item segmentation of continuous audio recordings of carnatic music for archival. In ISMIR, pages 487–492, 2013.

8. Jilt Sebastian, Manoj Kumar, and Hema A Murthy. An analysis of the high resolution property of group delay function with applications to audio signal processing. Speech Communication, 2016.

9. B Yegnanarayana, D K Saikia, and T R Krishnan. Significance of group delay functions in signal reconstruction from spectral magnitude or phase. IEEE Trans. Acoustics Speech and Signal Processing, ASSP-32(3):610–623, 1984.

10. Heiga Zen, Keiichi Tokuda, and Alan W Black. Statistical parametric speech synthesis. Speech Communication, 51(11):1039–1064, November 2009.

Annals of the Indian National Academy of Engineering
Vol. XV, April 2018

Full Scale Component to Miniature Specimen Tests and Analysis – Some Research Findings on Material and Fracture Mechanics Issues

J.Chattopadhyay[1]

Abstract : This paper gives a glimpse of the comprehensive work on component integrity test program that spans from fracture tests on around 60 full scale piping components to miniature specimens. It also briefly touches upon the development of several new analytical equations for improved integrity assessment of power plant piping.

Keywords : Fracture experiment, Miniature test, J-integral, Pipe, Elbow

1 Introduction

Integrity assessment of piping components is very essential for safe and reliable operation of all types of process power plants. It is especially important for nuclear power plants because of the application of leak-before-break (LBB) concept which involves detailed fracture mechanics assessment of primary heat transport piping systems taking into account the postulated cracks. The mechanical evaluation of pipe failures has evolved over time. While a considerable amount of work has already been done in the development of integrity assessment procedure of cracked/un-cracked piping components, some issues are still unresolved or not fully understood, especially regarding pipe bends.

Against this backdrop, a comprehensive program, both experimental and analytical, was initiated to address some of these issues related to materials and fracture mechanics. The outcome of this program has been the development several new formulas to evaluate various fracture parameters of piping components. In parallel, full scale piping component tests were also conducted to experimentally validate the predictions of the above new formulas. Additionally, improved correlation and methodology have been proposed to obtain the material fracture toughness using miniature specimens by invoking material damage mechanics model. Miniature specimen tests are very important in nuclear industry to estimate the degree of material degradation under service condition since volume of degraded material is extremely scarce for testing purpose. The following sections briefly explain various research findings of this program.

2 Experimental work on full scale components

In the experimental investigations, fracture mechanics tests were carried out on around 60 cracked pipes and elbows under quasi-static monotonic loading. Pipes of various sizes (200 - 400 mm diameter) with circumferential cracks of various angles (30^{o}-150^{o}), configurations (throughwall/surface), materials (base/weld) are tested under 4 point bending and combined loading of bending and internal pressure at RT and 300^{o}C. Elbows of various sizes (200 - 400 mm diameter) with throughwall cracks of various angles (60^{o}-120^{o}), locations (extrados/intrados/crown), configurations (circumferential/axial) and in-plane bending modes (opening/closing) have been tested. Tests on around 300 small tensile, CT and SE(B) specimens, machined from the pipe of same material and heat, have also been done to evaluate the actual stress-strain and fracture resistance properties of pipe/elbow material. Figures 1-2 show the photographs of fracture tests on pipe and pipe bend. Details may be found in Chattopadhyay, Dutta, Kushwaha (2000) and Chattopadhyay, Pavankumar, Dutta, Kushwaha (2005).

[1]Reactor Safety Division, Bhabha Atomic Research Centre, Mumbai - 400085, Email : jchatt@barc.gov.in

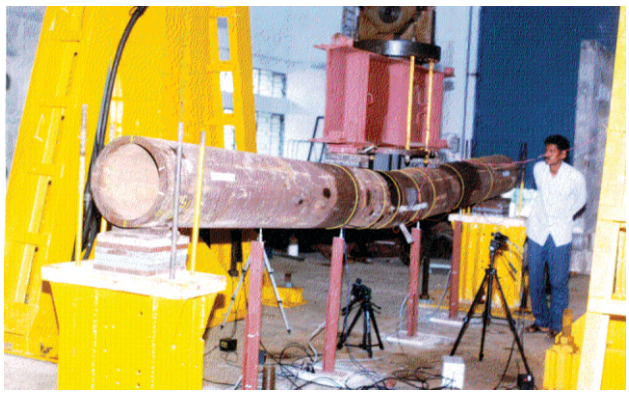

Figure 1: Photograph of pipe fracture test set-up

3 Analytical work

Various analytical work have also been undertaken to propose the improvements in the existing equations to evaluate various fracture parameters of piping components, specially for Leak-Before-Break analysis of nuclear power plant piping. The test data developed above have been extensively used for experimental

Figure 2: Photograph of elbow test set-up

validation of the proposed improvements. The major analytical works are as follows:

- Generalized equation of η_{pl} and γ to evaluate J-R curve
- Study of transferability of fracture properties from specimen to component
- New limit moment equations of elbows under combined loading of internal pressure and bending moment
- New J and COD estimation schemes of throughwall cracked elbows

These analytical works are described in brief in the subsequent sections.

3.1 General equations of η_{pl} and γ to evaluate J-R curve

The evaluation of J-integral from test data generally requires the experimental load vs. load-line-displacement and load vs. crack growth data. Rice, Paris and Merkle (1973) proposed splitting the total J-integral into elastic (J_e) and plastic (J_p) components:

$$J = J_e + J_p; \quad J_e = K^2 / E'$$

where, $E = E$ for plane stress case and $E = E/(1-\nu^2)$ for plane strain case, K is the elastic stress intensity factor, E is the Young's modulus and ν is the Poisson's ratio. The general expression to evaluate J_p from experimental data is as follows:

$$J_p = \int_{o}^{\Delta_{pl}} \eta_{pl}.P.d\Delta_{pl} + \int_{a_o}^{a} \gamma.J_p.da \qquad (1)$$

where, P is the total applied load, Δ_{pl} is the plastic load-line-displacement due to crack only, a_o is the initial crack length per crack tip, a is the current crack length per crack tip, η_{pl} and γ are two functions that depend on geometry and type of loading. The earlier η_{pl} and γ functions had been derived from dimensional analyses that were specific to the geometry and loading conditions. No general formula was available. Chattopadhyay, Dutta and Kushwaha (2001, 2004a, 2004b) derived the limit load-based general expressions of η_{pl} and γ functions as follows:

$$\eta_{pl} = -\frac{\partial F_L}{\partial A}.\frac{1}{F_L}; \qquad \gamma = \frac{\partial^2 F_L / \partial a^2}{\partial F_L / \partial a} \qquad (2)$$

where, F_L is the limit load expression of cracked component as a function of crack size, 'A' is the crack area and 'a' is the crack length per crack tip.

These general expressions of η_{pl} and γ functions have been extensively validated analytically by deriving almost all the existing η_{pl} and γ functions of TPB specimen and pipes with various crack configurations under different loading conditions. Utilizing these general expressions, new η_{pl} and γ functions for various cracked pipe/elbow geometry under various loading conditions, for which no solutions were available in the open

literature, were derived. These crack geometries are as follows:

- Throughwall circumferentially cracked thick pipe under combined bending and tension
- Pipe with constant depth and semi-elliptical part-through circumferential crack under combined bending moment and axial tension
- Pipe with full circumferential part-throughwall crack under axial tension
- Elbow with throughwall circumferential crack under in-plane bending moment
  - Crcak at extrados under closing moment
  - Crack at intrados under opening moment
- Elbow with throughwall axial crack at crown under in-plane bending moment
  - Closing moment
  - Opening moment

All these newly proposed equations are available in Chattopadhyay, Dutta and Kushwaha (2001, 2004a, 2004b).

3.2 Study of transferability of fracture properties from specimen to component

Ductile tearing resistance of a material is conventionally characterized by a J-resistance (J-R) curve, which is obtained from laboratory fracture specimens. However, J-R curve shows strong dependence on stress triaxiality ahead of the crack tip. The transferability of the specimen J-R curve to the component is thus an important issue in fracture mechanics. Two-parameter fracture mechanics approach have been tried to describe the effect of constraint on ductile tearing resistance and thereby resolving the issue of transferability. In this approach, the first parameter reflects the scale of crack tip deformation (e.g. J-integral) and the second parameter is used to quantify the level of stress triaxiality. If the triaxial conditions are found to be similar then it is believed that the J-R curves are transferable within certain circumstances. There are various parameters to quantify the stress triaxiality or constraint ahead of the crack tip. However, in this study, the multi-axiality quotient, 'q' as proposed by Clausmeyer, Kussmaul and Roos (1991) and later modified by Pavankumar, Chattopadhyay, Dutta and Kushwaha (2003) is used. The parameters are as defined below:

$$q = \frac{\sigma_e}{\sqrt{3}\sigma_m}; \quad A_{nq} = \frac{\int_{J/\sigma_0}^{5J/\sigma_0} q.dx}{\int_{J/\sigma_0}^{5J/\sigma_0} q_c.dx} \qquad (3)$$

where, $\sigma_m = (\sigma_1 + \sigma_2 + \sigma_3)/3.0$; $\sigma_e = [(\sigma_1 - \sigma_2)^2 + (\sigma_2 - \sigma_3)^2 + (\sigma_3 - \sigma_1)^2]^{1/2}/2$; σ_e = von-Mises effective stress; σ_m = hydrostatic stress; σ_1, σ_2, σ_3 are the principal stresses; q_c is the critical value of multi-axiality quotient (= 0.27); dx is the distance across the ligament ; J is the J-integral and σ_0 is the yield stress.

These parameters (i.e. q and A_{nq}) have been evaluated for side grooved TPB specimen (a/w = 0.5) which are machined from 200 mm NB pipes, 200 mm NB pipes having various sizes of throughwall circumferential crack subjected to four point bending load and also for 200 mm NB elbows having throughwall circumferential cracks at extrados/intrados subjected to closing/opening bending moment. Figure 3 shows the variation of 'A_{nq}' with J-integral for TPB specimen and pipes and elbows. It may be seen that stress triaxiality ahead of crack tip, quantified by the parameter 'A_{nq}' is almost identical for all these pipes and elbows and TPB specimen. This implies that J-R curves generated from all these components and specimens should also be identical. Figure 4 shows the J-R curve generated from TPB specimen, 3 pipes and 3 elbows. The J-R curves from pipes are taken from Chattopadhyay, Dutta, Kushwaha (2000). The J-R curves of elbows have been taken from and Chattopadhyay, Pavankumar, Dutta, Kushwaha (2005) which are evaluated using the newly proposed 'η_{pl}' and 'γ'. Figure 4 shows that J-R curve from all these components and specimens are indeed identical, because of similar stress triaxialities in a region ahead of the crack tip. This shows the role of stress triaxialities in the transferability of J-R curve from specimen to component.

3.3 Development of New Limit Load Equations for Elbows

Pipe bends or elbows are commonly used components in a piping system. It is important to know its limit moment for the safe operation of the plant. The term *'limit load'* is used in this paper in a generic sense to indicate plastic collapse load. In this paper, plastic collapse load has always been evaluated by twice elastic slope (TES) criterion. Elbows may potentially contain cracks due to manufacturing defects or service related degradation mechanisms. It is very important to know the effect of cracks on the plastic collapse moment (PCM) of elbows for integrity assessment of the piping system. Limit load equations for elbows are very meager in the open literature. Even the available equations are applicable for pure bending moment loading condition, whereas the elbows in actual service condition are mostly subjected to combined loading of internal pressure and bending moment. No limit load equation of elbows is available for this combined loading condition. The present work is an effort to fill this gap area.

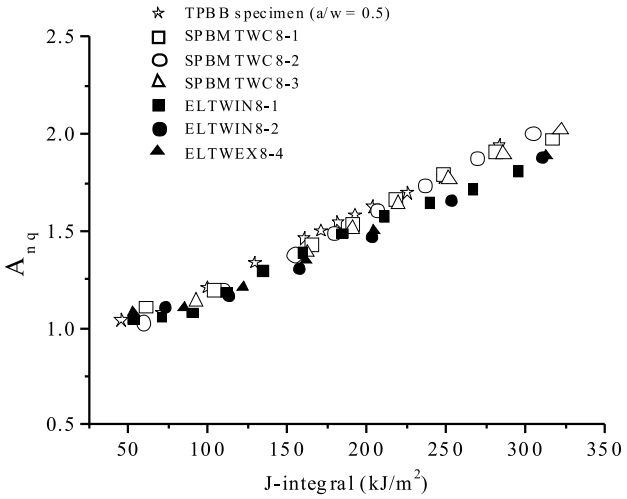

Figure 3: Variation of constraint parameter (A_{nq}) with J- integral for various pipes and elbows

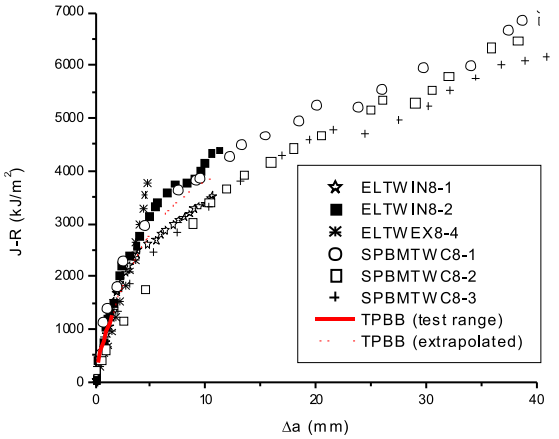

Figure 4: Comparison of J-R curves from side-grooved TPB specimen and throughwall circumferentially cracked pipes and elbows

The PCM of any cracked component is generally expressed as product of PCM of defect-free component and a weakening factor due to the presence of crack. Therefore, before studying the PCM of any cracked component, one should know the PCM of a defect-free component. In comparison to the straight pipe, the deformation characteristics of pipe bend has additional complexities due to ovalisation of elbow cross section, which makes its deformation behaviour completely different for opening and closing mode of bending moment. Additionally, bending moment induces both axial and circumferential stresses at a significant level in pipe bends, which makes it imperative to postulate both circumferential and axial crack configurations. Finally wall thickness and bend radius of elbows also determine its deformation characteristics. These large numbers of variables make the analysis of pipe bends quite elaborate and complex. As a part of the current research program on component integrity, new closed-form equations have been proposed to evaluate plastic collapse moments of pipe bends considering almost all the variables mentioned above. The following cases have been studied.

Three crack configurations: (i) Defect free elbow, (ii) Throughwall circumferentially cracked (TCC) elbow, (iii) Throughwall axially cracked elbow. For each crack configurations two in-plane bending modes: (i) Closing mode, (ii) Opening mode. For each bending mode two loadings: (i) Pure in-plane bending moment , (ii) Combined loading of internal pressure and in-plane bending moment. For each of the above geometry and load configuration, several radii to thickness ratio (R/t) and crack sizes (for cracked elbows) have been considered. Total 607 cases have been numerically analyzed using non-linear finite

element analyses considering both material and geometric non-linearity. More details may be found in Chattopadhyay, Nathani, Dutta and Kushwaha (2000), Chattopadhyay & Tomar (2006) and Chattopadhyay, Venkatramana, Dutta and Kushwaha (2009). Figure 5 shows the variation of normalized PCM $(m_o = M_o/(4R^2t\sigma_y))$ with normalized internal pressure $(p = PR/(t\sigma_y))$ for various elbow thicknesses (R/t) for defect-free elbows. It is seen from Fig.5 that there is a beneficial effect of internal pressure, especially for a thin elbow, which enhances the limit moment till certain extent. Figure 6a shows the variation of PCM of TCC elbows with crack angles for various R/t. Figures 6b shows the effect of internal pressure on the PCM of TCC elbows subjected to combined internal pressure and closing bending moment for one typical case of $R/t = 5$. All the data points are generated for long radius elbows ($R_b/R = 3$). To express the PCM of cracked elbows, a weakening factor (X) is defined as the ratio of PCM of cracked elbows to that of the defect-free elbows $(X = M_L/M_o)$. It is seen from Fig.6a that there is a threshold crack angle below which a through wall circumferential crack at elbow extrados does not weaken an elbow. This threshold crack angle increases with increasing R/t. It may be seen from Fig.6b that application of internal pressure reduces the threshold crack angle and increases the weakening due to the crack. The FE data of these normalized parameters (m_o, p, 2θ) have been best fitted and equations are proposed to evaluate the PCM of TCC elbows under pure in-plane bending moment and combined internal pressure and in-plane bending moment. The proposed equations are as follows:

$$M_L = M_o . X \tag{4}$$

M_o is the limit moment of defect-free pipe bend and X is the weakening factor due to presence of crack defined as a function of (θ/π) and normalized pressure (p) for various R/t. As typical examples, the equations for combined loading of internal pressure and in-plane closing bending moment are shown below:

$$\frac{M_o}{4R^2t\sigma_y} = \left[1.075h^{2/3} + \frac{2.071p^{1.418}}{h^{0.223}} + 8.41p^{12.129}\right][1-p] \tag{5}$$

For $R/t = 5$

$$X = 1.1194 - 0.7236\left(\frac{\theta}{\pi}\right) - 2.0806\left(\frac{\theta}{\pi}\right)^2 - 3.4164p^{0.8408}\left(\frac{\theta}{\pi}\right)^{2.1758} \tag{6}$$

For $R/t = 7.5$

$$X = 1.4423 - 1.495\left(\frac{\theta}{\pi}\right)^{0.6687} - 2.9803p^{0.7136}\left(\frac{\theta}{\pi}\right)^{1.7345} \tag{7}$$

For $R/t = 10$

$$X = 1.6039 - 1.0847\left(\frac{\theta}{\pi}\right)^{0.4082} - 3.1773p^{0.4807}\left(\frac{\theta}{\pi}\right)^{1.4381} \tag{8}$$

For $R/t = 15$

$$X = 1.4298 - 0.0789\left(\frac{\theta}{\pi}\right)^{0.5435} - 3.3789p^{0.2336}\left(\frac{\theta}{\pi}\right)^{0.9644} \tag{9}$$

For $R/t = 20$

$$X = 7.7803 - 6.8959\left(\frac{\theta}{\pi}\right)^{0.0231} - 4.1061p^{0.5464}\left(\frac{\theta}{\pi}\right)^{1.2776} \tag{10}$$

Applicability:

$0 \le X \le 1$, $2 \le (R_b/R) \le 3$, $2\theta \le 150^o$, $1 > p \le 0.1$

Eq.(5) is for un-cracked elbow and Eqs.(6-10) are for TCC elbow. For intermediate R/t, X can be linearly interpolated between the adjacent R/t values.

3.4 Development of elastic-plastic J and COD estimation scheme for throughwall circumferentially cracked elbow under in-plane bending moment

Leak-Before-Break (LBB) qualification of nuclear power plants requires detailed fracture analysis of piping components with postulated throughwall cracks. Since these piping components are mostly made of ductile material, one has to invoke the elastic-plastic fracture mechanics principles to deal with the large-scale plasticity ahead of the crack tip. For this purpose, the estimation of elastic-plastic J-integral and crack opening displacement (COD) is very essential. In LBB analyses, J-integral is used to calculate the crack initiation and unstable ductile tearing load while COD is used to obtain the crack opening area in the evaluation of leakage size crack. Elastic-plastic finite element analysis (FEA) is the most general technique to evaluate these parameters. But, FEA often requires large computational time, expertise and resources, which make the computation quite expensive. Moreover, it has to be carried out on a case-by-case basis for each piping component. To circumvent these problems, simple J and COD estimation schemes emerged. All these estimation schemes were based on large number of finite

element analysis for a wide range of geometry and material parameters. However, *J* and COD estimation schemes for cracked elbows, one of the very important geometry for LBB analyses is quite meager. As a part of the present research program, simple *J* and COD estimation schemes for elbow with throughwall circumferential crack at extrados / intrados subjected to in-plane

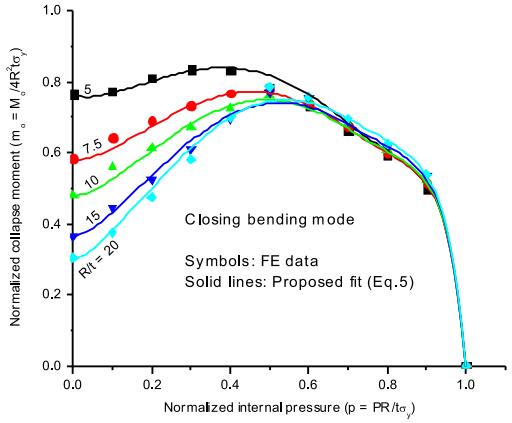

Figure 5: Variation of closing PCM with internal pressures for un-cracked elbows

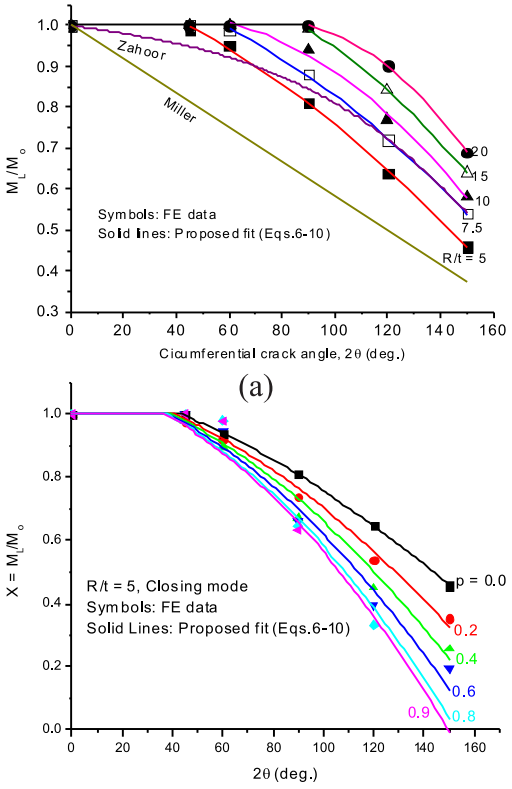

Figure 6: Variation of normalized plastic collapse moment with crack angle: (a) for pure closing moment and (b) combined internal pressure and closing moment

closing/opening bending moment have been proposed. The following paragraphs describe very briefly the estimation schemes. The basic approach has been same as that of GE/EPRI estimation schemes for pipe with through wall crack under bending moment. More details may be found in Chattopadhyay, Tomar, Dutta and Kushwaha (2005) and Chattopadhyay, Acharyya and Kushwaha (2007).

3.4.1 Proposed J and COD estimation scheme

Equations (11-19) are proposed to estimate the J-integral and COD of TCC elbows. The geometry constants i.e. V_2 to evaluate the elastic COD at inside and outside surface and also the plastic influence functions i.e. h_1 for J-integral and h_2 for COD at inside and outside surface are evaluated for various geometric cases and Ramberg-Osgood hardening index, n = 3,5,7. Typical comparisons between the FE results and predictions of estimation schemes for various cases of elbows with extrados crack under closing moment is shown in Fig.7. The conventional elastic-plastic J and COD estimation schemes overestimate the plastic J and COD in the transition from elastic to fully plastic condition. Chattopadhyay, Tomar, Dutta and Kushwaha (2005) and Chattopadhyay, Acharyya and Kushwaha (2007) investigated this issue in detail and proposed the modified plastic J-integral and COD equations by changing the terms in Ramberg-Osgood equation.

$$J = J_e + J_p \tag{11}$$

$$J_e = K^2 / E \tag{12}$$

$$J_p = \alpha^{\frac{1}{n+1}} \sigma_y \varepsilon_y \pi R \left(1 - \frac{\theta}{\pi}\right)^2 h_1\left(\frac{\theta}{\pi}, n, \frac{R}{t}\right)\left(\frac{M}{M_L}\right)^{n+1} \text{ for } \frac{M}{M_L} \le 1.0 \tag{13}$$

$$J_p = \alpha \sigma_y \varepsilon_y \pi R \left(1 - \frac{\theta}{\pi}\right)^2 h_1\left(\frac{\theta}{\pi}, n, \frac{R}{t}\right)\left(\frac{M}{M_L}\right)^{n+1} \text{ for } \frac{M}{M_L} \ge 1.2 \tag{14}$$

$$J_p = J_{p_1} + \frac{J_{p_{1.2}} - J_{p_1}}{0.2 M_L}\left(M - M_L\right) \text{ for } 1.0 < \frac{M}{M_L} < 1.2 \tag{15}$$

$$\delta = \delta_e + \delta_p \tag{16}$$

$$\delta_p = \alpha^{\frac{1}{n}} \varepsilon_y \pi R h_2\left(\frac{\theta}{\pi}, n, \frac{R}{t}\right)\left(\frac{M}{M_L}\right)^{n} \text{ for } \frac{M}{M_L} \le 1.0 \tag{17}$$

$$\delta_p = \alpha \varepsilon_y \pi R h_2\left(\frac{\theta}{\pi}, n, \frac{R}{t}\right)\left(\frac{M}{M_L}\right)^{n} \text{ for } \frac{M}{M_L} \ge 1.2 \tag{18}$$

$$\delta_p = \delta_{p_1} + \frac{\delta_{p_{1.2}} - \delta_{p_1}}{0.2 M_L}\left(M - M_L\right) \text{ for } 1.0 < \frac{M}{M_L} < 1.2 \tag{19}$$

where, the subscripts 'e' and 'p' indicate the elastic and fully plastic values respectively, M_L is the limit moment, J_{p1} and δ_{p1} are the plastic J-integral and COD evaluated at $M = M_L$ using Eqs.(13,17) and $J_{p1.2}$ and $1.2p\delta_{p1.2}$ are the plastic J-integral and COD evaluated at $M = 1.2\ M_L$ using Eqs.(14,18).

It may be observed from Fig.7 that the predictions of the proposed J and COD scheme match very well with FEM and test data in contrast to the conventional scheme, which highly over-predicts J and COD in the transition from elastic to fully plastic regime. It may be noted here that the conventional GE/EPRI plastic zone correction of elastic J-integral and COD is not recommended. Because, its contribution has been found to be negligible up to the load range considered and it makes the elastic J and COD estimation unduly complicated.

It may be observed from Fig.7 that the predictions of the proposed J and COD scheme match very well with FEM and test data in contrast to the conventional scheme, which highly over-predicts J and COD in the transition from elastic to fully plastic regime. It may be noted here that the conventional GE/EPRI plastic zone correction of elastic J-integral and COD is not recommended. Because, its contribution has been found to be negligible up to the load range considered and it makes the elastic J and COD estimation unduly complicated.

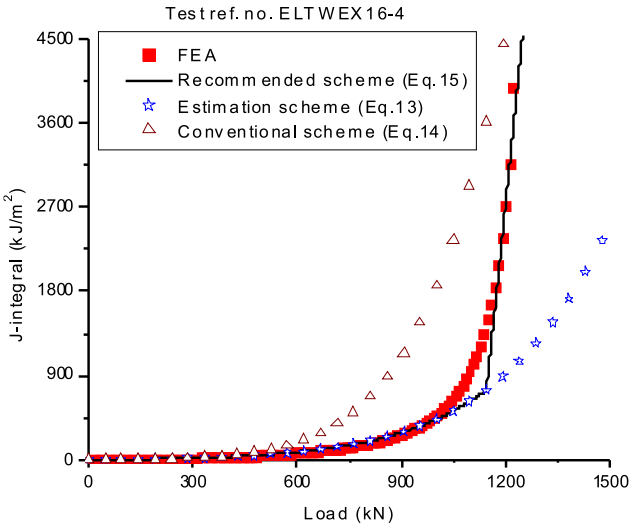

(a)

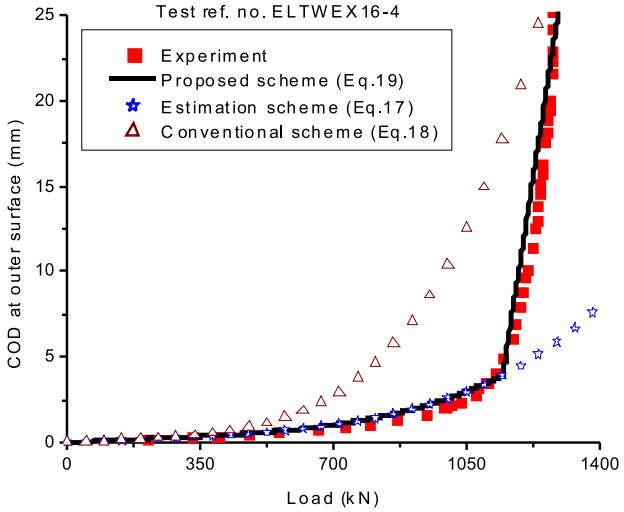

(b)

Figure 7: Comparison of conventional and proposed (a) *J* and (b) COD estimation scheme with FEM and test data for an TCC elbow under closing moment

3.5 Work on miniature specimens

The miniaturized specimens are in use to determine the mechanical properties of the materials, such as yield strength, ultimate tensile strength, ductility, fracture toughness etc. Use of such specimens is popular whenever the limited quantity of material is available for testing, such as aged/irradiated material. However, there are several unresolved issues in this field. The present research program tried to address few of them. They are as follows:

(a) To develop a correlation between minimum thickness and central deflection during small punch test (SPT)

(b) Numerical evaluation of J-R curve from SPT data using micro mechanical modeling

(c) Numerical development of a new correlation between biaxial fracture strain during SPT and material fracture toughness

(d) Fracture toughness prediction of nuclear materials using pre-notched SPT specimens

The following subsections very briefly explain the first 3 of these works. Details may be found in Kumar, Chattopadhyay and Dutta (2016), Kumar, Dutta, Chattopadhyay and Shriwastaw (2016) and Kumar, Dutta and Chattopadhyay (2017).

3.5.1 Correlation between minimum thickness and central deflection during SPT

During SPT (Fig.8), one gets the equivalent strain during fracture as

$$\bar{\varepsilon}_{qf} = \ln(t_0 / t_f) = \beta(\delta^* / t_0)^p \qquad (20)$$

where t_0, t_f, δ^* and $\bar{\varepsilon}_{qf}$ are the initial thickness, minimum thickness at fracture, central deflection at fracture and equivalent fracture strain respectively. This value of fracture strain is used to calculate the fracture toughness by using various equations. Using large number of experimental data from the literature, Mao and Takahashi (1987) determined the values of β and p as 0.09 and 2 respectively for the disk specimen having diameter φ=3 mm and thickness of 0.24-0.25 mm.

Finite element studies have been carried out to investigate the effect of various parameters which are expected to influence this correlation. The parameters under consideration were material hardening, material yield stress, coefficient of friction and initial thickness of the specimen. It is shown that the correlation remains unaffected with respect to change in material parameters. Similarly, the coefficient of friction beyond 0.2 also does not affect the correlation. However, change in thickness has significant effect on the correlation. (Fig.9). A modification has been suggested in the existing correlation to consider the influence of thickness change. Equation (21) shows the best fit quadratic relations between β and p as a function of initial thickness t_o. The coefficients of the quadratic equations are shown below.

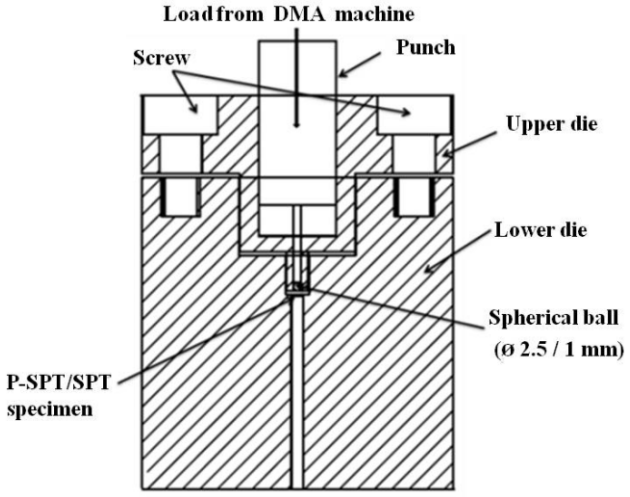

Figure 8: Specimen support configuration and loading in the test set-up of small punch test

$$\beta = a_1 t_0^2 + b_1 t_0 + c_1 \text{ and } p = a_2 t_0^2 + b_2 t_0 + c_2 \qquad (21)$$

where,

a_1=2.32, b_1=0.03, c_1=-0.03, a_2=12.13, b_2=-8.89, c_2=3.38

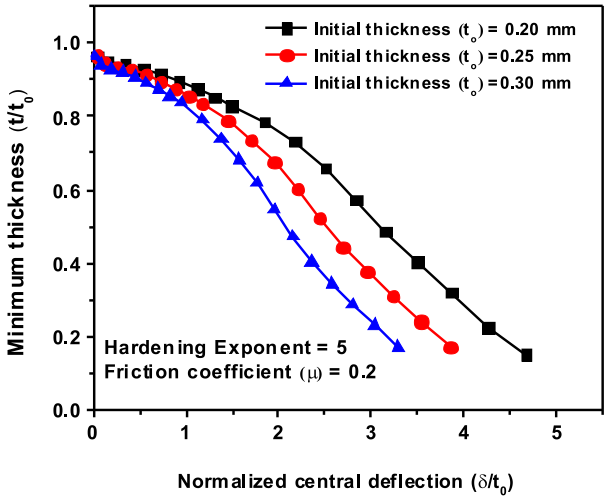

Figure 9: Comparison of minimum thickness v/s central deflection for various initial thicknesses of SPT specimens

3.5.2 Numerical evaluation of J-R curve from SPT data using micro mechanical modeling

Six miniaturized small punch tests have been carried out for three materials, viz., T91, AISI403 and 20MnMoNi55 which are commonly used as structural materials in nuclear reactors. The punch load v/s displacement data are collected up to fracture signified by a rapid drop in load carrying capacity of the specimens. The experimental data for each material is then used to evaluate yield strength and ultimate tensile strength making use of available correlations in the literature. These material data are then used to calculate Ramberg-Osgood hardening exponent leading to the generation of complete true stress-strain data. The next task is to determine Gurson-Tevergaard-Needleman (GTN) parameters of the materials which can simulate punch load v/s displacement through micromechanical modeling. These GTN parameters along with true stress-strain data are then used to numerically generate J-R data of the

materials by analyzing ASTM E1820 standard CT specimens. Calculated J-R data are then compared with the experimental values quoted in the literature (Fig.10). The above methodology may be used to determine J-R data of aged/irradiated materials using SPT.

3.5.3 A new correlation between biaxial fracture strain during SPT and material fracture toughness

Various empirical correlations are proposed in the literature to determine the value of fracture toughness (J_i) using biaxial fracture strain (ε_{qf}) as determined from SPT. There are number of such correlations available in the literature, which are

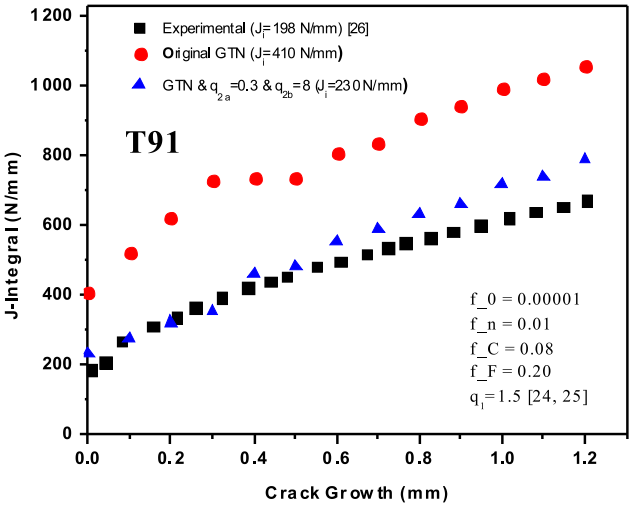

Figure 10: Predicted J-R data using GTN material model in comparison to experimental values for T91 material

generally not in agreement with each other. In the present work, an attempt has been made to determine the correlation between biaxial fracture strain (ε_{qf}) and crack initiation toughness (J_i) numerically. About one hundred materials are digitally generated by varying yield stress, ultimate stress, hardening coefficient and Gurson parameters. Each material of this set is then used to analyze a SPT specimen and a standard TPB specimen. Analysis of SPT specimen generated biaxial fracture strain (ε_{qf}) and analysis of TPB specimen generated value of J_i. A graph is then plotted between these two parameters for all the digitally generated materials. The best fit straight line determines the correlation. It has also been observed that it is possible to have variation in J_i for the same value of biaxial fracture strain (ε_{qf}) within a limit (Fig.11). Such variation in the value of J_i has also been ascertained using the graph. Experimental SPT data acquired earlier for three materials were then used to get J_i by using newly developed correlation. A reasonable comparison of calculated J_i with the values quoted in literature confirmed usefulness of the correlation.

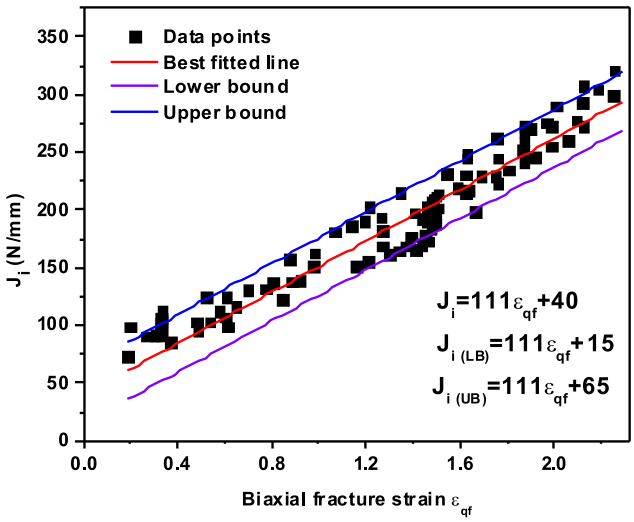

Figure 11: Relation between fracture toughness (J_i) and biaxial fracture strain (ε_{qf})

Conclusions

- Around 60 fracture tests are carried out on full scale piping components, which forms a valuable database for validation of future analytical developments.

- Several new correlations are proposed to obtain $_{pl}$ and to get material *J-R* curve from test data, limit load of elbows under combined pressure and bending moment, *J*-integral and COD for cracked elbows.

- The role of stress triaxiality in transferability of material fracture properties is studied and it is experimentally shown that if the stress triaxiality ahead of crack tip is same in a specimen and a component, *J-R* curve is transferable from specimen to component.

- In miniature small punch test (SPT), a new correlation is developed between minimum thickness and central deflection, *J-R* curve is

numerically calculated using micro mechanical modeling and a new correlation is developed between biaxial fracture strain during SPT and material fracture toughness (J_i).

5 References

1. **Chattopadhyay,J., Dutta, B.K. and Kushwaha, H.S.** (2000), "Experimental and analytical study of three point bend specimens and throughwall circumferentially cracked straight pipe", *International Journal of Pressure Vessels and Piping*, Vol.77, pp 455 – 471.

2. **Chattopadhyay,J., Pavankumar,T.V., Dutta,B.K. and Kushwaha,H.S.** (2005) Fracture experiments on throughwall cracked elbows under in-plane bending moment: Test results and theoretical/numerical analyses, *Engineering Fracture Mechanics*,Vol.72, pp 1461 – 1497.

3. **Rice,J.R., Paris,P.C. and Merkle, J.G.** (1973) Some Further Results of J-integral Analysis and Estimates, *Progress in Flaw Growth and Fracture Toughness Testing*, ASTM STP 536, American Society for Testing and Materials, Philadelphia, pp 231 – 245.

4. **Chattopadhyay,J., Dutta,B.K. and Kushwaha, H.S.** (2001) Derivation of γ parameter from limit load expression of cracked component to evaluate J-R curve, *International Journal of Pressure Vessels and Piping*, Vol.78, pp 401 – 427.

5. **Chattopadhyay,J., Dutta,B.K. and Kushwaha, H.S.** (2004a) New '$_{pl}$' and " functions to evaluate J-R curves from cracked pipes and elbows: Part I – Theoretical derivation, *Engineering Fracture Mechanic*, Vol.71, Issue no.18, pp 2635 - 2660

6. **Chattopadhyay,J., Dutta,B.K. and Kushwaha, H.S.** (2004b) New '$_{pl}$' and " functions to evaluate J-R curves from cracked pipes and elbows: Part II –Experimental and numerical validation, *Engineering Fracture Mechanics*, Vol.71, Issue no.18, pp 2661 – 2675

7. **Clausmeyer, H., Kussmaul, K. and Roos, E.** (1991) Influence of stress state on the failure behaviour of cracked components made of steel, ASME, *Applied Mechanics Rev.*, Vol.44 (2), pp77-92.

8. **Pavankumar, T.V., Chattopadhyay,J., Dutta,B.K. and Kushwaha,H.S.** (2003) Importance of stress triaxiality at crack tip in elastic-plastic fracture mechanics, 8th *International Symposium on Plasticity and Impact Mechanics*, *IMPLAST 2003*, 16-19th March, New Delhi, India.

9. **Chattopadhyay,J, Nathani,D.K., Dutta,B.K. and Kushwaha,H.S.** (2000) Closed-form collapse moment equations of elbows under combined internal pressure and in-plane bending moment, *Journal of Pressure Vessel Technology*, ASME Transactions, Vol.122, pp 431 – 436.

10. **Chattopadhyay,J. and Tomar, A.K.S.** (2006) New Plastic Collapse Moment Equations of Defect-free and Throughwall Circumferentially Cracked Elbows Subjected to Internal Pressure and In-plane Bending Moment", *Engineering Fracture Mechanics,* Vol.73, pp 829 – 854.

11. **Chattopadhyay, J., Venkatramana, W., Dutta, B.K. and Kushwaha, H.S.** (2009) Plastic Collapse Moment Equations of Throughwall Axially Cracked Elbows Subjected to Combined Internal Pressure and In-plane Bending Moment, *Engg. Fracture Mechanics,* Vol.76, 2009, pp 1380 – 1385.

12. **Chattopadhyay,J., Tomar,A.K.S., Dutta,B.K. and Kushwaha, H.S.** (2005) Elastic-plastic *J* and COD estimation

schemes for throughwall circumferentially cracked elbow under in-plane closing moment, *Engineering Fracture Mechanics*, Vol.72, 2005, pp 2186 – 2217.

13. **Chattopadhyay,J., Acharyya,S. and Kushwaha, H.S.** (2007) Elastic-plastic *J* and COD estimation schemes for 90° elbow with throughwall circumferential crack at intrados under in-plane opening moment, *International Journal of Fracture*, Vol.144, No.4, pp 227 – 245.

14. **Kumar,P., Chattopadhyay,J. and Dutta,B.K.** (2016) "On the correlation between minimum thickness and central deflection during small punch test", *Journal of Nuclear Materials*, Vol.475, pp 37-45.

15. **Kumar,P., Dutta,B.K., Chattopadhyay,J., and Shriwastaw, R.S.** (2016) "Numerical evaluation of J-R curve using small punch test data", *Theoretical and Applied Fracture Mechanics*, Vol.86, pp 292-300.

16. **Kumar,P., Dutta,B.K. and Chattopadhyay,J.** (2017) Numerical development of a new correlation between biaxial fracture strain and material fracture toughness for small punch test, *Journal of Nuclear Materials*, Vol.486, pp 332-338.

17. **Mao,X. and Takahashi,H** (1987) Development of a further miniaturized specimen of 3 mm diameter for TEM disk (φ 3 mm) small punch tests, *Journal of Nuclear Materials*, Vol.150, pp 42-52.

Acknowledgement

Author gratefully acknowledges the contributions of Mr.H.S.Kushwaha and Dr.B.K.Dutta who were his mentors in all the research activities. The contributions of Fatigue Testing Laboratory, SERC, Chennai for full scale component tests and that of Mr. Pradeep Kumar for miniature specimen tests are also acknowledged.

Annals of the Indian National Academy of Engineering
Vol. XV, April 2018

Remediation of Contaminated Water Soil and Aquifers

Ligy Philip[1]

Abstract : Water and soil in different parts of the world are polluted by various contaminants originating from natural and anthropogenic activities. The people in developing countries are severely affected by the pollution due to improper management of resources and weak enforcements of rules and regulations. A sustainable approach of managing recourses only can protect the environment. A few case studies dealing with the adoption of sustainable technologies along with awareness creation and practicing 3 R principle to tackle the pollution problem is discussed in this article.

1. Introduction

Our living environment is getting polluted at a rapid rate due to indiscriminate discharge of wastes. As the population increases, the consumption of resources and the production of goods increase enormously and consequently the generation of waste increases. Mother Nature is unable to satisfy the greed of everybody. Many contaminated sites are existing all over the world due to various industrial activities. Moreover, due to improper management of domestic/human waste, most of our water sources are contaminated by organics, emerging contaminants and pathogens. A sustainable approach is essential to manage the environment properly. Technologies for remediation should be developed based on a basic understanding of processes involved. It should also be realized that technology alone cannot find a solution for tackling many of the environmental problems. A combination of technologies along with awareness and practice of the "reduce, recycle, and reuse" principle will lead us to appropriate solutions. This article describes a few case studies, drawn from author's experience of last one decade, to illustrate these principles.

2. Bioremediation of Chromium Contaminated Soil and Aquifer

There are many chromium contaminated soils and aquifers in India (Ex: Ranipet in Tamil Nadu, Kanpur in Uttar Pradesh and Sukhinda in Odisha) and other parts of the world (Ex: Vancouver in Washington; Caspian in Kasakhstan and Meycauayn and Luzan). Hexavalent chromium is highly mobile and carcinogenic. Therefore these sites require immediate remediation. Remediation of contaminated sites poses a number of challenges and there is an urgent need to develop techniques that are cost-effective and environmentally friendly. Remediation based on biotransformation of Cr(VI) to Cr(III) is an attractive option and many studies have been conducted in the past in this area. However, most of these studies pertain to ex-situ treatment option. Also, earlier laboratory studies used batch and small laboratory scale columns to understand the combined transport and geo-chemical processes pertaining to Cr(VI) in different soils. These experiments do not truly represent the complex interplay between the biological and hydro-geological processes. Large scale systematic experimental studies have not been carried out for evaluating the effectiveness of bio-barrier and reaction zone techniques for containment of plumes. Data from pilot scale experiments is useful for validation of mathematical models for such systems.

Starting in the year 1998 author and her co-

[1]Professor, Department of Civil Engineering, IIT Madras, Chennai -600 036

workers have conducted a series of batch experiments for isolation and enrichment of chromium reducing bacteria (CRB) for bio-transformation of Cr(VI) to Cr(III) (Philip et al., 1998; Philip et al., 1999; Krishna and Philip, 2005; Jeyasingh and Philip, 2005; Elangovan et al. 2008a; 2008b; 2010; Elangovan and Philip, 2009; Somasundaram et al., 2009; Jeyasingh et al., 2010). Batch experiments were conducted to understand the biokinetics, optimal environmental conditions for bio-transformation, reaction pathways, formation of intermediate metabolites, effect of other contaminants presence of other bacteria such as iron reducing bacteria (IRB) and sulphate reducing bacteria on the bio-transformation process. These batch studies were complimented by laboratory column and bench scale experiments (Sashidhar et al. 2006; 2007; Somasundaram et al., 2011) to understand the interplay between biological fate and hydro-geological transport processes. These studies helped in assessing the effectiveness of bio-barriers in *in situ* containment of chromium contaminated plumes.

In a follow up study (Jeyaingh et al., 2011), remediation of Cr(VI) contaminated aquifers using bio-barrier and reactive zone technologies was evaluated using pilot scale reactors employing CRB isolated from a chromium contaminated site. The physical scale of the pilot scale reactors (3.0 x 1.0 x 0.5 m) employed in this study was much larger compared to scales in the earlier column studies (3.0 cm diameter and 45 cm long). As shown in Fig. 1, one of the reactors had a 10 cm wide portion, at 75 cm from the inlet end, filled with sand containing CRB to act as the bio-barrier. The other reactor without this bio-barrier was used as the control reactor. Same flow conditions (a Darcy velocity of 0.2 cm/h) were maintained in both the reactors. In another set of experiments, reactive zones were created by injecting bacteria into the aquifer through two wells having a diameter of 4 cm. Water samples were collected from the monitoring wells, located on both upstream and downstream sides of barrier and reaction zones, periodically and were analyzed for Cr(VI), total chromium, and COD concentrations. The long duration experiments revealed that Cr(VI) concentration was zero in wells located downstream of the biobarrier and in the influence zone of the well even after 180 days, whereas the concentration attained a maximum of 43 mg/L in the blank reactor.

Fig. 1: Pilot scale reactor for bio barrier

Once the technology was demonstrated successfully in the laboratory pilot scale system, it was taken for field demonstration. The filed demonstration (funded by Central Pollution Control Board CPCB) and coordinated by the Tamil Nadu Pollution Control Board (TNPCB)) was carried out in the chromium contaminated site in Ranipet, Tamil Nadu. The aquifer was contaminated with Cr(VI) and the concentration was as high as 150 mg/L where as the permissible concentration is as low as 0.05 mg/L. A demonstration project was undertaken to remediate a part of an aquifer with an areal extent of 25 m^2 and a depth of 10-20 m. The technology was demonstrated successfully by adopting the reactive zone technology. The Cr(VI) and Cr(III) concentrations in the aquifer test site were reduced to below detectable limit during the period. The remediation of sludge contaminated with hexavalent chromium was also demonstrated. Five tons of sludge with a Cr(VI) concentration varying between 3-6 mg/kg and total chromium varying between 10-16 mg/L was treated. After the remediation, the Cr(VI) concentration in the sludge was reduced to below detectable limits. The leachability test of the remediated sludge met all the prescribed standards stipulated by CPCB.

The success of the field demonstration led to the transfer of the technology to several industries.

Chromium contaminated aquifers near M/s Radiant Electroplating Industries, Chennai, M/s Munjal Showa Limited, Gurgoan and M/s Sriram Pistons Ltd, Gaziabad have been successfully remediated using the bacterial inoculums provided by the author and deploying that into the aquifer using reaction zone technology. It must be noted here that M/s Sriram Pistons Ltd. was using pump and treat technology based on chemical treatment before switching over to more cost-effective in situ bioremediation.. Recently, author was contacted by the CPCB for advice on implementation of this technology for remediating a chromium contaminated site in Kanpur. It is expected that the proposed bioremediation technology would cost (around Rs. 10 crores) much less compared to the cost (around Rs. 600 crores) estimated for application of chemical technology.

The above case illustrates how controlled studies, spanning from batch experiments in test tubes to pilot scale studies in laboratory and field, are crucial for successful development and implementation of technology for contaminant remediation in the field.

3. Effective Intervention to Improve the Quality of Rural Water Supply

A case study is described in this section to illustrate how significant improvement in the water quality in rural areas can be achieved through simple and novel interventions, which can be implemented by local population. . A project work involving community based water quality monitoring and sanitary surveillance has been carried out by the author (Philip, 2013) in some of the blocks of Krishnagiri and Hosur Districts of Tamil Nadu, India. . This work was supported by the Unicef because although drinking water systems already existed in the villages of these blocks, the prevalence of water related diseases was high due to poor water quality at household level. The overall objective of the project was to improve the water quality situation through simple interventions. This goal was achieved by making the members of the Panchayat Level Convergence Committee (PLCC) of the block aware of importance of water quality and sanitation for good health and training them for testing for basic water quality parameters without dependence on external actors. The trained PLCC members acted as agents of change. They spread the awareness on water supply, sanitation and hygiene among the local population and also put pressure on local government officials to undertake early remedial actions whenever water quality was poor.

Intervention was made in six blocks: (i) Veppanapally, (ii) Bargur, (iii) Thally, (iv) Krishnagiri, (v) Kaveripatnam and (vi) Mathur blocks of Krishnagiri district (Tamilnadu). A number of samples were collected from bore wells, hand pumps and water taps during two campaigns: (i) monsoon and (ii) non-monsoon, in the year 2008, prior to the intervention. These were analyzed for: (i) bacteriological quality; (ii) fluoride; (iii) TDS, (iv) pH, (v) iron, (vi) chloride and (vii) nitrate. Almost all samples from bore wells and 29% samples from hand pumps had bacteriological contamination. Fluoride concentration was more than 3.0 mg/L in 27% samples from hand pumps and 18% samples from bore wells.

The implementation of project consisted of following actions: (i) base line water quality and sanitary surveys, (ii) design and supply easy to use and make water quality test kits, (iii) training PLCC members on water quality monitoring system, (iv) review the progress and results every two months, (v) cross-check the quality of water samples to monitor the work carried out by the village volunteers and (vi) provide technical support to carry out appropriate action. Easy to use water quality test kit was designed and made by the author and her co-workers in the laboratories of IIT Madras. Training was imparted in the use of these easy to use field kits as well as making such kits using chemicals available easily in the market. These test kits could be used for testing for: bacteriological quality, , fluoride, chloride, residual chlorine, nitrate, alkalinity, hardness, Total dissolved solids and iron. To make the intervention effective even after the exit of the external actors, participation

and contribution of Tamilnadu Water Supply and Drainage (TWAD) Board, the local water supply service provider was co-opted.

Several three-day training programs for PLCC members (three volunteers from Panchayat) two-day training programs (about 30 participants each) for Panchayat Presidents, block development officers, ADWs, CFVP coordinators and Panchayat Secretaries were conducted. One-day final refresher programs were conducted for selected volunteers and Panchayat Presidents in each block. Volunteers carried out: (i) water quality analyses of almost all water sources, (ii) survey of sanitary practices and (iii) inventory of all drinking water sources. TWAD Board carried out confirmatory tests for water quality analyses and coordinating tem took appropriate remedial actions in case of discrepancy in the results. Review meetings were conducted once in two months to discuss about the problems being faced in the field, offer advice and replenish the the chemicals, along with H_2S bottles. A stakeholder workshop was conducted to evolve a plan for scaling up and sustainability of the intervention.

The water quality parameters were monitored until September 2012. As shown in Fig. 2 for Thally block, a decreasing trend in bacteriological contamination was clearly visible. 42% of samples showed bacterial contamination in June 2011, while only 2% of samples were bacterially contaminated in September 2012. The improvement in health of people in intervened blocks was assessed using secondary data for occurrence of water borne diseases. This data was collected from primary health centers. -As illustrated in Fig. 3 for Barur PHC, there was a visible decrease in the number of cases of dysentery and cholera. This project illustrates how simple and properly designed interventions can positively and significantly improve the environment and public health.

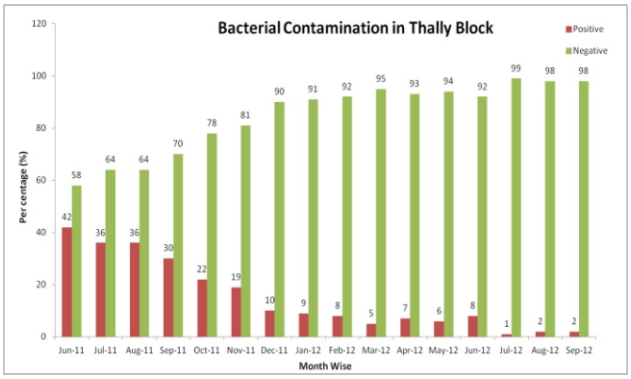

Fig. 2: Decrease in bacterial contamination in Thally

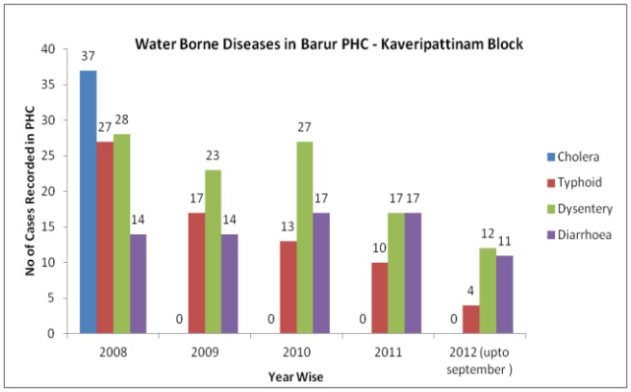

Fig. 3: Decrease in water borne diseases in Barur PHC

4. Environmentally Friendly Water Treatment System using N-doped TiO_2

One cannot overemphasize that the water which is consumed should be free from pathogens and any organic pollutants in order to prevent occurrence of water borne diseases. However, only 89% of world population has access to improved water sources and access to drinking water remains a challenge in most of the developing and underdeveloped countries. Therefore, it is necessary to disinfect the water before it is supplied as drinking water. Chlorine is commonly used in many countries as disinfectant because it is inexpensive. However, chlorination results in the formation of disinfection byproducts such as trihalomethanes and haloacetic acids which are carcinogenic and mutagenic. Thus there is an urgent need to develop a simple and low cost water treatment system.

Author and her co-workers have carried out

extensive studies on the application of photocatalysis for treating contaminated water (Senthilnathan and Philip, 2009; 2010a; 2010b; 2010c; 2012; Arya and Philip, 2014; Priya and Philip, 2015; Surenjan et al., 2017). This is an advanced oxidation process, wherein highly reactive oxygen species, mainly hydroxyl radicals, are produced and used for oxidizing the contaminants. During the course of these studies it was recognized that a photocatalyst like titanium dioxide can be used for bacterial inactivation. However, this process is expensive and unsustainable as it requires UV light for excitation. One way to make this process viable is to modify TiO_2 by doping in order to excite it under sunlight. Even though studies on antimicrobial activity of TiO_2 have started almost three decades ago; solar radiation for disinfection has not been demonstrated. Also, continuous reactor studies have not been conducted. Author (Arya and Philip, 2014) has developed a treatment system utilizing immobilized nitrogen doped TiO_2 to achieve disinfection under solar radiation.

Batch experiments were conducted to evaluate bacterial inactivation w using immobilised and suspended form of N doped TiO_2. Batch experiments were conducted to (i) compare activities of Degussa P-25 and N doped TiO_2, (ii) determine optimal catalyst loading and (iii) study The effect of anions on the efficiency. These studies were followed by continuous reactor studies, which used N doped TiO_2 coated glass plates (Fig. 4). It was found that a 3 log inactivation of bacteria can be achieved within 40 mins. The variation in concentration along the length of the reactor for two different flow rates is shown in Fig. 5.

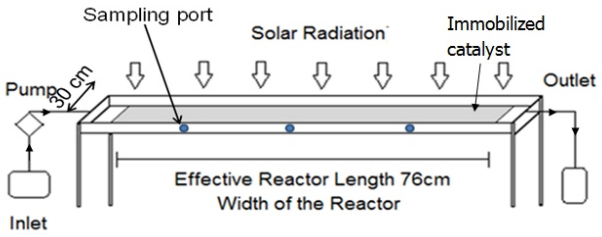

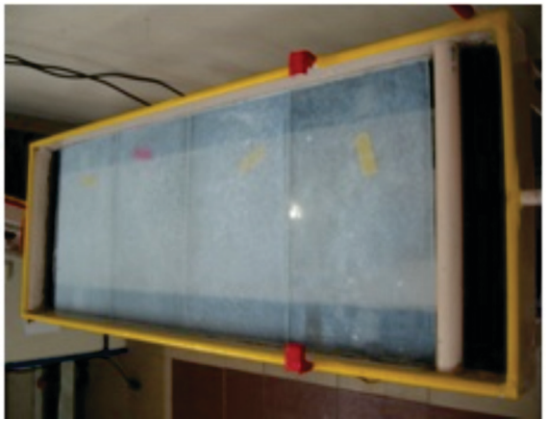

Fig. 4. Thin film continuous photo reactor for disinfection

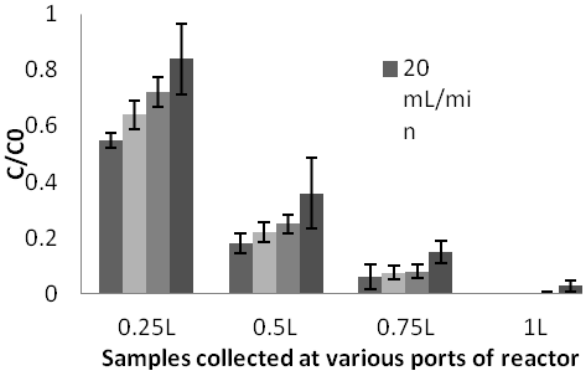

Fig. 5. Concentration variation along the length of the photo reactor

It was found that the efficiency of system decreases due to turbidity, bicarbonate ions and organic matter. However, efficiency in such situations can be improved by reducing the flow rate. As compared to popular SODIS system which took 6 hours for complete inactivation, the developed solar photocatalytic treatment took only one hour for complete inactivation. Also, unlike in SODIS treatment, bacterial inactivation is irreversible in solar photocatalytic treatment system.

5. Water Recycling for Reducing Pollution and Stress on Resources

There is growing interest in recent years on the on-site treatment and reuse of grey water as a means to reduce the water demand at household level. Also, the current paradigm (Fig. 6) is to treat the water to a specified level, depending on its use, i.e., one need not treat the water used for flushing

to the same level as water used for drinking. It is in this context the treatment and reuse of grey water becomes important. Around 60 – 70% of water used in a household is converted into grey water (bathroom, laundry and kitchen) and this is less polluted than black water coming out of toilets. The low-load grey water coming out of bath, showers and hand basins makes up around 40% of total household consumption, depending on socio-economic and cultural factors and climatic conditions.

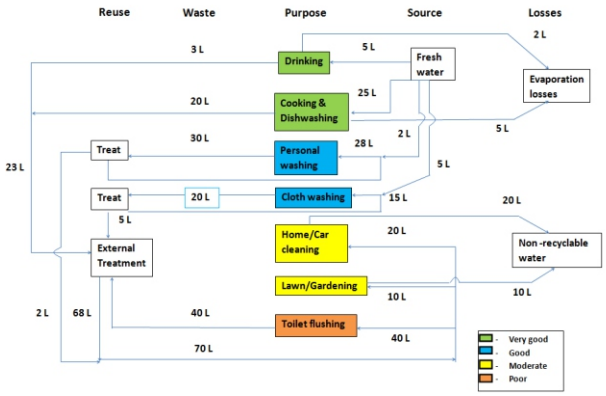

Fig. 6. Closing the loop at household level with on-site recycling

Over the years it has been perceived that grey water is easiest to treat and recycle due to its composition. *For rapidly increasing per capita water consumption in an emerging economy country like India, grey water recycling (GWR) systems appear to become a future requirement at household level* However, it may contain emerging contaminants and wastes besides contaminants such as body fats, hair, soil, pathogens etc. The group of emerging contaminants commonly found in bathroom wastewater belongs to pharmaceuticals, personal care products (PCPs), detergents etc., which are endocrine disrupting compounds (EDC), and care should be taken to treat grey water for removing them. The current preferred treatment technologies used for grey water include physical and biological/natural systems. Chemical systems like coagulation, adsorption and advanced oxidation processes (AOPs) have also been successful.. However, most of these technologies defied commercialization mainly due to (i) lack of knowledge, (ii) cost of treatment and (iii) socio-economic and cultural issues. Also, most studies considered grey water from combined sources and are not focused on segregated source of grey water. Moreover, removal of EDCs which are hazardous micro-pollutants from bathwater is not studied.

Author and her co-workers have developed a treatment system for bathroom wastewater using combination of chemical treatment (coagulation) followed by advanced treatment (ultra filtration) in removal of various pollutants and to attain a high recovery of treated water for the purpose of reuse. Figure 7 shows the quality of treated wastewater after different stages of treatment.

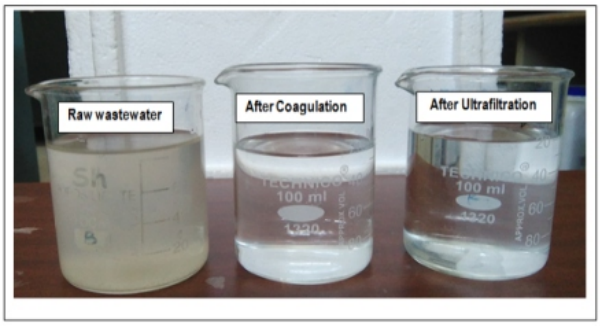

Fig. 7. Bathroom wastewater after different stages of treatment

Author and her associates also focused on treatment of greywater from washing machines using coagulation with cationic synthetic polymer as coagulant aid followed by polyethersulfone (PES) ultra filtration membrane and disinfection. The study showed good removal of various organics, solids and emerging contaminants (>90%) and 100% removal of pathogens (Table 1). The recovery of treated water was found to be greater than 90% which can be recycled and reused within the washing machine itself.

Table-1: Characteristics of recycled wastewater from washing machines

PARAMETERS	UNIT	RINSE 1		RINSE 2		RINSE 3	
		Raw	Treated	Raw	Treated	Raw	Treated
pH		8.92	8.56	7.34	7.32	7.18	6.33
Electrical conductivity (EC)	mS	1.974	1.23	0.715	0.603	0.638	0.43
Turbidity	NTU	136	35.3	17.47	3.44	9.68	1.62
Total Dissolved Solids (TDS)	mg/L	2157	1010	1320	656	1015	318
Total Organic Carbon (TOC)	mg/L	333.4	68.9	42.94	20.2	23.87	12.4
Total Coliform (TC)	CFU/100 mL	340	50	60	BDL	20	BDL
Faecal Coliform (FC)	CFU/100 mL	200	42	40	BDL	10	BDL

6. Zero Discharge Toilets

Reuse of toilet wastewater at household level after appropriate treatment and recovery of fertilizers from the waste yields twin benefits of prevention of water pollution and production of cheap natural soil conditioner. Such a technology leads to zero waste discharge. Author and her co-workers (Sharon et al., 2017) utilized the concept of treating toilet waste using solar energy to produce treated water for non-potable applications and dried solid waste for fertilizer. As illustrated in Fig. 8, the system consists of urine separation toilet, solar drying unit, evacuated solar distillation unit and solar PV panel with batteries. Human waste is dried in the solar drying unit while the wastewater is distilled in the distillation unit. The dried products can be used as fertilizer and distilled water can be used for non-potable applications such as flushing of the toilet. The quality of solar distilled and dried products were assessed by conducting experiments solar inclined still and solar dryer with synthetic wastewater and synthetic human faeces prepared as per NASA CR1802 report standards. Figure 9 shows synthetic wastewater and feaces after treatment. The distilled wastewater falls within USEPA reuse limit. Nitrogen (N), phosphorus (P) and potassium (K) contents of dried feacal powder were found to be 28.9 g/kg, 4.8 g/kg and 2.17 g/kg, respectively. Its calorific value was found to be 2220 kcal/kg and has a high stability to be used as soil conditioner. Pilot scale study confirmed the suitability of treating toilet waste using solar energy.

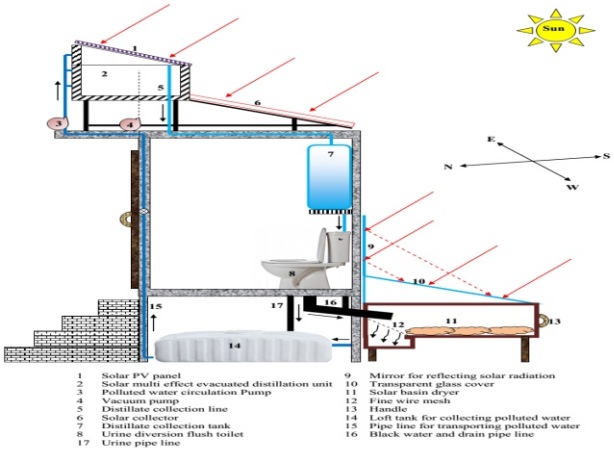

Fig. 8. Concept of toilet waste treatment using solar energy

Fig. 9. Solar Distilled Wastewater and feaces

6. Summary

Case studies on remediation of contaminated water and soil by Cr(VI) using environmental friendly technology has been discussed. The effectiveness of the reactive zone technology has been successfully demonstrated in the field. The effectiveness of awareness program and intervention through water quality monitoring using easy to use water quality test kit for improving the public health in rural areas is demonstrated. The concept of zero liquid discharge homes and sustainable usage of resource in household through recycling of water within utilities is demonstrated.

Acknowledgement

Author likes to express her gratitude to all her collaborators, students, project staffs, funding agencies and others who directly or indirectly contributed to this work. Without their help, this would not have been possible.

7. References

1. Arya V. and Philip L (2014) Visible and solar light photocatalytic disinfection of bacteria by N-doped TiO_2. Water Science & Technology: Water Supply, IWA Publishing, Vol. 14(5), pp. 924 – 930.

2. Elangovan R, Ligy Philip and Chandraraj K (2008b). Biosorption of Chromium Species by Aquatic Weeds: Kinetics and Mechanism Studies. Journal of Hazardous Materials, Elsevier, Vol. 152(1), pp. 100-112.

3. Elangovan R, Philip L (2009) Performance

evaluation of various bioreactors for the removal of Cr(VI) and organic matter from industrial effluent. Biochemical Engineering Journal, Elsevier, Vol. 44(2-3). pp. 174-18.

4. Elangovan R, Philip L and Chandraraj K (2010). Hexavalent Chromium Reduction by Free and Immobilized Cell-Free Extract of Arthrobacter rhombi-RE. Appl. Biochem. and Biotech, Springer, Vol. 160(1), pp. 81-97.

5. Elangovan R, Philip L and Chandraraj K (2008a). Biosorption of Hexavalent and Trivalent Chromium by Palm Flower (*Borassus aethiopum*). Chemical Engineering Journal, Elsevier, Vol. 141 (1-3), pp. 99-111.

6. Jeyasingh J, Somasundaram V, Philip L, Bhallamudi, S. M (2010). Bioremediation of Cr (VI) Contaminated Soil/Sludge: Experimental Studies and Development of a Management Model. Chemical Engineering Journal. Elsevier, Vol. 160 (2), pp. 556-564.

7. Jeyasingh J, Somasundaram V, Philip L, Bhallamudi, S.M (2011). Pilot scale studies on the remediation of chromium contaminated aquifer using bio-barrier and reactive zone technologies. Chemical Engineering Journal. Elsevier, Vol. 167(1), pp. 206-214

8. Jeyasingh, J. and Philip L (2005) Bioremediation of chromium contaminated soil: optimization of operating parameters under laboratory conditions. . Journal of Hazardous Materials. Elsevier, Vol. 118 (1-3), pp. 113-120.

9. Krishna K.R and Philip L (2005). Treatment of Chromium Contaminated Soils using a Bioreactor –Biosorption System. Journal of Hazardous Materials, Elsevier, Vol. 121(1-3), pp. 109-117

10. Philip L, Leela Iyengar and C. Venkobachar (1998). Cr(VI) Reduction by Bacillus coagulans Isolated from Contaminated Soils. J. Environmental Engineering, ASCE, Vol. 124(12), pp. 1165-1170.

11. Philip L, Leela Iyengar and C. Venkobachar (1999), Immobilized Microbial Reactor for the Biotransformation of Hexavalent Chromium. Int. J. Environment and Pollution. Vol. 11(2), pp. 202-210.

12. Philip, L. (2013), "Final Report on Scaling up of the community based water quality monitoring and sanitary surveillance in Veppanapalli Block, Krishnagiri district, Tamilnadu", UNICEF Chennai office for Tamilnadu and Kerala.

13. *Priya V.S and Philip L (2015).* Photocatalytic Degradation of Aqueous VOCs Using N Doped TiO2: Comparison of Photocatalytic Degradation under Visible and Sunlight Irradiation. International Journal of environmental science and development. Vol. 6(4): pp 286-291

14. Putnam DF. Composition and concentrative Properties of human urine. National Aeronautics and Space Administration Washington, D.C. July 1971; Report No. NASA CR-l802.

15. Senthilnathan J and Philip L (2009). Removal of Mixed Pesticides from Drinking Water System by Photodegradation using Suspended and Immobilized TiO2. J. Env Sci and Health Part-B, Taylor & Francis Ltd. Vol. 44 (3), pp 262-270.

16. Senthilnathan J and Philip L (2010a). Photocatalytic Degradation of Lindane under UV and Visible Light using N-doped TiO_2. Chemical Engineering Journal. Elsevier, Vol. 161(1-2), pp. 83-92. (IF – 4.321)

17. Senthilnathan J and Philip L (2010b). Investigation on Degradation Of Methyl Parathion Using Visible Light in the Presence of Cr^{3+} and N-Doped TiO_2. Advanced Materials Research, Vols. 93-94, pp. 280-283. (IF – 0.086)

18. Senthilnathan J and Philip L (2010c). Removal of mixed pesticides from drinking water system using surfactant assisted nano

TiO_2. Air, water and Soil Pollution. Springer, Vol. 210(1-4), pp143-154

19. Senthilnathan J and Philip L (2012). Elimination of Pesticides and their Formulation Products from Drinking Water using Thin Film Continuous Photoreactor under Solar Radiation. Solar Energy Journal. Elsevier, 86(9), pp 2735-2745.

20. Sharon, H. Reddy, K.S., Krithika, D., Philip, L.(2017). Experimental performance investigation of tilted solar still with basin and wick for distillate quality and enviro-economic aspects. Desalination, 420, pp 30-54

21. Shashidhar, T. Philip L, Bhallamudi, S.M (2006). Bench Scale Column Experiments to study the Containment of Cr(VI) in confined aquifers by Biotransformation. Journal of Hazardous Materials. Elsevier, Vol. 131(1-3), pp. 200-209.

22. Shashidhar, T., Bhallamudi, S.M, and Philip L (2007). Performance evaluation and modeling of bio-barriers for remediation Cr (VI) contaminated confined aquifers. Journal of Hazardous Materials. Elsevier, Vol. 145(3), pp. 437-452

23. Somasundaram V, Philip L, Bhallamudi, S. M (2009). Experimental And Mathematical Modeling Studies on Cr(VI) Reduction by CRB, SRB and IRB, individually and in Combination. Journal of Hazardous Materials, Elsevier, Vol. 172(2-3), pp. 606-617.

24. Somasundaram V, Philip L, Bhallamudi, S.M (2011). Laboratory Scale Column Studies on Transport and Biotransformation of Cr (VI) through Porous Media in Presence of CRB, SRB and IRB. Chemical Engineering Journal, Elsevier, Vol. 171(2), pp. 572-581.

25. Surenjan A, Sambandam B, Pradeep T and Philip L (2017). Synthesis, characterization and performance of visible light active C-TiO2 for pharmaceutical photodegradation. Journal of Environmental Chemical Engineering, 5 (1), pp. 757 – 767.

Annals of the Indian National Academy of Engineering
Vol. XV, April 2018

Low Carbon Desalination & Water Purification

P.K. Tewari[1]

Abstract : India has a highly seasonal pattern of rainfall, with 50% of precipitation falling in just 15 days. As per Central water Commission, total annual rain-fall in the country is estimated as 4000 Billion Cubic Metre (BCM). The utilizable or internally renewable water resources are estimated to be 1200 BCM (i.e. average inflow of rivers and recharge of aquifers). The annual water demand is increasing. It was about 800 BCM in 2010 and estimated to touch 1500 BCM in 2050. The emerging scenario is alarming. There are areas which face perennial water shortage. Several regions are suffering from excess contaminants like salinity, fluoride, nitrate, iron, arsenic, heavy metals and microbial contaminations of ground water. The contaminants lead to water borne diseases and cause hardships to the inhabitants. The problems are not limited to providing adequate quantities of good quality water. Growing population, cities and industries are putting great stress on the aquatic environment. Disputes between the States in sharing of water are well-known. Today's challenge is to effectively use the available water and to increase the availability of right quality of water. Adding to the general concern over the sustainable use of water, are the uncertainties about the possible impact of global climate change. The temperature rise due to green-house effect may lead to change in rainfall patterns and evaporation rates. Any such changes would have major implication on water and environment. Low carbon desalination such as nuclear desalination and water purification has potential to offer solutions to the challenging water issues.

Keywords: Low carbon desalination, nuclear desalination, water purification.

1 Low Carbon Desalination

Seawater desalination provides an additional source of fresh water, thus enhancing fresh water availability in the coastal areas. Interest in using nuclear energy for producing potable water from seawater has been growing worldwide [1]. Nuclear energy has capability to reduce the carbon foot print and provides low carbon desalination. It can be usedin the form of heat/ electricity for producing fresh water from seawater. As per International Atomic Energy Agency (IAEA), nuclear desalination means production of potable water from sea water in a facility in which a nuclear reactor is used as the source of energy for the desalination process. Electrical and/or thermal energy may be used in the desalination process. The facility may be dedicated solely to the production of potable water, or may be used for the generation of electricity and the production of potable water. In either case, it is an integrated facility and energy is produced on-site for use in the desalination system. It also involves some degree of common or shared facilities, services, staff, operating strategies, outage planning and control facilities, and seawater intake and outfall structures.' Nuclear desalination involves three technologies: nuclear, desalination and their coupling system. A Nuclear Desalination Demonstration Plant (NDDP) based on hybrid technology was developed in BARC and is operational at Kalpakkam in Tamilnadu (Fig. 1). The hybrid 4500 m^3 per day Multi-Stage Flash (MSF) and1800 m^3 per day Reverse Osmosis (RO) desalination system, together constitute the largest capacity 6300 m^3 per day operating nuclear desalination plant based on hybrid technology

[1]Homi Bhabha National Institute (HBNI), Bhabha Atomic Research Centre (BARC), Mumbai- 400085

attached to Madras Atomic Power Station (MAPS). It produces two qualities of desalinated water from seawater: distilled water for high end applications and potable water for drinking and other uses. Co-location of desalination and power plants has benefit of sharing the resources and infrastructural facilities.

There is scope to use low grade heat/ waste heat of nuclear reactors as energy source. A 30,000 litres per day low temperature evaporation (LTE) seawater desalination plant utilizing waste heat of nuclear research reactor was also set up in BARC. The technology has been transferred for deployment in a commercially viable manner.

Fig. 1: Nuclear Desalination Demonstration Plant (NDDP) at Kalpakkam (Tamilnadu)

2 Low carbon Water Purification

BARC has developed several types of low carbon water purification technologies (Indian Patent nos. 19596, 186210, 186375, 194101, 194106, 195317) addressing the unique challenges faced by the country particularly in rural and remote areas. knowhow of the technologies have been transferred to several entrepreneurs for wider deployment in a commercially viable manner. Rural adaptability of the technologies has been demonstrated (Fig. 2). Field demonstration of the technologies for purification of raw water contaminated with bacteria, virus, fluoride, arsenic, iron and other contaminants has been carried out in different parts of the country.

In the tribal hamlets located at about 100 kilometres from Mumbai (India), an eco-friendly and low cost water filtration technology has changed lives in around 200 households. Residents of these un-electrified settlements have access to potable water round-the-clock owing to a domestic purifier developed by the Bhabha Atomic Research Centre (BARC). The water purifier does not require electricity. It causes no wastage of water and can be maintained easily. The low carbon technology, if widely adopted, could do away with the hazards of adding chemicals such as chlorine, or using filtration units that guzzle power or require professional maintenance. The purifier uses the ultrafiltration (UF) technique: a membrane made up of polysulphone, a kind of tough plastic. It selectively allows water to pass while keeping out dirt, suspended particles, cysts, viruses, bacteria including the dreaded E-coli. Purified water is piped out of the filter and stored. The output of the filter is five litres per hour for every membrane, without the aid of a pump. One of the licensees M/s Sonadka has installed several units in community projects (where electricity was not available) serving 200 to 300 people each in Imphal Manipur, India (Fig. 3). Apart from tribal and rural settlements, the purifier has been set up in hospital and residential colonies and rural schools. The company is now running a pilot project at railway stations to provide low carbon purified potable water to passengers.

Fig. 2: Nanocomposite Membrane Based Water Purification Unit requiring no Electricity

Fig. 3: Community Level Water Purification Unit for Remote Areas

Renewable energy based low carbon desalination and water purification systems have also been developed. Small and community size solar energy driven Reverse Osmosis (RO) and Ultra-Filtration (UF) units have been demonstrated for producing clean water. Bicycle mounted solar based units, 10 and 80 Litres per hour capacity– RO based and UF based respectively, have been demonstrated and technology transferred.

Contaminants, both inherently present in environment in certain places and pollution arising from industrial and other human activities, often impact water quality to varying degrees in different locations in India and in other countries. It is estimated that more than 85% of rural water supply is sustained by ground water source. Though the ground water is less susceptible to pollution as compared to surface water, water quality is a major issue.

Membrane based water purification systems, to remove or mitigate contaminants, are essential pre-requisites for ensuring acceptable water quality (and in turn, taking care of health and sanitary needs of communities, including in rural areas). Thermal and membrane based technologies for waste water treatment and water recycle have very high potential in industrial sectors leading to effective water management, product recovery from effluent and minimal waste disposal.

3 Specific Aims

There is need for enhanced research and development in the field of low carbon desalination and water purification so that carbon foot print can be brought down. In several parts of the world, water is available but quality is a major issue. Affordability is another aspect to be kept in mind by the researchers. General view point all over the world is that water is a simple compound which is not true. It is full of surprises. Normally, researchers prefer to work in the field of 'High Value, Low Volume' projects. The research work in the field of water is a 'Low Value, High Volume' which itself is quite challenging, however, motivation is huge as it concerns with the socity at large across the globe. In low carbon desalination and water purification, the R&D work need to be oriented in the direction of cost reduction strategies through technological innovations.

4 Methods

R&D efforts may be directed in the following directions:

i. Nuclear Desalination
   a. Reduce the energy requirement through technological innovations
   b. Need to understand coupling aspects
   c. Nuclear fuel cycle and reactor type as energy source
   d. Small reactors
   e. Low grade and waste heat utilization
   f. Hybrid desalination technologies

ii. Membrane Processes
   a. Enhance membrane life

b. Enhance membrane flux
c. Selectivity aspects
d. Development of fouling resistance membrane
e. Spent membrane management

iii. Thermal Desalination
a. High heat transfer coefficient
b. Enhanced heat transfer performance
c. Reduction in terminal temperature difference
d. Material of construction

iv. Reject Management
a. Recovery of valuables from brine

v. Emerging technologies:
a. Nano-composite membrane
· Stability
· High temperature application
b. Membrane Distillation
c. Forward Osmosis

5 Outcomes

The outcome of the above mentioned R&D efforts are as following:

i. Potential to bring down the carbon foot print in desalination and water purification technologies
ii. Make the water technologies more affordable to the bottom of the pyramid in society
iii. Environmental Considerations

There is need to step up research in the field of nanocomposite membrane which appear to be quite promising. Besides tuning the physicochemical properties of membranes (hydrophilicity, porosity, charge density, thermal, and mechanical stability), the incorporation of nanomaterials can provide membranes with unique properties of nanomaterials and also induce new characteristics and functions based on their synergetic effects. It provides a new dimension to design the next generation of polymeric membranes with high performance and antifouling properties. The potential applications of nanocomposite membranes could cover the whole filtration spectrum including micro-filtration, ultra-filtration, nano-filtration, reverse osmosis and forward osmosis.

Several challenges need to be addressed to optimize the design of the nanocomposite membranes [1]:

- Fundamental understanding need to be developed to systematically reflect the effects of nanomaterials on membrane structures and correlate them to the membrane performance changes.
- Approaches for better dispersion of nanomaterials need to be further explored.
- Compatibility of nanofillers with polymers should be ensured to avoid leaching of nanomaterials into to the environment.
- Large scale production and industrial application with cost effectiveness

All references should be listed at the end of the paper [Ramakrishnan and Francavilla (1975)]. The names of the authors should be in bold, with the last name(s) first. The year in which the paper is published follows the name(s) of the author(s). Journal and book titles should be in italic.

Acknowledgement
Add an acknowledgement when appropriate.

References :

1. **Intr** *Introduction of Nuclear Desalination- a Guidebook*, Technical Report Series No. 400, International Atomic Energy Agency (IAEA), Vienna, 2000

2. **P.K.P.K. Tewari** (2016) *Nano-composite Membrane Technology: Fundamentals & Applications,* CRC Press, Taylor & Francis Group, pp 146.

Annals of the Indian National Academy of Engineering
Vol. XV, April 2018

Urban Floods : An Evolving Engineering Challenge

Chandra Rupa R. and P.P. Mujumdar[1,2,3]

Abstract : Globally, urban flooding is the biggest and severest natural disaster faced year after year. Managing floods in cities is evolving as an engineering challenge due to several factors. Urban flooding cannot be managed in isolation and responses to potential impacts of floods are complicated by interlinked environmental and socio-economic changes. To manage flooding, an integrated framework is required in which a leap from the current, poorly managed system to a highly efficient and technology-driven automated management is achieved. Such an integrated approach should provide clarity regarding the flood management, risk, vulnerability and resilience as well, and how the interactions across various systems can be achieved. This paper discusses about challenges and various sights in modelling, managing floods and lists different structural and structural measures to attain a sustainable urban drainage system. An integrated approach is shown for urban planning and water management for a viable and sustainable environment, bringing together researchers, government agencies, policy makers and stake holders. A city scale pioneering and experimentation are essential to build resilience through bottom-up initiatives that can shape strategy and policy development.

Keywords: urban flooding, integrated approach, flood risk management, sustainability.

1 Introduction

The global population is increasingly getting concentrated in cities, with more than 50% of the world's population currently living in urban areas (UN, 2011). The United Nations urbanization prospects (2005) reported that twentieth century is observing rapid urbanization, globally. This population growth has led to urban sprawl with rapid increase in urban areas. Urbanization, leading to changes in land use/land cover, has created substantial contrasts in land surface characteristics between urban areas and surrounding rural areas, manifesting in different hydrologic signatures. Advances in the science and practice of urban hydrology have therefore been significant over the last two decades. New methodologies for modelling urban precipitation have emerged, with the aim of addressing the challenges of modelling urban flooding precisely. Despite these advances, management of flood in urban areas is still a challenge to policy makers in many countries. This paper discusses on the issues why management of urban flooding is an engineering challenge and give insights of an integrated approach to manage flooding in cities.

2 Why Urban Flooding is a Challenge?

It is well understood that urbanization alters the hydrologic response of a catchment. However, precise modeling of the hydrologic response and then the assessment of the flooded areas, including the management of flooding in cities is still a major challenge for various reasons. Following are some of the challenges in modeling and management of urban flooding.

2.1 Availability of data

Flood and environmental risks are always dependent on correct designs, which in turn depend on the quality and quantity of data. Data requirements for urban applications are different

[1] Dept. of Civil Engg., Indian Institute of Science, Bangalore-560012.
[2] Divecha Centre for Climate Change, Indian Institute of Science, Bangalore-560012.
[3] Interdisciplinary Centre for Water Research (ICWaR), Indian Institute of Science, Bangalore-560012.

compared to applications in rural catchments (Schilling, 1991). Especially, fine resolution data in both temporal and spatial scales are required. Urban infrastructure design and evaluation is in general based on hydraulic simulations using short-duration, local precipitation data as input. For example, a sustainable urban storm water drainage system requires handling a short duration, low frequency precipitation event without excessive flooding or other problems (Olsson et al., 2012). Most urbanized catchments are relatively small, with low catchment response times, typically of hourly to sub-hourly scales. Therefore, the precipitation data from sub-hourly to hourly time scales are required for assessing urban runoff behavior. However, the availability of precipitation time series recorded at such short time steps is in general sparse leading to uncertainties.

In the urban designs, it is also important to consider the spatial variability of short duration high intensity precipitation events. The areal extent of such events is in general limited, and the events evolve as a nature of convective storms, where, the precipitation producing cells are typically of the order of a few square kilometres in areal coverage and have durations of between 10 and 40 min (Patrick and Stephenson, 1990). However, the data is not recorded at a high spatial resolution leading to high uncertainties in estimations of the spatial variation of precipitation in urban areas. Therefore, understanding spatial variation of short duration events along with uncertainty quantification is also crucial in the urban hydrologic designs.

New research methods have been emerging to quantify the uncertainties due to insufficient quantity and quality of data and propagate the uncertainties in the urban hydrologic designs. For example, methods like Monte Carlo simulations, Bayesian techniques are incorporated to quantify the uncertainties due to insufficient quantity of data in the design precipitation intensities. Fig. 1 shows the Intensity Duration Frequency (IDF) relationships for the Bangalore City obtained from the classical approaches using standard statistical techniques (Maximum Likelihood Estimation (MLE) approach) and from the Bayesian method. It should be noted that the uncertainties in the short duration (at sub-hourly scales) precipitation events are high when compared to that of the high duration, of order daily.

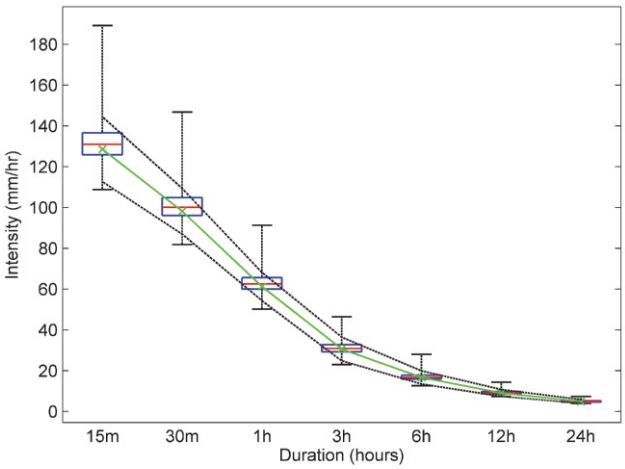

Figure 1: Variation in return levels for 10-year return period for different durations (historical period, 1969-2003) for Bangalore City. Boxplot gives the uncertainty in return levels obtained from Bayesian analysis. Intensity using Classical approach (MLE method) is shown in solid green line; black dashed lines give the uncertainty band using delta method

2.2 Climate change impacts

Although it is evident that urbanization significantly influences the local climate, the climate change also effects the extreme precipitation, adding further complications in modeling the extremes in urban areas. According to IPCC (2012), climate change is believed to increase the frequency and magnitude of the extreme precipitation events. As growing urban communities seek to minimize their impact on already stressed water resources, an emerging challenge is to design for resilience to the impact of climate change, particularly in regard to ensuring secure water supplies and the protection of water environments. For the Bangalore City, short duration precipitation increases considerably in future (Chandra Rupa et al., 2015). Fig. 2 shows the

IDF relationships for future time slices for RCP8.5 scenario for 10-year return period.

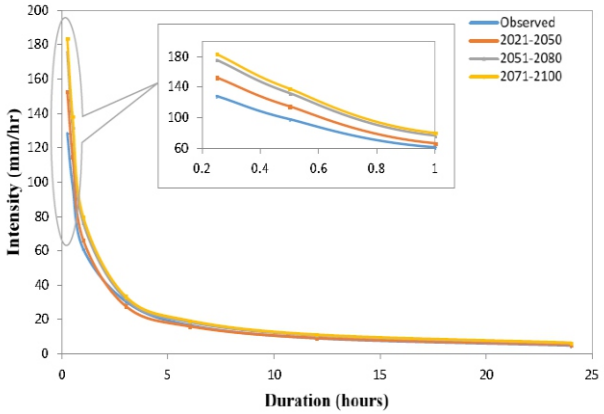

Figure 2: Projected IDF relationships for Bangalore City for RCP 8.5 scenario for 10-year return period (Chandra Rupa et al., 2015)

2.3 Reliable forecasts

Simulating emergent behaviors and predicting precipitation extremes are significant research challenges because the interactions between drivers are highly complex and uncertain. A major challenge of extreme weather forecasting in urban areas is the underrepresentation of the local or regional influences of the urban areas of interest. Weather forecasting is essentially an initial value problem, and misrepresentation of the regional heterogeneities in land use and land cover (LULC), and the consequent land-atmospheric feedback, cascades to errors in local and regional extreme rainfall prediction. Currently, most numerical weather prediction (NWP) models are good for developing regional and large simulations but for urban flooding, urban scale weather forecasts are needed.

Therefore, the objective should be to develop components for community NWP forecasting models that can be applied for cities. The widely-used Weather Research Forecasting (WRF) model is considered as the base, and the challenge is to adapt the model for high resolution (sub km) grid spacing runs. For developing urban scale NWP forecasts, with the availability of high-resolution LULC or LiDAR datasets, there is a need for a robust methodology to incorporate these datasets as an input into (NWP)/mesoscale weather forecasting models. Additionally, the corresponding dynamic, thermal and radiative properties (e.g. albedo, emissivity, roughness length, specific heat capacity etc.) of the land cover types from these datasets need to be parameterized into the models (Mujumdar et al., 2017).

Current approach used in weather models for representing urban areas have been based on a simple parametrization that alters surface albedo, thermal capacity, hydraulic conductivity, and roughness. These variables and the corresponding parameterizations are embedded within appropriate land surface models (LSMs) which have water, temperature, radiation, balance and predictions in a prognostic manner. That is, the atmospheric information such radiation, winds, temperature, humidity, and rainfall are needed as inputs to the LSM to generate surface energy balance, and hydrological responses such as surface and deeper soil moisture/ temperature fields. These surface variables in turn modulate the development of boundary layer, regional thermals, winds, cloud convection and ultimately the rainfall timing, amount, location, and intensity. Changes in LULC, impact the hydrological balance of the region and could potentially result in urban flooding. Further, since urbanization also implies increasing population, the flood risk, vulnerability and consequence of such events should they occur, drastically increases (Mujumdar et al., 2017). Therefore, a critical factor in developing high-resolution urban weather prediction model is the representation of land surface and the associated parameters This challenge of representing the land surface that can be linked within high-resolution WRF needs to be undertaken for urban areas.

2.4 Management of urban infrastructure

Despite research issues like assessing the climate change impacts and modelling reliable forecasts, poor maintenance and management of urban water infrastructure is a major cause for flooding in cities. Though reliable forecasts are available, if the drainage system cannot cater the needs of the storm, flooding is inevitable. Besides poor

maintenance, some of the other factors which causes flooding are listed in the following sub-sections.

2.4.1 Encroachments

Storm water channels overtops their banks if developments encroach floodplains, obstructing floodways and causing loss of natural flood storage. Drainage systems back up because they cannot cope with the volume of water or are blocked by urban waste. Also, there could be cases where the sewer systems obstruct the natural flow in the drains.

2.4.2 Unplanned urbanization

Over a longer historical period, cities have always successfully adapted to changing environmental conditions and thus have been extremely resilient. Due to the unprecedented growth of population in urban areas in the recent past, cities couldn't adapt to the quick changes. This increase in population has led to unplanned urbanization in most of the cities. Research work by Sheppard (2007) revealed that the spatial distribution of urban population in nearly all 90 cities surveyed is by and large not the result of conscientious planning. This lack of careful planning, or even uncontrolled urbanization, will exacerbate the trend of increasing flood vulnerability of cities due to a combination a) development in areas previously in nonurban use, leading to encroachment and expansion onto flood-prone areas b) redevelopment of built-up areas and infill of the remaining open spaces in already built-up areas, leading to an overall density increase and subsequent increase of surface imperviousness and disruption of natural drainage channels and c) conversion of water bodies (lakes, ponds in low lying areas) to residential layouts (Zevenbergen et al., 2008).

2.5 Extended events of precipitation

The worst flooding occurs after prolonged rainfall when the soil is saturated and the water levels in drains, lakes rise. Then, if an intense rainfall burst occurs, causing a large amount of rain within a brief period, flash flooding may occur with little or no warning. This is one of the reasons for devastating flooding in the Bangalore City during September $1^{st} - 10^{th}$, 2017.

3 Integrated Urban Flood Management

Cities have witnessed tremendous growth in the last few decades, as a result of the rise in urban population. Unfortunately, infrastructure development has lagged with the economic and population growth, resulting in mismanagement of resources. Changing rainfall patterns, due to both natural and anthropogenic causes, have made the flooding problem more exaggerated, frequent, and widespread. Cities' drainage infrastructure, coupled with soil erosion, have proved ineffective in the face of intense rainfall, making flash floods a common occurrence. Consequently, cities losing their capacity to deal with quick changes (like changes in extreme rainfall events) and the ability to anticipate and adapt to slow changes and trends (population increase, climate change) pose new challenges for urban flood management research and touch upon various disciplines (e.g. urban planning, regional economy, etc.). Because urban floods cannot be managed in isolation, there is a need for integrated approaches that address the problem of urban flooding.

Best management techniques and practices are required to achieve a leapfrog from the current, poorly managed state to a highly efficient, technology-driven automated end-to-end management of urban flood, thus overcoming the institutional constraints to a significant extent. An innovative use of sensor and communication technologies coupled with ultra-high resolution real-time nested forecasts of high intensity rainfall, state-of-the-art hydrologic models, GIS and control systems are required for implementable operational decisions in real time. Hydro-meteorological forecasts with sufficient lead times of a few hours to a day or more, need to be developed using a suite of data driven, pattern recognition models as well as process based numerical urban weather prediction models. Forecasts of high intensity rainfall should be

converted to flood forecasts with in-situ as well as remote sensed measured data. Measurements from in-situ sensors provide information on rainfall intensity, and geospatial location of water levels, which should be assimilated within the hydrologic models.

A comprehensive GIS driven data base, integrated with the flood forecast models is required to graphically depict flooding in real time at various locations in the city. Control systems algorithms should be developed to provide operational decisions, communicated instantly through internet and/or mobile technologies. Long term adjustments in the hydrologic designs for urban flooding are to be recommended based on likely changes in frequencies of high intensity rainfall. To achieve this, cross-sectional collaborations between hydrologists, climatologists, government agencies and policy makers is required. Through involvement of government agencies, policy makers and with the support of NGOs implementing post-flood management solutions is possible. Involvement of stakeholders is also crucial in achieving a flood free city. A citizen driven portal should be developed to upload digital pictures or tweets on the flood levels, which provides visual, numerical input to complement the sensor data in a bi-directional information flow mode.

A collaborative project titled "Integrated Urban Flood Management in India: Technology driven Solutions" by Indian Institute of Science, Bangalore with other partners from Karnataka Natural Disaster Monitoring Center (KSNDMC), NIT Warngal, ITS Pilani Hyderabad Campus and C-DAC Trivendrum aims at an integrated urban flood management in urban areas (Mujumdar et al., 2017). The project has its focus set on two cities: Bangalore and Hyderabad, and on a controlled watershed in Bangalore. The graphical overview of the project is shown in Fig. 3

Figure 3: Graphical overview of "Integrated Urban Flood Management in India – Technology Driven Solutions"

The key activities carried out towards this project are summarized in following points.

- The changes in the hydro-climatic variables' extremes (which are the main causes of floods) are analysed using historical observed data for Bangalore and Hyderabad city. Especially, the spatial distribution of return levels of extreme rainfall, are studied. Fig. 4 shows the variation in return levels in and around the Bangalore City. The return levels and the associated uncertainty on the western part of the Bangalore City are higher by 10% compared to the other parts for annual maxima (Chandra Rupa and Mujumdar, 2017). In addition, temporal non-stationarity in the extreme rainfall series is studied. Fig. 5 shows the methodology developed for obtaining the non-stationary rainfall IDF curves by modelling non-linear trend in the extreme rainfall series (Agilan and Umamahesh, 2017).

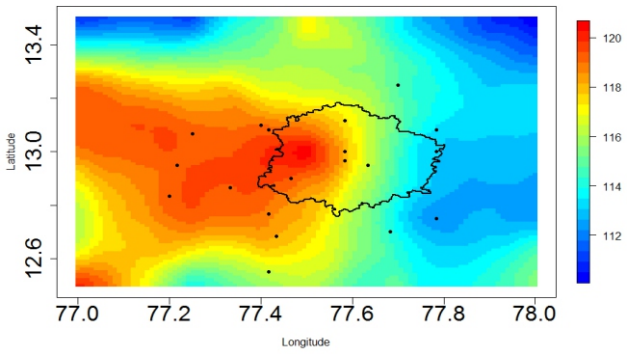

Figure 4: Spatial map of mean return levels (mm) for 10-year return period for Bangalore City. The city boundary is marked, and the stations used for modelling are shown as black dots (Chandra Rupa and Mujumdar, 2017)

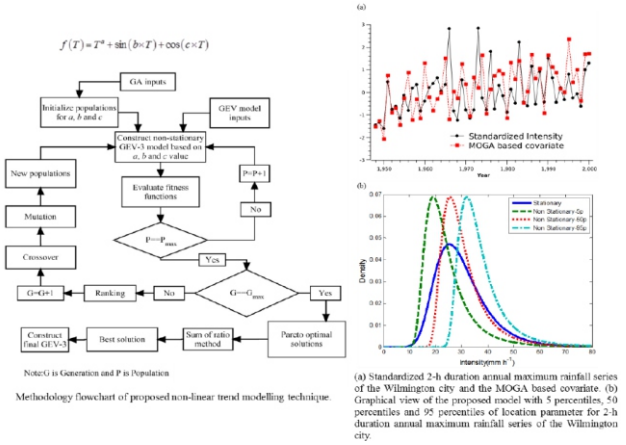

Figure 5: Proposed methodology for developing non-stationary rainfall IDF curves for Hyderabad City by modelling non-linear trend in the extreme rainfall series. Results of the proposed methodology are shown on the right panel of the Figure (Source: Agilan and Umamahesh, 2017)

- The climate change impacts on hydro-climatic variables and its extremes are projected for the future time periods. Solving research problems like - model and parameter uncertainty in IDF relationships under climate change, the capability of covariate based non-stationary rainfall IDF curve in encompassing future rainfall changes etc.
- 2D overland flow models are built for the study regions to simulate the flood event accurately. The developed two-dimensional overland flow model is capable of simulating floods with obstructions due to buildings and other structures.
- The adequacy of capacity of the existing structural measures to cope with the changing climate is studied for Bangalore and Hyderabad city.
- Enhanced laboratory setup is created, and experiments are conducted to reproduce the field situations under floods.

Figure 6: Experimental setup and facilities

Implementation on ground:

- Flow level sensors are installed in pilot study areas. Fig. 7 shows the flow level sensor installed in the storm water drain in IISc campus and Fig. 8 shows the flow level sensors installed in a storm water drain and in a lake (Gottigere Kere) in Bangalore City.
- LiDAR survey is carried out in IISc Campus for obtaining very high resolution (0.2m resolution) terrain information that will eventually help in producing accurate flood forecast and inundation maps.
- The flow level and weather sensors are connected to wireless communication systems for getting hydro-meteorological data in real-time.

Figure 7: Water level sensor installed at the outlet of the drainage network inside the IISc Catchment

- Flood maps are created by combining hydrological simulations with GIS environment. Fig. 9 shows the flood inundation map of a catchment in Bangalore City.
- Flood events are characterised into different classes for management activities.
- Flood management decision support system is developed by integrating Rainfall Forecast-Hydrologic Models-Flood Forecast on Real time

Figure 8: Water level sensor installed in a storm water drain and in a lake – Bangalore City case study

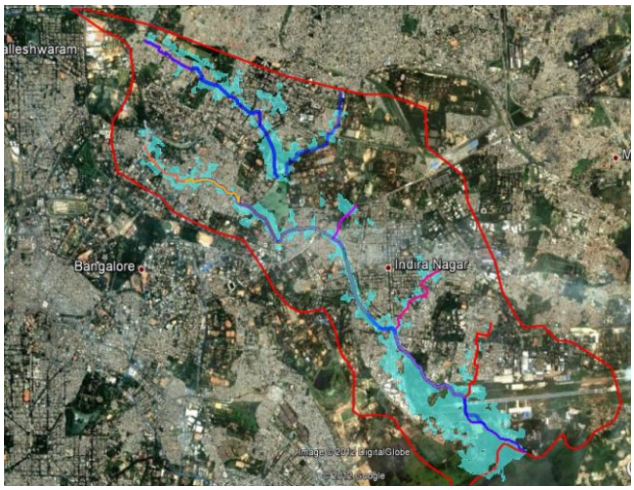

Figure 9: A flood inundation map superimposed over the Google map for a valley in Bangalore City

In addition to research and modelling, a few value additions are made in the project – a) revised urban landcover and climate zone maps of Bangalore city are created for accurate meteorological forecasts using weather research forecast model, b) communication systems such as WhatsApp Group, Website, Twitter page, Facebook page, e-mails and customised mobile SMS are created to disseminate flood forecast to administrative departments and public and c) a number of outreach activities are conducted during the project period to train faculty members of premier institutes of India, engineers from different municipalities, scientists and research scholars. In particular, the team has organized three Monsoon schools, two short-term courses, two workshops and a training program.

The disaster management i.e., emergency preparedness and response activity, is also planned in the project. As the response to a natural disaster warning must be immediate, comprehensive, and demonstrate very clear lines of command, the hierarchy in the chain of command was established for all responsible personnel. Further to the specification of roles and responsibilities for those involved in disaster management activities, the main tasks responding to different disaster scenarios were identified. Fig. 10 shows the summary of disaster management activities.

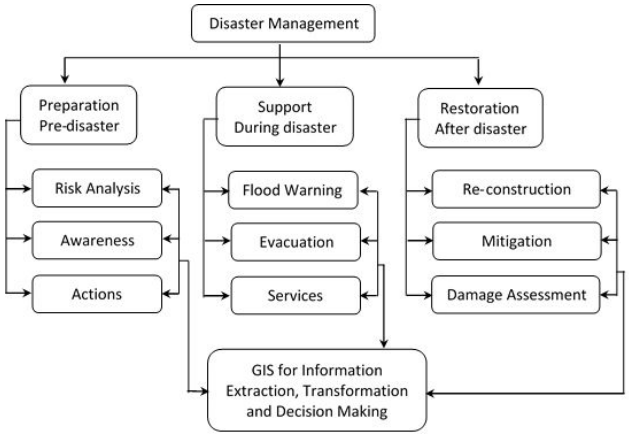

Figure 10: Disaster management framework (Modified from Price and Vojinovic, 2008)

4 Flood Risk Management

It is unrealistic to expect a no flooding scenario in urban areas and therefore risk management in case of flooding is a must. Flood risk management requires the holistic development of a long-term strategy, balancing current needs with future sustainability. Integrated flood risk management also includes the recognition that flood risk can

never be fully eliminated and that resilience to flood risk can include enhancing the capacity of people and communities to adapt to and cope with flooding. Four capacities for reduced vulnerability and increased resilience are illustrated in Fig. 11.

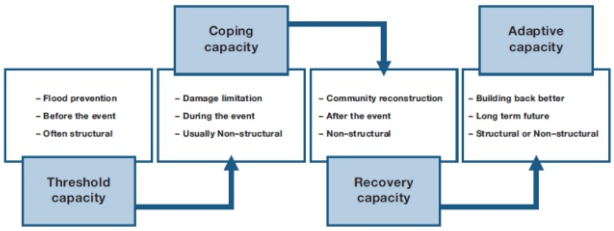

Figure 11: The four capacities towards increased resilience (Source: Jha et al., 2012)

An integrated strategy usually requires the use of both structural and non-structural solutions. It is important to recognize the level and characteristics of existing risk and likely future changes in risk.

4.1 Structural and non-structural measures

Structural measures range from heavily-engineered interventions, such as floodways and reservoirs, to more natural approaches like wetlands and greening measures. They cover water management at the catchment and urban level. A few structural measures are:

- Providing temporary storage for storm water in urban areas by making use of areas with other primary functions, for example, parkland, play grounds or car parks
- Increasing the drainage capacity or altering the line
- Reopening culverts
- Floodplain restoration
- Relief channels - re-direct some of the flow at flooded areas, by using an off-take structure, to an area where water can be safely discharged without adverse impacts
- Protecting the banks from erosion
- Introduce flood mitigation structural measures, (restriction removal, widening/deepening)

Non-structural measures do not require extensive investment in hard-engineered infrastructures, but rely instead on a good understanding of flood hazard and adequate forecasting systems. There are four main categories are i) increased preparedness, ii) flood avoidance iii) emergency planning and management and iv) speeding up recovery and using recovery to increase resilience.

Many of the measures, such as early warning systems, will form part of any flood risk management scheme. They can be seen as a first step in protecting people in the absence of more expensive structural measures, but they will also be needed to manage residual risk where such schemes have been constructed.

Engagement of the community at risk and encouragement of citizen preparedness is critical to the success of non-structural flood risk management. Communication is, therefore, a key element. Develop and implement awareness programs. Land use planning and regulation of new development is a central measure for reducing future flood risk, particularly in rapidly urbanizing emerging economies. Control land use/development.

Heavily-engineered structural measures can be highly effective when used appropriately, but they share one characteristic: that they tend to transfer flood risk from one location only to increase it in another. In some circumstances this is acceptable and appropriate, while in others it may not be. Therefore, a careful study of the area is required before implementing a solution.

4.2 Sustainable drainage

It is possible to return the catchment response to a more natural state by using natural methods of drainage. The use the infiltration and storage properties of semi-natural devices such as infiltration trenches and ponds, not only help in preventing floods, but also improve water quality. In addition, they can enhance the physical environment and in urban areas. These techniques are term 'best management practices' (BMPs), or

the Sustainable Urban Drainage Systems (SUDS) (Woods-Ballard et al. 2007; Butler and Davies 2011). There is growing awareness that sustainable urban drainage systems can offer a more sustainable option for the management of storm water runoff than conventional drainage systems.

SUDS devices are most effective in avoiding flooding. Like all drainage systems, SUDS are designed to provide capacity for a storm event of a particular frequency. For more extreme events, exceedance flows are likely to be generated and must be carried by the major drainage system. Many SUDS devices are based on infiltration to the ground, the risk of groundwater pollution is an important consideration, especially where surface runoff is likely to be polluted and the groundwater is used for drinking supplies. The design of a permeable pavement system, for example, can be adjusted to allow infiltration, or not, in order to account for this.

The main types of SUDS devices can be listed as: Inlet control - Inlet control devices provide storage close to the point where the rainfall is first collected.

Green roofs/vegetated surfaces - Rooftop ponding uses the storage potential of flat roofs; as this creates an additional load there is an increased need for water tightness, as well as good maintenance of outlet control devices. A green roof is a planted area that provides storage, encourages evapo-transpiration and improves water quality.

Infiltration devices - Instead of connection to the drainage system, water collected from roofs can be diverted at the bottom of the downpipe to in filtrate in nearby stable pervious areas. Paved area ponding, to accommodate heavy rainfall, can be achieved by restricting in flow to the piped drainage system, thereby reducing flood risk downstream.

Detention ponds - Detention basins are storage facilities formed from the landscape with controlled outflow. They store stormwater temporarily, and are dry between storms.

Retention ponds - They provide storage within a permanent body of water. They allow natural treatment of the water and provide environmental and amenity benefits.

Constructed wetlands - A water store, consisting of a water butt or a tank near to ground level, can store rainwater and make it available for garden use, though some outflow must be assured to provide capacity for subsequent rainfall.

Permeable paving - Permeable paving (also known as pervious or porous pavement) are surfaces that allow water to pass through voids in the paving material or between pavers while providing a stable, load-bearing surface. This allows storm water to filter through the soil below the paved surface, reducing the numerous environmental issues associated with water runoff.

5 Concluding Remarks

Historically, disasters were viewed as 'act of God', but, floods in the recent past can be viewed as 'negligence of man'.

Establishing healthy urban conditions through planning, design, and management, while ensuring a resilient future for people in cities, requires a novel understanding of how numerous elements converge and interact to form and influence urban functions and dynamics (McPhearson et al., 2016, Alberti, 2017). Given the uncertainties surrounding these complex interactions, urban policy makers need reliable empirical evidence, innovative decision-making tools, and novel approaches (Rosenzweig et al., 2010).

Strategic decisions about urban planning and investments in infrastructure require synthesis of the complex and evolving knowledge of how coupled human–natural systems work. Only a new collaboration among scholars from diverse disciplines can develop a research agenda that will deliver a shared framework and generate a productive knowledge synthesis, connecting recent advancements in complex systems science, engineering, and urban design and planning. Such

synthesis is essential to transforming the study of cities into an integrative urban science to address the challenges confronting humanity in an urbanizing world. Therefore, an integrated urban planning and water management, bringing together researchers, government agencies, policy makers and stake holders is required for a more viable and sustainable urban environment.

Cities are becoming smarter and huge amount of information flowing in an urban network must be used for multiple purposes. So, investing in a 'digital city' is another way of improving the preparation for natural disasters. In this respect, the application of hydroinformatics technologies in urban water systems plays a vital role. Increasingly, urban policy makers are turning to the collection, archiving and analysis of data for their cities, especially through facilities like advanced geographic information systems (GIS) and remote sensing. Properly presented GIS maps of flooded areas, and areas at risk become important means of communicating information on potential natural disasters.

Acknowledgement : The project "Integrated Urban Flood Management in India – Technology Driven Solutions" is funded by Information Technology Research Academy (ITRA), Media-Lab Asia, Ministry of Electronics and Communications and Information Technology (MeitY), Government of India. The project is a multi-institution collaborative project, and the authors thank all partners in the project. The work presented here is primarily the component carried out by the authors, in the project.

References :

1. **Agilan V; Umamahesh N. V.** (2017) Modeling non-linear trend for developing non-stationary rainfall intensity-duration-frequency curve, *International Journal of Climatology*, Vol. 37, Issue 3, pp 1265–1281, DOI: 10.1002/joc.4774.

2. **Alberti, M.** (2017) Grand Challenges in Urban Science, *Front. Built Environ.*, Vol. 3, Article 6, DOI: 10.3389/fbuil.2017.00006.

3. **Chandra Rupa R; Ujjwal Saha; Mujumdar, P. P.** (2015) Model and parameter uncertainty in IDF relationships under climate change, *Advances in Water Resources*, Vol. 79, pp 127–139.

4. **Chandra Rupa, R; Mujumdar, P. P. (2017)** Quantification of uncertainty in spatial return levels of urban precipitation extremes, *ASCE Journal of Hydrologic Engineering*, Vol. 23, Issue 1, 04017053, DOI: 10.1061/(ASCE)HE.1943-5584.0001583.

5. **IPCC - Intergovernmental Panel on Climate Change** (2012) *Special report on Managing the risks of extreme events and disasters to advance climate change adaptation (SREX), a special report of Working groups I and II of the Intergovernmental Panel on climate change*, (ed.) C.B. Field, V. Barros, T.F. Stocker, D. Qin, D.J. Dokken, K.L. Ebi, Mastrandrea, M.D., Mach, K.J., Plattner, G.-K., Allen, S.K., Tignor, M. and P.M. Midgley, Cambridge University Press, Cambridge and New York.

6. **Jha, A. K; Bloch, R; Lamond, J.** (2012) *Cities and Flooding : A Guide to Integrated Urban Flood Risk Management for the 21st Century*, World Bank. © World Bank. https://openknowledge.worldbank.org/handle/10986/2241 License: CC BY 3.0 IGO.

7. **McPhearson, T; Pickett, S. T. A; Grimm, N; Niemelä, J; Alberti, M; Elmqvist, T; Weber, C; Haase, D; Breuste, J; Qureshi S.** (2016) Advancing urban ecology towards a science of cities. *Bioscience*, Vol. 66, pp 198–212. DOI:10.1093/biosci/biw002.

8. **Mujumdar P.P; Mohan Kumar, M. S; Srinivasa Raju, K; Umamahesh, N.V; Valsalam, R; Srinivasa Reddy, G. S; Niyogi D.** (2017) *Integrated Urban Flood Management in India – Technology Driven Solutions*, Monograph submitted to ITRA, Government of India Jul. 2017.

9. **Olsson, J; Willén U; Kawamura A.** (2012) Downscaling extreme Regional Climate

Model (RCM) precipitation for urban hydrological applications, *Hydrology Research* 43 341–351.

10. **Patrick N. A; Stephenson D.** (1990) Spatial variation of rainfall intensities for short duration storms, *Hydrological Sciences Journal*, Vol. 35, Issue 6, pp 667-680, DOI:10.1080/02626669009492471.

11. **Price, R. K; Vojinovic, Z.** (2008) Urban flood disaster management, Urban Water Journal, Vol. 5, No. 3, pp 259-276, DOI: 10.1080/15730620802099721.

12. **Rosenzweig, C; Solecki, W; Hammer, S.A; Mehrotra, S.** (2010) Cities lead the way in climate-change action. *Nature*, Vol. 467, pp 909–911.

13. **Schilling, W.** (1991) Rainfall data for urban hydrology: what do we need?, Atmospheric Research, Vol. 27, Issue 1–3, pp 5-21, https://doi.org/10.1016/0169-8095(91)90003-F.

14. **United Nations**, Department of Economic and Social Affairs, Population Division (2011) *World population prospects: The 2010 revision*, Volume I: Comprehensive Tables, ST/ESA/SER.A/313.

15. **Zevenbergen, C.; Veerbeek, W; Gersonius, B; van Herk, S.** (2008) Challenges in urban food management: travelling across spatial and temporal scales, *J. Flood Risk Management*, Vol. 1, pp 81–88, DOI:10.1111/j.1753-318X.2008.00010.x.

Annals of the Indian National Academy of Engineering
Vol. XV, April 2018

Leveraging Formal Methods for Design Certification of Integrated Circuits : Beyond Functional Correctness

A. Hazra[1]

Abstract : The increasing complexity and safety-criticality of modern-day systems have introduced the need for comprehensive validation and provable safety assurance of integrated circuit designs. Consequently, there has been a constant urge to deploy formal methods for early-stage certification of various design requirements, ranging from correctness and timing to power, reliability, quality and security etc. This article presents a roadmap for formal validation and certification of integrated circuit design requirements using formal analysis techniques.

Keywords : Formal methods, VLSI CAD, Design validation.

1 Introduction

The rapid increase in complexity of electronic designs and electronically controlled systems has continued to pose fresh challenges in electronic design automation (EDA) for several decades. Validation challenges are among the most complex ones, especially for large component-based hierarchically developed integrated systems. Recently, model-based development frameworks, as illustrated in Figure 1, have been adopted in diverse domains and appear to be the key to address some of the verification challenges.

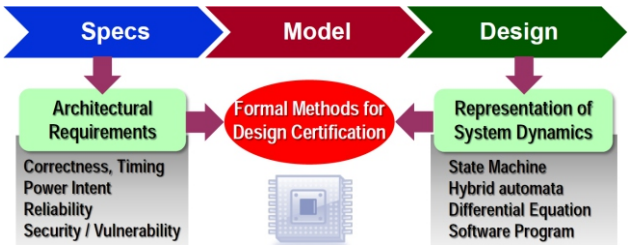

Figure 1: Modern Engineering System Design Framework

Functional validation, which accounts for more than 70% of the design time, is essential for ensuring the safety and correctness of designs. In view of the fact that electronic systems drive many of the safety-critical embedded systems that we use at present, it has been recommended that formal methods be used to mathematically prove the correctness of a design. Specifically, formal certification of correctness (including timing) has been recommended in the safety standards for several domains, including aeronautics (DO-178C), automotive (ISO 26262), industrial process automation (IEC 61508), nuclear (IEC 60880), railway (EN 50128) and space (ECSS-Q-ST-80C).

During the development phase, the designers need to certify a design based on its various attributes, namely functional correctness, end-to-end timing, power performance, functional reliability, quality of control, security and vulnerability etc. Formal methods have been traditionally confined to ensure the functional correctness of a system using techniques such as model checking [Clarke, Grumberg and Peled (1999)] and design intent verification [Dasgupta (2006)]. Recent research [Dixit, Dasgupta and Ramesh (2010)] also focuses on guaranteeing stringent timing requirements of a system by choosing the timing layout for the constituent components.

However, functional correctness is only one of many aspects in modern engineering design. Performance parameters, such as power, reliability etc., have also become equally dominant aspects in determining the acceptability of a design. It has been witnessed that formal

[1] Dept. of Comp. Sc. & Engg., IIT Kharagpur, West Bengal - 721302

methods can be aptly used to enable early-stage certification of such diverse design requirements. In particular, this paper illustrates the following non-functional aspects (power and reliability) of design certification (beyond functional correctness) in details.

Architectural Power Intent Validation: The rapid increase in design complexity and a stringent low-power budget make the power management schemes highly sophisticated. The logic behind these strategies is decided at the architectural level. Today there is a disconnection between the high-level architectural power management strategy which relates multiple power domains and the low-level assertions for controlling individual power domains. This poses an interesting challenge in ensuring the accurate implementation of the architectural power management strategy in the power-managed designs. We propose a verification [Hazra, Goyal, Dasgupta and Pal (2013)] and coverage analysis framework [Hazra, Dasgupta, Banerjee and Harer (2012)], enabled by our developed tool, named POWER-TRUCTOR, that bridges the disconnect between high-level properties capturing the architectural power management strategy and the implementation of the power management control logic using low-level per-domain control signals [Hazra, Mukherjee, Dasgupta, Pal, Harer, Banerjee and Mukherjee (2013)].

Functional Reliability Analysis: There has been a continuous effort to improve the reliability limits in safety-critical systems and often this is carried out in the component-level design phase with appropriate redundancy allocations. In many cyber-physical domains, such as automotive, avionics etc., it is very important to formally specify the functional reliability from an early-stage of design, so that the resource requirements can also be budgeted at an early-stage from a cost vs. reliability perspective. We analyze the spatial and temporal redundancy requirements upfront with the objective of making it an integral part of the specification. The underlying problem of synthesizing formal specifications with built-in redundancy artifacts has been studied from formal properties of the error-free system, the control component reliabilities, and an overall system reliability target [Hazra, Dasgupta and Chakrabarti (2016)].

2 Certification for Power Intent of Designs

The battle to tackle increasing power-densities within a chip has led to awareness about the need for better architectural power management. Consequently, the task of developing efficient on-chip power management strategies [Bailey, Chidolue and Crone (2007)], [Keating, Flynn, Aitken, Gibbons and Shi (2008)] has been pushed up to the architectural level and has become a significant challenge for micro-architects. Power performance analysis typically leads to the development of a *global* power management strategy, which demarcates the boundaries of various architectural power domains and specifies the properties relating these power domains at a high level of abstraction. Though global power management strategies are designed upfront, they can be implemented only much later in the design flow. This is because power intent specification is not supported in high-level design languages (such as Verilog or SystemVerilog), which are used to specify the design implementation at behavioral or Register-Transfer Level (RTL).

2.1 Power-Managed Designs

Typically, a power-managed digital design consists of the following three components:

1) The digital logic of the circuit, called the *design*, which is partitioned into a set of power domains.
2) The *power control circuitry* (PCC) is the power control interface, consisting of isolation cells, voltage regulators, level shifters, switches and retention cells.
3) The power management logic (PML) drives (digital) control inputs to the PCC to effect changes in the power states of a power managed domain. For large circuits the PML consists of two entities, namely:

a) the *global power manager (GPM)* which is responsible for implementing the architectural power management strategy, and
b) a set of per-domain *local power managers*

(LPM) which are responsible for issuing valid control sequences for ensuring correct transition between power states of individual power domains.

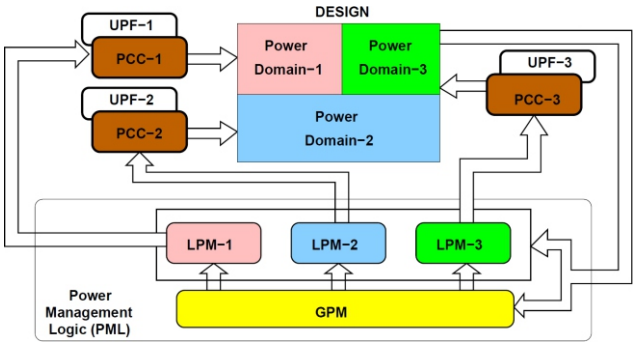

Figure 2 : Power-Managed Design Components

Figure 2 illustrates the different components of a power-managed design. Typically, both the design and the PML can be expressed in digital logic and can be coded using hardware description languages (such as Verilog/VHDL). Since the power lines, voltage regulators or level-shifter circuits cannot be described in RTL, it is not possible to directly express the PCC in RTL. The adoption of new standards like UPF (Unified Power Format) [UPF2.0 (2008)] and CPF (Common Power Format) [CPF (2008)] for specifying PCC has led to new opportunities for accelerating the verification of power-managed designs.

2.2 Power Intent Validation

Verification of low-power designs [Jadcherla, Bergeron, Inoue and Flynn (2009)] involves verifying the design in multiple power states, and ensuring that only the intended transitions and sequences of transitions have occurred. Assertions extracted from UPF specifications typically target the verification of individual local power managers (LPMs) and are per-domain in nature. The properties meant for the global power manager (GPM) are typically inter-domain in nature and are decided top-down, often at the architectural level. This introduces the need to explore the following two primary verification aspects:

- Formally express the architectural power intent properties using pre-defined predicates related to abstract interpretations of the states of the power domains, and
- Formally verify these generated global properties and determine the completeness of the validation effort by formal coverage analysis of global power states.

To enable the above mentioned goals, we develop a tool-flow, called POWER-TRUCTOR, having *six* major steps (also shown in Figure 3), which are summarized below:

Step-1: The architectural power intent properties are expressed formally using several pre-defined predicates related to abstract interpretations of the states of the architectural power domains.

Step-2: A set of per-domain low-power control sequences are synthesized from UPF specifications leveraging on a considerable amount of low-power domain knowledge.

Step-3: A novel mechanism is provided to automatically extract the timing information for per-domain sequences using LPMs, which is not purely a syntactic procedure.

Step-4: Formal properties (as SystemVerilog Assertions or SVAs), which capture the global power intent, are automatically generated using the per-domain sequences.

Step-5: Model checkers are used to formally verify global assertions over the architectural power management logic.

Step-6: A formal coverage analysis of the global power states is conducted to explore the completeness of our verification effort. The global power state reachability analysis indicates the consistency (unreachability of any illegal global power states by PML) and completeness (reachability of all legal global power states by PML) for the architectural power management strategies.

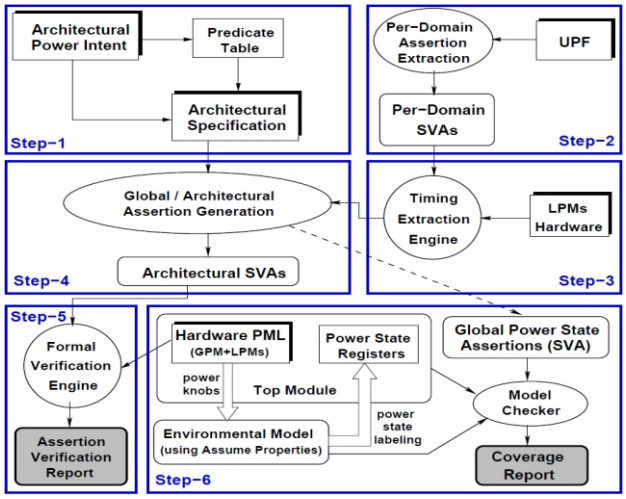

Figure 3: Formal Verification and Coverage Analysis Framework (enabled by POWER-TRUCTOR Tool)

2.3 Verification with Mixed-Signal Power Domains

The power management logic is primarily digital in nature, but it relies on analog components such as Low Dropout Regulators (LDO) and Phase-Locked Loops (PLL) for delivery of regulated voltages and clock frequencies. In low power designs, such analog components may also be powered down at times, and hence power domains are defined around modules containing these components. The digital brain of the power management logic must correctly consider the latencies of the analog components in the power management fabric while switching the power domains driven by these components. This is a task which has become extremely complex by virtue of the multitude of LDOs and PLLs in a modern integrated circuit, and the numerous domains that they drive.

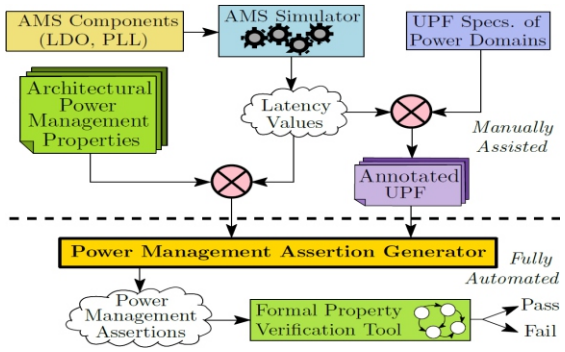

Figure 4: Formal Verification with Mixed-Signal Domains

A formal verification methodology [Mandal, daCosta, Hazra, Dasgupta, Naware, Mohan and Basu (2017)], as projected in Figure 4, is proposed for automatically generating the necessary assertions from an extended syntax of the UPF and proving them on the power management logic. To enable this, inter-domain power sequencing strategies (such as the start-up sequence for waking up the different power domains) are translated into corresponding timing properties over the signals of the power management logic.

2.4 Experimental Results over Industrial Test-Cases

To demonstrate the efficacy and scalability of the proposed power intent verification framework, we present experiments (using Magellan as the formal verifier tool) over industrial Enhanced Leon3 (eLeon3) processors in Table 1.

Table 1: *Formal Power Intent Verification Results*

Name of the Design	Number of Power Domains	Number of Assertions		Formal Verification Time	
		Per-Domain	Arch	Build-Time	Run-Time
eLeon3-DualCore	7	100	22	726 sec.	978 sec.
eLeon3-QuadCore	15	192	40	1656 sec.	2219 sec.

Moreover, the proposed coverage analysis framework also reveals both the inconsistency and incompleteness of the power management strategy by assessing the reachability of the illegal and legal global power states, respectively (using Magellan), as shown in Table 2.

Table 2: Power State Coverage Analysis Results

Name of the Design	Global States	Reachable States		Unreachable States	Analysis Time
		Legal	Illegal		
eLeon3-SingleCore	288	63	12	213	2364 sec.
eLeon3-DualCore	288	39	72	177	3294 sec.

The extension of the power intent verification framework has been applied to a mixed-signal design, namely *D-PHY TX-Master*. The number (#) of generated assertions and their estimated for formal verification time is presented in Table 3.

Table 3: Formal Verification Results over D-PHY TX-Master

# Per-dom. Assert.	Time (in sec.)		# Arch. Assert.	Time (in sec.)			
	Gen.	Verif.		Gen.	Verification		
					Formal	BMC	Reset
140	12	510	20	5	33660	4260	10260

[2]https://standards.ieee.org/findstds/standard/1800-2012.html
[3]www.synopsys.com/verification/static-and-formal-verification/vc-formal.html

3 Certification for Functional Reliability of Designs

The growing need to deploy reliable systems in safety-critical environments has paved newer ways for developing highly reliable functional components in modern-day embedded systems. The necessity to attain higher reliability in safety-critical component-based systems is overcome by introducing various fault-tolerance methods leveraging redundancy and diversity in these systems [Johnson (1989)], [Siewiorek and Swarz (1998)]. Several fault-tolerance methods have been implemented that include hardware, software, time and information redundancies [Koren and Krishna (2007)].

To improve the overall functional reliability of the system, typically, different combinations of component-level spatial and temporal redundancy provisions are explored during design time – finally leading to choosing the most efficient one available. We believe that the reliability preserving specifications for a system need to incorporate such spatial and temporal redundancies in order to dictate a more reliable implementation of the system, along with its functional requirements and carry the same through the design flow. This gives rise to the following two objectives:

- Developing new formalisms to suitably overlay the functional reliability specifications along with the safety-critical properties of embedded designs, and

- Computing the maximum reliability values attainable for the component-level as well as system-level properties with respect to the overlaid reliability specs.

3.1 Formal System Model

An embedded controller of a Cyber-Physical System (CPS) comprises of three primary modules, namely Sensor, Controller and Actuator – which interacts with the Plant (or the environment) to perform desired behaviors. The sensor is responsible for sensing input scenarios from the plant model (or the environment). The controller performs the control decision based on the sensed input. The actuator delivers actuation signals to the plant (or the environment). Some of the activities in the CPS control may be implemented using software and the rest may be controlled via hardware. For example, sensing a scenario where the brake should be applied automatically, the computation of appropriate brake-pressure may be carried out using a software program. However, maintaining the same break-pressure for certain duration is performed by a hardware-control. The resultant outcome while applying such actions is the application of the wheel-brakes and thereby reductions in the vehicle speed.

Figure 5 provides a schematic representation of the embedded CPS framework. Here, the events responsible for sensing inputs, actions (actuations) and outcome activities are termed as sensed-events, action-events and outcome-events, respectively. The controller receives the sensed-events, interacts with the plant model with appropriate actions/actuations to produce the desired outcome-events. The outcome of an action may take place after many control cycles and may also be durable over a period of time.

Figure 5 : Representation of Embedded CPS Framework

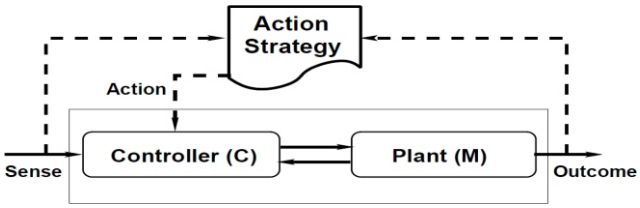

3.2 Formal Specifications

From an abstract point of view, the activities of a CPS can be visualized in terms of sequence of events. The early-stage specification narrates the outcome activity based on a sensed scenario which is to be met with a specified reliability value. Such specifications describe the correctness requirements for a CPS. In addition to this, the meta-level action-strategy specifies the supervisory control where the redundancies in actions are described for a sensed scenario. Such requirements are termed as the reliability specifications for CPS. Let us present an example to explain this.

Example 1: Adaptive Cruise Control (ACC) supports features to – (a) maintain a minimum following interval to a lead vehicle in the same lane and (b) control the vehicle speed whenever any lead obstacle is present. Let us consider the functional requirements of ACC, which senses the proximity of any lead vehicle by the sense-event, **lead_gap.** The required action-events issued by the ACC controller for reducing throttle by 10% and applying proper pressure in wheel-brakes are denoted as, **act1** and **act2**, respectively. The corresponding outcome-events are given as, **thrt_adj** and **brk_adj.** Now, consider the following functional correctness requirement of ACC as follows:

ACC_C1: *Whenever a lead vehicle is sensed in a close proximity, then within a total of 300ms, the throttle is adjusted (reduced by 10%) followed by the application of wheel brakes after 50-150ms.*
The property is formally expressed as:

ACC_C1: lead_gap ##[1:3]thrt_adj ##[1:3]brk_adj
It is to be noted that a single time-unit delay is considered to be of *50ms* in the above mentioned functional spec.

Suppose, the desired reliability of the given correctness requirements be **0.99** for **ACC_C1.** Here, the actions **act1** and **act2** are responsible for producing the outcome-events **thrt_adj** and **brk_adj**, respectively. The outcomes are unreliable and their reliability values are given as follows :

$$R_{thrt\_adj} = \text{Prob(thrt\_adj | act1)} = 0.8,$$
$$R_{brk\_adj} = \text{Prob(brk\_adj | act2)} = 0.9.$$

Since the outcomes are unreliable, the ACC must issue the action - events with appropriate redundancy in order to meet the desired reliability target, as given by the following reliability specification.

ACC_R1: *Whenever a lead vehicle is sensed in a close proximity, then the overall action of 10% throttle-reduction applied successively twice, followed by brake-application in the next time-unit is re-executed twice within an overall time limit of 300ms.*

The property is formally expressed as :

ACC_R1: lead_gap ##[1:3](act1[*2] ##1 act2)[=2] ■
Now, it is imperative to find the maximum reliability attainable for the given correctness specification from the specified reliability strategy. Such an assessment will also ensure whether the desired reliability target can be fulfilled by the formal specifications.

3.3 Functional Reliability Analysis

The problem of obtaining the maximum reliability for a correctness requirement with respect to the given reliability specification is formulated in recursive manner and AND/OR tree search procedure is used to solve the problem.

Example 2: Let us revisit Example 1 for the assessment of reliability. Now, given the reliability specification, **ACC_R1**, and assuming that sense-event (**lead_gap**) is present in **Cycle-0,** the reliability for the correctness specifications, **ACC_C1** is calculated in Table 4, with respect to each action/control strategy derived.

Table 4: Possible Options of Action-Events for *ACC_R1*

Action Events (Cycle-wise)						Computed Reliability
Cycle-1	Cycle-2	Cycle-3	Cycle-4	Cycle-5	Cycle-6	
act1	act1 act1	act2 act1	act2			0.9999
act1	act1	act2 act1	act1	act2		0.9983
act1	act1	act2	act1	act1	act2	0.9216
	act1	act1 act1	act2 act1	act2		0.9995
	act1	act1	act2 act1	act1	act2	0.9780
		act1	act1 act1	act2 act1	act2	0.9216

The highlighted rows of Table 4 indicate the *admissible* action-strategies (first one providing the maximum reliability) that meet the desired reliability requirements (**0.99**) for **ACC_P1.** ■

3.4 Experimental Results over Industrial Test-Cases

Table 5 provides few reliability results for Brake Controller (BC) and Collision Mitigation Controller (CMC) components leveraging the proposed AND/OR search procedure.

Table 5: **Reliability Estimation for Component Specifications**

Component Specifications		# States in AND/OR Tree			Analysis	Maximum
Functional	Reliability	Total	Explored	Solution	Time	Reliability
BC_Prop5	BC_Rel5	2974	2470	54	0.275 sec.	0.999900
CMC_Prop2	CMC_Rel2	533	480	108	0.068 sec.	0.993141

4 Conclusion

The focus of this article is to present a framework for the specification and analysis of architectural-level power and functional reliability requirements. In the process of this exercise, several novel solutions are reported to address the challenges of formally validating the power management schemes as well as estimating the functional reliability of a system at an early-stage of the design flow. We believe that this work is helpful in validating the performance guarantees (beyond functional correctness) of designs from a higher level of abstraction so that, in future, the low-power and reliable systems can be automatically synthesized.

Acknowledgement

The author acknowledges the support of Synopsys Inc., Intel Inc. and DST for this work.

References:

1. **Bailey, S.; Chidolue, G.; Crone, A.** (2007); Low Power Design and Verification Techniques, White Paper by Mentor Graphics Inc.
2. **Clarke, E. M.; Grumberg, O.; Peled, D. A.** (1999); Model Checking, MIT Press, ISBN: 9780262032704.
3. **Dasgupta, P.** (2006); A Roadmap for Formal Property Verification, Springer, ISBN: 978-1-4020-4758-9.
4. **Dixit, M.; Dasgupta, P.; Ramesh, S.** (2010); Taming the Component Timing: A CBD Methodology for Real-time Embedded Systems, In the Proc. of DATE, pp. 1649-1652.
5. **Hazra, A.; Dasgupta, P.; Banerjee, A.; Harer, K.** (2012); Formal Methods for Coverage Analysis of Architectural Power States in Power-Managed Designs, In the Proc. of ASP-DAC, pp. 585-590.
6. **Hazra, A.; Dasgupta, P.; Chakrabarti, P. P.** (2016); Formal Assessment of Reliability Specifications in Embedded Cyber-Physical Systems, In the Elsevier Journal of Applied Logic (JAL), vol. 18, pp. 71-104.
7. **Hazra, A.; Goyal, S.; Dasgupta, P.; Pal, A.** (2013); Formal Verification of Architectural Power Intent, In IEEE Trans. on VLSI, vol. 21, no. 1, pp.78-91.
8. **Hazra, A.; Mukherjee, R.; Dasgupta, P.; Pal, A.; Harer, K.; Banerjee, A.; Mukherjee, S.** (2013); POWER-TRUCTOR: An Integrated Tool Flow for Formal Verification and Coverage of Architectural Power Intent, In IEEE Trans. on Comp.-aided Design of Integrated Cir. & Sys. (TCAD), vol. 32, no. 11, pp. 1801-1813.
9. **Jadcherla, S.; Bergeron, J.; Inoue, Y.; Flynn, D.** (2009); Verification Methodology Manual for Low Power (VMM-LP), Synopsys, ISBN: 978-1607434139.
10. **Johnson, B.** (1989); Design and Analysis of Fault Tolerant Digital Systems, Addison-Wesley Longman Publishing Co., MA, ISBN: 0-201-07570-9.
11. **Keating, M.; Flynn, D.; Aitken, R.; Gibbons, A.; Shi, K.** (2008); Low Power Methodology Manual (LPMM) – For System-on-Chip Design, Springer (Second Ed.), ISBN: 978-0-387-71819-4.
12. **Koren, I.; Krishna, C. M.** (2007); Fault-Tolerant Systems, Morgan Kaufmann, ISBN: 9780120885251.
13. **Mandal, S.; daCosta, A. A. B.; Hazra, A., Dasgupta, P.; Naware, B.; Mohan, C. R.; Basu, S.** (2017); Formal Verification of Power Management Logic with Mixed-Signal Domains, In the Proc. of VLSID, pp. 239-244.
14. **Siewiorek, D. P.; Swarz, R. S.** (1998); Reliable Computer Systems: Design and Evaluation (3rd Ed.), A. K. Peters, Ltd., MA, ISBN: 978-1568810928.

Annals of the Indian National Academy of Engineering
Vol. XV, April 2018

Secure Multi-Party Computation

ArpitaPatra[1]

Abstract : Secure multi-party computation (MPC) permits a collection of parties to compute a collaborative result, without any of the parties gaining any knowledge about the inputs provided by other parties, except what is derivable from the final result of the computation.

The primary aim of this work is to study the feasibility and efficiency of MPC protocols in various network and adversarial settings.

Keywords: MPC, Network, Adversary, Garbled Circuits, Broadcast, Byzantine Agreement, synchronous, asynchronous, static, adaptive.

1 Introduction

MPC, arguably termed as the holy-grail problem of cryptography, not only makes privacy-preserving collaborative computation on sensitive data a reality, but also removes a single point of attack by allowing for distribution of secrets and computation on the distributed secrets. Applications of MPC include prevention of satellite collision, e-action, secure outsourcing to cloud, secure benchmarking, data analytics, machine learning, supply chain collaboration, email filtering, aggregation to name a few. MPC has seen monumental progress in recent years and has been translated to technology from concept in order to solve problems such as e-auction and prevention of satellite collision.

Informally, the problem of MPC enables a set of n parties connected over a network to jointly perform a computation, represented by a function f, on their private inputs in a secure way, so that no adversary **A** corrupting a coalition of t parties can learn more information than their outputs (*privacy*), nor can they affect the outputs of the computation (*correctness*). Solving MPC is easy in the presence of a trusted third party (TTP). The challenge therefore is to solve the problem without the help of a TTP.The approach used by a generic MPC protocol is to "securely" evaluate Boolean circuit (with AND, OR and XOR gates) or arithmetic circuit (with Addition and Multiplicationgates) representing the function $f$to be computed. MPC being a complex problem, needs and introduces a rich set of primitives which apart from serving as building blocks for MPC protocols, have found independent applications. The study of MPC encompasses the various feasibility and efficiency questions for these primitives and MPC. The primary questions include: (a) How many corruptions can be tolerated; (b) How many bits need to be communicated? (c) How many interactions are needed? The answers to these questions rely on the underlyingnetwork and adversarial setting. We discuss several of our recent advances made in the domain of MPC and its building blocks.

2 Organization

In Section 3, we discuss our results for circuit garbling, a central primitive for MPC. In Section 4, we discuss our results on Byzantine broadcast and agreement extension problems. In section 5, we discuss our results on oblivious transfer (OT) extension problems. In section 6, we discuss our resultson bridging feasibility and efficiency gaps between synchronous and asynchronous MPC. In section 7, we state our results on bridging efficiency gaps between static and adaptive MPC.

[1] Department of Computer Science & Automation, Indian Institute of Science, Bangalore, 560012

3 Privacy-free Garbling: Size-zero and Information-theoretic

Garbled circuits (GC) are of paramount importance in in MPC. Roughly speaking, a GC allows evaluation of a circuit in its encoded form on an encoded input, and produces an encoded output.

GCs first made their appearance in Yao's secure two-party computation protocol. Their theoretical importance and potential to serve asa cryptographic primitive has been recognized recently and they have been elevated from a technique to be used in other protocols, to a cryptographic primitive. Tofacilitate abstraction as a primitive, recent fundamental works formalize three notions of security that a garbling scheme may achieve; namely privacy, obliviousness, and authenticity, and shows separation between them. Informally, privacy aims to protect the privacy of encrypted inputs, while obliviousness hides both the input and the output when the output decoding information is withheld. However, once the output decoding information is revealed, obliviousness does not necessarily imply privacy of inputs. Lastly, authenticity captures the unforgeability of the outputof a garbled circuit evaluation.

In the original scheme of Yao, each wire in the GC was assigned two strings called “keys”, each corresponding to bit values zero and one on that wire. A garbled gate in the circuit was represented by ciphertexts encrypting its output wire keys using the corresponding input wire keys as per the gate's truth table. A garbled gate for a gate with fan-in two is thus constituted of four ciphertexts. Thefinal garbled circuit was a composition of the garbled gates, and its size was definedas the number of bits of ciphertext needed overall. The size of the garbled circuits is a very important parameter as it directly impacts the communication complexity of MPC protocols.

We are interested in a particular kind of garbling scheme, termed privacy-free in the literature.We show that Boolean formulas can be garbled information-theoretically in the privacy-free setting, producing no ciphertexts at all. Existing garbling schemes either rely on cryptographic assumptions (and thus require cryptographic operations to construct and evaluate garbled circuits), produce garbled circuits of non-zero size, or are restricted to low depth formulaic circuits. Our result has both theoretical and practical implications for garbled circuits as a primitive. On the theory front, our result breaks the known theoretical lower bound of one ciphertext for garbling an AND gate in this setting. As an interesting implication of producing size zero garbled circuits, our scheme scores adaptive security for free. On the practical side, our garbling scheme involves only cheap XOR operations and produces size zero garbled circuits. As a side result, we propose several interesting extensions of our scheme. Namely, we show how to garble threshold and high fan-in gates. This result appears in [Kondi and Patra (2017)].

4 Optimal Extension Protocols for Byzantine Broadcast and Agreement

The problem of Byzantine Broadcast (BB) andByzantine Agreement (BA) are of interest to both distributedcomputing and cryptography community. In the BB problem, a designated party(called the sender) holds an input message m, and the goalis for all parties to learn m and agree on it. In the related BA problem, every party P_i holdsa message m_i, and the goal is for all parties to agree ona common message. Extension protocolsfor these primitives have been introduced to handle longmessages efficiently at the cost of small number of single-bitbroadcasts, referred to as seed broadcasts. The communicationoptimality has remained the most sought-after propertyof an extension protocol in the literature. In this paper, weprioritize both communication and round optimality. A concreteprotocol from an extension protocol is obtained by replacingthe seed broadcasts with a BB protocol for single bit.Towards building concrete protocols efficient both in termsof communication and round, we minimize the seed roundcomplexity of the extension protocols, where this measurerefers to the number of rounds

in which seed broadcasts areinvoked in an extension protocol.

In a setting with n parties and an adversary controlling at most t parties in Byzantine fashion, we present BB and BA extension protocols with $t<n$, $t < n/2$ and $t<n/3$ that are simultaneously optimal in terms of communication and round complexity. The best communication that an extension protocol can achieve in any setting is $O(l\ n)$bits for a message of length l bits. The best achievable round complexity is $O(n)$ for the setting $t< n$ and $O(1)$ in the other two settings $t < n/2$ and $t<n/3$. The existing constructions are either optimal only in terms of communication complexity, or require more rounds as well as seed rounds than our protocols, or achieve optimal round complexity at the cost of sub-optimal communication. Specifically, we construct communication-optimal protocols in the following three settings with the following round and seed round complexities:

- $t <n/3$: Our protocol requires three rounds and a single seed round. The best-known protocol in this setting is only communication optimal and requires a round complexity and a seed round complexity of at least $O(n^3)$.
- $t <n/2$: Our protocol provides a round complexity of 5 and a seed round complexity of one. The best-known protocol in this setting requires a round complexity of 6and a seed round complexity of 3.
- $t <n$: Our protocol has a round as well as a seed round complexity of $O(n)$. The same complexities for the best-known protocol in this domain are $O(n^2)$.

These results appear in [Patra (2011)] and [Ganesh and Patra (2016)].

5. Fast Actively Secure OT Extension

Oblivious Transfer (OT) is one of the most fundamental cryptographic primitives with wide-spread application in general secure multi-party computation (MPC) as well as in a number of tailored and special-purpose problems of interest such as private set intersection (PSI), private information retrieval (PIR), contract signing to name a few. Often the instantiations of OT require prohibitive communication and computation complexity. OT extension protocols are introduced to compute a very large number of OTs referred as extended OTs at the cost of a small number of OTs referred as seed OTs.

We present a fast OT extension protocol for small secrets in active setting. Our protocol when used to produce 1-out-of-nOTs outperforms all the known actively secure OT extensions. Our protocol is built on the semi-honest secure extension protocol of Kolesnikov and Kumaresan of CRYPTO'13 (referred as KK13 protocol henceforth) which is the best-known OT extension for short secrets. At the heart of our protocol lies an efficient consistency checking mechanism that relies on the linearity of Walsh-Hadamard (WH) codes. Asymptotically, our protocol adds a communication overhead over KK13 protocol that is independent of the number of extended OTs.

Concretely, our protocol when used to generate a large enough number of OTs adds only 0.011-0.028% communication overhead and 4-6% runtime overhead both in LAN and WAN over KK13 extension. The runtime overheads drop below 2%when in addition the number of inputs of the sender in the extended OTs is large enough.

These results appear in [Patra and Sarkar and Suresh (2017)].

6. Bridging the Gap between Synchronous and Asynchronous MPC

The problem of MPC has been studied in the two important settings of synchronous and asynchronous networks, respectively. MPC protocols for the synchronous setting assume a network in which parties proceed in rounds, with the guarantee that messages sent by any party in any given round are delivered to all recipients in the same round. Consequently, in all such protocols the parties are assumed to be synchronized, i.e., to be in the same round at all times. On the other hand, asynchronous MPC can

be deployed even in networks like Internet that deliver messages in an arbitrary order and impose arbitrary delays on them.

Perfectly-secure verifiable secret sharing (VSS) and multi-party computation (MPC) protocols inasynchronous network tolerate only at most one-fourth of corruption, while their counterparts in synchronousnetwork sustain against at most one-third corruption. Moreover property-wise, synchronousprotocols provide much stronger guarantees than the asynchronous counterparts. Taking note of the factthat asynchronous network is more realistic on one hand and on the other, synchrony of a network haspositive impact on several aspects of distributed protocols including properties and fault-tolerance, weexplore the power of hybrid network that combines best of both the worlds by supporting a few synchronousrounds at the onset of a protocol execution, before turning to asynchronous mode. In hybridnetwork, we investigate various feasibility questions pertaining to protocols giving guarantees attainablein synchronous as well as asynchronous networks.

For the asynchronous protocols in hybrid network, we hope to leverage the initial synchronous roundsto bridge the gap in the fault-tolerance with the synchronous protocols under minimal synchrony assumption.We ask the following fundamental question of both theoretical and practical importance: What isthe minimum number of initial synchronous rounds necessary and sufficient in a hybrid network to constructasynchronous perfectly-secure VSS and MPC protocols with the fault-tolerance of synchronousprotocols? On the positive note, we show that the answer is one for VSS which is clearly optimal. Notablyno broadcast oracle is invoked in the synchronous round of our proposed VSS protocol. On thenegative side, we prove that one synchronous round is not enough for MPC, putting MPC on a higherpedestal than VSS in terms of difficulty.

For synchronous protocols in hybrid network, we hope to save on the synchronous rounds leveragingconveniently the available asynchronous phase. We settle the question for VSS in negative showing thatthree rounds that are known to be necessary (and sufficient) for VSS in synchronous network, is alsorequired in hybrid network. VSS being a special case of MPC, the lower bound holds true for MPC. Wematch the lower bound with a 3-round protocol. Notably, synchronous MPC with cryptographic securityis known to be achievable in hybrid network with one synchronous round.

A part of these results appears in [Choudhury and Patra (2017)]. Some of the results are submitted to IEEE Transactions on Information Theory [Patra and Ravi (2017)]

7. Bridging the Efficiency gap between Adaptive and Static MPC

The initial model considered for MPC was one of a static adversarywhere the adversary controls a subset of the parties (who are called corrupted) before the protocol begins,and this subset cannot change. A stronger corruption model that allows the adversary to choose which partiesto corrupt throughout the protocol execution, and as a function of its view; such an adversary is calledadaptive. Adaptive corruptions model "hacking" attacks where an external attacker breaks into parties'machines in the midst of a protocol execution. In the case where protocols run over a long period of time(e.g., consider a "secure database search protocol" where a party can ask queries over time without revealingthe query to the database), such attacks are very realistic.

There are two types of adaptively-secure protocols: adaptive with erasures and adaptive without erasures. Achieving adaptivity without erasures is preferable, since secure erasures are not always trivial. However, it seems far harder. We introduce a new model of adaptive security called adaptive security with partial erasures that allows erasures, but only assumes them in a very weak sense. Specifically, if all parties are corrupted then security holds as long as any single party successfully erases. In addition, security

holds if any proper subset of the parties is corrupted without erasures. We initiate a theoretical study of this new notion and demonstrate that MPC in this setting is as efficient as static secure computation.

We introduce yet another weaker model of adaptive security where only one of the parties is adaptively corrupted. We refer the security model as one-sided adaptive security. We demonstrate that MPC in this setting is as efficient as static secure computation.

These results appear in [Hazay and Patra (2017)] and [Hazay, Lindell and Patra (2015)].

References :

1. **Kondi, Yashvanth;Patra, Arpita.** Privacy-Free Garbled Circuits for Formulas: Size Zero and Information-Theoretic. *CRYPTO2017*.

2. **Patra, Arpita.** Error-free Multi-valued Broadcast and Byzantine Agreement with Optimal Communication Complexity. *15th International Conference on Principles of Distributed Systems (OPODIS 2011)*, LNCS 7109, pp. 34-49, 2011.

3. **Ganesh, Chaya;Patra, Arpita.** Broadcast Extensions with Optimal Communication and Round Complexity. *35th Annual ACM Symposium on Principles of Distributed Computing (PODC 2016)*, pp. 371–380, ACM Press, 2016.

4. **Patra, Arpita; Sarkar, Pratik; S, Ajith.** Fast Actively Secure OT Extension for Short Secrets. *24th Annual Network and Distributed System Security Symposium (NDSS 2016)*, Internet Society, 2017.

5. **Choudhury, Ashish; Patra, Arpita.** An Efficient Framework for Unconditionally Secure Multiparty Computation. *IEEE Transactions on Information Theory*, vol. 63, no. 1, pp.428–468, 2017.

6. **Hazay,Carmit; Patra, Arpita.** Efficient One-Sided Adaptively Secure Computation. *Journalof Cryptology*, vol. 30, no. 1, pp. 321–371, 2017.

7. **Hazay,Carmit; Lindell, Yehuda;Patra, Arpita.** Adaptively Secure Computationwith Partial Erasures. *34th Annual ACM Symposium on Principles of Distributed* Computing(PODC 2015), pp. 291–300, ACM Press, 2015.

Annals of the Indian National Academy of Engineering
Vol. XV, April 2018

Design and Development of Refocusing System for High Resolution Imaging Satellites

Naimesh Patel[1]

Abstract : This paper presents design and development of a refocusing system, It is used to sense misalignment in optical system using wavefront sensor and correct the same using thermal actuator based hexapod. Novel thermal actuator is developed which provided bidirectional actuation. Using six thermal actuators and indigenously designed backlash free structural spherical joint, hexapod is realized. Hexapod is characterized in thermos-vacuum chamber for its operation. An algorithm is developed, which computes misalignment in two mirror optical system using measured wavefront. Re-focusing methodology is proposed in two mirror optical system using indigenous developed hexapod and algorithm.

Keywords Hexapod, Wavefront sensor, Telescope, optical aberrations, Misalignment, Zernike coefficients.

1 Introduction

In general, space borne telescopes are subjected to orbital loads like temperature excursion, absence of gravity, moisture de-sorbption of metering structure etc, which leads to misalignment of optical system and loss of the optical performance. Future space based large telescope will be made from number of smaller mirrors, which are aligned together to create a larger segmented mirror. Due to orbital loads misalignment will occur in these smaller mirrors supported by large structures and intern this will introduce aberrations in imaging. Hence, there is a need of some technique which measures the onboard optical misalignment and corrects it. The focus of this paper is to develop a system, which sense misalignment using wavefront and correct the same using hexapod. This work includes design and development of thermal actuator, backlash free structural ball joint, hexapod and algorithm to sense misalignment in optical system. Using Thermal actuator based hexapod and algorithm, re focusing in two mirror optical system is demonstrated.

2 Development of thermal actuator

Using aluminum rods in appropriate geometrical configuration along with heaters and thermistors, highly reliable bi-directional thermal actuator is designed. Fig.1 shows details of thermal actuator.

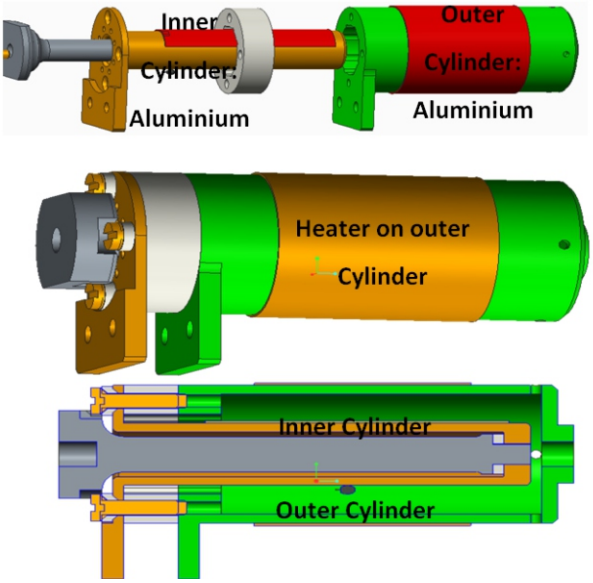

Figure 1: Thermal Actuator-CAD

By selectively heating aluminum rods, elongation and contraction of actuator is achieved. Performance of actuator is ensured by theoretical simulation. Fig.2 shows details of simulation results of thermal actuator.

[1] Space Applications Centre, ISRO, Ahmedabad-380015

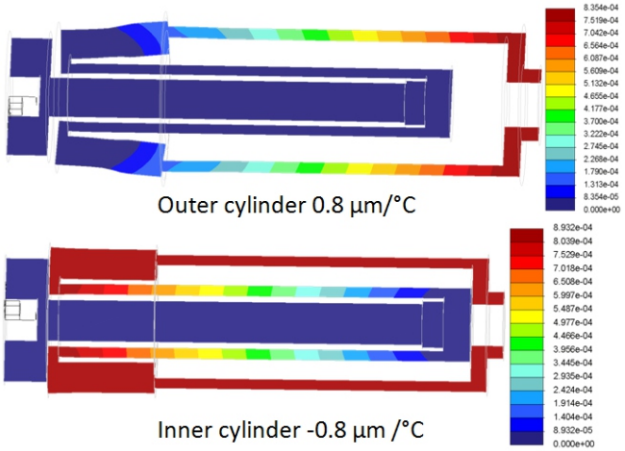

Figure 2: Simulation of Thermal Actuator

Actuators are fabricated and integrated with thermal elements like heaters, thermistors and low emittance tape. Fig.3 shows details of hardware.

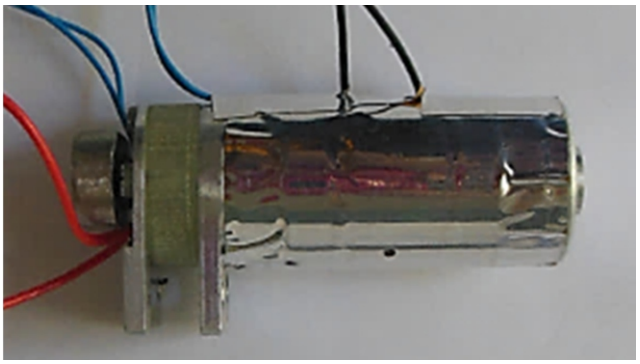

Figure 3: Thermal Actuator-Prototype

3 Characterization of Actuator

Thermal actuator is characterized in thermos-vacuum chamber for its performance. Test setup is shown in fig.4

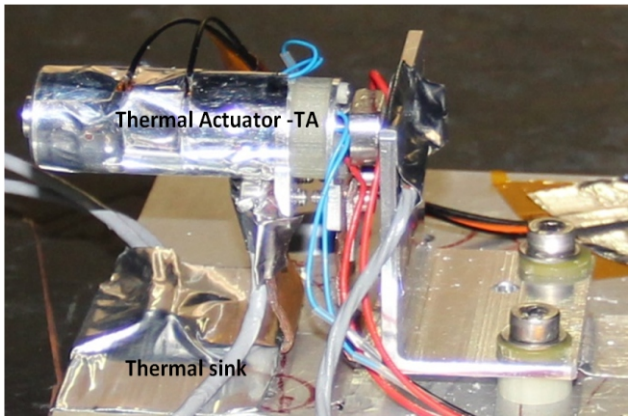

Figure 4: Testing of actuator in thermo-vacuum chamber

Selectively heating inner and outer cylinder, temperature difference between two cylinder is controlled. Temperature V/S time plot is shown in fig-5(a). Range of actuation depends on magnitude of temperature difference between inner and outer cylinder. To check maximum temperature difference, test was performed by heating outer cylinder alone. Same is shown in fig-5(b). Maximum temperature difference of 22°C is achieved, which is corresponds to 20-micron of actuation.

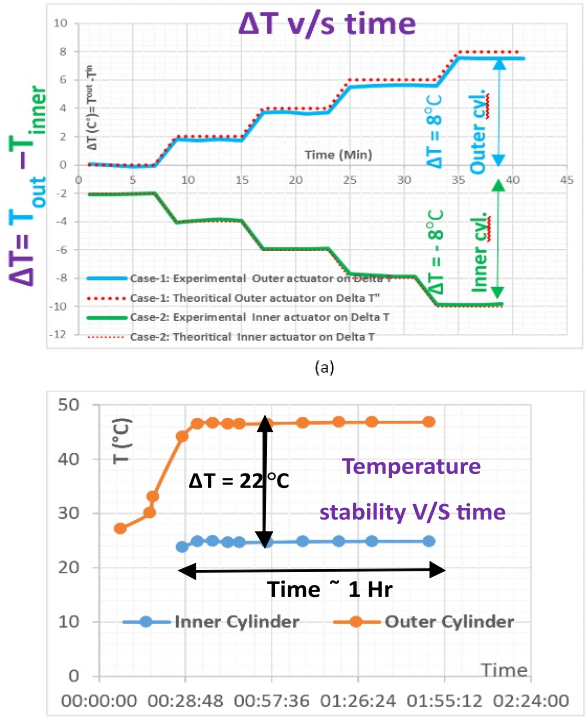

Figure 5: Temperature characteristic of actuator

4 Virtual ball joint

Spherical joint is required at either side of actuator in hexapod, conventional spherical joint has backlash which results in to poor accuracy of hexapod. Novel structural ball joint is designed with desired stiffness to provide three rotational DOF. This structural joint will act as a virtual spherical ball joint without backlash. Detailed view of virtual ball joint is shown in fig.6.

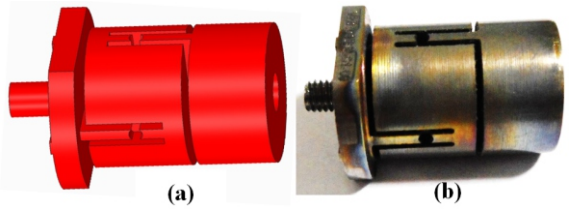

Figure 6: Virtual ball joint, (a) CAD, (b) Hardware

5 Hexapod

Hexapod consists of a moving plate, fixed plate, and six thermal actuators connected to the moving and fixed plate with virtual spherical joint at either end. In order to achieve desired 6 DOF of the moving plate relative to the fixed plate, all the six actuators are actuated with computed temperature. Detailed view of hexapod is shown in fig.7.

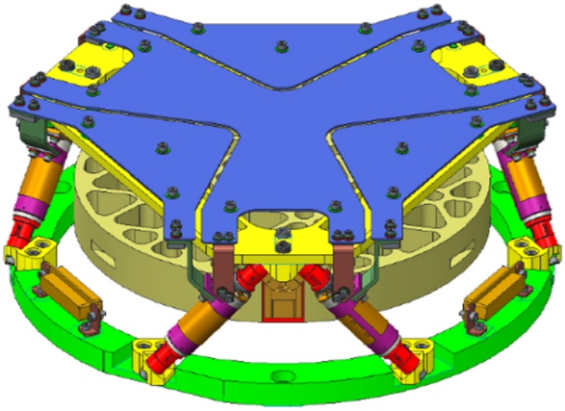

(a)

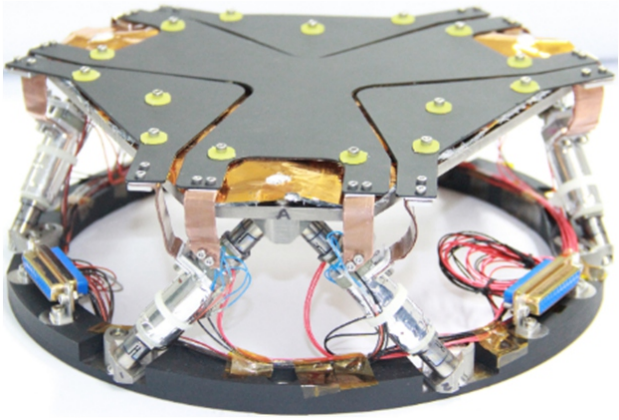

(b)

Figure 7: Hexapod, (a) CAD model (b) Prototype

Hexapod is controlled by indigenously developed computer algorithm, which takes 6 DOF as input, computes desired length and temperature of each actuator and control power supply to corresponding heaters to achieve it. There by it demonstrates the performance with actuating translation and rotational degree of freedom.

Characterization of Hexapod is carried out in thermo vacuum chamber for its degree of actuation. Detailed characterization setup is shown in fig.8.

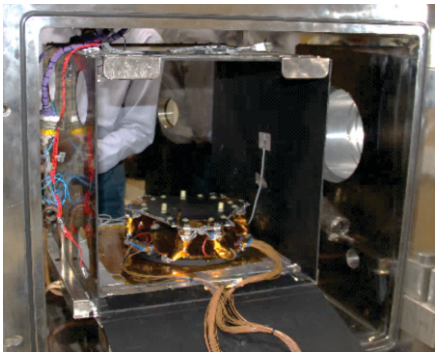

Figure 8: Characterization of Hexapod in thermos-vacuum chamber

Temperature difference of each actuator is controlled in thermos-vacuum chamber for degree of actuation. Typical characteristic for transnational DOF is shown in fig.9.

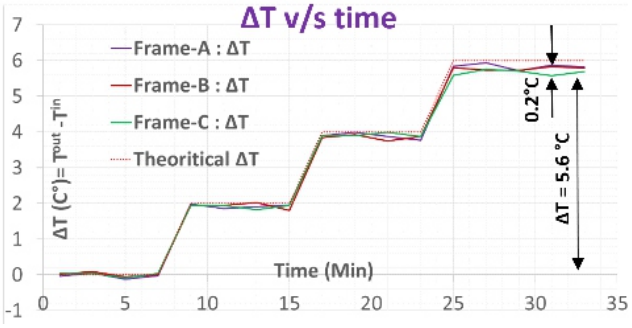

Figure 9: Temperature characteristic of hexapod

6 Development of wavefront sensor

Wavefront sensor based on Shack-Hartmann principal is developed. Opto-mechanical configuration of wavefront sensor is shown in Fig 10. It consists of front cover, adaptor, lenslet mount, back cover etc. Front cover supports lenslet with respect to detector at focal distance. Thermo-elastic mount with appropriate flexure is design to hold lenslet without transferring mechanical and thermal distortion to lenslet[1]. Lenslet mount is fixed on adaptor. Adaptor has external threads which engage with front cover. Using adaptor, coarse focusing and angular adjustment of lenslet with respect to detector were done. Two screws allowed fine focusing and angular adjustment of lenslet with respect to detector. Modal wavefront reconstruction algorithm is used to fit sensed wavefront using Zernike polynomial.

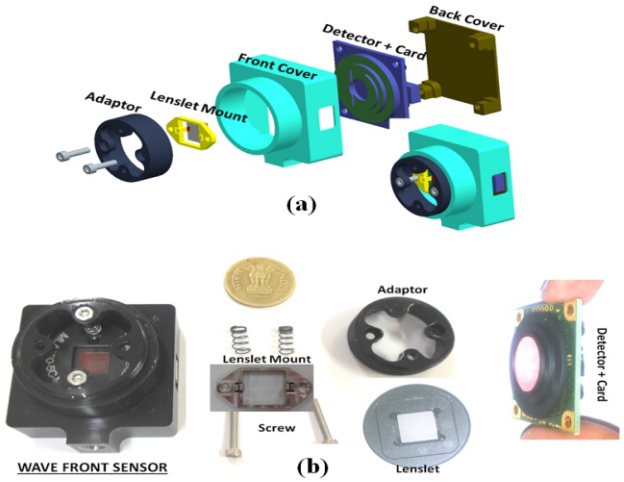

Figure 10: Wavefront sensor, (a) CAD, (b) Hardware

7 Algorithm to estimate misalignment in optical system

Developed an algorithm for measurement of misalignment in an optical system using wavefront sensing [2]. Sensed wavefront is decompose to Zernike coefficients. Sensitivity matrix is derived from optical design. Using sensitivity matrix and wavefront aberrations, algorithm is developed to estimate misalignment in two mirror optical system. Details of algorithm is shown in fig-11. Here, {ΔX} are misalignments and {ΔZ} are change in Zernike coefficients.

Schematic of close loop correction for misalignment sensing and correction using hexapod and wavefront sensor in two mirror optical system is shown in fig – 12.

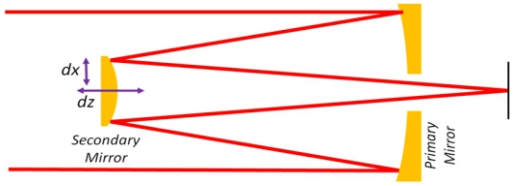

$$\{\Delta X\} = [A]^{-1}\{\Delta Z\}$$

$$\begin{Bmatrix} dx \\ dy \\ dz \\ d\theta_x \\ d\theta_y \end{Bmatrix} = \begin{bmatrix} \frac{\partial Z_2}{\partial x} & \frac{\partial Z_2}{\partial y} & \frac{\partial Z_2}{\partial z} & \frac{\partial Z_2}{\partial \theta_x} & \frac{\partial Z_2}{\partial \theta_y} \\ \frac{\partial Z_3}{\partial x} & \frac{\partial Z_3}{\partial y} & \frac{\partial Z_3}{\partial z} & \frac{\partial Z_3}{\partial \theta_x} & \frac{\partial Z_3}{\partial \theta_y} \\ \frac{\partial Z_4}{\partial x} & \frac{\partial Z_4}{\partial y} & \frac{\partial Z_4}{\partial z} & \frac{\partial Z_4}{\partial \theta_x} & \frac{\partial Z_4}{\partial \theta_y} \\ \frac{\partial Z_7}{\partial x} & \frac{\partial Z_7}{\partial y} & \frac{\partial Z_7}{\partial z} & \frac{\partial Z_7}{\partial \theta_x} & \frac{\partial Z_7}{\partial \theta_y} \\ \frac{\partial Z_8}{\partial x} & \frac{\partial Z_8}{\partial y} & \frac{\partial Z_8}{\partial z} & \frac{\partial Z_8}{\partial \theta_x} & \frac{\partial Z_8}{\partial \theta_y} \end{bmatrix}^{-1} \times \begin{Bmatrix} \Delta Z_2 \\ \Delta Z_3 \\ \Delta Z_4 \\ \Delta Z_7 \\ \Delta Z_8 \end{Bmatrix}$$

Figure 11: Algorithm for estimation of misalignment

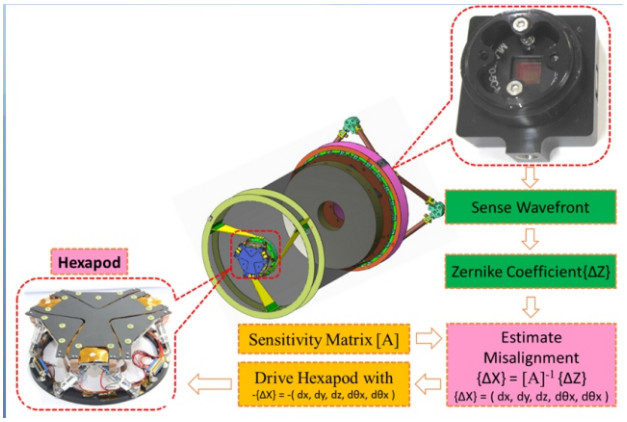

Figure 12: Misalignment sensing and correction

8 Conclusion

Indigenously designed and realized, novel most reliable thermal actuator based hexapod for re-alignment and wavefront sensor for sensing wavefront in optical system. Also, developed an algorithm to sense and correct misalignment in optical payloads. Proposed an algorithm for misalignment sensing and correction using hexapod in two mirror optical system.

9 REFERENCES

1. **Naimesh Patel**, Rakesh Kumar Singh, C.S.Narayanamurthy, "Opto-mechanical design of lenslet mount for Shack Hartmann Wavefront Sensor", Proceedings of the International conference on optics and optoelectronics, ICOL 2014,IRDE, Dehradun, March 5-8,2014.

2. **Naimesh Patel**, C.S.Narayanamurthy, "Measurement of optical misalignment using wavefront sensing" is published in SPIE journal of Optical engineering,Vol-54(10), 104106 (October2015).doi: 10.1117/1. OE.54.10.104106.

Annals of the Indian National Academy of Engineering
Vol. XV, April 2018

Three-Dimensional Solutions for Hybrid laminates Subjected to Arbitrary Boundary Conditions using Extended Kantorovich Method

Poonam Kumari[1], **Susanta Behera**[1]

Abstract : This paper presents the glimpse of development of three-dimensional solutions for arbitrary supported piezolaminated plate using multi-term multi-field Extended Kantorovich method. Here, extended Kantorovich method is used to develop 3D elasticity solution of hybrid plate using the mixed variational principle. Two-way electromechanical coupling is considered, all boundary conditions and continuity conditions at the interface are satisfied exactly at all points. The aim of the research is to develop solution which can accurately characterize the edge effects for piezolaminated plates under electromechanical excitation. The results can be used as benchmark for assessing the accuracy of the two-dimensional laminate theories.

Keywords: Analytical, Three-dimensional, extended Kantorovich method, Piezoelectric plate

1 Introduction

In recent years, laminated composite structures integrated with piezoelectric layers are also knowns as smart structures and extensively used in some of the weight sensitive and sophisticated engineering applications such as in aerospace, structural health monitoring devices and naval industries where these are subjected to various combination of loading (static and dynamic loads) and boundary conditions. Unlike the isotropic structures, smart laminates experience coupling between electrical and mechanical material properties and further couplings among bending, extension, and twisting matrices pertaining to its varied stacking order among layers. Near the clamped/free edges, the stress field changes sharply, and it is three-dimensional (3D) in nature. Therefore, various two-dimensional, numerical, semi-numerical and approximated methods have been developed to accurately predict this 3D boundary layer stress field [Mittelstedt and Becker (2007)].

For such cases, the general purpose displacement based finite element may not be reliable in the vicinity of the edges [Sheng et.al. (2007)]. The limitations of the general finite element solution for addressing the edge effects has also been pointed out in recent review article. Analytical/semi-analytical three-dimensional solutions of piezoelectric plates with clamped/free support conditions can help to understand the edge effects and effect of electromechanical coupling. Since exact 3D analytical solution is possible for all round simply supported hybrid plates. Very few research articles have been presented for non-simply supported elastic and piezoelastic plates based on 3D elasticity/piezoelasticity using approximate analytical techniques [Vel and Batra (2000), Vel et. al. (2004), Huang and Kim (2014)]. In these articles, boundary and interfacial continuity conditions are satisfied in approximate sense. Stress field near or in the vicinity of boundaries is very sensitive and such approximation may lead to erroneous prediction of stress field.

Some approximate methods such as Ritz/Galerkin are also used to develop the solution of non-simply supported plates [Reddy (2007)]. But the accuracy and convergence of the final solution depends upon the initial guess function. The Kantorovich method, originally proposed by Kantorovich and Krylov (1958) to

[1] Department of Mechanical Engineering, IIT Guwahati, Guwahati-781039

eliminate this dependence along one direction, and later modified by introducing the concept of iterative step techniques to eliminate the dependence along both direction as extended Kantorovich method by Kerr [Kerr(1968), (1969)] . It is a very powerful and elegant semi-analytical method for solving partial differential equations (PDEs). In this method, the PDEs of a bivariate problem is converted into two sets of ordinary differential equations (ODEs) in the two directions, by approximating the solution as a series of products of two separable functions. The ODE in a given direction is obtained by assuming the functions in the other direction as known from intial guess or previous iteration. The iterative process converges fast (generally in two/three iterations), even when the initial trial functions do not satisfy the boundary conditions, and unlike in Ritz's and Galerkin's methods, the accuracy of the final solution is independent of the initial guess. The method has been shown to yield accurate results for several problems of elastic single layer, and multi-layer plates, and shells subjected to arbitrary boundary conditions. The further details of application of method for bending, vibration and bucking can be found in recent review article [Singhatanadgid and Singhanart (2017)]. The commonly EKM was applied for solutions based on 2D plate/shell theories and not on the 3D elasticity theory, and involve only homogeneous boundary conditions. In year 2011, first time, Kapuria and Kumari (**2011**) presented a three dimensional analytical solution of flat panel using single-term extended Kantorovich method. A mixed formulation approach was followed, considering both displacements and stresses as primary variables, which allows:

i) Exact satisfaction of all homogeneous and non–homogeneous boundary conditions, as well as interface continuity conditions at all points, and
ii) Ensures the same order of accuracy for both displacements and stresses.

But single-term solution does not predict the sharp variation of stresses near the clamped, free supports. Then multi-term 3D EKM [Kapuria and Kumari (2012)] was developed for the cylindrical bending of anisotropic laminated panels subjected to arbitrary boundary conditions. Its efficiency and accuracy was rigorously verified by comparing with other available 3D elasticity solution and detailed 3D finite element analysis. It was found that the multi-term solution yields accurate results for all response entities including the stress field near the edges, with just two to three terms in the solution. After onward, the method has been extended to the multi-field problem of the 3D piezoelasticity solution for the cylindrical bending of hybrid piezolaminated panels with edge effects, considering full electromechanical coupling [Kapuria and Kumari (2013)]. Recently, the multi-term EKM solution in conjunction with Fourier series is further developed to obtain the general bending response of elastic rectangular laminated plates [Kumari et. al. (2013)] and piezoelectric plate [Kumari et. al. (2016)] and free vibration of elastic plate [Kumari and Behera (2017)]. Very recently, this method has been extended to develop analytical 3D solution for longitudinally functionally graded plates [Kumari et. al. (2017)]. Presently, I and my Ph.D students are working for developing solution for shells and FGM piezo plates. In this article, brief mathematical formulation for levy-type piezoelectric plate and some typical examples are presented from our existing work.

2 Overall Mathematical Modelling

2.1 Geometry and basic governing equation

A hybrid cross-ply composite plate with span length 'a' along direction x, and total thickness h along the z-axis is considered for modeling (Fig.1). The hybrid laminated plate is made of L perfectly bonded generally orthotropic laminas, some of which can be orthotropic piezoelectric or PFRC material with poling along the thickness direction z, which can be used as distributed sensors and actuator. The thickness of the kth layer is $t^{(k)}$, and the z-coordinate of its bottom surface is denoted as z_{k-1}. The interface between the kth and the (k+1)th layer is denoted as the kth interface. The layer superscript is omitted unless needed for clarity. Let us take, u, v and w are

displacements along *x,y* and *z*-zxis. ε_i and γ_{ij} denotes mechanical strains and E_i denotes electrical strains and ϕ denote the electric potential The following linear strain-displacement and electric field-potential relations are used:

$$\varepsilon_x = u_{\square x}\ ;\ \varepsilon_y = v_{,y}\ ;\ \varepsilon_z = w_{,z}\ ;\quad \gamma_{xy} = v_{,x} + u_{,y}$$
$$\gamma_{zx} = w_{,x} + u_{,z};\ \gamma_{yz} = w_{,y} + v_{,z};$$
$$E_x = -\phi_{,x}\ ;\ E_y = -\phi_{,y};\ E_z = -\phi_{,z} \qquad (1)$$

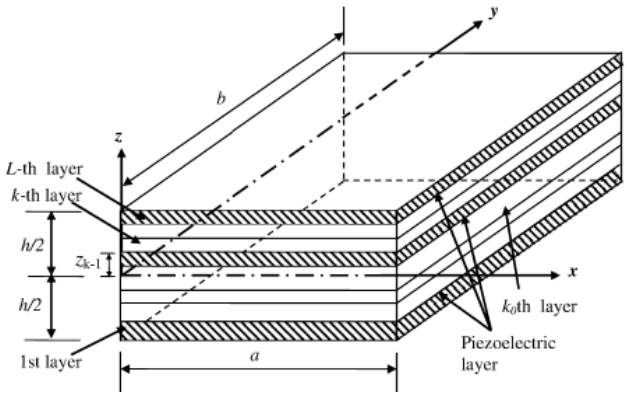

Figure 1. Geometry of Piezolaminated Plate

The Ressiner type variational principal considering mixed form of piezoelectric medium without body force and internal charge source can be written for the bending case as

$$\int_a \int_b \int_h [\delta u(\sigma_{x,x} + \tau_{xy,y} + \tau_{zx,z}) + \delta v(\tau_{xy,x} + \sigma_{y,y} + \tau_{yz,z})$$
$$+ \delta w(\tau_{zx,x} + \tau_{yz,y} + \sigma_{z,z}) + \delta\sigma_x(\varepsilon_x - u_{,x}) + \delta\sigma_y(\varepsilon_y - v_y)$$
$$+ \delta\sigma_z(\varepsilon_z - w_{,z}) + \delta\tau_{yz}(\gamma_{yz} - v_{,z} - w_{,y}) + \delta\tau_{zx}(\gamma_{zx} - u_{,z} - w_{,x})$$
$$+ \delta\tau_{xy}(\gamma_{xy} - v_{,x} - u_{,y}) + \delta\phi(D_{x,x} + D_{y,y} + D_{z,z}) - \delta D_x(E_x + \phi_{,x})$$
$$- \delta D_y(E_y + \phi_{,y}) - \delta D_z(E_z + \phi_{,z})]\mathrm{dzdydx} = 0,$$
$$\forall\ \delta u_i,\ \delta\phi,\ \delta\sigma_i,\ \delta\tau_{ij},\ \delta D_i \qquad (2)$$

Using the expression of *zD* from 3D-linear piezoelectric constative relations, $\varepsilon_x, \varepsilon_y, \varepsilon_z, \gamma_{xy}, \gamma_{zx}, \gamma_{yz}, E_x, E_y$ and Ez can be expressed in terms of σx, σy, τxy, τxz, τyz, σz, Dx, Dy and Dz is substituted in Eq. (2). Thus, governing equation in mixed form is obtained as

$$\int_a \int_b \int_h [\delta u(\tau_{xz,z} + \sigma_{x,x} + \tau_{xy,y}) + \delta v(\tau_{yz,z} + \tau_{xy,x} + \sigma_{y,y})$$
$$+ \delta w(\sigma_{z,z} + \tau_{zx,x} + \tau_{yz,y}) + \delta\phi(D_{x,x} + D_{y,y} + D_{z,z})$$
$$+ \delta\sigma_x(\bar{s}_{11}\sigma_x + \bar{s}_{12}\sigma_y + \bar{s}_{13}\sigma_z + \bar{d}_{31}D_z - u_{,x})$$
$$+ \delta\sigma_y(\bar{s}_{12}\sigma_x + \bar{s}_{22}\sigma_y + \bar{s}_{23}\sigma_z + \bar{d}_{32}D_z - v_{,y})$$
$$- \delta\sigma_z(w_{,z} - \bar{s}_{13}\sigma_x - \bar{s}_{23}\sigma_y - \bar{s}_{33}\sigma_z - \bar{d}_{33}D_z)$$
$$- \delta\tau_{yz}(v_{,z} + w_{,y} - \bar{s}_{44}\tau_{yz} - \bar{d}_{24}D_y)$$
$$- \delta\tau_{zx}(u_{,z} + w_{,x} - \bar{s}_{55}\tau_{zx} - \bar{d}_{15}D_x) + \delta\tau_{xy}(s_{66}\tau_{xy} - v_{,x} - u_{,y})$$
$$- \delta D_x(\phi_{,x} + \bar{\epsilon}_{11}D_x - \bar{d}_{15}\tau_{zx}) - \delta D_y(\phi_{,y} + \bar{\epsilon}_{22}D_y - \bar{d}_{24}\tau_{yz})$$
$$- \delta D_z(\phi_{,z} - \bar{d}_{31}\sigma_x - \bar{d}_{32}\sigma_y - \bar{d}_{33}\sigma_z + \bar{\epsilon}_{33}D_z)]\,\mathrm{dzdydx} = 0,$$
$$\forall\ \delta u_i,\ \delta\phi,\ \delta\sigma_i,\ \delta\tau_{ij},\ \delta D_i \qquad (3)$$

Detailed expression can be find out in Ref. [Kumari et.al**.** (2016)]. Dimensionless in-plane coordinates considered is $\xi = x/a$ along the *x*-direction, respectively. A thickness coordinate ζ for a layer along the *x*-direction is defined which vary from 0 to 1. The boundary conditions considered at the top and bottom surface are as follows : at $z = \pm h/2$ $\sigma_z = -p_i$, $\tau_{zx} = 0$, $\tau_{yz} = 0$, $\phi = \phi_i$ or $D_z = 0$ The plate are subject to arbitrary boundary conditions at 0,1ξ= e.g. simple supported-simply supported (SS), clamped-clamped (CC) and free-free (FF).

2.2 Fourier series in conjunction with EKM

The solution is expressed in terms of Fourier series in y, which identically satisfies the boundary conditions at two simply supported edges y (0, b) and in this way, Eq. (3) reduced containing derivative along **x** and *z*-axis.

The solution of the field variables, $\mathbf{X} = [u\ \ v\ \ w\ \ \sigma_x\ \ \sigma_y\ \ \sigma_z\ \ \tau_{xy}\ \ \tau_{yz}\ \ \tau_{zx}\ \ \phi\ \ D_x\ \ D_y\ \ D_z]^{\mathrm{T}}_m$ is assumed in terms of an n-term series of the products of separable functions in the two independent variables ξ (=*x*/a) andς (=$(z - z_{k-1})/t^k$) The solution for the variables are assumed in the following form:

$$X_l(\xi_1, \zeta) = \sum_{i=1}^{n} f_l^i(\xi_1) g_l^i(\zeta) + \underline{\delta_{l6}[p_a + zp_d]} + \underline{\delta_{l,10}\bar{g}_{10}}$$
$$\text{for } l = 1,2,.....13 \qquad (4)$$

wherein $f_l^i(\xi)$ and $g_l^i(\zeta$ are the univariate functions of ξ and ζ respectively, for the *i*th term of the n-term series solution. There is no sum over *l* and δ_{l6}

is Kroneckor's delta. The underlined terms are used to satisfy the non-homogenous boundary conditions at the top and bottom of the plate.

$p_a = -(p_{1_m} + p_{2_m})/2, p_d = -(p_{2_m} - p_{1_m})/h$, and $\bar{g}_{10}$ is given by

$$\bar{g}_{10} = \begin{cases} \phi_1(1-\zeta) & \text{for } k = 1 \\ \phi_2\zeta & \text{for } k = L \end{cases}$$

These functions are to be determined iteratively, satisfying all homogenous boundary conditions.

2.2.1 First Iteration step

In this step, functions $f_l^i(\xi)$ are assumed, for which the variation δX_i

$$\delta X_l = \sum_{i=1}^{n} f_l^i(\xi)\, \delta g_l^i \qquad l = 1,2,.....13 \tag{5}$$

Functions $g_l^i(\zeta)$ are partitioned into a column vector $\bar{G}$ which contains those 8n that appear in the boundary and interface conditions, and a column vector $\hat{G}$ consisting of 5n the reaming variable. Substituting Eq. (4) and (5) in Eq. (3), integrating over ξ direction and considering the variations δg_l^{III} are arbitrary, the coefficients of δg_l^{III} are equated to zero individually. This results in the following set of 8*n* differential-algebraic equation for the *k*th layer:

$$M\bar{G}_{,\zeta} = \bar{A}\bar{G} + \hat{A}\hat{G} + \bar{Q}_p \tag{6}$$

$$K\hat{G} = \tilde{A}\bar{G} + \tilde{Q}_p \tag{7}$$

Where M, $\bar{A}$, $\hat{A}$, K and $\tilde{A}$ are 8*n*x8*n*, 8*n*x8*n*, 8*n*x5*n*, 5*n*x5*n* and 5*n*x8*n* matrices. The load vectors $\bar{Q}_p$ and $\bar{Q}_p$ are load vectors of size *8n* and *5n*, and linear function of ζ. The algebraic equations in (6) can be solved to obtain $\hat{G}$ and put into (5) which yields a set of 8*n* first-order homogeneous ODEs as:

$$\bar{G}_{,\zeta} = A\bar{G} + Q_p \tag{8}$$

This is a first order non homogenous differential equation which is solved using standard approach given in Ref. [Kumari et.al. (2016)].

2.2.2 Second Iteration step

In this step, the solution of the previous step is taken as the known approximated solution for $g_l^i(\zeta)$ while functions f_l^i are considered as unknown. The variation $X\delta$ for this case is given by

$$\delta X_l = \sum_{i=1}^{n} g_l^i(\xi)\, \delta f_l^i \qquad l = 1,2,.....13 \tag{9}$$

The functions $f_l^i(\xi)$ are partitioned into vector $\bar{C}$ consisting of those variables appear that in the boundary conditions along x-axis and a vector $\hat{F}$ of the remaining variables. Performing integration over ζ direction on the known functions of ζ, applying integration by parts wherever necessary, and equating the coefficient of δf_l^i to zero individually, yields the following system of differential-algebraic equations for f_l^i:

$$\begin{aligned} N\bar{F}_{,\xi} &= \bar{B}\bar{F} + \hat{B}\hat{F} + \bar{P}_m \\ L\hat{F} &= \tilde{B}\bar{F} + \tilde{P}_m \end{aligned} \tag{10}$$

Where N, $\bar{B}$, $\hat{B}$, L and $\tilde{B}$ are 8*n*x8*n*, 8*n*x8*n,* 8*n*x5*n*

5*n*x5*n* and 5*n*x8*n* matrices. The load vectors and $\bar{P}_m$ are load vectors of size *8n* and *5n.* The same procedure is followed as in the first step and a system of 13*n* differential-algebraic equations are obtained for f_l^i, which are solved in a similar fashion as mentioned in the previous step.

3 Results and Discussion

3.1 Stress field at the interface of long bi-material strip

A long bi-material strip under uniform tension is studied under uniform tension (see Fig.2 (a)) by taking material (mat 1: E =100 GPa, v=0.3; Mat 2: 1 GPa, v=0.3). Normal stress is plotted (Fig.2 (b)) along the interface at *z*=0 with non-dimensional parameter r/a (r=distance from the free edge) by taking converged results of 4 terms in EKM. The order of stress singularity for the present curve is -0.271(which is obtained by fitting the power low over the graph) and for this configuration Akisanya and Fleck [1997] reported stress singularity equal to -0.277. So present results are in excellent agreement and it establishes the methods efficacy and accuracy in predicting the stress behaviour near the free or clamped edge.

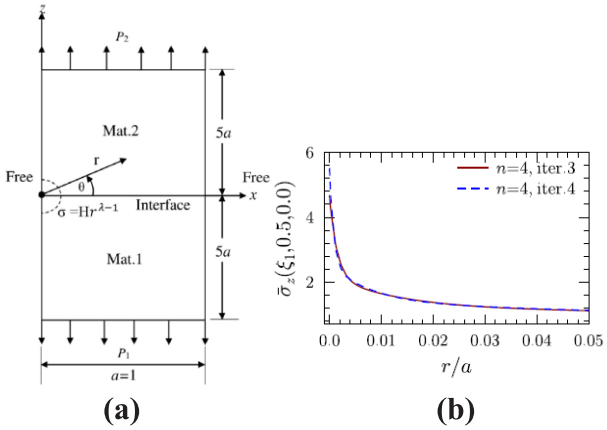

Figure 2. (a) Geometry of Bi-material strip; (b) Stress distribution along the interface.

3.2 Sandwich plate under electromechanical excitation

Some typical results of piezoelectric sandwich plate (material property and layup configuration can be found in Ref (Kumari et al. 2016) under the pressure and electric potential loading are presented in Figs. 3, 4. The present results are presented in Figs 3 and 4 and compared with converged results obtained by 3D FE (ABAQUS). It can be seen that present methodology are able to capture the sharp variation of stresses and electrical displacement for clamped (C), free (F) and simply supported edge under electromechanical excitation. At the very edge, the present results are in disagreement with 3D FE. This mismatch is because the FE Solution does not satisfy the condition of zero shear traction at the top and bottom surfaces, and interfacial continuity of transverse shear stresses at the clamped edge, and the free edge which can be verified in Fig. 5. Effect of adhesive thickness on the interfacial stress behaviors is depicted in Fig. 6. Stress concentration at the interfaces reduce with the increase in adhesive layer thickness and significant reduction in the magnitude for transverse shear stress is observed.

4 Conclusions

The state-of-art of the development of 3D piezoelsaticity solutions for Levy-type piezoelectric laminated plate using the EKM is presented. Some typical results which show efficiency and power of the method is presented. The present methodology can be used to develop 3D analytical solutions for functionally graded beams, plates and shells under bending, vibration and bucking cases.

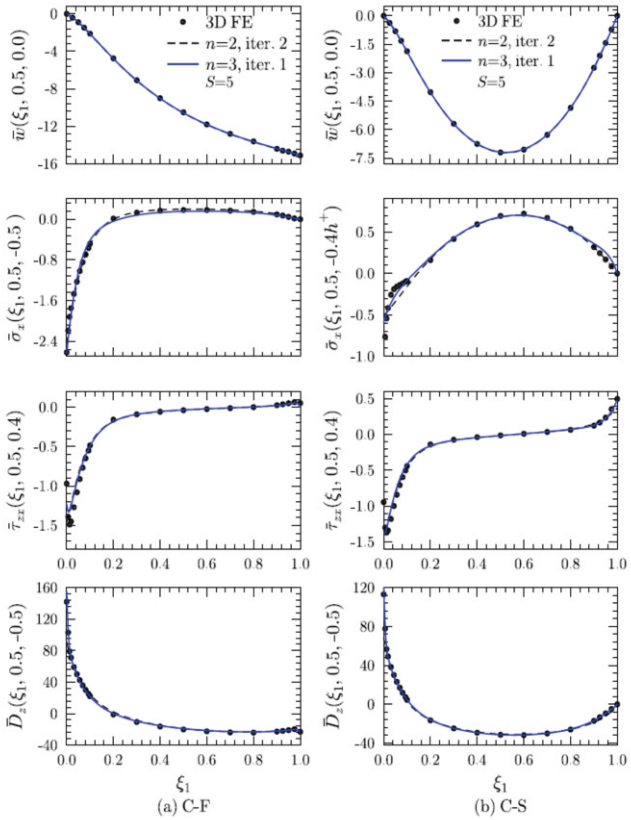

Figure 3. Longitudinal variations of deflection, stresses and electric displacement for hybrid sandwich plate with C–F and C–S boundary conditions under pressure loading.

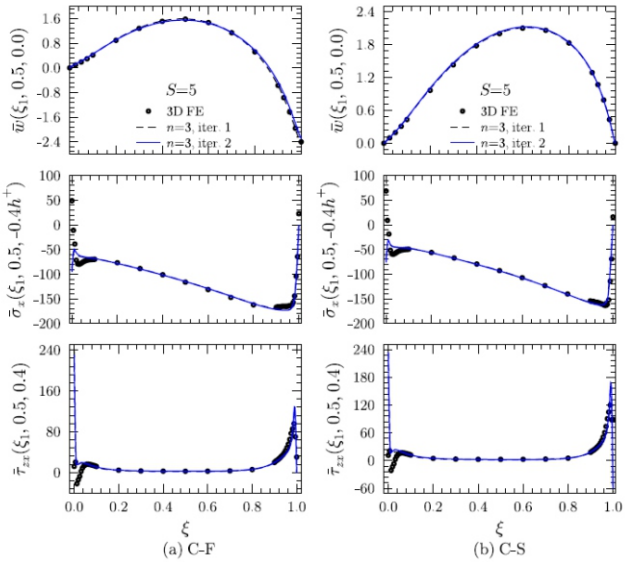

Figure 4. Longitudinal variations of deflection and stresses for sandwich plate with free–free (F–F) boundary condition under potential loading.

These results can be used as benchmarks to assess the accuracy of 2D and numerical solution.

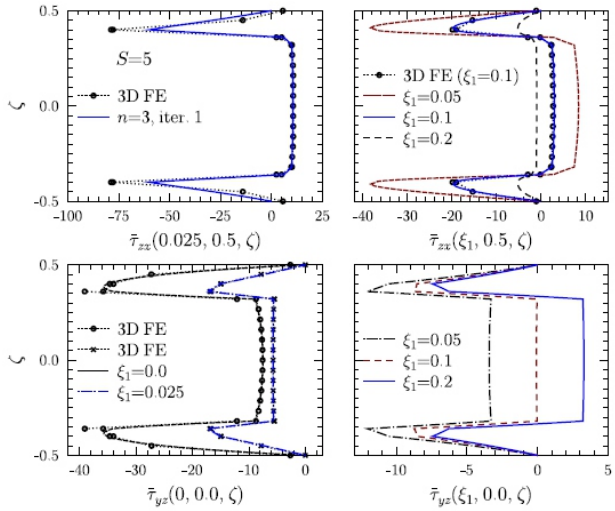

Figure 5. Through-thickness variations of stresses for F–F boundary condition at different locations of square sandwich plate under potential loading

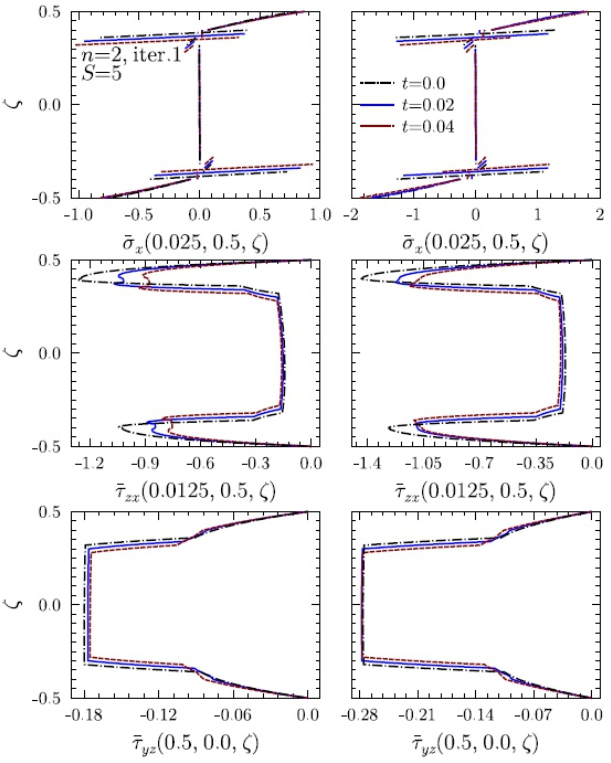

(a) C-C (a) C-F

Figure 6. Through-thickness variations of stresses for different adhesive thickness under pressure loading.

References :

1. **Mittelstedt C; Becker W**. (2007) Free-edge effects in composite laminates, *Appl. Mech. Rev.*, vol.60, pp 217–24.

2. **Sheng H.Y.; Wang H; Ye J.Q.** (2007) State space solution for thick laminated piezoelectric plates with clamped and electric open-circuited boundary conditions, *Int. J. Mech. Sci.*, vol.49, pp 806–18.

3. **Vel S.S.; Batra R.C.** (2000) Three-dimensional analytical solution for hybrid multilayered piezoelectric plates, *J Appl Mech Trans ASME,* vol. 67, pp 558–67.

4. **Vel S.S.; Mewer R.C.; Batra R.C.** (2004) Analytical solution for the cylindrical bending vibration of piezoelectric composite plates, *Int. J. Solids Struct.*, vol. 41, pp1625–43.

5. **Huang B,; Kim H.S.** (2014) Free-edge interlaminar stress analysis of piezo-bonded composite laminates under symmetric electric excitation, *Int. J. Solids Struct.*, Vol.51, pp 1246–52.

6. **Reddy J. N.** (2007) Theory and Analysis of Elastic Plates and Shells, CRC, Boca Raton, FL.

7. **Kantorovich L.V.; Krylov V. I.** (1958) Approximate Methods of Higher Analysis, Interscience, New York.

8. **Kerr A.D.** (1968) An Extension of the Kantorovich Method, *Q. Appl. Math., vol.* 4, pp 219–229.

9. **Kerr A. D.** (1969) An Extended Kantorovich Method for the Solution of Eigenvalue Problems, *Int. J. Solids Struct.*, vol. 5, pp. 559–572.

10. **Singhatanadgid P; Singhanart T.** (2017) The Kantorovich method applied to bending, buckling, vibration, and 3-D stress analyses of plates: a literature review, *Mech. Adv. Mater. Struc.*, doi:10.1080/15376494.2017.1365984.

11. **Kapuria S.; Kumari P.** (2011) Extended Kantorovich method for three-dimensional elasticity solution of laminated composite structures in cylindrical bending, *J Appl Mech Trans ASME* , vol. 78, Art. No. (061004).

12. **Kapuria S.; Kumari P.** (2012) Multi-term extended Kantorovich method for three dimensional elasticity solution of laminated plates*, J Appl Mech Trans ASME,* vol. 79, Art. No. (061018).

13. **Kapuria S.; Kumari P.** (2013) Extended Kantorovich method for coupled piezoelasticity solution of piezolaminated plates showing edge effects, *Proc R Soc A,* vol. 469, Art. No. (20120565).

14. **Kumari P.; Kapuria S.; Rajapakse R.K.N.D.** (2013) Three-dimensional extended Kantorovich solution for levy-type rectangular laminated plates with edge effects, *Compos Struct.,* vol. 107, pp 167–76.

15. **Kumari P.; Behera S.; Kapuria S.** (2016) Coupled three-dimensional piezoelasticity solution for edge effects in Levy-type rectangular piezolaminated plates using mixed field extended Kantorovich method, *Composite Structures*, vol.140, pp 491-505.

16. **Kumari P.; Behera S.** (2017) Three-dimensional free vibration analysis of levy-type laminated plates using multi-term extended Kantorovich method, *Composites Part B: Engineering,* vol. 116, pp 224-238.

17. **Kumari P.; Singh A.; Rajapakse R.K.N.D.; Kapuria S**. (2017) Three-dimensional static analysis of Levy-type functionally graded plate with in-plane stiffness variation, *Compos Struct*, vol. 168, pp 780-791.

18. **Akisanya A.R.; Fleck N.A. (**1997) Interfacial cracking from the free edge of a long biomaterial strip, *Int J Solids Struct*., vol. 34, pp 1645–65.

Annals of the Indian National Academy of Engineering
Vol. XV, April 2018

Effect of Electric Field on Mechanical Properties of Vertically Aligned Carbon Nanotube Porous Structure

Praveen Kumar[1]

Abstract : Vertically aligned carbon nanotubes (CNT) porous structures, also known as CNT forests (CNTF), are multifunctional materials, with commendable mechanical, electrical and sensing properties. Here, we describe effects of electric field on a few time-independent mechanical properties (e.g., stress-strain behavior, energy absorption) and time-dependent mechanical properties (e.g., creep and stress relaxation) of CNTF. An increase in the load bearing capacity of CNTF was observed upon application of an electric field in the direction of compression. If the electric field was "on" while loading and "off" while unloading, then the energy absorption capacity of CNTF increased several folds under quasi-static loading conditions. However, this enhancing effect of electric field on energy absorption reduced under dynamic loading conditions. On other hand, CNTF became creep resistant upon application of electric field, wherein a distinct steady state was observed that could be quantified using a power-law function. Nevertheless, stress relaxation increased and hence saturation load bearing capacity of CNTF reduced in presence of an electric field. It is suggested that the electric field induced polarization of CNT strands is responsible for the observed effects of electric field on mechanical properties of CNTF.

Keywords: CNT forests, Mechanical properties, Effect of electric field, Polarization.

1 Introduction

Carbon nanotube (CNT) is a 1-D tubular structure of carbon, which can manifest itself in myriad of bulk structures, e.g., Buckeye paper, vertically aligned porous ensemble of CNT (often called CNT forests (CNTF) or CNT mats) (see Fig. 1), etc. Although some of the properties of the individual strands of CNT are retained as well as revealed dominantly in the bulk structures (e.g., gas sensing properties [1,2]), the additional physical interactions between multiple strands of CNT in the bulk structures lead to different sets of properties also. One of the examples where the difference between the properties of individual strands and ensemble of several CNT strands (as in CNTF) is dramatically revealed is in terms of mechanical properties; for example, while the Young's modulus of an individual CNT strand may reach 106 MPa [3], the elastic modulus of CNTF may be in the order of 10 MPa only [4,5]. This colossal difference between elastic moduli originates from the fact that while the C-C bonds are stretched during deformation of an individual CNT strand, the van der Waal's interactions between adjacent CNT strands determines the resistance to deformation of CNTF. Since the bond strength of van der Waals is much weaker than that of the covalent bond between carbon atoms forming the CNT, the stiffness of CNTF becomes orders of magnitude smaller than that of a CNT strand. Nevertheless, the ensemble configuration not only allows handling and manipulation of CNT easier, thereby allowing regular engineering applications of these materials, but also proffers an additional control for tuning the overall mechanical (or other physical) properties of CNTF. For example, van der Waal's interactions between CNT strands may be changed by introducing a liquid medium (e.g., by impregnating CNTF by mixture of glycerin and water [6], etc.), nano-particles [7], etc. inside the open spaces or pores of CNTF, thereby

[1] Department of Materials Engineering, IISc/Bangalore, Bengaluru-560012.

altering the overall mechanical response of CNTF. This is interesting to note that the presence of pores, which is a microscopic length scale feature associated with CNTF, allows altering the van der Waal's interactions, which is an atomic level phenomenon, through the methodologies mentioned above and hence the later cannot be achieved without the presence (or assistance) of the earlier one. Therefore, all length scales shown in Fig. 1 provide a method for tuning the overall mechanical behavior of CNTF and hence they must be considered separately as well as in tandem with others for understanding the mechanical response, as well as any other physical property, of CNTF.

Furthermore, CNTF have demonstrated tremendous reversible compressibility of > 80 % [8], and due to the energy loss involved in sliding of CNT strands over each other and breaking of nodes formed between CNT strands, they also have very high energy absorption capacity [4,9]. CNTF can remain chemically stable even at temperatures of > 400 ºC [10]. As shown in Fig. 2a, it has been predicted that single walled CNT can be polarized upon application of an electric field and hence it can show electrostriction induced actuation (see Fig. 2b) [11]. This was experimentally exploited previously by proposing the usage of CNT structures – especially Buckeye paper – as artificial muscles [12]. Finally, as shown in Fig. 2c, the band-structure and hence the net polarization of the CNT have been predicted to change upon application of a mechanical stress or deformation [13]. Therefore, CNTF presents itself as a quite interesting material for studying mechanical behavior, as its overall response can be tuned at various length scales, its mechanical response can potentially be varied by applying electric field (i.e., harnessing its mechanical stress or electro-mechanical coupling dependent electrostriction property) and it has superb compressibility along with exceptional energy absorption capacity. Realizing this potential of CNTF, which may in near future be translated into a real engineering application of a CNT based structure, we initiated the study of effect of electric field on both the time-dependent and the time-independent mechanical behavior of CNTF, which form the subject of this manuscript. Particularly, effects of electric field on actuation, stress-strain curves under quasi-static condition, energy absorption under quasi-static as well as dynamic loading condition, creep and stress relaxation behavior of CNTF will be discussed. Results obtained in this study would allow to actively tune various mechanical properties of CNTF using electric field for enhancing its utility in protecting microelectronic, MEMS devices, etc. by absorbing energy during a drop, nudge or mishandling.

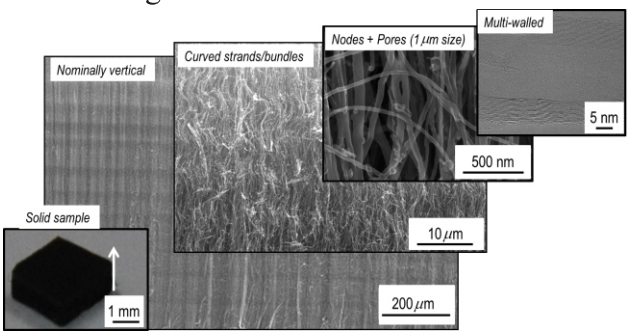

Figure 1: Micrographs obtained at different magnifications showing various length-scale features of CNTF. The left-bottom image shows a real test specimen, the right-top micrograph was a taken using a transmission electron microscope (TEM) and other micrographs were taken using a scanning electron microscope (SEM). CNTF were made up of multi-walled CNT strands (see the TEM micrograph). Significant open space was available inside the sample, making these samples porous. Nodes were formed where CNT strands crossed each other.

2 Experimental Procedure

CNTF shown in Fig. 1 and used in this study were prepared using thermal chemical vapor deposition technique. Ferrocene was used as the iron (i.e., catalyst) source, whereas toluene was used as the carbon source. A mixture of vaporized ferrocene and toluene was brought into the reaction zone in a tubular furnace maintained at 825 ºC using Ar, enabling growth of a ~1 mm thick mat of vertically aligned CNT or CNTF on SiO_2/Si substrate. The mat of CNTF was then separated from SiO_2/Si

substrate using a surgical knife. Test samples with various cross-sections (e.g., ~4 × 3 mm^2, ~2 × 2 mm^2, etc., depending on the test) were sliced from the CNTF mat using a surgical knife. An example photograph of the test specimen is shown in Fig. 1. Through this CVD process, as shown in Fig. 1, only multi-walled CNT were grown, and the macroscopic structure of the sample was highly porous. The overall density of sample was only 0.28 g/cm^3, which is ~20 % of the theoretical density, thereby qualifying these samples as cellular (foam).

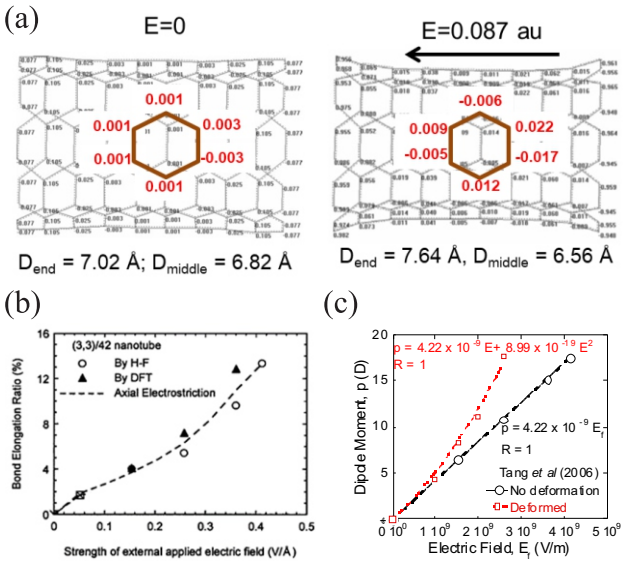

Figure 2: Density functional theory (DFT) based prediction showing effect of electric field on (a) polarization of CNT rings [11], (b) bond elongation (leading to overall actuation of the sample) [11] and (c) dipole moment in presence of mechanical deformation (or load) [based on data reported in 13] in single walled CNT. H-F in (b) stands for Hartree-Fock ab initio quantum mechanics model. In (a), for clarity, a ring in the center was redrawn using thick lines and the charge values were written using larger letters.

Electric field induced actuation behavior of CNTF was studied using a simple test setup, shown in Fig. 3a, which allowed application of different electric fields across the height (or thickness) of the sample using a source-measurement unit as well as measurement of the change in the length using a laser-based non-contact extensometer. In this set of experiments, the electric field and the extension of sample height was recorded as function of time and only the saturation value of the actuation strain at a given electric field is reported in this manuscript. The details of the experimental setup are available in reference 7.

All mechanical tests were performed in compression at room temperature using standard universal mechanical tester (UTM) having low load capacity using a 100 N load cell. A schematic of the test fixture is shown in Fig. 3b and the details of the test methodology are available in references 5, 9 and 14. Since the mechanical testing involved application of electric field along the sample height, which was same as the direction of application of load, proper insulation between the sample and the load-train of the UTM was ensured by introduction of glass in between the sample and the metallic loading rods (see Fig. 3b). Displacement and force data was recorded as function of time in all tests. For each set of tests performed in this study, a couple of experiments were repeated under identical condition to verify the repeatability of the data obtained.

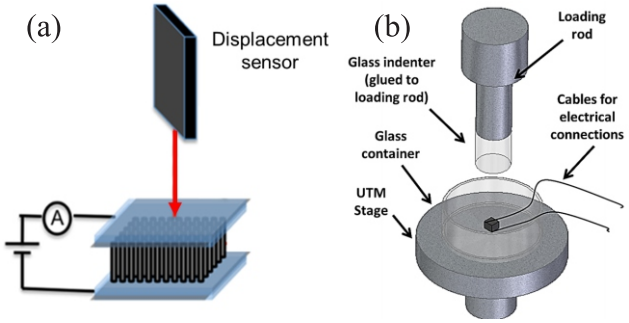

Figure 3: (a) A schematic illustration of the setup used to measure electric field induced actuation in CNTF. A known electric potential, varying between – 5 V to + 5 V, was applied across the height of the sample and the corresponding actuation in the direction of electric field was measured using a laser based non-contact displacement sensor (with a resolution of 10 nm). A polymer-Buckeye paper based foil was affixed onto each end of the sample as electrode. (b) A schematic illustration of the test fixture – that was

attached to the loading rods of the universal mechanical tester - used for studying effect of electric field on the mechanical behavior of CNTF [14]. The glass container at the bottom (which allows, in principle, submerging the sample in a liquid medium, e.g. 20 % H_2SO_4, etc., also) and the glass rod on the top ensured electrical insulation of the sample from rest of the mechanical tester.

For studying the stress-strain response and energy absorption capacity and effect of electric field on these properties of CNTF, the samples were compressed at a constant nominal strain rate 1.0×10^{-3} s^{-1} and then unloaded under the same nominal strain rate. The area of the stress-strain curve over one loading-unloading cycle was equal to the strain energy absorbed by the sample per unit volume.

For studying the load bearing capacity and energy absorption behavior of CNTF under dynamic loading condition, a custom built experimental setup shown in Fig. 4 was used. Herein, a steel ball was dropped from a height of 1 m (i.e., a known potential energy) and the time between the first two load peaks, which is a direct measure of the velocity of the ball after a collision, was used to determine the total mechanical energy of the ball after the first collision with the sample. Loss of the total mechanical energy (or sum of potential and kinetic energies) before and after collision of ball with the sample was used to calculate the energy absorbed by the sample. During the dynamic loading test, the electric field was applied along the height of the sample only when it was being loaded (i.e., when the ball was decelerating during its collision with the sample), and it was switched off during unloading.

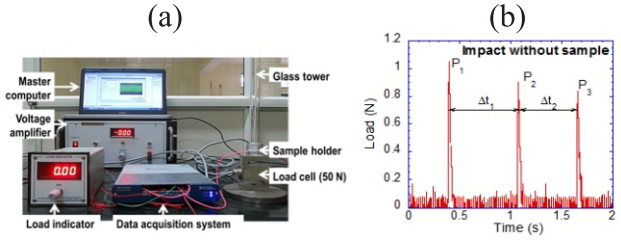

Figure 4: (a) A digital pictograph of the setup used for studying effect of electric field on the energy absorption capacity of CNTF [15]. A steel ball was dropped from the top of the glass tower, which then impacted the CNTF sample placed inside the sample holder at the bottom of the glass tower. The sample holder was affixed onto a load cell and hence the load applied onto the sample was measured as function of time. (b) An example load vs. time data obtained from one of the ball-drop impact tests, showing distinct peaks representative of an impact [15]. The time duration between the two consecutive impacts (Δt) is the time of flight of the ball in the air, which can be used to calculate the kinetic energy of the ball once it left the sample after a collision with the sample.

For performing creep and stress relaxation tests, samples were loaded at a constant nominal stress and a constant nominal strain, respectively, using the setup shown in Fig. 3b and the corresponding increase in the strain and the decrease in the nominal stress, respectively, was observed as function of time. Here also, the electric field was applied in the direction of the applied load or strain.

The structure of CNTF was observed using scanning electron microscope (SEM) and transmission electron microscope (TEM) at different magnifications (see Fig. 1). The structure of CNTF was observed before the tests and, at several occasions, after the test also to gain insights into effect of mechanical deformation on the structure of CNTF.

3 Results and Discussions

3.1 Actuation

Fig. 5 shows the effect of electric field on the overall strain, i.e., actuation, generated in a free-standing CNTF, as measured using the setup shown in Fig. 3a. Fig. 5a clearly reveals that the sign of the actuation strain was independent of the sign of the electric field, and the relationship between the strain, ε, and the electric field, E, can be represented aptly by a parabolic function: $\varepsilon = CE^2$, where C is a constant. Interestingly, a strain of ~12 % was observed in these samples at an electric field of only ~ 4 kV/m, which translates

into an electric potential of 4 V over 1 mm distance (i.e., height of sample). This actuation is extraordinarily high for any CNT based structure reported experimentally as well as predicted using DFT (e.g., see Fig. 2b).

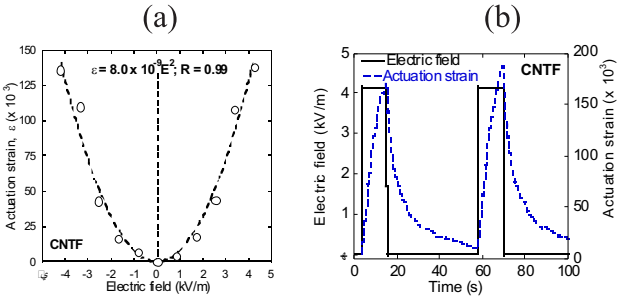

Figure 5: Variation of (a) strain as function of applied electric field, and (b) electric field and actuation as function of time. The equation along with the regression parameter (R) in (a) represent the best fit curve (shown in broken curve) passing through the experimental datum points (shown using open circles). Reproduced from [7].

Another salient feature of the actuation in CNTF is shown in Fig. 5b, which reveals that there was a lag between the stimulus (i.e., "on" or "off" of the electric field) and the actuation strain. The actuation appeared to saturate only after a few seconds of application of an electric field, and it also only gradually became zero upon switching off the electric field. Moreover, careful observation of the nature of the rise and fall of the actuation due to the "on" and "off" of electric field, respectively, suggests an exponential behavior, akin of charging and discharging of a capacitor As a matter of fact, fitting a curve of exponential nature (e.g., for rising and for retracting strain segments, where t and τ are time and a time constant, respectively) gives the same value for the time constant, equal to 8 × 1 s, for both the rising and retracting curves shown in Fig. 5b. This confirms a charging – discharging based phenomenon in response to the on-off events of the electric field responsible for the actuation in CNTF.

As shown in Fig. 2, the DFT based calculations reveal generation of a net charge in the CNT ring upon application of an electric field, thus creating a dipole (and hence dipole moment in the direction of the electric field). According to Fig. 2c, the dipole moment generated in absence of any mechanical load (or deformation) varies linearly with the electric field. Since the force on a dipole placed in an electric field is proportional to the electric field, the net force applied onto a CNT strand due to an applied electric field will be proportional to the square of the electric field; this is consistent with the experimentally observed expression for actuation strain as shown in Fig. 5a. Furthermore, since charging (and discharging) of CNT ring due to the electric field is not instantaneous, the "capacitor" like lag between the stimulus and the response, as shown in Fig. 5b, is also consistent with the theoretical models. It should be noted that the current through a multi-walled CNT is carried often by only a few concentric shells, especially the outer ones [16]. Hence, the several shells of multi-walled CNT (as prepared in this study), especially the interior ones in presence of electric field, could be polarized, even if the overall CNTF sample behaves like a conductor. The electromagnetic interaction between two CNT strands due to the Lorentz force was observed to be negligible [9]. Furthermore, such an electromagnetic interaction would lead to reduction in height of CNTF [9], which is contrary to the experimental observation.

3.2 Stress-Strain Behavior under Quasi-Static Loading

Fig. 6 shows the effect of electric field on the stress-strain behavior of CNTF. As shown in Fig. 6a, the stress required to hold the sample at a certain compressive strain increased upon application of an electric field. Moreover, in this small strain regime the stress-strain curve was completely recovered to the "regular" values (i.e., if electric field was never applied during the mechanical test) if the electric field was turned off, thereby erasing any memory of the application of electric field. Fig. 6a also shows that the stress jump increased with electric field and, accordingly, the area of the hysteresis loop increased if the electric field was applied during the loading segment of the mechanical testing. It should be noted that a stress-strain hysteresis loop during the loading-unloading of CNTF within the

linear region of stress-strain curve was observed. This is due to dissipation of some strain energy when either two CNT strands slide against each other or the nodes formed at the CNT-CNT intersection are broken. Hence, the stress-strain curve of a CNTF sample is not fully reversible even if the sample is loaded only in the linear regime. Nevertheless, the overall height of the sample was recovered at conclusion of the test.

As shown in Fig. 2c, the dipole moment of the electric field induced polarized CNT rings increases in the presence of deformation or mechanical stress. DFT calculations have shown that the presence of mechanical stress changes the relative position of the highest occupied molecular orbital and the lowest unoccupied molecular orbital [13], and hence the electric field induced polarization changes in presence of a mechanical stress. Due to this electro-mechanical coupling induced enhancement in polarization, the overall electric field induced actuation in CNTF would increase in presence of a mechanical stress. A first order estimate, as shown in Fig. 2c, suggests that the polarization should vary as square of the electric field and hence the actuation strain should vary as cube of the electric field (as opposed to the square in the free-standing CNTF – see Fig. 5a). Assuming the stress-strain relationship to be linear (which is reasonable in the linear region of stress-strain curve of CNTF), the stress required to maintain a compressive strain will increase as cube of the applied electric field. Now, as shown in Fig. 6b, this is indeed the case, because if this electro-mechanical coupling is neglected (e.g., blue broken line), the experimentally observed stress jump upon application of an electric field could not be captured. Therefore, the enhancement in the strength of CNTF in presence of electro-mechanical coupling is significantly more than that predicted from the "accommodation" of the electric field induced macroscopic actuation strain of the freestanding CNTF.

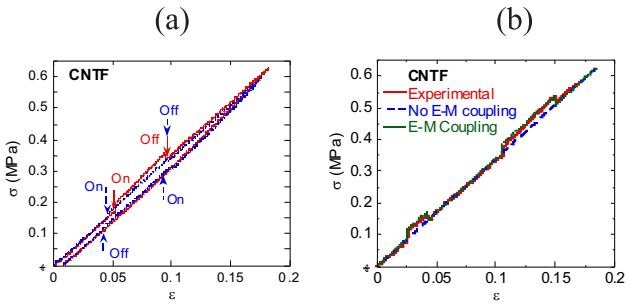

Figure 6: (a) Effect of application of electric field on the stress-strain curve within linear region of CNTF. The vertical arrows show the instances of electric field "on-off" events. (b) The prediction of the model assuming electro-mechanical coupling (i.e., E-M coupling) and without assuming such coupling (i.e., No E-M coupling). In (b), the applied electric field at two instances was ~1.5 kV/m. Tests were performed in compression at a constant nominal strain rate of 1.0×10^{-3} s^{-1}. Reproduced from [5].

3.3 Energy Absorption under Quasi-Static and Dynamic Loading Condition

Fig. 7 shows the effect of electric field, applied only during the loading segment of the loading-unloading cycle, on the stress-strain behavior as well as the size of the hysteresis loop (or, accordingly, the total energy absorbed per unit volume) of CNTF samples. It is apparent from Fig. 7a that an increase in the electric field (applied during loading segment only) enhances not only the stress bearing capacity of CNTF at any strain, but also the overall size of the hysteresis loop. One of the most striking features of the unloading curve is the sudden drop in the load as soon as the electric field was switched off (which coincides with the onset of unloading). This feature of unloading segment appears to be eventually responsible for increasing the overall size of the hysteresis loop. It should be noted that, as shown in Fig. 7a, the original height of the CNTF samples was recovered at the end of the test, thereby confirming exceptional reversible compressibility of these samples.

Consistent with Fig. 7a, Fig. 7b shows a rapid increase in the total energy absorbed per unit volume with the applied electric field.

Interestingly, the energy absorption capacity of these samples increased by a factor of > 7 upon application of an electric field of only ~1 kV/m, which translates into 1 V over the height of samples (i.e., 1 mm). Such voltages are readily available in all handheld microelectronic and MEMS devices, and hence this observation opens a new avenue for using this material in the mobile devices to protect them against mishandling and accidental nudge or drop. It should be noted that other schemes of applying electric field, such as application of electric field throughout the loading-unloading cycle or only during the unloading cycle, did not show an increase in the energy absorption capacity and hence they are not discussed here. However, one can refer to reference [9] for a detailed discussion on effect of these testing conditions on energy absorption capacity and structure of CNTF.

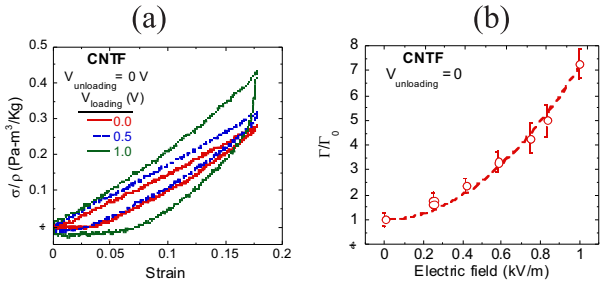

Figure 7: Effect of application of electric field on (a) stress-strain behavior within linear stress-strain region of CNTF and (b) total normalized energy absorbed (per unit volume) over a loading-unloading cycle. For normalization of energy absorbed, the energy absorbed by the sample in presence of electric field, Γ, was divided by that observed in absence of electric field, Γ0. Electric field (or, electric potential, V) was applied only during the loading segment, which are listed in legend of (a). The broken curve shown in (b) is the best-fit curve, obtained using a parabolic function. Reproduced from [9].

Fig. 8 shows the effect of the scheme of application of electric field during a loading-unloading cycle on the structure of CNTF samples. A comparison of Figs. 8a and 8b readily reveals that the CNT strands in the samples loaded under electric field and unloaded without electric field were highly buckled, suggesting more distortion (and hence non-uniform deformation) as compared to the as-fabricated structure (e.g., see Fig. 1). On the other hand, Fig. 8 also suggests that if the sample was unloaded under electric field (and loaded without electric field), the CNT strands became straighter, and comparable to that observed in the as-fabricated sample. Hence, this scheme of application of electric field can be used to "heal" CNTF that have undergone some damage due to the previous loading-unloading cycles. This further adds to extension of the useful life of such energy absorbers.

Fig. 9 shows the effect of application of electric field during the loading segment on the energy absorption capacity of CNTF under dynamic loading condition, as obtained using the ball-drop setup shown in Fig. 4a. A comparison of Figs. 9a and 9b clearly reveals that the time between the first two impacts (which could be unambiguously identified in these tests) reduced if the electric field was applied during the loading segment, thereby suggesting more energy absorption by the sample (i.e., more energy loss by the ball) in presence of an electric field under the dynamic condition also. Furthermore, the maximum load exerted by the ball onto the sample during the second collision significantly reduced relative to the maximum load applied during the first collision. This further confirms that the ball rose to a shorter height (relative to the original height from which the ball was dropped from the rest) after the first collision if an electric field was applied during the loading segment. Fig. 9c, accordingly, shows a monotonous increase in the total energy absorbed by the sample due to application of an electric field during the loading segment.

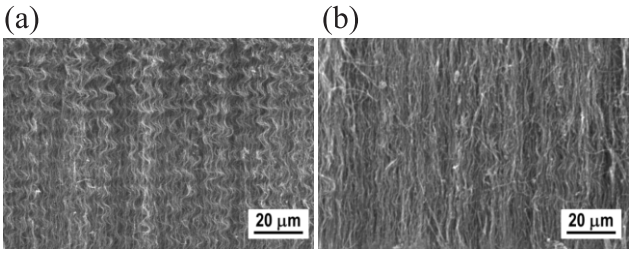

Figure 8: SEM micrographs obtained within a short time after the conclusion of a loading-unloading cycle: The electric field was applied only during the (a) loading and (b) unloading segment of the loading-unloading cycle [9].

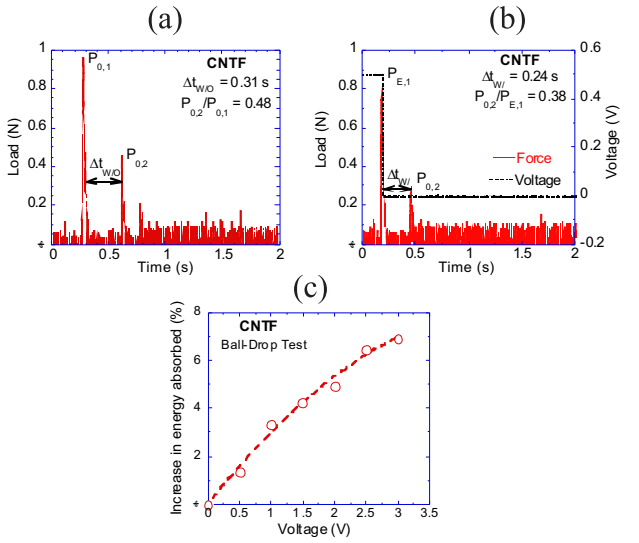

Figure 9: The load-time signal obtained using the ball-drop setup (see Fig. 4) for CNTF when electric field was (a) not applied throughout the test, and (b) applied only during the loading segment. (c) Effect of electric field on the total energy absorbed during the impact test (i.e., under dynamic loading). Reproduced from [9].

Nevertheless, a comparison of Fig. 7b and Fig. 9c shows that the increase in the energy absorption capacity of CNTF upon application of electric field was lost dramatically in the dynamic condition as compared to the quasi-static loading condition. Interestingly, this difference between the quasi-static and dynamic loadings is consistent with the understanding that the effect of electric field on the stress-strain behavior originates mainly due to the electric field induced polarization of CNT rings which does not occur instantaneously (e.g., see Fig. 5b and related discussion in Section 3.1). Therefore, while the CNT rings get sufficient time to polarize and depolarize upon "switching on" and "switching off" of the electric field, respectively, during quasi-static loading, they do not get enough time to depolarize under dynamic loading condition. Due to retention of the strength by CNTF during unloading segment (i.e., upon switching off the electric field), the sudden drop in the value of stress at the onset of the unloading segment (which is predominant during quasi-static loading – see Fig. 7a) was not observed during dynamic loading condition, leading to only a small increase in the hysteresis loop (and hence energy absorption) as compared to that under quasi-static loading.

3.4 Creep

Creep behavior of CNTF was studied in ambient condition by applying a constant nominal compressive stress and measuring the accumulated strain as function of time. As shown in Fig. 10a, the creep curves of CNTF samples show the standard primary and secondary (or steady state) stages of creep. Furthermore, application of an electric field increased the creep resistance of CNTF, resulting in a decrease in overall creep strain as well as the strain rate in the secondary stage (i.e., steady state strain rate). A standard creep equation, known as Garofalo equation, that represents total creep strain as sum of an exponentially decaying primary creep term and a linearly varying steady state creep term was used to fit the creep curves for all tests performed in this study. Fig. 10a reveals that the curve fitting using this equation was reasonably good. Various creep parameters, such as steady state creep (c), total primary creep strain (b), etc., were calculated from such a curve fitting exercise.

Fig. 10b shows the variation of the calculated steady state strain rate (c) as function of the applied stress for tests performed with or without application of an electric field. Interestingly, Fig. 10b shows that the steady state creep rate varied with stress as a power-law, with the exponent increasing upon application of an electric field. This is interesting as it shows that at higher stresses, the strengthening effect of electric field may become negligible or even reverse into weakening effect. However, we did not perform experiments at such higher stresses to validate the above inference in this study.

One of the striking features of the creep of CNTF in compression is that its behavior is like that of a crystalline material at high temperature (i.e., observation of distinct primary and steady state creep). However, CNTF neither have vacancies nor dislocations, which are often employed to explain such behavior in crystalline materials. Hence, a different set of softening and hardening mechanisms should be active in these sample

responsible for observation of strengthening (at reducing rate) during primary creep and a balanced strengthening and softening rates during the steady state. It can be postulated that as CNTF sample is compressed, the existing nodes break (or slide) and new nodes form as more CNT strands come closer to each other. Since compression is associated with densification (by bringing CNT strands closer), compression creep will lead to formation of more nodes than their breaking. This will strengthen CNTF, thereby hardening of the structure. However, at the same time, the CNT strands may also rotate to relax the stress applied from the adjacent CNT strands, as the nodes are not strictly rigid against rotation. In addition, the load bearing capacity of CNT strands upon buckling gets minimized. This has been revealed from observation of confinement of progression of buckling of CNT strands – and hence overall deformation – in the region wherein CNT strands have which been buckled before the buckling propagates to the neighboring region [8]. These two processes of rotating and buckling soften CNTF. It is reasonable to assume that the rate of softening will increase with increase in strain. Hence, the structure becomes stronger with strain at a reducing rate in the primary, finally establishing a balance between strengthening and softening in the secondary stage, thus attaining the classical steady state.

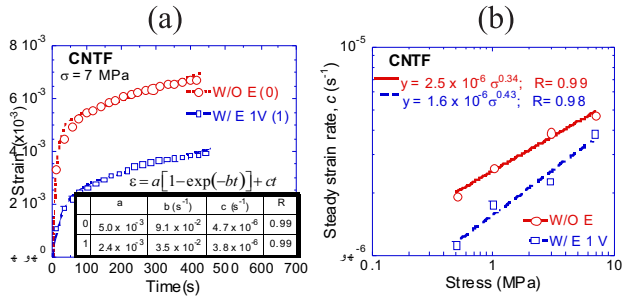

Figure 10: Effect of electric field on creep: Variation of (a) creep strain as function of time, and (b) steady state strain rate as function of stress. In (a), curves represent the best curve-fits obtained using a simple primary-cum-secondary stage creep equation (i.e., Garofalo equation). The equation is given above the table at the bottom of the graph, whereas the table gives the values of various parameters of this equation as obtained from curve fitting. W/O E and W/E 1V stand for without electric field and with an electric potential of 1 V (which translates into an electric field of ~1 kV/m), respectively. Reproduced from [14].

3.5 Stress Relaxation

As shown in Fig. 10, creep occurs in CNTF samples and hence it is expected that stress relaxation, another time dependent mechanical behavior, may also be important in these samples. Hence, stress relaxation was studied by loading CNTF under compression at a fixed nominal strain and then measuring the nominal stress required to maintain the same compressive strain. As shown in Fig. 11a, CNTF indeed show significant stress relaxation, wherein the overall stress relaxation decreased with an increase in the pre-strain. This can be attributed to the fact that an increase in the pre-strain will densify the sample, thereby increasing the CNT-CNT contact area and hence the friction opposing any rearrangement. However, Fig. 11a also shows that the stress relaxation increased with the application of an electric field. This can be explained as follows: Electric field increases the "effective" height of CNTF samples and hence the effective compressive strain, which leads to an increased driving force for stress relaxation. In addition, the Coulombic repulsion between the adjacent CNT strands aids to sliding and rotating of CNT strands and breaking of nodes formed at intersection of CNT strands (see Fig. 1), which would then enhance the stress relaxation process.

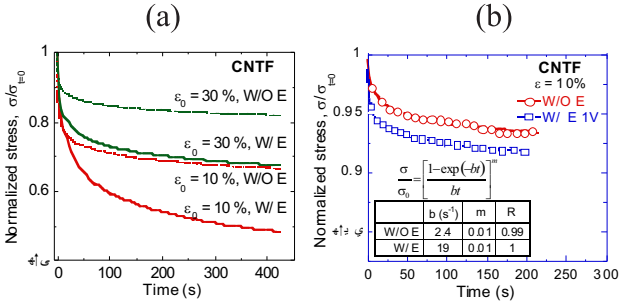

Figure 11: Effect of electric field on stress relaxation: (a) Variation of normalized stress, defined as the stress at any instant divided by the stress at the beginning of the stress relaxation, as function of time, and (b) curve fits using the expression derived for the stress

relaxation using the Garofalo creep equation shown in Fig. 10a. In (b), the equation is given above the table at left-bottom, whereas the table gives the values of various parameters of this equation as obtained from curve fitting. W/O E and W/E 1V stand for without electric field and with an electric potential of 1 V (which translates into an electric field of ~1 kV/m), respectively. Reproduced from [17].

Since creep and the stress relaxation has the origin in the same viscous properties of CNTF, it is imperative to derive expression for the stress relaxation from the creep expression used in Fig. 10a (i.e., Garofalo equation). An attempt was made for the same and a simple equation with exponential-cum-power law dependence for the stress on time was derived (see legend of Fig. 11b). The curve fits using this derived expression are shown in Fig. 11b, which confirms the efficacy of the derived expression in capturing the stress relaxation in CNTF. Further, this aids to the physical meaning of different terms of these empirical expressions. It further confirms the same origin for stress relaxation and creep behavior – or in general the time dependent mechanical behavior – in CNTF.

4 Conclusions

- Electric field induces very large actuation in CNTF. There is a little degradation in actuation due to the repeated usage.
- Electric field enhances short term strengthening of CNTF, which is repeatable. Electric field actuation may be further enhanced if CNT foam is compressed to small pre-strain
- Electric field dramatically increases energy absorption capability of CNT foams at low strain rates; however, the relative advantage decreases with strain rate
- Electric field makes CNTF more creep resistant.
- Electric field enhances the stress relaxation in CNTF.

Acknowledgement : This work was financial supported by Council of Scientific and Industrial Research (CSIR), India. The help of Professor Abha Misra with CNT samples and Drs. Piyush Jagtap, Prarthana Gowda, and Sivakumar Reddy, and Messrs. Bikramjit Das, Pravin Kavale and Amit Kumar with experiments is greatly appreciated.

References:

1. **Cantalini, C.; Valentini, L.; Armentano I.; Kenny, J. M.; Lozzi, L.; Santucci, S.** (2004) Carbon nanotubes as new materials for gas sensing applications, *J. Euro. Cer. Soc.* Vol. 24, pp. 1405

2. **Misra, A.** (2009) Carbon nanotubes and graphene based chemical sensors, *Current Science* Vol. 107, pp. 419

3. **Harris, P.J.F.** (2009) Carbon nanotube science: Synthesis, properties and applications, Cambridge University Press, Cambridge UK

4. **Misra, A.; Greer, J. R.; Daraio, C**. (2008) Strain rate effects in the mechanical response of polymer anchored carbon nanotube foams, *Adv. Mater.* Vol. 20, pp. 1.

5. **Jagtap, P.; Gowda, P.; Das, B; Kumar, P.** (2013) Effect of electro-mechanical coupling on actuation behavior of a carbon nanotube cellular structure, *Carbon* Vol. 60, pp. 169.

6. **Misra, A.; Kumar, P; Raney, J.R.; Singhal, A.; Lattanzi, L; Daraio, C.** (2014) Effect of fluid medium on mechanical behavior of carbon nanotube foam, *Appl. Phys. Lett.* Vol. 104, pp. 221910.

7. **Gowda, P.; Kumar, P; Tripathi, R; Misra, A.** (2014) Electric field induced ultra-high actuation in a bulk carbon nanotube structure, *Carbon* Vol. 67, pp. 546.

8. **Cao, A.; Dickrell, P.L.; Sawyer, W.G.; Nejhad, N.M.G.; Ajayan, P.M.** (2005) Supercompressible foam like carbon nanotubes, *Science* Vol. 310, pp. 1307.

9. **Jagtap, P.; Reddy, S. K.; Sharma, D.; Kumar, P.** (2015) Tailoring energy absorption capacity of CNT forests through application of electric field, *Carbon* Vol. 95, pp. 126.

10. **Shastry, V.V.; Ramamurty, U.; Misra, A.** (2012) Thermo-mechanical stability of a cellular assembly of carbon nanotubes in air, *Carbon* Vol. 50, pp. 4373.

11. **Guo, Y.; Guo, W.** (2003) Mechanical and electrostatic properties of carbon nanotubes under tensile loading and electric field, *J. Phys. D Appl. Phys.* Vol. 36, pp. 805.

12. **Baughman, R.H.; Cui, C.; Zakhidov, A.A.; Iqbal, Z.; Barisci, J.N.; Spinks, G.M.; Wallace, G.G; Mazzoldi, A.; De Rossi, D.; Rinzler, A.G.; Jaschinski, O; Roth, S.; Kertesz, M.** (1999) Carbon nanotubes actuators, *Science* Vol. 284, pp. 1340.

13. **Tang, C.; Guo W.; Guo, Y.** (2006) Electrostrictive effect on electronic structures of carbon nanotubes, *Appl. Phys. Lett.* Vol. 88, pp. 243112.

14. **Jagtap, P.; Kumar, A.; Kumar, P.** (2016) Effect of electric field on creep and stress-relaxation behavior of carbon nanotube forests, *RSC Adv.* Vol. 6, pp. 67685.

15. **Jagtap, P.; Kumar, P.** (2014) Evaluating shock absorption behavior of small-sized systems under programmable electric field, *Rev. Scientific Inst.* Vol. 85, pp. 113903.

16. **Collins, P.G.; Arnold, M.S.; Avouris, P.** (2001) Engineering carbon nanotubes and nanotube circuits using electrical breakdown, *Science* Vol. 292, pp. 706.

17. **Misra, A; Kumar, P.** (2014) Tailoring viscoelastic response of carbon nanotubes cellular structure using electric field, *Nanoscale* Vol. 6, pp. 13668.

Annals of the Indian National Academy of Engineering
Vol. XV, April 2018

Silicon Based Efficient Scalable Photodetector for Visible to Near Infrared Wavelengths

Samaresh Das[1] **and Veerendra Dhyani**[1]

Abstract : This paper summarizes the investigation of semiconductor nanostructure based high efficient photodetector for Si photonics. Devices such as junctionless (JL) NW phototransistor, Si/MoS_2 heterojunction photodetector and Ge nanocrystals (NCs) based MOS-photodetector have been fabricated on Si substrate using highly scalable process. These photodetectors have shown improved responsivity in the visible to infrared wavelengths with fast transient response.

Keywords: Scalability, nanowire, Si-photonics, High speed photodetector.

1 Introduction

In the recent time silicon photonics is widely accepted as a key technology for the next-generation communications systems and data interconnects [1]. Over the past few decades the rapid advances in Si photonics have been driven due to need of higher functionality with excellent performance in integrated circuits [1, 2]. Compared to the other compound semiconductors (II-VI, III-V etc.) Si brings the advantages of high device density with low manufacturing costs [1-3]. One of the challenges in integration of optoelectronics and microelectronics is the lack of high efficient Si-compatible light emitters and detectors. To enhance the device performance, researchers have developed several photodetector and waveguide-based structure for high power and large bandwidth [1-3]. Unfortunately, most of these approaches are not compatible with small scale structures and thus not suitable for complex nanoscale electronic integration. At the same time, the developments of nano-materials such as nanowires (NWs), nanocrystals and two dimensional materials with precise control over the chemical compositions, morphologies, and sizes have enabled researchers to fabricate novel nanodevices. Lots of research is still going on the size and shape dependent electrical, optical and mechanical properties of these nanomaterials [2-5]. However, a large number of questions regarding the performance of nanostructure-based device and scalability in fabrication process need to be addressed. To address these questions some of the nanostructure based photodetectors well-suited on Si platform have been fabricated in this work. The photodetector characteristics of the Si and Ge nanostructure have been investigated over a visible to near infrared wavelengths range. Also the integration of MoS_2, one of the 2D transition metal dichalcogenides (TMDCs) on the Si substrate has been carried out using a scalable fabrication process for high speed photodetector [5]. The process used for the device fabrication is highly scalable and reproducible.

2 High sensitive Junctionless (JL) NW phototransistor

A highly sensitive junctionless (JL) phototransistor has been fabricated on the silicon-on-insulator (SOI) wafers with top silicon thickness of 10 nm [2]. The tri-gate silicon junctionless n-transistors with 1μm gate length were made by E-beam lithography and dry etching. The basic structure of a junctionless phototransistor consists of a uniformly doped nanowire wrapped by the gate material as shown in Fig. 1. The conduction of charge carriers between source and drain can be controlled by the gate similar to a conventional junction transistor.

[1]Centre for Applied Research in Electronics, Indian Institute of Technology Delhi, New Delhi-110016, India.

Therefore, junctionless phototransistor can be considered as resistors in which the carrier density is modulated by a gate. In junctionless phototransistors due to the work difference between gate and channel, carriers get depleted in the channel. Thus with a very small dimension (10 nm) and for a negative gate voltage the channel can be considered almost fully depleted, which shows very small current under a zero or negative gate voltage.

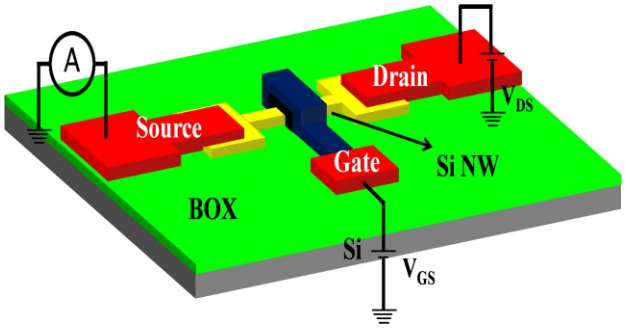

Fig.1. Schematic view of JL phototransistor

In presence of light electron-hole pairs are generated in the channel. The negatively charged electrons moves towards the drain contact due to applied source-drain bias, while holes are trapped inside the channel [2]. These trapped holes will decrease the barrier height at the source-channel interface, just like in conventional npn phototransistor [2]. Due to this lowering of barrier, holes are now allowed to diffuse into source region. At the same time more number of electrons now can easily pass through the channel from source to drain. As a result photocurrent in the circuit get enhanced. I-V charactristics of the JL phototransistor under constant drain-source bias of 0.30 V is presented in Fig.2 (a). A large enhancement in the photocurrent under the illumination of very low intensity demonstrates that high sensitivty of the fabricated devices. Responsivity of the NWs were also measured in the wavelength range 710 to 860 nm and it is observed that the responsivity and gain increases as the wavelength increases from 710 to 860 nm.

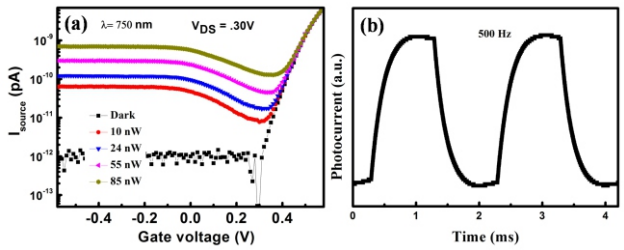

Fig. 2 (a) Photoresponse of the JL phototransistor at different gate bias and at 300 mV Drain bias, (b) Time response of the JL phototransistor under the illumination of modulated light source (at ~5pW and 500 Hz)

The dynamic response of the device has been measured using a modulated light source. This response is shown in the Fig. 2(b). The measured value of rise time and fall time are 300 µs and 480 µs, respectively. From the mesurments it is observed that a small change in the intensity (~5pW) of the light caused a large change in the current, which proves the outstanding photosensitity of the JL phototransistors. The internal gain (defined as *N(carrier)/(N(photon*))for these devices reaches up to more than 40 for a source to drain voltage of 200mV for 860 nm wavelength light.

2. High speed Si/MoS_2 heterojunction photodetector

Here, we report Si/MoS_2 (p-n) heterojunction based photodetector with a very simple and scalable fabrication process. To fabricate the heterojunction, chemical vapor deposition process is used for the growth of MoS_2thin film on Si substrate. Two step photo-lithography process has been used for the fabrication of Si/MoS_2 hetero-junction [5]. In the first photo-lithography step, squares of dimension 100 µm X 100 µm were opened in SiO_2, which define the Si/MoS_2 junction area. Afterwards, the metal contact (Cr/Au) has been pattern in the second lithography process. Fig.3 (a) shows a schematic representation of the device structure. A typical current-voltage (I-V) characteristic of the Si/MoS_2 heterojunction under the light and dark condition is depicted in Fig. 3(b). The asymmetry in the IV characteristics clearly indicates the

formation of very good p-n junction between n-type MoS_2 and p-type Si. During the measurement the p-type substrate was kept at ground and the bias voltage was given at the top MoS_2 contact and therefore a negative voltage at top contact makes the junction forward bias. These devices have shown quite low dark current of ~1.8 X 10^{-7} (at reverse bias of 3V), with an enhancement of ~ 127 times upon the illumination of 5 mW/cm^2(560 nm).

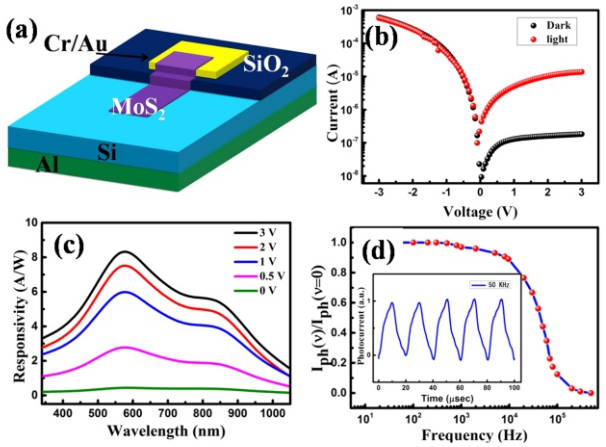

Fig. 3 (a) Schematic representation, (b) I-V characteristics , (c) spectra and (d) frequency response of Si/MoS_2 heterojunction (inset shows the time response of Si/MoS_2 heterojunction under 50 kHz modulation light) [5]

The photoresponse properties of the Si/MoS_2 heterojunction in the wavelength range 350 nm to 1050 nm were evaluated as shown in Fig. 3 (c). Spectral responsivity (wavelength dependent responsivity) of a photodetector is directly proportional to the internal gain, which shows efficiency of a detector to the optical signals. The devices exhibit a wide spectral response ranging from 450 nm-1000 nm. In case of Si/MoS_2 two prominent peaks centered around 580 nm and 860 nm were observed in spectral response for Si/MoS_2 heterojunction. The high responsivity at 580 nm is in accordance with the absorption of MoS_2 film in the visible region [5, 6]. Other peak at wavelength 860 nm corresponds to absorption of the Si substrate. For the wavelength 580 nm the measured value of responsivity is 8.50 A/W for MoS_2-Si photodetectorrespectively. The transient response of the devices has been measured under the modulated laser source (660 nm). The response has been extracted in terms of voltage across a parallel resistor connected to the photodetector. Further analysis to the measurement reveals a small τ_r of 10 μs, as well as a small τ_f of 19 μs. The values obtained here are remarkably high and much faster than any other reported MoS_2 -based PDs. Fig. 3(d) shows the relative change in the current ($I_{ph}(\upsilon)$) of the photocurrent as a function of frequency. The relative change (defined as $I_{ph(\upsilon)=} I_L - I_d$) of the photocurrent only decreases by 50 % at a high frequency of ≈ 40kHz, implying that the Si/MoS_2 based PDs can operate at much higher frequencies. The inset shows the time response of Si/MoS_2 heterojunction under 50 kHz modulations light.

3 Broadband high speed Porous Si/MoS_2 heterojunction photodetector

Motivated from the excellent performance of MoS_2 heterostructure with Si, photodetection properties of MoS_2 with Porous Si (PSi) have been explored. Fabricated PSi/MoS_2 heterojunction have shown much better characteristics compare to planar Si/MoS_2, as the responsivity of the heterojunction get improved in the infrared region. Fig. 4(a) shows the Atomic force microscopy (AFM) image of the MoS_2/PSi interface. Porous Si was made by electrochemical etching of c-Si (p-type), which results in textured surface with depth of 4-5 μm. On the top PSi MoS_2 has been deposited. Inset shows the SEM image of MoS_2 thin film. Afterwards, a 200 nm indium tin oxide (ITO) was deposited by RF sputtering using a metal shadow mask for transparent top electrode.

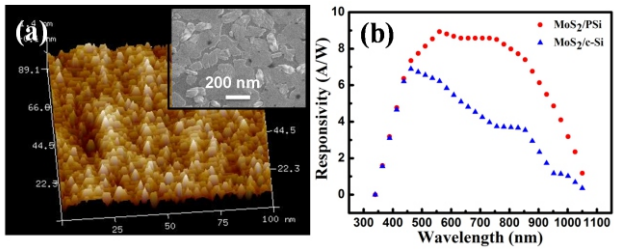

Fig. 4 (a) Atomic force microscopy image MoS_2/PSi interface (inset shows the SEM image of MoS_2 thin film) and (b) Responsivity MoS_2/Si heterojunction on the planar(c-Si) and porous (PSi)

The spectral response of the Si/MoS_2 heterojunctions were measured in the wavelength range 350 nm to 1050 nm. As shown in Fig. 4(b). In case of MoS_2/c-Si high responsivity is observed due to photoresponse of MoS_2 (in 400-600 nm) and Si (near to 800 nm). On introducing nanostructure at the MoS_2-Si interface in case of PSi quite large and a broader spectral response have been noted compared to planar Si substrate [7]. Maximum responsivity upto 9 A/W for the MoS_2/PSi device has been observed for 550 nm.

4 Oxide embedded Ge nanocrystals for optical sensors

A high speed two-terminal metal-oxide-semiconductor (MOS) photodetector has been fabricated, in which Ge-NCs embedded silicon oxide is capped between the metal and semiconductor. The distribution in the size of Ge-NCs was achieved by annealing the samples at temperature range of 800-950 °C. Fig. 5 (a) shows the Schematic diagram of the Ge NCs based MOS-photodetector. These Ge-NCs annealed at different temperature posses size dependent absorption, which led to the tunable spectral response. Ge and SiO_2 composite films (60 nm)was deposited by co-sputtering method on p-type Si wafers with target areal ratio of 1.5:10. Three different samples were annealed in inert environment (N_2) at temperature range 850–950 °C for the crystallization of Ge. For the fabrication of photodetector, a transparent top contact of size 1 mm^2 was made using 100 nm thick sputtered deposited ITO film.

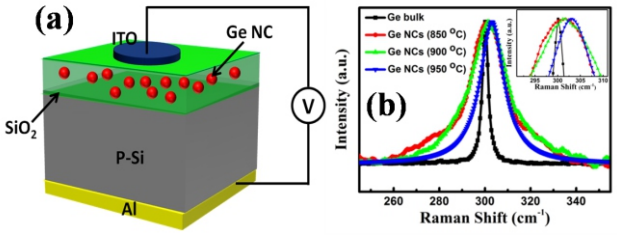

Fig. 5 (a) Schematic diagram of the Ge NCs based MOS-photodetector, (b) Raman spectra of Ge NCs (Inset shows the zoom view of peak shift)

Fig. 5 (b) shows Raman spectroscopy of post annealed samples to realize the crystallization of Ge nanocrystals. It is observed that the peak corresponding to Ge-Ge TO mode shifts towards higher wave number with increasing annealing temperature. The possible reason for this shifting is due to compressive stress arises during annealing. Also this shifting casts a signature of quantum confinement in Ge NCs. Further it can be observed that for lower annealing temperature (i.e. size of NCs) the peak in Raman spectra was observed for lower wave number. Higher temperature also favor to high crystallinity of Ge-NCs, as the FWHM of Raman peak for lower annealing temperate is quite large as compare to high temperature samples.

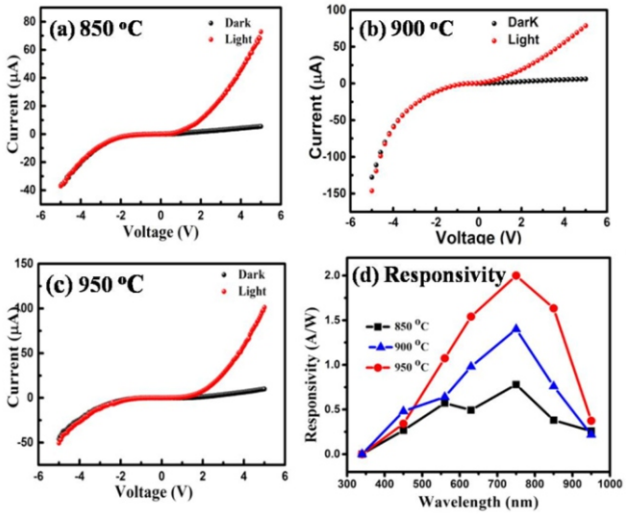

Fig.6 (a), (b) &(c)I-V characteristic (dark and light) and (d) Responsivity of the Ge NCs based photodetector annealed at different temperature

The dark-light current-voltage characteristics of the fabricated Ge NC devices under the normal incidence 5mW/cm^2 intensity are shown in figure. Fig. 6(a) shows that sample annealed at 850 °C posses small photoresponse as the change in photocurrent is not much significant compare to dark current. This indicates that at lower temperature thermal energy in not sufficient for the crystal formation during the annealing process and thus the optical absorption in SiO_2 matrix is poor due to lack of absorption of light in Ge NCs. Increasing the temperature caused the efficient crystallization of bigger Ge NCs in SiO_2 matrix. As a result of that a large absorption is expected in the Ge NCs, which results in huge change in the photocurrent as shown in Fig. 6 (b) and (c). The

spectral photoresponse at a particular reverse bias of 3 V for Ge QDs annealed at different temperatures is shown in Fig. 6(d). A broad response in the spectral range 300-1100 nm could be observed with a maximum responsivity of 1.1 A/W around 750 nm has been observed for Ge NCs formed at 950 °C. Change in responsivity has been observed with the annealing temperature, which is appearing due to the change in the size of the NCs with temperature. Previous studies have shown that electron-hole separation is less probable for smaller NCs due to stronger Coulomb attraction resulting in lower photocurrent and lower photoresponse [8]. With strong probability of charge separation the large size NCs possessed high absorption, resulting in the increased photocurrent.Fig.7 (a) Time response of Ge NCs based MOS-photodetector annealed at 950 °C and (b) Frequency dependence of normalized relative change in photocurrent.

Fig. 7 (a) shows the time response of the Ge NCs MOS photodetector (annealed at 950 °C) under the illumination of 10 kHz laser light). Very fast rise of 6 µsec and fall time of 8 µsec range has been observed. The measurements have been carried out with a modulation up to 80 kHz. The relative change in the current ($I_{ph}(\upsilon)$) of the photocurrent as a function of frequency in the range from 10 Hz to 80 kHz is depicted in Fig. 7 (b). The relative change (defined as $I_{ph}(\upsilon)= I_L - I_d$) of the photocurrent only decreases by 50 % at a high frequency of ≈ 30kHz, implying that the Ge-NCs based PDs can operate at much higher frequencies.

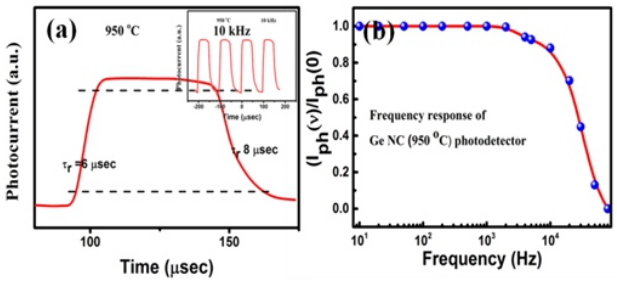

Fig.7 (a) Time response of Ge NCs based MOS-photodetector annealed at 950 °C and (b) Frequency dependence of normalized relative change in photocurrent.

Acknowledgement

The authors would like to thank Ministry of Electronics and Information Technology (MEITY) and Department of Science and Technology (DST) for their financial support. We are very grateful to the Nanoscale Research Facility (NRF), IIT Delhi for providing assistance in the characterization facilities

References:

1. **Thomson David et al.** (2016) Roadmap on silicon photonics, *J. Opt.,* 18, 073003.

2. **Das S.; Dhyani V.; Georgiev Y. M.; and Williams D. A.** (2016) High sensitivity silicon single nanowire junctionless phototransistor, *Appl. Phys. Lett.* 108, 063113.

3. **Jamois C. et al.** (2003), Silicon-based two-dimensional photonic crystal waveguides, *Photonics Nanostructures - Fundam. Appl.*, 1, 1–13,

4. **Gasparyan F. et al.** (2016), Double-gated Si NW FET sensors: Low-frequency noise and photoelectric properties, *J. Appl. Phys*., 120, 064902,

5. **Dhyani V.; Das S.** (2017) High-Speed Scalable Silicon-MoS_2 P-N Heterojunction Photodetectors, *Scientific Reports*. 44243.

6. **Mukherjee, S et al.** (2016) Novel Colloidal MoS2 Quantum Dot Heterojunctions on Silicon Platforms for Multifunctional Optoelectronic Devices. *Sci. Reports* 29016.

7. **Dhyani, V. et al.** (2017) High performance broadband photodetector based on MoS_2/porous silicon heterojunction, *Appl. Phys. Lett.* 111, 191107.

8. **Kim, S. et al.** (2009) Size-dependent photocurrent of photodetectors with silicon nanocrystals, *Applied Physics Letters*, 94, 25-28.

Annals of the Indian National Academy of Engineering
Vol. XV, April 2018

Extraction Efficiency Based Approach for Health Monitoring of Aluminum Electrolytic Capacitors in Single Phase Grid-Feeding SolarInverters

Sandeep Anand[1]

Presentation is based on the work published as:Nikunj Agarwal, Abhinav Arya, Md Waseem Ahmad, and Sandeep Anand, "Lifetime Monitoring of Electrolytic Capacitor to Maximize Earnings from Grid Feeding PV System" IEEE Trans. Ind. Electron., vol. 63, no. 11, pp. 7049-7058, Nov. 2016

Abstract : Photovoltaic (PV) panels are usually connected to single phase grid using the single stage, grid feeding inverters. These inverters offer less operational life as compared to the PV panels due to the use of Aluminum Electrolytic Capacitor (AEC). With time, AEC degrades, resulting in an increase in ripple voltage on PV panel. This reduces the power extraction efficiency (PEE) of the system, thereby a loss of revenue.This work proposes a technique to determine the health of capacitor and indicate its replacement.Time of replacement is determined based on the status of PEE so as to maximize profit from the grid connected system. The online method to evaluate PEE is suggested. A mathematical model relating PEE to the health of AEC is developed. Detailed simulations are carried out in MATLAB-Simulink. The effectiveness of the technique is verified experimentally by implementing it in a scaled down solar PV inverter prototype.

Keywords:Electrolytic capacitor, online monitoring, photovoltaic (PV) inverter, power extraction efficiency.

1 Introduction

Growing concerns about climate change and global warming resulting from carbon emissions have pushed for more use of renewable sources such as solar photovoltaic (PV), wind, solar thermal etc. The estimated cumulative potential of different renewable energy sources in India is 900 GW, among which potential of solar PV stands at 750 GW. As of August2017, total installed PV capacity has surpassed 14.5 GW and by 2022, the target is to increase the total installed capacity to 175 GW. Currently, 96.4 % of solar PV systems are grid connectedas per the data of MNRE, Govt of India (2017).A grid connected solar PV system consists of solar panels, power electronic converters (PEC) and other balance of systemcomponent. Apartfrom focus on developing high efficient PEC, increased attention is being paid on the field performance of these converters, including their reliability.

An All-India Survey of Photovoltaic Module Reliability carried out jointly by NCPRE (IIT Bombay) and NISE (Haryana) in 2013, reported by Dubey, Chattopadhyay,Kuthanazhi, John, Solanki, Kottantharayil, Arora, Narasimhan,Kuber, Vasi, and Kumar (2013),suggests that PV power output decrease over operating years from its rated output with rates which vary from less than 0.6%/year to more than 4%/year. This reduction in power is mainly due to degradation of solar PV panels and solar inverters. No documented reliability data of PEC in PV system is available with the particular context of India. The reliability data of the performance of PV system collected over by different centers across the world gives an idea of the reliability problem faced by PV installation in India. Florida Solar Energy Center analyzed 103 gridconnectedPV systems which indicates that inverters are the most vulnerable componentsin solar PV systems, see Dhere (2005). It is recorded that out of 213 failure events, 139 failure(65%) events were the result of malfunctioning of inverters.Similarly, an assessment of 5 MW plant at Springerville Crystalline Silicon Systems during 5 year of operation published by Moore and Post(2008) suggests that 37% of unscheduled

[1]Department of Electrical Engineering, Indian Institute of Technology, Kanpur 208016

maintenance hasto be carried out because of the failure of PV inverter. These unscheduled breakdowns of PEC would result in loss of generation from renewable power plant as the plant cannot be operated till repair of faulty components is complete. Furthermore, these unscheduled repair cost may be sometimes considerably high as it is subjected to the availability of replacement of faulty components at the site. Therefore, unscheduled shutdown and outrage need to be avoided to improve performance and availability of renewable sources based power processing system.

Industrial surveys have revealed that Aluminum electrolytic capacitor (AEC) is among the most fragile component in the PEC. With aging, due to evaporation of electrolyte, equivalent series resistance (ESR) offered by the AEC increases and capacitance decreases. This leads to an increase in voltage ripple across solar PV terminals, which reduces the average power extracted from solar PV due to oscillations around maximum power point (MPP). Capacitor manufacturers suggest replacement of AECs when the ESR or capacitance reaches a critical value.

Review of the various technique for health monitoring of AECs is available in Soliman, Wang and Blaabjerg (2016). Most of the previously suggested techniques in publications and in patents are based on the estimation of ESR or capacitance of AEC to monitor its health. The criteria for replacement of capacitor based on ESR or capacitor may not optimize earnings from the grid connected PV system. An early replacement of capacitor would add to the cost of the system and thereby decrease the earnings. On the other hand late replacement would adversely affect PEE and thereby reducing the power output and revenue generated by the system. This work suggests a novel method to determine the time for replacement of capacitor based on power extraction efficiency (PEE). The proposed approach for replacement of capacitor ensures maximum profit from the grid feeding system.

The paper is organized as follows. In section 2, proposed technique and its mathematical modeling is presented. Detailed simulation and experimental results are presented in section 3. Section 4 concludes the paper.

2 Proposed Approach

Fig. 1 shows a single phase full bridge solar PV inverter along with its controller. Due to single phase inverter, dc-link voltage oscillates at twice the grid frequency. This leads to oscillations of the same frequency in the power supplied by solar PV panels. As the health of the dc-link capacitor deteriorates, its capacitance value decreases, causing an increase in the voltage oscillations, thereby increasing the oscillations in PV power. Due to increased oscillations in PV power around its maximum power point (MPP), the average output power reduces. This leads to the reduction in PEE. The proposed method is based on the determination of PEE and indicating capacitor replacement based on a critical value of PEE. The subsequent subsection discusses the method to calculate PEE and the criteria for replacement of capacitor. Furthermore, mathematical modeling of the technique is discussed at the end of the section.

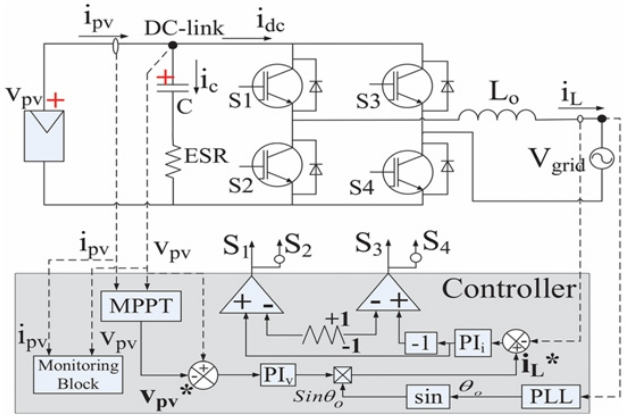

Figure 1: Single Phase grid-feeding PV system

2.1 Approach for PEE calculation

At steady state, PV voltage (v_{pv}) and PV current (i_{pv}) are sampled using analog-to-digital converter (ADC). The sampled values of v_{pv} are multiplied to the correspondingly sampled i_{pv}values to get instantaneous PV power ($P_{pv}[k]$) The number of samples (N) considered for computation is integer multiple of $2\pi/T_s\omega_0$, where T_s is the sampling period and ω_0

is the fundamental grid frequency in rad/s. This ensures that complete power cycle is covered while calculating the extraction efficiency. The average PV power P_{pv} is calculated as :

$$P_{av} = \sum_{k=3}^{N} P_{pv}[k] / N \quad (1)$$

Direct measurement of maximum power would be erroneous due to the presence of noise. Therefore, a modified approach to calculate $P_{\max}$ is suggested based on the evaluation of root mean square (RMS) power and ripple power, as follows,

$$P_{rms}^2 = \sum_{i=1}^{N} \left(p_{pv}[k]\right)^2 / N \quad (2)$$

$$P_{ripp,rms} = \sqrt{P_{rms}^2 - P_{av}^2} \quad (3)$$

Using the above expression, maximum power is evaluated as,

$$P_{max} = \sqrt{2} \times P_{ripp,rms} + P_{av} \quad (4)$$

PEE is calculated as the ratio of average power to the maximum power.

$$\text{PEE} = P_{av} / P_{max} \quad (5)$$

The flowchart of the proposed technique is shown in Fig. 2.

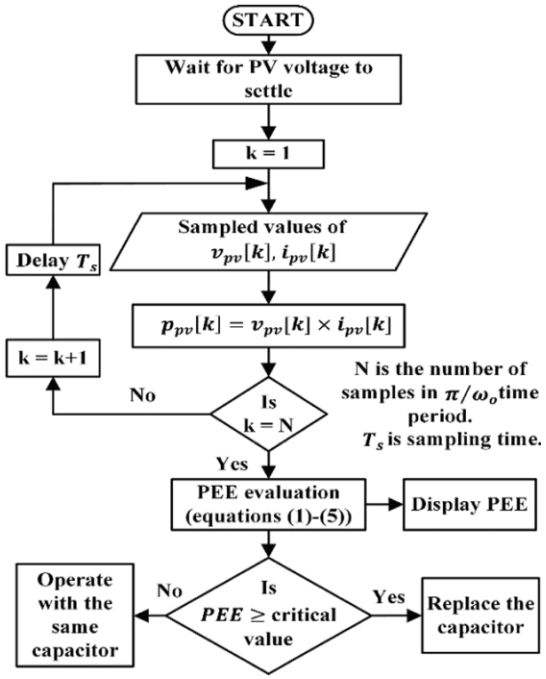

Figure 2: Flowchart of proposed health monitoring technique

2.2 Criteria for replacement of capacitor

As a result of degradation of AEC, ripple in dc-link voltage increases which decrease the PV PEE. This negatively impactsthe earnings from the PV system. Frequent replacement of capacitor would increase the revenue but would add to the system cost. Therefore a criteria based on PEE for replacing the capacitor is required.

An analytical expression of PEE(t) with the change in AEC parameter is required in the first step. This expression could be obtained using simulation studies with a suitable capacitor degradation model or experimentation based on the accelerated aging of the capacitor. Once PEE(t), it is compared with the critical value of PEE. If the calculated PPE is less than PEE_{cr}, incremental revenue (Δr) per hour is calculated using the following equation,

$$\Delta r = (\text{PEE}(t) \times P_{PV\_max} \times \eta_{MPPT} \times \eta_{conv}) \times \text{FIT} \quad (6)$$

where,$P_{pv,max}$ is the maximum possible PV power in t^{th} hour (in kW),η_{MPPT} is the extraction efficiency of MPPT algorithm,η_{con} is the power conversion efficiency of the inverter and FIT is feed-in tariff (in $ /kWh). The incremental revenue obtained from (6) is added to the previously calculated revenue. This process of updating the revenue is repeated after every 1 hour till PEE reaches the value of PEE_{cr}.Once this value is reached, capacitor is replaced. With the new capacitor, the process of revenue calculation is repeated to determine the instant of capacitor replacement. This process of repeating the calculation is carried out for 20 years. Profit generated by this system in its lifetime (20 years) is calculated as,

Profit = Revenue (in 20 years) - Gross System Cost (7)

where, the gross system cost (GSC) is calculated by

GSC = PV system cost + i × capacitor replacement cost (8)

where*i*is the number of replaced electrolytic capacitors in 20 years. The replacement cost of the capacitor includes the cost of a new capacitor, labor cost, and revenue loss due to the shutdown of the inverter. The above process of profit calculation is repeated for different PEE_{cr}. Based

on the plot of profit from the system and $PPE_{cr,}$ an optimal value of PEE_{cr} is obtained to maximize profit from the system.Simulation results for a test system to obtain the plot of profit with PEE_{cr} are presented in Section 3.2.

2.3Mathematical expression for PEE

As stated already that PEE is evaluated as a ratio of average and maximum power available from PV source. Since the ripple in PV voltage and current are dependent on the status of capacitor, an analytical model is developed for calculation of ripple in PV system. Based on the derived expression, PEE is evaluated.

Using double Fourier series analysis (DFSA), dc-link current,*dci* is given by,

$$i_{dc}(\omega_o t,\omega_c t) = |\overrightarrow{C_{00}}|/2 + \sum_{\substack{m=0\\(m=n)\neq 0}}^{\infty}\sum_{n=-\infty}^{\infty}[|\overrightarrow{C_{mn}}|\sin(m\omega_c t + n\omega_o t + \angle\overrightarrow{C_{mn}})] \quad (9)$$

where $|C_{mn}|$ and $C_{\blacksquare}$ are the magnitude and the phase of the $(m\omega_c t+n\omega_0 t)$ frequency component in the dc-link current, which are given by,

$$\overrightarrow{C_{mn}} = \frac{1}{2\pi^2}\int_{-\pi}^{\pi}\int_{-\pi}^{\pi} i_{dc}(t)e^{j(m\omega_c+n\omega_o)t}\,\mathrm{d}(\omega_c t)\mathrm{d}(\omega_o t) \quad (10)$$

The high frequency dc-link current component$(m\omega_c t+n\omega_0 t)$ is absorbed by the AEC as it offers less impedance when compared to PV panel. The voltage ripple due to this frequency component is given,

$$\overrightarrow{V_{mn}} = \overrightarrow{C_{mn}}\{ESR + \frac{1}{j(m\omega_c + n\omega_o)C}\} \quad (11)$$

Adding all these harmonic components would contribute to the total ripple voltage across the PV panel and is given by

$$\tilde{v}_{pv} = \sum_{\substack{m=0\\(m=n)\neq 0}}^{\infty}\sum_{n=-\infty}^{\infty}|\overrightarrow{V_{mn}}|\sin(m\omega_c t + n\omega_o t + \angle\overrightarrow{V_{mn}}) \quad (12)$$

The instantaneous PV current is given by Femia, Petrone, Spagnuolo, and Vitelli,(2017).

$$i_{pv} = I_{MPP} + (\partial I_{MPP}/\partial V_{MPP})(v_{pv} - V_{MPP}) + (1/2)(\partial^2 I_{MPP}/\partial V_{MPP}^2)(v_{pv} - V_{MPP})^2 \quad (13)$$

Expressing the above equation as,

$$i_{pv} = A.v_{pv}^2 + B.v_{pv} + D \quad (14)$$

where, constants

$$A = \frac{1}{2}\frac{\partial^2 I_{MPP}}{\partial V_{MPP}^2},\ B = \frac{\partial I_{MPP}}{\partial V_{MPP}} - V_{MPP}\frac{\partial^2 I_{MPP}}{\partial V_{MPP}^2}$$

$$\text{and, } D = \frac{1}{2}\frac{\partial^2 I_{MPP}}{\partial V_{MPP}^2}V_{MPP}^2 - V_{MPP}\frac{\partial I_{MPP}}{\partial V_{MPP}} + I_{MPP}$$

Invoking $v_{pv} = V_{MPP} + \tilde{v}_{pv}$ results in,

$$i_{pv} = A(V_{MPP} + \tilde{v}_{pv})^2 + B(V_{MPP} + \tilde{v}_{pv}) + D \quad (15)$$

Using (13) and $v_{pv} = V_{MPP} + \tilde{v}_{pv}$ to calculate instantaneous PV power would result in,

$$p_{pv}(t) = AV_{MPP}^3 + BV_{MPP}^2 + DV_{MPP} + A(\tilde{v}_{pv}^3 + 3V_{MPP}\tilde{v}_{pv}^2 + 3V_{MPP}^2\tilde{v}_{pv}) + B(\tilde{v}_{pv}^2 + 2V_{MPP}\tilde{v}_{pv}) + D\tilde{v}_{pv}) \quad (16)$$

Substituting the value of $v_{\blacksquare}$ from (12) in (16) to evaluate average power over second harmonic time period using

$$P_{av} = \frac{1}{(\pi/\omega_o)}\int_t^{t+(\pi/\omega_o)} p_{pv}(t)dt \quad (17)$$

This would result in,

$$P_{av} = P_{MPP} + \frac{1}{2}(3V_{MPP}A + B)\sum_{\substack{m=0\\(m=n)\neq 0}}^{\infty}\sum_{n=-\infty}^{\infty}|\overrightarrow{V_{mn}}|^2 \quad (18)$$

Evaluating PEE result in,

$$\text{PEE} = 1 + \frac{3V_{MPP}A + B}{2P_{MPP}}\sum_{m=0}^{\infty}\sum_{n=-\infty}^{\infty}|\overrightarrow{V_{mn}}|^2 \quad (19)$$

where, $P_{MPP} = V_{MPP}I_{MPP}$

Substituting the value of $|V_{mn}|$ from (11) in the above expression would give,

$$\text{PEE} = 1 + \frac{3V_{MPP}A + B}{2P_{MPP}}.\sum_{\substack{m=0\\(m=n)\neq 0}}^{\infty}\sum_{n=-\infty}^{\infty}|\overrightarrow{C_{mn}}|^2\left(\text{ESR}^2 + \left(\frac{1}{(m\omega_c + n\omega_o)C}\right)^2\right) \quad (20)$$

This mathematical model of PEE would be compared with the simulation result in the next section to verify its validity.

3. Results and Discussion

3.1 Simulation Results

A closed loop controller with outer dc-link voltage loop and inner grid current for single

phase grid feeding inverter is realized in Matlab / Simulink environment. The dc-link voltage reference is generated using Perturb and Observe (P&O) MPPT technique. The dc-link capacitor is selected such that the low-frequency ripple is below 10% at full power rating, for a new capacitor.To simulate the aging of the capacitor, ESR and capacitance value at any time t is calculated using the method outlined in Abdennadher, Venet, Rojat, Rétif, and Rosset,(2010). PEE values obtained from the simulation and from the mathematical model (discussed in section 2.2) are tabulated in Table 1. It is observed that with degradation of AEC, PEE decrease. Also, extraction efficiency obtained from simulation is lower when compared to that of the mathematical model. This is mainly because the mathematical model does not consider non-idealities in the circuitelement (such as switch resistance, diode resistance, inductor resistance etc.) and uses an approximate PV model. Therefore, prediction using simulation is more accurate when compared to that of the mathematical model. Using simulation data, an expression of PEE (t) is obtained by curve fitting the data points as,

$$\mathrm{PEE}(t) = 0.9902 - k_1(e^{t/k_2} - 1) - k_3 t \qquad (21)$$

where, k_1=0.002461, k_2=2.55 10^4, k_3= 9.902 $10^{-8.}$

Table 1: Simulation results @ 25^{0}C operating temperature and solar irradiance of 1000 W/m^2

Time (hours)	ESR (?)	C (μF)	%PEE (by Simulation)	%PEE (by Mathematical model)
0	0.210	330	99.02	99.11
5000	0.2356	315.5	98.93	99.04
10000	0.2684	301	98.93	98.94
15000	0.3118	287	98.7	98.84
20000	0.3721	272	98.55	98.71
25000	0.4609	258	98.39	98.57
30000	0.6057	243	98.2	98.39
35000	0.8832	229.5	97.97	98.18
40000	1.63	215	97.71	97.86

3.2 Determination for criteria for the replacement of capacitor

Details of the PV system considered for this analysis are as follows.

1) System power rating is 2 kW.
2) Cost of PV system is $2000($1 per watt).
3) Replacement cost of capacitor is $20.
4) FIT is $0.15 per kWh.
5) Extraction efficiency of MPPT algortithm $\eta_{MPPT}$is 0.95
6) Power conversion efficiency of inverter η_{conv} = 0.98.

Based on the above system description, profit from the system over 20 year period is calculated using the equation and method outlined in Section 2. Fig. 3 shows plot between profit and various values of PEE_{cr}. The profit from PVsystem is low if the capacitor is replaced at higher PVPEE_{cr}. This is because of frequent replacement of capacitor that would result in higher gross system cost(GSC). Though GSC would decrease for the lower value of PEE_{cr}, but profit would also decrease due to lower PEE_{cr}. The replacement of the capacitor at certain optimal PEE_{cr} results in the maximum profit generation from the system. For PEE_{cr}equal to 98.4%, the profit generated from this PV system is expected to be maximum.

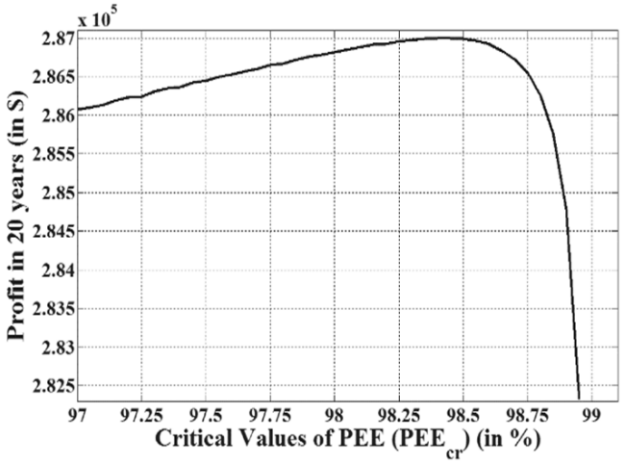

Figure 3: Variation in Profit for different values of PEE_{cr}

3.3 Experimental Verification

In order to validate the proposed technique, a scaled-down laboratory prototype of single phase grid connected PV system, as shown in Fig.1, is developed for experimentation. Specifications of solar PV is : Open-circuit voltage is 100 V, Short-circuit current is 2.2 A., PV current at MPP is 1.7 A, PV voltage at MPP is 80 V. The

experimentation is performed with two different values of dc-link capacitors (C_1=820 µF, ESR=0.062 Ω and C_2=410 µF, ESR=0.134 Ω).

To emulate the PV characteristic, Agilent technologies made E4360 solar emulators is used. The proposed technique is implemented in TI made TMS320F2808 digital signalprocessor (DSP) which besides this, also performs MPPT function and control of the converter. LEM-LA-25P current sensors are used to measure the PV current and inductorcurrent.For control of converter, feedback signals (PV voltage, grid voltage, and current) are attenuated using OP-AMP based differential amplifier circuits. These attenuated signals are fed to analog-to-digital converter (ADC) of theDSP. The complete experimental setup is shown in Fig. 4. The waveform of inverter PWM voltage, grid voltage, and grid current are shown in Fig. 5.

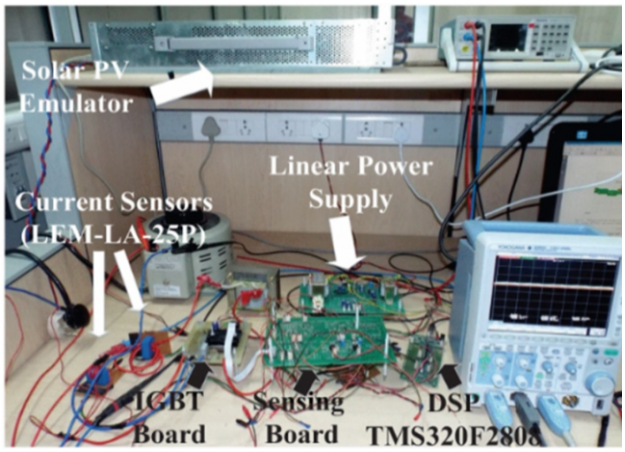

Figure 4: Experimental setup

The P&O MPPT algorithm generates the PV reference voltage to be tracked. Fig. 6 shows the ripple in dc-link voltage and current for capacitor C_1 connected to the dc-link. The voltage and current ripples are about 4.53% and 8.23% respectively. The technique for PEE estimation is implemented experimentally with both set of capacitor and the results are tabulated in Table 2. As expected maximum powerremains almost constant but with the reduction in capacitance value average value of power decreases. Experimentally, the extraction efficiency deteriorates from 95.53% to 93.126%. The experimental and simulated values are within 1% of each other. This confirms the operation of the PEE estimation method.

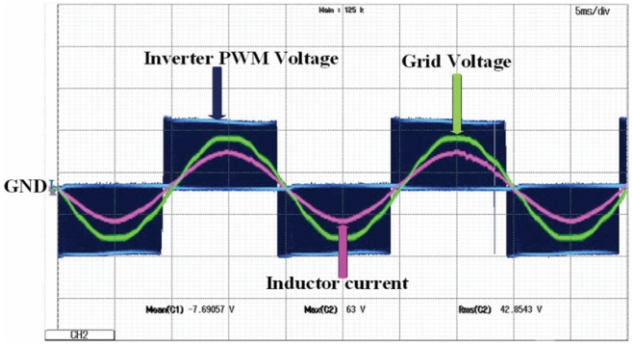

Figure 5 : Waveforms of inverter PWM voltage (50 V/div), grid voltage (50 V/div) and inductor current (5 A/div), time:5 ms/div.

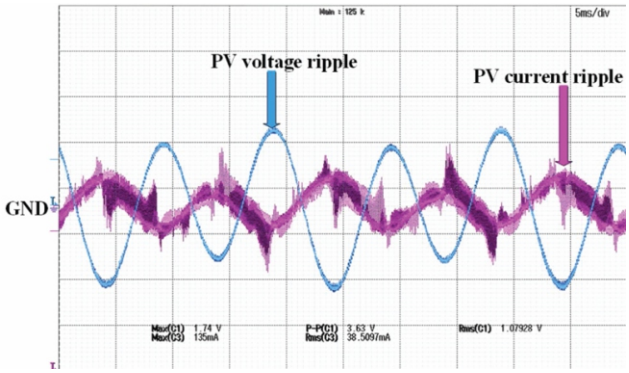

Figure 6 : Waveforms of PV voltage ripple (1 V/div) and current ripple (100 mA/div) for C_1:820µF, ESR=0.062 Ω, time:5ms/div (observed by keeping oscilloscope in ac mode).

Table 2: Experimental and Simulation Results

Time (hours)	C_1=820 µF ESR=0.062 ?		C_2=410 µF ESR=0.134 ?	
P_{avg}	0129.9	130.8	126 W	127.9 W
P_{max}	135.97	135.9	135.3 W	135.9 W
PEE	95.53 %	96.24%	93.126%	94.11%

4 Conclusion

With aging, AEC degrades, resulting in an increase in ripple voltage on PV panel. This reduces the power extraction efficiency of the system, which causes loss of revenue. A technique is suggested for replacement of capacitor based on PEE to maximize earning from the system in 20 years. Detailed steps for finding the optimum value of PEE for replacement of capacitor is outlined. A mathematical model of PEE which relates the ESR and C is developed. Experimental

verification is done on a prototype of single phase grid connected PV system with the different set of capacitor. PEE is found to decrease with decrease in C value. Key advantage of the proposed technique is that it determines the health of capacitor during the normal operation of the inverter without additional sensors.

References

1. **http://mnre.gov.in/mission-and-vision-2/achievements/ Dubey, R.; Chattopadhyay, S.;Kuthanazhi, V;, John, J.J; Solanki, C.S;Kottantharayil,A; Arora, B.M;Narasimhan, K.L., Kuber, V;Vasi, J; and Kumar, A.**(2013). All India survey of PV module degradation: 2013. Nat. Cent. Photovoltaic Res. Educat., Mumbai, India, [Online]. *Available:www.ncpre.iitb.ac.in/uploads/All_India_Survey_of_Photovoltaic_Module_Degradation_2013.pdf*

2. **Dhere, N. G.** (2005) Reliability of pv modules and balance-of-system components," in Conf. Record of the Thirty-first IEEE Photovoltaic Specialists Conference, 2005, pp. 1570-1576, 2005

3. **Moore, L.M; and Post, H. N**. (2008) Five years of operating experience at a largeutility-scale photovoltaic generating plant," *Progress in Photovoltaics: Researchand Applications*, Vol. 16, No. 3, pp. 249-259.

4. **Soliman, H; Wang, H; and Blaabjerg, F.** (2016) A review of the condition monitoring of capacitors in power electronic converters. *IEEE Trans. on Indus. Appl.*, Vol.52, No.6, pp-4976-4989.

5. **Femia, N; Petrone, G; Spagnuolo, G., and Vitelli, M.** (2017) *Power electronics and control techniques for maximumenergy harvesting in photovoltaic systems*.CRC press

6. **Abdennadher, K; Venet, P; Rojat, G; Rétif, J. M., and Rosset, C.** (2010) A real-time predictive-maintenance system of aluminum electrolytic capacitors used in uninterrupted power supplies. *IEEE Trans. on Indus. Appl.*, Vol. 46, No.4, pp-1644-1652.

Annals of the Indian National Academy of Engineering
Vol. XV, April 2018

Predicting evolution of antibiotic resistance

Supreet Saini[1]

With the discovery of antibiotics in the first half of the 20th century, many thought that the area of microbiology was completely understood. The microbes were thought to be a menace, and we were equipped with this tool called antibiotics. However, a few decades later, a new phenomenon was observed – microbial populations were observed to have become resistant to antibiotics. As a result, the list of antibiotics working against a particular microbial species becomes smaller. Together with this, the discovery of newer antibiotics has slowed down considerably. These two facts combined, make search for newer attention towards understanding evolution of resistance imperative.

Broadly, the mechanisms which enable a bacterium to become resistant to antibiotics can be classified into three main area:

1. Mutating the target of the antibiotic so the antibiotic is no longer able to bind and act on the target,
2. Evolve alternate pathways, so that the cellular function compromised by the action of the antibiotic can be accomplished via an alternate pathway, and
3. Altering cellular physiology, like forming spores, so that the metabolic activities in the cell are reduced to a minimum and are only resumed once the cellular stress is overcome.

All three can be accomplished by either using in-house genes, or by acquisition of foreign genes by the bacterium.

In enteric bacteria (those that reside in the human gut), one of the key elements which enable the cell to become resistant to antibiotics are three target protein systems, called, Mar, Sox, and Rob. Each one of the three, binds a wide range of chemicals/stress agents and thereafter alters cellular physiology to best cope with the present stress. In this way, these three systems are the interface between what is present in the environment surrounding the bacteria (the chemical stressers) and the physiological response of the bacterium to this stress.

One of the ways in which the effect of a particular protein in combating antibiotic resistance can be quantified is characterization of its minimum inhibitory concentration (MIC). MIC is that minimum quantity of a drug at which the bacteria do not exhibit any growth. In the case of enteric bacteria, the MIC associated with antibiotics decreases if we were to remove either one of the Mar, Sox, or Rob systems from the cell. What these results exhibit is the role played by these three systems in modulating the cellular physiology to increase the effective concentration of the drug needed to halt growth.

In addition to each of these systems responding to an environmental stimulus, and altering physiology – they form an intricate regulatory network, where they influence each other's levels too. For instance, the Mar system, when activated, positively controls Rob amounts in the cell. The Sox system, when active, increases the number of Mar protein numbers inside the cell. Hence, there exists this extensive regulatory crosstalk between these three systems. Our first challenge in this direction was to answer the following question:

[1]Associate Professor, Chemical Engineering, Indian Institute of Technology Bombay, Powai, Mumbai – 400 076

Why does the regulatory network between Mar, Sox, and Rob have a particular topological structure? Is there something unique conferred by this structure, or was this structure just one of many possibilities which would have helped the cell accomplish the same task. In this regard, we performed experiments, and computational analysis to show that the Mar, Sox, Rob regulatory topology observed in nature is "optimal" in nature.

But the main question we were interested in this area was the following: should the wild type regulatory network be "re-wired", how does the cell react to that challenge? Does the cell change the "re-wired" network and if so, does it come back to the structure it started from, or does it evolve towards another structure?

To answer a question such as this, we perform evolutionary experiments in laboratory. In these experiments, we grow bacteria in a defined environment in a test tube, and on exhaustion of resources, we pick a few bacteria from this test tube and add them to a tube with fresh resources but identical conditions as the one before. This process is continued for several thousand generations. In evolutionary experiments, the relevant time scale is the number of generations that the experiment went on for, and not the hours/days etc. over which it was conducted.

The logic behind this experiment is as follows. During growth in this environment, one of the bacteria, by a random accident, pick up a beneficial mutation which enables it to survive better in the new environment. This new mutant, because it is better adapted to survive in the test tube environment, grows faster than the original cells we started with, and soon begins to outcompete them for resources. As a result, the fraction of total cells which are progenies of the mutant cell increases with time, and eventually, all cells in the test tube will be of this kind. The same process then repeats itself – where a newer mutant arises which outcompetes the original mutant in the test tube. Since mutations occur by random chance, and their location could be anywhere in the genome, the dynamics of this evolutionary process are dictated by a random process.

The regulatory structure defining the Mar, Sox, and Rob proteins is as shown in **Figure 1**. In order to do the evolutionary experiments, we need to change the original regulatory structure to an altered one. We do this in two distinct ways. In the first scheme, we go into the genome of the organism and alter its DNA such that one of the nodes in the network is missing. In the other scheme, all three nodes are intact, but one of the arrows (representing interaction between the two nodes) is missing. The mutated strain is, thereafter, allowed to evolve for several thousand generations in identical conditions. By doing the same evolutionary experiment in parallel (for the same mutant), we hope to generate data which allows us to understand the dynamics and statistics of this evolutionary process better.

The key result from these experiments is that once we allow the cells with mutated networks to evolve, they all recover their ability to deal with the stress posed by the antibiotics. However, parallel lines do it differently. That is, different lines "acquire" different mutations – each altering the regulatory topology in its own unique way – but enabling the cell to cope with the stress. Thus, the cell has many ways to solve the same problem!

This is exciting and challenging. This is exciting in case we want to engineer microorganisms for applications related to health, energy, environment – there are many ways to do this. And suppose one of our approaches to engineer microorganisms fails, many alternates do exist. However, from the perspective of antibiotic resistance, this result is challenging. It exhibits that, should the cell be compromised in its ability to deal with the antibiotics in any way, there are multiple avenues available to it to recover and re-establish its resistance towards antibiotics.

Acknowledgements
This work is supported by Chemical Engineering PAC in Department of Science and Technology, Government of India.

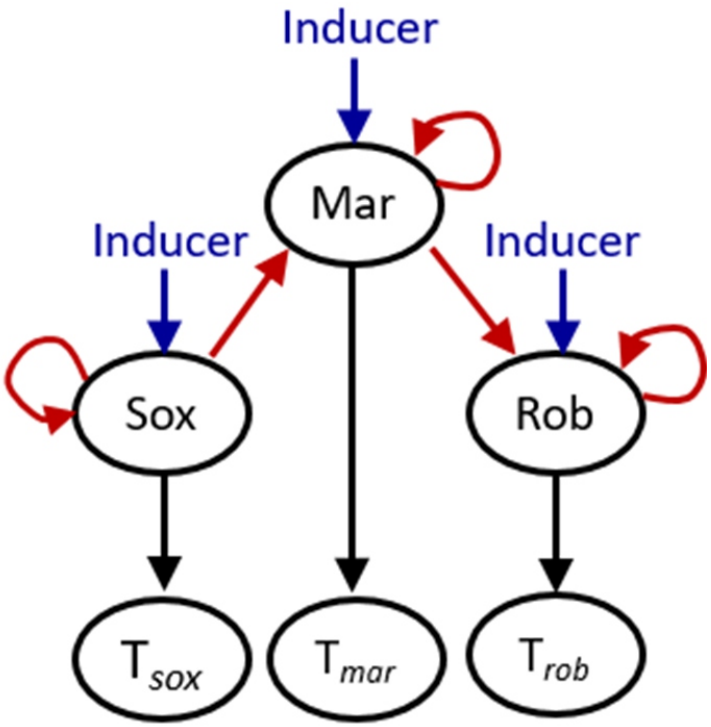

Figure 1. The regulatory network of Mar, Sox, and Rob systems in the common bacterium *Escherichia coli.*

Annals of the Indian National Academy of Engineering
Vol. XV, April 2018

Nanomaterials based low cost flexible and wearable electronics for healthcare

Parikshit Sahatiya[1] and Sushmee Badhulika[2*]

Abstract : The demand for the flexible and wearable electronics have increased significantly due to its excellent advantages such as low cost, variety of substrates, ease of fabrication and holds potential applications in the field of healthcare. In this paper, we discuss the fabrication of temperature and IR senor, flexible touch pad and strain sensor based on carbon nanomaterials. Fabrication of temperature and IR sensor was performed using conventional lithography techniques while fabrication of touch pad and strain sensor was performed by a novel rolling pin method. Substrate properties of polyimide and eraser were utilized for the fabrication of efficient sensors. Further, the fabricated strain sensor were real time tested for its application by integrating onto various human body parts. Pressure sensors was applied for flexible electronic skin and was able to detect the shape and location of the object kept on it. Simple fabrication techniques demonstrated in this paper is a major step ahead in the field of flexible and wearable electronics which finds tremendous applications in field of healthcare, human machine interaction, sensors etc.

Keywords: Flexible electronics, graphene, carbon nanotubes, sensors, wearable electronics.

1 Introduction

Flexible electronics is a technology which allows us to fabricate device on flexible substrates. Fabricating devices on flexible substrates is important as conventional Silicon technology is rigid and cannot be integrated onto human body which is soft and curvilinear. To overcome the gap, there is an urgent need to develop flexible electronics devices which can be integrated onto human and other curved surfaces.

There are variety of substrates that can be utilized for flexible electronics which include polymer films, rubbers, cellulose paper, cotton thread etc. Among various polymer films, polyimide is most suitable for use in flexible electronics because of its compatibility with microfabrication techniques such as sputtering and electron beam evaporation. Moreover, it is resistant to acid which makes them suitable for etching process. Hence polyimide substrate was utilized as a substrate for fabrication of flexible temperature and IR photodetector. Further, the low tear resistant nature of polyimide when compared to cellulose paper was used to develop flexible touch pad with novel rolling pin technique. Rolling pin technique requires the substrates to be pressed with high pressure and also fabricating flexible touch pad requires the keys to be pressed numerous time and hence the substrates needs to be highly tear resistant. Therefore polyimide was used as a substrate for fabricating flexible touch pad. Apart from that, the development of strain and pressure sensors on a single platform requires the substrate not only to be flexible but also stretchable and hence PVC free eraser was chosen as a substrate for the development of both strain and pressure sensor. Similar rolling pin approach was utilized for deposition of MWCNTs on both sides of eraser wherein pressure sensing was capacitive in nature and strain sensing was resistive. For both pressure sensor fabricated on polyimide and eraser, pressure spatial mapping experiments were performed wherein random objects were positioned on the array of sensors and the sensor was able to detect the accurate

[1]Department of Electrical Engineering, IIT Hyderabad, Hyderabad, India.

shape and location of the object which finds tremendous applications in healthcare diagnostics. The fabricated sensors were utilized in healthcare applications such as temperature monitoring, electronic skin for acid and burn victims and also for consumer electronic applications.

2 Flexible Temperature and Infrared photodetector

This paper describes an approach for fabrication of flexible electronics i.e., a wearable temperature sensor and IR photodetector on flexible polyimide (PI) substrate. Solar exfoliated reduced graphene oxide (SrGO) and graphene flakes are used as the sensing materials for developing the sensors on PI substrate. PI, apart from being flexible and compatible with microfabrication processes also helps in reducing the mobility and recombination of the photogenerated electrons of graphene due of its dielectric nature, thus enabling IR detection. Current responsivity and external quantum efficiency of IR photodetector for graphene flakes and SrGO based devices were found to be 0.4AW^{-1}, 16.53% and 0.8AW^{-1}, 33.06% respectively which are higher to those of commercially available photodetectors. In addition, we demonstrate an ultrasensitive wearable human body temperature sensor in temperature range of 35°C to 45°C, wherein both graphene flakes and SrGO based devices exhibited negative temperature coefficient of -41.30 x 10^{-4} $°C^{-1}$ and -74.29 x 10^{-4} $°C^{-1}$ respectively which are higher than commercial available counterparts. Plausible underlying mechanisms to both IR sensing and temperature sensing have been studied. Furthermore, as a proof of concept, we investigated the effect of IR radiation emitted by human hand on the device. Interestingly it was found that the device was very sensitive to it indicating that the sensor can be used for motion detection that has potential applications in security, surveillance etc. The strategy presented here provides a new simple, cost effective approach for the fabrication of next generation wearable and bio-implantable devices based on polyimide substrate that can be easily integrated onto the surface of leaf, skin, paper, clothes etc. owing to its versatile nature.

Figure 1 shows the fabrication of graphene and solar exfoliated rGO based temperature and IR sensor which uses conventional photolithography to pattern metal contacts on PI substrate. SrGO and Gr solutions were drop casted in the channel region and subsequently utilized for temperature and IR sensing. The fabricated device was transparent, flexible and wearable. Due to the adhesive at the back of PI, it has ubiquitous nature of integrating the device to any object of the choice. Fig 1 shows the integration of the device onto human skin, cloth, leaf and bark of tree. Responsivity and EQE calculated for SrGO and Gr were found to be 0.4 A/W and 0.8 A/W respectively suggesting that SrGO was more responsive to IR illumination. The reason for the higher responsivity was the defects (thermal traps) that are present in SrGO which gets activated upon IR illumination. Both SrGO and Gr possess negative temperature co-efficient of -41.3 x 10^{-4} /deg and -74.29 x 10^{-4} /deg again suggesting that SrGO was more sensitive to temperature changes when compared to Gr. It can be further used to monitor the human body temperature.

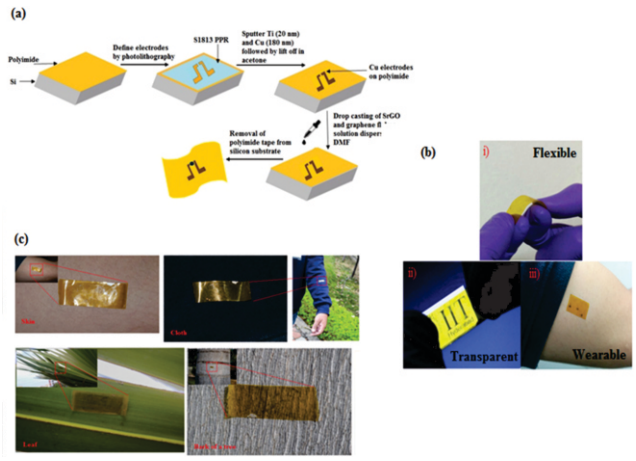

Figure 1: fabrication of graphene and solar exfoliated rGO based temperature and IR sensor and its integration onto human skin, cloth, leaf and bark of tree

3 Fabrication of pressure and strain sensor for flexible touch and electronic skin applications

This paper describes a solvent free, low cost fabrication of an ultrasensitive touch pad by sandwiching multi walled carbon nanotubes (MWCNTs) between bottom polyimide (PI) substrate and top cellulose paper using pre-compaction mechanical pressing technique. The sensing mechanism is due to pressing force dependent contact between MWCNTs and metal electrodes. Unlike, bulk flexible metal, cellulose paper is soft and has nanofiber-like structure which allows for more MWCNTs to be in contact with metal electrodes when pressed, resulting in more conductive paths under a fixed voltage thereby ensuring high sensitivity. The as fabricated sensor has sensitivity of 0.549KPa-1, response time of <32 ms and low power consumption of <1.9 mW. The entire fabrication process is scalable and could be integrated to large area for mapping spatial pressure distribution. Apart from measuring pressing, tensile and compressive forces, the sensor can identify acoustic vibrations from a loud speaker. We further demonstrate flexible touch pad which consists of an array of buttons which serve as a user interface in flexible electronics. This proposed flexible touch pad fabricated by a solvent free, low cost and low energy fabrication process paves way for future wearable electronics such as flexible touch pads, human-machine interfaces and electronic skin

Figure 2 shows the solvent free fabrication of flexible touch pad on flexible PI substrate. Conventional patterning techniques utilize lithography which are not very expensive. Further the integration of carbon based materials in conventional CMOS technology has its own problems. Here MWNCTs are utilized as active sensing material. Butter paper mask was prepared having square pattern of 5mm2. The deposition was performed by unique and novel rolling pin method. The method has a drawback of non-uniformity as the pressure applied varies from person to person. Hence to overcome the above problem, pre-compaction press of uniform pressure was performed so as to minimize the variations caused in the rolling pin method. The fabricated device was further utilize for touch pad on both smooth and curved surface without change in the performance. Further, it was utilize as artificial electronic skin wherein the device was able to recognize the shape and location of the object kept on the device.

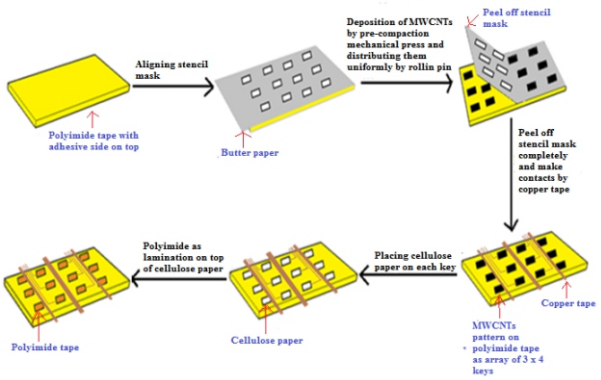

Figure 2: solvent free fabrication of flexible touch pad on flexible PI substrate

The same rolling pin method was applied on eraser substrate due to its inherent property of both stretchablity and bendability. In this case MWNCTs were rolled pin on top and bottom side of the eraser. In this case, eraser not only acts as a substrate but also as dielectric for capacitive pressure sensing. Also, MWCNTs deposited on top of top and bottom of eraser not only acts as active sensing material for strain sensing but also as metal contacts for capacitor. This greatly reduces the effort in depositing dielectric and metal using conventional sputtering and evaporation method. Strain sensing was resistive which utilize the change in resistance of MWCNT channel when bend or stretched. Pressure sensing was capacitive wherein the press changes the distance d of the eraser. Since both strain and pressure sensing are independent it eliminates the need for further frontend processing of data which needs sophisticated statistical tools such as principal component analysis and pattern recognition.

Figure 3 shows the photographic images for integration of eraser based sensor on different parts of human and fig to the right shows the spatial pressure mapping data when letter “IITH”

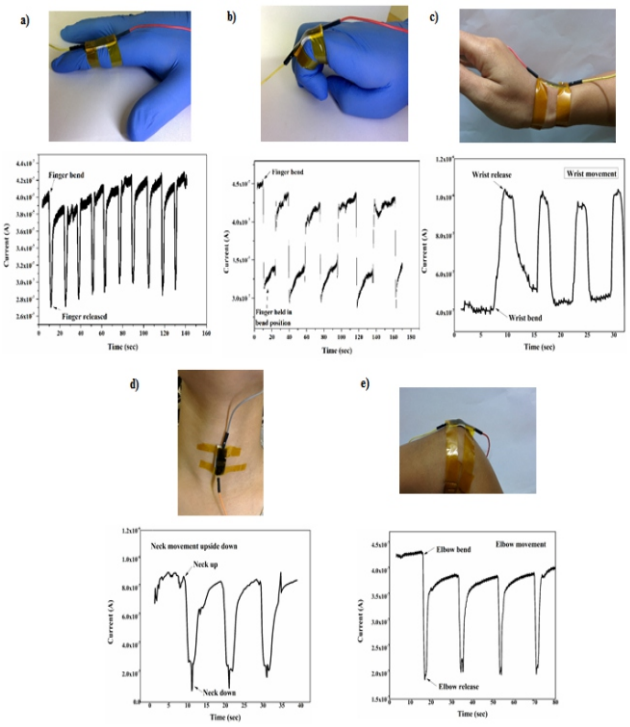

Figure 3: photographic images for integration of eraser based sensor on different parts of human and fig to the right shows the spatial pressure mapping data when letter "IITH"

Acknowledgement

A part of the reported work (characterization) was carried out at the IITBNF, IITB under INUP which is sponsored by DeitY, MCIT, Government of India.

References:

1. P. Sahatiya, S. Puttapati, S. Vadali, S. Badhulika. Wearable temperature sensor and infrared photodetector based on flexible polyimide substrate. *Flex. Print. Electron.* **2016**; 1 025006

2. P. Sahatiya & S. Badhulika. Solvent-free fabrication of Multi-walled carbon nanotube based flexible pressure sensor for ultra-sensitive touch pad and electronic skin applications. *RSC Advances*. **2016**, 6, 95836-95845

3. P. Sahatiya & S.Badhulika. Eraser-based eco-friendly fabrication of a skin-like large-area matrix of flexible carbon nanotube strain and pressure sensors. *Nanotechnology*. **2017**; 28, 9

Indian National Academy of Engineering
Unit No. 604-609, SPAZE, I Tech Park, 6th Floor, Tower A, Sector 49, Sohna Road
Gurgaon – 122 002; Phone: +91 0124 4239480 Fax: +91 0124 4239481
email : inaehq@inae.in website : www.inae.in